

CRANFIELD UNIVERSITY

AVER HEMBEN

**DEVELOPMENT OF IMMUNOSENSORS FOR THE DETECTION  
OF MALARIA**

SCHOOL OF AEROSPACE, TRANSPORT AND MANUFACTURING

PhD Thesis

Academic Years: 2014 - 2017

Supervisor: Professor Ibtisam E. Tothill

May 2017



**CRANFIELD UNIVERSITY**

**SCHOOL OF AEROSPACE, TRANSPORT AND  
MANUFACTURING**

**PhD Thesis**

**Academic Years 2014 - 2017**

**AVER HEMBEN**

**DEVELOPMENT OF IMMUNOSENSORS FOR THE DETECTION  
OF MALARIA**

Supervisor: Professor Ibtisam E. Tothill

May 2017

© Cranfield University 2017. All rights reserved. No part of this publication may be reproduced without the written permission of the copyright owner.



## ABSTRACT

Malaria is a disease of global importance caused by an Apicomplexan *Plasmodium* parasite and transmitted by adult female *Anopheles* mosquitoes. Malaria affects approximately 50% of the world's population causing millions of deaths every year. Mostly affected are pregnant women and children under 5 years of age. Morbidity and mortality rates are on the decline in some areas. Despite control efforts the disease continues to affect productivity. Productivity can be increased by early detection. Methods for malaria detection include blood film microscopy, immunochromatographic, serological and molecular tests. Blood film microscopy shows the highest sensitivity and specificity when used by trained personnel with reliable instruments. It is however time-consuming and cannot be applied as a point-of-care diagnostic method.

Two electrochemical immunosensors for malaria biomarkers *Plasmodium falciparum* histidine rich protein 2 (*PfHRP 2*) and parasite L-Lactate dehydrogenase (LDH) were developed in this work for the detection and quantification of *Plasmodium* species. The methods were based on screen-printed gold electrodes (SPGEs) with on board carbon counter and silver /silver chloride (Ag / AgCl) pseudo-reference electrode. The first stage of the work involved comparison by characterization of the bare SPGEs using potassium ferricyanide. Electrochemical techniques were used to compare bare and self-assembled monolayers of mercaptoundecanoic acid (MUA) and 3,3'-dithiodipropionic acid (DTDPA) against bare SPGE. The optimal sensor was then used for antibody attachment.

For the second stage of the work, adsorption was investigated for capture antibody immobilization on the SPGE. HuCAL monoclonal antibodies against *PfHRP 2* conjugated to the electroactive enzyme horseradish peroxidase (HRP) were then applied for signal generation. Electrochemical measurements were conducted using 3,3',5,5'-tetramethylbenzidine dihydrochloride and hydrogen peroxide (TMB / H<sub>2</sub>O<sub>2</sub>) as the mediator / substrate system at potential of -0.2 V. The sensors utilized sandwich enzyme-linked immunosorbent assay (ELISA) format with HuCAL monoclonal antibodies against *Plasmodium* immobilized on

the gold working electrode. The developed biosensor was capable of detecting sub-microscopic Plasmodium infection with a linear range from 1 to 100 ng mL<sup>-1</sup> and a limit of detection (LOD) as low as 2.14 ng mL<sup>-1</sup> and 2.95 ng mL<sup>-1</sup> for *PfHRP 2* in buffer and serum assays respectively. When compared with AuNP enhanced assays, the LOD was 36 pg mL<sup>-1</sup> and 40 pg mL<sup>-1</sup>.

Another biomarker *Plasmodium falciparum* parasite Lactate dehydrogenase (LDH) was also investigated and another sensor developed using a sandwich assay similar to the *PfHRP 2* sensor, but incorporating different antibodies against LDH. LOD 1.80 ng mL<sup>-1</sup> and 0.70 ng mL<sup>-1</sup> for LDH was obtained in buffer and serum assays. When compared with AuNP enhanced assays, the LOD was 19 pg mL<sup>-1</sup> and 23 pg mL<sup>-1</sup> respectively.

As part of the work, culture medium supernatant containing *PfHRP 2* and LDH was used to compare the immunosensor sensitivity for the pan-malaria antigen LDH. Sensitivity of the immunosensor was compared against commercially available *Plasmodium* immunochromatographic (ICT) kits: OptiMAL-IT and BinaxNOW Malaria kits. The optimized immuno-electrochemical biosensor detected the antigen at 0.002 % parasitaemia whereas the OptiMAL-IT ICT was only able to detect the LDH antigen when concentrations were of 2% parasitaemia. BinaxNOW ICT detected both the LDH and *PfHRP 2* antigens in concentrations of 4% parasitaemia and showed negative reading at 0.5% parasitaemia in both synchronized and asynchronized samples.

This study has developed two highly sensitive, portable and low cost malaria immunosensors for the first time on JD SPGEs. LDH immunosensor detects all Plasmodium species while *PfHRP 2* immunosensor is specific for the detection of *Plasmodium falciparum* biomarker. Both immunosensors detect quantifiable, sub-microscopic levels of the biomarkers with sensitivities higher than the ICT tests. The immunosensors are therefore recommended for field trial.

Keywords: Malaria, Diagnosis, *PfHRP 2*, LDH, immunosensor.

## ACKNOWLEDGEMENTS

Many thanks to all (too numerous to mention) who have been part of a most interesting journey. Many thanks for supporting the research spiritually, financially, scientifically, technically and personally; my amazing family, friends and colleagues particularly project supervisor Professor Ibtisam E. Tohill, whose careful, considerate guidance and tremendous hard work, has seen the project through its stages. I would also like to thank other review panel members: Professor Selim Cellek, Professor Seamus Higson, Professor Naresh Magan, Dr. Fady Mohareb, Dr. Iva Chianella and Dr. Jeff Newman whose professional input has been very helpful.

I am delighted to have had the opportunity for collaboration with Professor Paul Horrocks (Keele University, UK) and his team who kindly invited me to visit their laboratory to participate in *Plasmodium falciparum* Dd2<sup>luc</sup> cell culture and luciferase assay. In kind support of the research, this group also provided the soluble malarial biomarkers *Plasmodium falciparum* histidine rich protein 2 and lactate dehydrogenase in culture medium supernatant.

I would like to thank all IT staff particularly at the service desk and training room and also library staff, especially Heather Woodfield for being there at the start of student-led journal club. The journal club greatly supports students' technical writing skills. Thanks as well to Dr. Kolios and all the students who participated.

I also thank Professor Richard Luxton, University of the West of England (Bristol, UK) and Dr. Iva Chianella for joining Professor Ibtisam Tohill in the final oral examination of this work.





# TABLE OF CONTENTS

ABSTRACT .....	i
ACKNOWLEDGEMENTS.....	iii
LIST OF FIGURES.....	ix
LIST OF TABLES .....	xviii
LIST OF EQUATIONS.....	xx
LIST OF ABBREVIATIONS .....	xxi
1 INTRODUCTION AND LITERATURE REVIEW .....	3
1.1 INTRODUCTION .....	3
1.2 MALARIA INCIDENCE .....	3
1.2.1 Malaria transmission .....	8
1.2.2 The malaria parasite.....	12
1.2.3 Parasite development within the human body .....	14
1.2.4 Plasmodium species variants.....	15
1.2.5 Signs and symptoms of malaria .....	15
1.2.6 Cerebral malaria (CM).....	16
1.3 TREATMENT OF MALARIA .....	16
1.3.1 Prevention of malaria .....	18
1.4 MALARIA BIOMARKERS .....	20
1.4.1 Parasite lactate dehydrogenase (pLDH) .....	22
1.4.2 <i>P. falciparum</i> histidine rich proteins ( <i>PfHRP</i> ) 1, 2 and 3.....	23
1.4.3 Hemozoin .....	24
1.4.4 Aldolase .....	25
1.4.5 Glutamate dehydrogenase (GDH).....	26
1.4.6 Serological markers for cerebral malaria (CM).....	26
1.5 DETECTION OF MALARIA .....	27
1.5.1 Peripheral blood smear (Malaria detection gold standard) .....	27
1.5.2 Quantitative buffy coat method (QBC).....	29
1.5.3 Immunochromatographic tests (ICTs) .....	31
1.5.4 Serological tests.....	34
1.5.5 Molecular tests .....	35
1.5.6 Coffee stain malaria detection .....	37
1.5.7 Laser desorption mass spectroscopy (LDMS).....	37
1.5.8 Flow Cytometry (FCM) .....	39
1.5.9 Surface Enhanced Raman Spectroscopy (SERS) .....	40
1.5.10 Resonance imaging.....	41
1.6 BIOSENSORS .....	42
1.6.1 Biosensing receptors.....	44
1.6.2 Transducers .....	47
1.6.3 Optical biosensors.....	47
1.6.4 Mass sensitive biosensors .....	50

1.6.5 Electrochemical biosensors.....	52
1.6.5.1 Amperometric biosensors .....	54
1.7 Aims and objectives .....	58
2 SCREEN-PRINTED ELECTRODE STUDIES .....	65
2.1 INTRODUCTION .....	65
2.2 MATERIALS .....	66
2.2.1 General chemicals and instrumentation .....	66
2.2.2 Screen-printed electrodes .....	66
2.3 METHODS.....	68
2.3.1 Characterization measurements and data analysis.....	68
2.3.2 Preparation of working buffer .....	72
2.3.3 Preparation of H <sub>2</sub> O <sub>2</sub> (substrate).....	72
2.3.4 TMB (mediator) solution preparation.....	72
2.3.5 Preparation of TMB / H <sub>2</sub> O <sub>2</sub> (mediator / substrate) stock.....	73
2.3.6 Characterization of mediator / substrate system .....	73
2.3.7 Chronoamperometric analysis to determine assay potential .....	73
2.3.8 Characterization of the bare electrode surface.....	74
2.3.9 Characterization of modified electrode surface .....	76
2.4 RESULTS AND DISCUSSION .....	76
2.4.1 CV analysis of JD 1 SPGE against potassium ferricyanide.....	76
2.4.2 CV analysis of JD 2a SPGE against potassium ferricyanide.....	83
2.4.3 CV analysis of JD 2b SPGE against potassium ferricyanide.....	91
2.4.4 Data comparison of the three electrodes.....	92
2.4.1 CV analysis of modified JD 2b SPGE against potassium ferricyanide.....	94
2.4.2 TMB / H <sub>2</sub> O <sub>2</sub> System .....	96
2.4.3 Confirmation of suitable potential for the JD 2b electrode .....	98
2.4.4 Atomic Force Microscopy .....	99
2.4.5 Scanning Electron Microscopy .....	100
2.4.6 Electron Emission Spectrum of the Bare SPGE .....	102
2.5 CONCLUSIONS.....	102
3 ELECTROCHEMICAL IMMUNOSENSOR FOR <i>Pf</i> HRP 2.....	107
3.1 INTRODUCTION .....	107
3.2 MATERIALS .....	109
3.2.1 General chemicals and instrumentation .....	109
3.3 METHODS.....	111
3.3.1 Direct ELISA Assay.....	111
3.3.2 Sandwich assay .....	114
3.3.3 Capture antibody optimization (HCA 160) on JD 2b sensor.....	116
3.3.4 Detection antibody optimization on JD 2b SPGE .....	117
3.3.5 Standard curve for <i>Pf</i> HRP 2 antigen (PIP001) in buffer .....	117
3.3.6 Signal enhancement using gold nanoparticles .....	118

3.3.7 AuNP conjugation to detection antibody (HCA 159 P)	119
3.3.8 P $\beta$ HRP 2 detection limit using AuNP	120
3.3.9 Blocking agent	121
3.3.10 P $\beta$ HRP 2 detection in 100% spiked serum	121
3.3.11 P $\beta$ HRP 2 detection using AuNP in 100% serum	121
3.4 RESULTS AND DISCUSSION	122
3.4.1 Direct ELISA	122
3.4.2 Sandwich ELISA	124
3.4.3 Capture antibody (HCA 160) optimization on SPGE	126
3.4.4 Detection antibody (HCA 159 P) optimization on SPGE	127
3.4.5 P $\beta$ HRP 2 standard curve in buffer samples	129
3.4.6 P $\beta$ HRP 2 standard curve in serum samples	131
3.4.7 Scanning electron microscopy of SPGE JD 2b assay	134
3.4.8 Signal amplification using gold nanoparticles	138
3.4.9 Dynamic light scattering for the particle size determination of colloidal gold	138
3.4.10 Conjugation of AuNP to HRP- conjugated detection antibody	139
3.4.11 P $\beta$ HRP 2 standard curve in buffer samples with AuNPs	140
3.4.12 P $\beta$ HRP 2 standard curve in serum samples with AuNPs	142
3.5 CONCLUSIONS	143
4 ELECTROCHEMICAL IMMUNOSENSOR FOR L-LDH	147
4.1 INTRODUCTION	147
4.2 MATERIALS	149
4.2.1 General chemicals and instrumentation	149
4.3 METHODS	149
4.3.1 Parasite L-LDH capture antibody (HCA 158) optimization	149
4.3.2 Parasite L-LDH detection antibody (HCA 157 P) optimization	151
4.3.3 LOD recombinant L-LDH (CSB-EP632935PLS) detection in buffer	151
4.3.4 Transmission electron microscopy of gold nanoparticles	152
4.3.5 Conjugation of AuNP to reporter protein (HCA 157 P)	153
4.3.6 Detection of L-LDH in spiked serum	154
4.3.7 LOD spiked serum L-LDH AuNP-enhanced detection	154
4.4 RESULTS AND DISCUSSION	154
4.4.1 Capture antibody (HCA 158) optimization on SPGE	154
4.4.2 Detection antibody (HCA 157 P) optimization on SPGE	155
4.4.3 L-LDH standard curve in buffer samples	156
4.4.4 L-LDH standard curve in serum samples	158
4.4.5 Conjugation of AuNP to detection antibody (HCA 157 P)	159
4.4.6 LDH standard curve in buffer samples with AuNPs	160
4.4.7 LDH standard curve in serum samples with AuNPs	161
4.5 CONCLUSIONS	163
5 SAMPLE ANALYSIS USING COMMERCIAL KITS	167

5.1 INTRODUCTION .....	167
5.2 MATERIALS .....	169
5.2.1 General chemicals and instrumentation .....	169
5.3 METHODS.....	170
5.3.1 Preparation of the culture medium .....	170
5.3.2 Culture of Dd2 <i>luc</i> in RPMI medium.....	171
5.3.3 Culture medium supernatant of Dd2 <i>luc</i> (in RPMI) .....	173
5.3.4 Preparation of malaria thin film.....	173
5.3.5 Estimation of percentage parasitaemia .....	175
5.3.6 Sorbitol lysis to obtain developmental stage parasites.....	175
5.3.7 Luciferase assay .....	176
5.3.8 LDH detection using OptiMAL-IT Malaria kit .....	178
5.3.8.1 LDH recombinant detection in 100% serum on OptiMAL-IT ....	179
5.3.8.2 LDH detection using positive control on OptiMAL-IT .....	180
5.3.8.3 LDH detection using culture medium supernatant on OptiMAL-IT .....	180
5.3.8.4 LDH detection using culture medium supernatant on biosensor .....	180
5.3.9 <i>Pf</i> HRP 2 and LDH detection using BinaxNOW Malaria kit .....	181
5.3.9.1 <i>Pf</i> HRP 2 / LDH detection using culture supernatant on BinaxNOW .....	181
5.4 RESULTS AND DISCUSSION .....	182
5.4.1 Estimation of percentage parasitaemia of <i>P. falciparum</i> .....	182
5.4.1 Luciferase assay .....	183
5.4.2 LDH detection using OptiMAL-IT Malaria dipstick kit.....	186
5.4.3 LDH detection on immunosensor using culture supernatant.....	188
5.4.4 BinaxNOW Malaria on ICT .....	191
5.5 CONCLUSIONS.....	193
6 FINAL CONCLUSIONS AND FUTURE WORK.....	197
6.1 Overview.....	197
6.2 ELECTROCHEMICAL IMMUNOSENSORS .....	198
6.3 MALARIA IMMUNOCHROMATOGRAPHIC KITS .....	200
6.4 LIMITATIONS .....	200
6.5 FUTURE WORK.....	201
6.6 FINAL CONCLUSIONS .....	202
REFERENCES.....	203
APPENDICES .....	239
Appendix A Conference posters .....	239

## LIST OF FIGURES

Figure 1-1: Countries by stage of malaria elimination (WHO, 2014). The boundaries and names shown and the destinations on this map do not imply the expression of any opinion whatsoever on the part of the World Health Organisation concerning the legal estate of any country, territory, city or area of its authorities, or concerning the delimitation of its frontiers or boundaries. Dotted and dashed lines on the maps represent approximate border use for which there may not yet be full agreement. Trends in global malaria incidence may show variation in regional and distribution factors in relation to intervention. ....	5
Figure 1-2: Projected changes in malaria incidence (WHO, 2015). The boundaries and names shown and the destinations on this map do not imply the expression of any opinion whatsoever on the part of the World Health Organisation concerning the legal estate of any country, territory, city or area of its authorities, or concerning the delimitation of its frontiers or boundaries. Dotted and dashed lines on the maps represent approximate border use for which there may not yet be full agreement. Trends in global malaria incidence may show variation in regional and distribution factors in relation to intervention. ....	7
Figure 1-3: <i>A. gambiae</i> (Centres for Disease Control and Prevention, 1994)....	8
Figure 1-4: Dominant malaria vectors (Sinka et al., 2012). Malaria mosquitoes dominant in Africa are <i>A. arabiensis</i> , <i>A.fenestus</i> and <i>A. gambiae</i> . In the Americas there are nine dominant species: <i>A. albimanus</i> , <i>A. albitarsis</i> , <i>A.aquasalis</i> , <i>A. darlingi</i> , <i>A. freeborni</i> , <i>A. marajoara</i> , <i>A. nuneztovari</i> , <i>A. pseudopunctipennis</i> and <i>A. quadrimaculatus</i> . In South East Asia and the Pacific there are 13 known species: <i>A. koliensis</i> , <i>A. dirus</i> , <i>A. minimus</i> , <i>A. lesteri</i> , <i>A. sinensis</i> , <i>A. balabacensis</i> , <i>A. farauti</i> , <i>A. punctulatus</i> , <i>A. barbirostris</i> , <i>A. flavirostris</i> , <i>A. macularus</i> and <i>A. sundaicus</i> . In India / Western Asia there are 3 dominant malaria vectors: <i>Anopheles culicifacies</i> , <i>A. stephensi</i> and <i>A. fluviatilis</i> . ....	10
Figure 1-5: Vector life cycle (American Mosquito Control Association, 2014). .	11
Figure 1-6: Apicomplexan parasite (Slapeta and Morin-Adeline, 2011). ....	13
Figure 1-7: Plasmodium life cycle (University of California, 2013).....	14
Figure 1-8: Bed nets protect many from malaria (CDC, 2014). ....	19
Figure 1-9: Molecular sizes of some malaria proteins (Akinyi et al., 2015).....	22
Figure 1-10: <i>Plasmodium falciparum</i> parasite LDH (Read et al., 1999). ....	23
Figure 1-11: Molecular sizes of some genes that code for Plasmodium proteins .....	<b>Error! Bookmark not defined.</b>
Figure 1-12: Hemozoin crystal (Pisciota and Sullivan, 2002). ....	25

Figure 1-13: <i>P. falciparum</i> blood stages in thin blood smear (Coatney et al., 1971). Laveran's bib is known as the outline of the red blood cell and is not always visible in thin film preparations viewed under high magnification (100x objective) with oil immersion. ....	28
Figure 1-14: Quantitative buffy coat malaria detection (Kakkilaya, 2011). Quantitative buffy coat column (a) trophozoites of <i>P. falciparum</i> stained with AO (b) and BCP (c) in the QBC fluorescence method. ....	30
Figure 1-15: Schematic of lateral flow device (adopted from Innovabiosciences, 2017). The sample pad absorbs the applied sample which progresses to the conjugate pad. Conjugated pad carries immobilized antibody labelled with enzyme, gold nanoparticles or fluorescent dye. Primary antibody is immobilized on the test line. An antibody against the conjugate antibody is immobilized on the control line. The wick absorbs excess moisture at the end of the flow. ....	31
Figure 1-16: Diagnosis of malaria suspected blood samples (Ittarat et al., 2013). Diagnosis of malaria suspected blood samples (n=30) by the agarose gel electrophoresis. M is the ladder on the far left and right. Samples in lane 6, 9 and 20 were reported as negative by microscopic examination but showed a malaria positive DNA band at 120 bp (Ittarat et al., 2013). ....	36
Figure 1-17: Coffee ring malaria detection (University of California, 2010). ....	37
Figure 1-18: Schematic - Laser Desorption Mass Spectrometry (scienceaid.co.uk).....	38
Figure 1-19: Schematic of a biosensor (Uludag, 2011). ....	43
Figure 1-20: Construction of biosensor assays (Tothill, 2009).....	44
Figure 1-21: Label – free SPR detection (Sierra sensors, 2014).....	49
Figure 1-22: Schematic of an electrochemical immunosensor (Binder, 2014). ....	53
Figure 1-23: The flow chart shows relationship between the chapters during progress of this research to develop immunosensors for malaria detection. ....	61
Figure 2-1: DuPont JD 2b SPGE is of similar construct to other batches. The JD 1 base carbon print (BQ 221) had been IR dried, the subsequent inks had been box-oven dried at 140°C for 30 minutes ....	67
Figure 2-2: Electrochemical set-up with single channel Dropsens (Spain) edge connectors (a) SPE preparation (b) Faraday cage (c) to reduce interference and multichannel measurements using banana connectors (Palmsens, Netherlands) (d).....	68
Figure 2-3: Cyclic voltammogram redox curve during oxidation and reduction of electroactive species (adopted from Higson, 2003). ....	69

Figure 2-4: Scanning electron microscope (A) was used to generate an image of the gold working electrode surface, when an electron beam was incident on the mounted SPGE (B). An adhesive was used to stabilize the SPGE. .... 75

Figure 2-5: Cyclic voltammogram with 0.1 mM potassium ferricyanide on JD 1 at scan rates of 10, 20, 50, 70 and 100 mV s<sup>-1</sup> using 100 μL 0.1 mM potassium ferricyanide solution for the characterization of JD 1 SPGE. The graph represents the average of two scans per three sensors. .... 77

Figure 2-6: Cyclic voltammogram JD 1 with potassium ferricyanide 0.5 mM at scan rates of 10, 20, 50, 70 and 100 mV s<sup>-1</sup> using 100 μL 0.5 mM potassium ferricyanide solution for the characterization of JD 1 SPGE. The graph represents the average of two scans per three sensors. .... 79

Figure 2-7: Cyclic voltammogram with 1 mM potassium ferricyanide on JD 1 at scan rates of 10, 20, 50, 70 and 100 mV s<sup>-1</sup> using 100 μL 1 mM potassium ferricyanide solution for the characterization of JD 1 SPGE. The graph represents the average of two scans per three sensors. .... 81

Figure 2-8: Generalized peak measurements for JD 1 SPGE (1 mM) with indicated parameters for the calculation of active surface area. .... 83

Figure 2-9: Cyclic voltammogram with 0.1 mM potassium ferricyanide on JD 2a at scan rates of 10, 20, 50, 70 and 100 mV s<sup>-1</sup> using 100 μL 0.1 mM potassium ferricyanide solution for the characterization of JD 2a SPGE. The graph represents the average of two scans per three sensors. .... 84

Figure 2-10: Cyclic voltammogram with 0.5 mM potassium ferricyanide on JD 2a at scan rates of 10, 20, 50, 70 and 100 mV s<sup>-1</sup> using 100 μL 0.5 mM potassium ferricyanide solution for the characterization of JD 2a SPGE. The graph represents the average of two scans per three sensors. .... 86

Figure 2-11: Cyclic voltammogram with 1 mM potassium ferricyanide on JD 2a at scan rates of 10, 20, 50, 70 and 100 mV s<sup>-1</sup> using 100 μL 1 mM potassium ferricyanide solution for the characterization of JD 2a SPGE. The graph represents the average of two scans per three sensors. .... 88

Figure 2-12: Cyclic voltammograms of JD 1 and JD 2a overlay (A); potassium ferricyanide concentrations JD 1 (B) and JD 2a (C) SPGEs. Percentage active area taken between 10 - 100 mV s<sup>-1</sup> (n =5). Higher signal in JD 1 while 20 mV s<sup>-1</sup> is the best scan rate. .... 90

Figure 2-13: Cyclic voltammogram with 1 mM potassium ferricyanide on JD 2b at scan rates of 10, 20, 50, 70 and 100 mV s<sup>-1</sup> using 100 μL 1 mM potassium ferricyanide solution for the characterization of JD 2b SPGE. The graph represents the average of two scans per three sensors. .... 91

Figure 2-14: Profile of performance of JD 1, JD 2a and JD 2b gold working electrodes at scan rates of 10-100 mV s<sup>-1</sup>. The average of two scans was used to compute these results. .... 93

Figure 2-15: Cyclic voltammogram with 1 mM potassium ferricyanide on JD 2b. Percentage active area of gold working electrode after deposition of the thiol monolayer on the SPGE JD 2b using potassium ferricyanide 1 mM at 50 mV s<sup>-1</sup> scan rate. Average of two scans was used. .... 95

Figure 2-16: Characterization CV of H<sub>2</sub>O<sub>2</sub> (A) and TMB / H<sub>2</sub>O<sub>2</sub> system on JD 2b (B). The TMB / H<sub>2</sub>O<sub>2</sub> system for signal generation was characterized using cyclic voltammetry with a bandwidth ranging from -0.3 to 0.8 V at ambient temperature. The 100 μL working solution comprised 10 μL of TMB solution (0.6 M) and 10 μL 1:10 (30%) hydrogen peroxide diluted in 480 μL of working buffer (1:1 KCl and 0.05 M phosphate citrate buffer, pH 5). .... 97

Figure 2-17: Determination of a suitable potential. The measurement was normalized by first obtaining baseline current of the TMB / H<sub>2</sub>O<sub>2</sub> system at each potential then injecting monoclonal antibody-HRP conjugated (10 μg mL<sup>-1</sup>) at 100 s. at ambient temperature between 18°C and 25°C. Results were calculated from 10 measurements before and after enzyme addition. Blank response subtracted from the measurement produced the signal for the optimal current for the system as -1.4 μA. .... 99

Figure 2-18: AFM image of bare JD 2b SPGE at 25 μm (A) and 50 μm (B). Images show the uneven surface of the gold working electrode prior to antibody immobilization. .... 100

Figure 2-19: SEM of JD 2b bare SPGE 50x magnification (A) enlarged to 500x (B) and 3,500x magnification (C). Arrows show lithographic pattern. ... 101

Figure 2-20: Elemental composition of bare SPGE using electron emission spectrum. The average of three scans showed 89.14 % gold, 9.28 % carbon and 1.59 % oxygen. .... 102

Figure 3-1: Working principle of the immunosensor with HRP as the electroactive species (adapted from Binder, 2014). .... 107

Figure 3-2: Human combinatorial antibody library (Bio-Rad, 2016). Fab region recombinant conjugates are generated through the use of viral proteins, removing the need to use animals in antibody generation. .... 112

Figure 3-3: Schematic of a direct ELISA (adopted from Abcam.com, 2016). The antigen is first immobilized on the platform. .... 113

Figure 3-4: Direct ELISA assay flow chart. .... 114

Figure 3-5: Schematic sandwich ELISA format (adopted from Abcam.com, 2016). The capture antibody is immobilized first. .... 115

Figure 3-6: Sandwich assay flow chart. .... 116

Figure 3-7: AuNP detection of malaria antigen. Malaria mosquito transmits the Plasmodium parasite. The parasite produces the soluble biomarkers during red blood cell stages of its development. These biomarkers have been detected in sandwich assay format on the DuPont SPGE using horse radish



peroxidase as the enzyme label on detection antibody. On application of current at optimal potential, a signal is measured in  $\mu\text{A}$ , proportional to the amount of target analyte present in sample. The enhanced assay makes using of gold nanoparticles to enhance the signal. .... 118

Figure 3-8: Flow diagram of AuNP conjugation to detection antibody (HCA 159 P)..... 120

Figure 3-9: Direct ELISA standard curve (A) and linear regression (B) obtained from Log concentration. Standard curve of the direct ELISA format with HuCAL antibody HCA 159 P conjugated to enzyme horse radish peroxidase ( $20 \mu\text{g mL}^{-1}$ ) as detection reagent ( $n=3$ )..... 123

Figure 3-10: Sandwich ELISA standard curve using paired antibodies (A) and linear regression obtained from Log values (B). Standard curve of the sandwich ELISA format with HuCAL antibody HCA 160 as capture antibody and HCA 159 P conjugated to horse radish peroxidase ( $20 \mu\text{g mL}^{-1}$ ) as detection reagent. LOD =  $0.89 \mu\text{g mL}^{-1}$ . Coefficient of correlation  $R^2 = 0.9755$  ( $n=3$ )..... 125

Figure 3-11: *Pf*HRP 2 Capture antibody optimization on JD 2b sensor. Capture antibody optimization was conducted by immobilizing 10, 20 and  $30 \mu\text{g mL}^{-1}$  of the capture antibody (HCA 160) in sodium carbonate-bicarbonate, pH 9.6, overnight. Antigen concentration of  $30 \mu\text{g mL}^{-1}$  was applied after the wash and block steps. Antigen detection was carried out by applying detection antibody ( $30 \mu\text{g mL}^{-1}$ ) ( $n=3$ )..... 127

Figure 3-12: Detection antibody optimization on JD 2b. Optimization of the detection antibody was carried out using  $20 \mu\text{g mL}^{-1}$  of the capture Ab in buffer on the electrode. Incubation was carried out overnight at  $4^\circ\text{C}$ . Antigen detection was carried out with  $30 \mu\text{g mL}^{-1}$  antigen in dissolved in PBS (0.01 M, pH 7.4). The detection antibody was used in concentrations of 10, 20 and  $30 \mu\text{g mL}^{-1}$ ..... 128

Figure 3-13: Calibration curve of the chronoamperometric response of *Pf*HRP 2 detection in buffer. The lower limit of detection of the immunosensor was assayed using the optimized capture and detection antibodies. The standard curve showed a response that is linear with a long linear range. The range of the assay was determined by the low limit of detection sought. Average of three sensors was used. .... 130

Figure 3-14: Calibration curve of the chronoamperometric response of *Pf*HRP 2 detection in commercial serum (A) and linear regression (B). A 100% concentration of commercial serum was used to dilute recombinant *Pf*HRP 2 to a concentration of 1 –  $100 \text{ ng mL}^{-1}$ . Correlation coefficient and  $R^2$  value of 0.9815 serum matrix was observed from the formula generated by the data in Excel. Average of three sensors was used to plot the curve. .... 132

Figure 3-15: Capture antibody immobilization on the SPGE at 50x magnification (A) and enlarged to 500x (B) and 3,500x magnification (C)..... 135

- Figure 3-16: *Pf*HRP 2 antigen added following the immobilization step. The three electrodes were blocked using 100  $\mu\text{L}$  of a 1:10 solution of milk concentrate in 0.01 M PBS and incubated at 37°C for 1 hour. SEM of JD 2 SPGE treated with capture antibody, blocking buffer and antigenic interaction at 50x magnification (A) and enlarged to 500x (B) and 3,500x magnification (C). ..... 136
- Figure 3-17: Sandwich assay for *Pf*HRP 2 immobilized on SPGE. The final step in the sandwich format was applied using 10  $\mu\text{L}$  of 0.02 mg mL<sup>-1</sup> of the *Pf*HRP 2 horse radish peroxidase-conjugated detection antibody. Incubation at 37°C for 1 hour was followed by washing two times with 1 mL 0.01 M PBST (0.05 v/v). Detection antibody interaction at 50x magnification (A), enlarged to 500x (B) and 3,500x magnification (C)..... 137
- Figure 3-18: AuNP in working concentration (A) and stock dilution (B). ..... 140
- Figure 3-19: Linear regression of the chronoamperometric response of *Pf*HRP 2 detection in buffer, enhanced with gold nanoparticles. Concentrations of recombinant *Pf*HRP 2 (0.05 – 0.5 ng mL<sup>-1</sup>) were diluted in PBS (0.01 M). Correlation coefficient, R<sup>2</sup> value of 0.955 was observed from the formula generated by the data in Excel. Average of three sensors was used to plot the curve. .... 141
- Figure 3-20: Linear regression of the chronoamperometric response of *Pf*HRP 2 detection in serum, enhanced with gold nanoparticles. Concentrations of recombinant *Pf*HRP 2 (0.05 – 0.5 ng mL<sup>-1</sup>) were diluted in 100% commercial serum. R<sup>2</sup> value of 0.9844 was obtained. Average of three sensors was used to plot the curve. .... 142
- Figure 4-1: PStouch application (A) useful for analysing and up-loading data from remote locations, and DropSens hand-held potentiostat (B). ..... 149
- Figure 4-2:** TEM set up (A) mesh (B) and AuNP droplet (C). A 20  $\mu\text{L}$  drop of BBI gold colloid was applied to the mesh. The particle was air dried on the mesh before microscopic examination. .... 152
- Figure 4-3: Schematic sandwich ELISA with HRP and antibody-labelled gold nanoparticles on SPGE. .... 153
- Figure 4-4: Amperometric measurements for *Pf*LDH capture antibody optimization. Capture antibody concentration assayed were 2.5, 5, 10 and 20  $\mu\text{g mL}^{-1}$  in sandwich format. Detection of the LDH analyte is evident in the profile of averages of 3 sensors used. .... 155
- Figure 4-5: Amperometric measurements for *Pf*LDH detection antibody optimization. A 10  $\mu\text{g mL}^{-1}$  capture antibody (HCA 158) and 30  $\mu\text{g mL}^{-1}$  recombinant L-LDH concentrations were used. The detection antibody (HCA 157 P) was however diluted in 1: 40 milk PBS to working concentrations of 10, 20 and 30  $\mu\text{g mL}^{-1}$ . Detection antibody (HCA 159 P) showed saturation at 10  $\mu\text{g mL}^{-1}$  concentration, and best signal response

for the assay confirming capture antibody optimization. Average of three sensors was used to show profile (embedded plot).....	156
Figure 4-6: Standard curve of the chronoamperometric signal of L-LDH detection in buffer (A) and linear regression (B). The range was from 0.1, 1, 10, 100, 1000, 10000 and 100,000 ng mL <sup>-1</sup> . The lower limit of detection of the immunosensor showed a response that is linear with a long linear range. Correlation coefficient R <sup>2</sup> value of 0.9916 was observed in buffer matrix. Limit of detection was 1.80 ng mL <sup>-1</sup> , using an average of three sensors.....	157
Figure 4-7: Standard curve of the chronoamperometric signal of L-LDH detection in serum (A) and linear regression (B). The range was from 0.1, 1, 10, 100, 1000, 10,000 and 100,000 ng mL <sup>-1</sup> . The lower limit of the immunosensor in this assay shows response as per available antigen. Correlation coefficient and R <sup>2</sup> value of 0.9851 was observed, while limit of detection was 0.70 ng mL <sup>-1</sup> in spiked serum.....	158
Figure 4-8: TEM AuNP before (A) and after (B) antibody conjugation. Nanoparticle sizes range between 1 and 100 nm. The size of commercial gold nanoparticles was determined by transmission electron microscopy. ....	159
Figure 4-9: Calibration curve of the enhanced chronoamperometric response of LDH detection in buffer (A) and linear regression (B) using 1: 10 AuNP stock dilution used. Independent variable range was taken to be 0.001, 0.01, 0.1, 1 and 10 ng mL <sup>-1</sup> with the logarithm of the values plotted in the linear regression curve. Limit of detection was 0.019 ng mL <sup>-1</sup> and correlation coefficient (R <sup>2</sup> ) 0.975. Average of three sensors was used to plot the curve.....	160
Figure 4-10: LDH AuNP enhanced assay standard curves (A) and linear regression (B) in 100 % serum matrix. A 100% concentration of commercial serum was used to dilute recombinant LDH to a concentration of 0.001, 0.01, 0.1, 1 and 10 ng mL <sup>-1</sup> . Limit of detection 0.023 ng mL <sup>-1</sup> while R <sup>2</sup> value of 0.9805.....	161
Figure 5-1: Preparation of culture. Following inoculation, the samples were gassed to mimic physiological conditions of human internal environment (A). When the two groups were sufficiently gassed (foamy), as in (B), they were incubated at 37°C(C). ....	172
Figure 5-2: Preparation of malaria thin film. Preparation of the thin film involved Giemsa staining (A) gently drying (B) stained film (C) microscopic examination (D). ....	174
Figure 5-3: Aspiration of the supernatant. After incubation, the surface layer above was aspirated (removed) to leave the cell sediment in the bottom of the tissue culture flask. The growth of the cells was then determined in luciferase assay.....	176

- Figure 5-4: Schematic of luciferase reporter assay. Light emission is brought about by a reaction in which luciferin is converted to oxyluciferin by luciferase, with some of the energy of conversion produced as light. .... 177
- Figure 5-5: Pellet obtained before sorbitol lysis and luciferase assay. Synchronized and asynchronized pellets were used for luciferase assay to determine cell growth. The luciferin (50  $\mu\text{L}$ ) was added to 10 $\mu\text{L}$  passive lysis buffer and then 40  $\mu\text{L}$  of *P. falciparum* cells was added. Samples were prepared in triplicate in a 96 –well microtitre plate..... 178
- Figure 5-6: OptiMAL-IT test. Contents include reaction well (A) wash well (B) well cover (C) buffer ampoule (D) and pipette (E). .... 179
- Figure 5-7: Contents of BinxNOW Malaria kit (A) and application of sample (B). Buffer A can be added to the sample pad to increase the flow rate if after 1 minute the sample is yet to reach the end of the strip. .... 182
- Figure 5-8: *Plasmodium falciparum* trophozoite in RBC. Following the Giemsa staining of the thin film, ~20  $\mu\text{L}$  of immersion oil is placed in the centre of the film. Thus the cells are viewed at high resolution with the exclusion of refraction as light travels from air to liquid medium..... 183
- Figure 5-9: Relative light unit for luciferase expression at the start and end of incubation during *Plasmodium falciparum* Dd2<sup>luc</sup> cell culture viability test. Synchronized and asynchronized samples were tested for cell growth by luciferase expression. Asynchronous samples contain all stages of parasite development while synchronous samples contain parasites at same developmental stage assayed at 0 hour incubation time. Both control samples are constant against 0.5%, 1%, 2% and 4% parasitaemia. Control for the experiment comprised neat culture medium RPMI 1640 referred to as 'M' and neat medium + uninfected red blood cells, referred to as 'RBC'. Three replicates were used for luciferase response. .... 184
- Figure 5-10: Chart staging *Plasmodium falciparum* cultured cells (Silamut, 2000). Trophozoite stage of parasite development is just prior to vegetative reproduction by schizogony. It is at this stage that sorbitol lysis was conducted to destroy other stage cells and obtain a synchronized culture. Box contains trophozoites of the age range used in the research. .... 185
- Figure 5-11: OptiMAL-IT dip stick assay with recombinant LDH. Concentrations of recombinant LDH in 100% serum (10  $\mu\text{g mL}^{-1}$ ) (A) and neat recombinant protein (0.8  $\text{mg mL}^{-1}$ ) showing negative control band (B). Internal control confirms test validity. The results also confirm kit manufacturer's assertion that the test kit is only positive when live parasites are present in the sample. This was further confirmed in the results of the LDH positive control assay (C). .... 186
- Figure 5-12: OptiMAL-IT dip stick assay. Arrows show internal control negative band. OptiMAL-IT dip stick assay with 3-fold dilution of Dd2<sup>luc</sup> culture medium supernatant. No band in dilution number two..... 187

Figure 5-13: Amperometric signal for LDH detection in culture medium supernatant (A). A concentration of  $10 \mu\text{g mL}^{-1}$  capture antibody was immobilized on the working electrode. For analyte detection, a concentration of  $10 \mu\text{g mL}^{-1}$  detection antibody with horse radish peroxidase conjugated was immobilized on the working electrode. The 6% parasitaemia was diluted in blank RPMI 1640 culture medium supernatant. The diluted sample was beyond the detection limit of the OptiMAL-IT malaria dipstick test. The graph was plotted minus the zero value of background from the observed measurements without gold nanoparticle signal enhancement on immunosensor (B). Red lines show smallest measurement obtained at lowest parasitaemia. .... 189

Figure 5-14: BinaxNOW Malaria kit for *Pf*HRP 2 and LDH detection. The blank (A) showed internal control line validation of the test. The antigens were however not detected in the samples. Synchronized samples of (B) showed negative low parasitaemia and positive *Pf*HRP 2 / LDH high parasitaemia (C). Asynchronized and synchronized low parasitaemia samples however failed to detect both HRP 2 and LDH malaria biomarkers in culture medium supernatant. The immunoassay however detected LDH in less than 5% parasitaemia (section 5.4.3). .... 192

## LIST OF TABLES

Table 1-1: <i>Plasmodium sp.</i> variants (adopted from Kim et al., 2010).....	15
Table 1-2: Malaria protein biomarkers.....	21
Table 1-3: Immunochromatographic tests.....	33
Table 1-4: Biosensors for malaria detection.....	57
Table 1-5: Some malaria detection methods.....	58
Table 2-1: Batches of electrochemical screen-printed electrodes.....	67
Table 2-2: Scan parameters for potassium ferricyanide for SPGE characterization.....	70
Table 2-3: Characterization of JD 1 SPGE using potassium ferricyanide (0.1 mM).....	78
Table 2-4: Characterization of JD 1 SPGE using potassium ferricyanide (0.5 mM).....	80
Table 2-5: Characterization of JD 1 SPGE using potassium ferricyanide (1 mM). .....	82
Table 2-6: Characterization of JD 2a SPGE using potassium ferricyanide (0.1 mM).....	85
Table 2-7: Characterization of JD 2a SPGE using potassium ferricyanide (0.5 mM).....	87
Table 2-8: Characterization of JD 2a SPGE using potassium ferricyanide (1 mM).....	89
Table 2-9: Characterization of JD 2b SPGE using potassium ferricyanide (1 mM).....	92
Table 2-10: Comparison of three JD batches at 20 mV s <sup>-1</sup> (1 mM).....	93
Table 2-11: Effect of surface chemistry modification.....	95
Table 3-1: Direct and Sandwich ELISA.....	126
Table 3-2: Physical properties of the gold nanoparticles.....	139
Table 3-3: Sensitivity of histidine rich protein 2 curves.....	144
Table 4-1: Parasite L-Lactate dehydrogenase standard curves.....	162
Table 4-2: Comparison with some malaria electrochemical immunosensor assay detection limit.....	162
Table 5-1: Advantages and disadvantages of Immunochromatographic tests	167

Table 5-2: Comparative sensitivity of some immunochromatographic tests...	168
Table 5-3: Amperometric signal of LDH immunosensor assay.....	190
Table 5-4: Methods compared in this research for detection of malaria .....	193

## LIST OF EQUATIONS

( 1-1).....	49
(1-2).....	51
(2-1).....	70
(2-2).....	71
(2-3).....	81
(2-4).....	81
(3-1).....	122
(5-1).....	175



## LIST OF ABBREVIATIONS

ACTs	- Artemisinin combination therapies
AFM	- Atomic force microscope
AMCA	- American Mosquito Control Association
AMP	- Adenosine -5'- monophosphate
ATP	- Adenosine triphosphate
AuNPs	- Gold nanoparticles
CDC	- Centres for Disease Control and Prevention
CM	- Cerebral malaria
CNTs	- Carbon nanotubes
CSP	- Circumsporozoite protein
DDT	- Dichlorodiphenyltrichloroethane
DMSO	- Dimethyl sulphoxide
DNA	- Deoxyribonucleic acid
DPI	- Dual polarization interferometry
DTDPA	- 3,3'-dithiodipropionic acid
EDC	- 1-Ethyl-3-(3-dimethylaminopropyl) carbodiimide
EDTA	- Ethylenediaminetetracetic acid
EIA	- Enzyme immunoassay
EIS	- Electrochemical impedance spectroscopy
ELISA	- Enzyme linked immunosorbent assay
FACS	- Fluorescence activated cell sorting
GAP 50	- Glideosome associate protein 50
GCE	- Glassy carbon electrode
GDH	- Glutamate dehydrogenase
GPx	- Gluthione peroxidase
ICG	- Indocyanine green
ICT	- Immunochromatographic tests
IFAT	- Indirect fluorescent antibody test

iRBC	- Infected red blood cells
ITO	- Indium tin oxide
KAHRP1	- Knob associated histidine rich protein 1
LAMP	- Loop mediated isothermal amplification
LDH	- Lactate dehydrogenase
LDMS	- Laser desorption mass spectrometry
LLNTs	- Long lasting insecticide treated bed nets
MDGs	- Millennium development goals
MoAb	- Monoclonal antibody
MUDA	- Mercaptoundecanoic acid
MWCNTs	- Multiwall carbon nanotubes
NAD <sup>+</sup>	- Nicotinamide adenine dinucleotide ion
NADP	- Nicotinamide adenine dinucleotide phosphate
Ni II NTA	- Ni Nitrilotriacetic acid
NTDs	- Neglected tropical diseases
PANI	- Polyalanine
PCR	- Polymerase chain reaction
PDB	- Protein data bank
<i>Pf</i> AMP 1	- <i>Plasmodium falciparum</i> apical membrane protein 1
<i>Pf</i> CRT	- <i>P. falciparum</i> chloroquine resistance transporter
<i>Pf</i> CSP	- <i>Plasmodium falciparum</i> circumsporozoite protein
<i>Pf</i> GDH 1	- <i>Plasmodium falciparum</i> glutamate dehydrogenase1
<i>Pf</i> HRP 1	- <i>Plasmodium falciparum</i> histidine rich protein 1
<i>Pf</i> HRP 2	- <i>Plasmodium falciparum</i> histidine rich protein 2
<i>Pf</i> HRP 3	- <i>Plasmodium falciparum</i> histidine rich protein 3
<i>Pf</i> MDR	- <i>Plasmodium falciparum</i> multi drug resistant protein
pLDH	- Parasite Lactate Dehydrogenase
PoAb	- Polyclonal antibody
PPi	- Inorganic pyrophosphate

<i>Pv</i>	- <i>Plasmodium vivax</i>
PVS	- Polyvinyl sulfonate
QCM	- Quartz crystal microbalance
RBC	- Red blood cell
RLU	- Relative Luminescence Units
RPMI	- Roswell Park Memorial Institute
SAM	- Self- assembled monolayer
SELEX	- Systematic evolution of ligands by exponential enrichment
SEM	- Scanning electron microscope
SHARP	- Small histidine -alanine - rich protein
SNPs	- Single nucleotide polymorphisms
SPGE	- Screen-printed gold electrode
SPR	- Surface plasmon resonance
SPP	- Surface plasmon polariton
SPW	- Surface plasmon wave
TMB	- 3,3',5,5' - Tetramethylbenzidine dihydrochloride
TRAP	- Thrombospondin - related anonymous protein
WBCs	- White blood cells
WHO	- World Health Organization



## **CHAPTER ONE**

### **INTRODUCTION AND LITERATURE REVIEW**



# **1 INTRODUCTION AND LITERATURE REVIEW**

## **1.1 INTRODUCTION**

Malaria is an acute febrile illness caused by an ancient parasite *Plasmodium falciparum*. The Greek physician, Hippocrates once wrote on the coming into being of certain diseases and some of the terms used to describe malaria were then coined from his writings. 'Bad air' was from the early association of the disease with marshy areas (Cox, 2010). The origin of the parasite however remained a mystery (Baron et al., 2011). Towards the end of the 19<sup>th</sup> century, it was found that mosquitoes transmit the malaria parasite (CDC, 2012).

Malaria infection distinguished itself from other illnesses by showing periodic fevers and response to quinine treatment (CDC, 2012). In areas where the disease was common, people built houses on higher ground in order to escape the marshy air and avoid morbidity and mortality. They also tried to avoid being bitten by mosquitoes. With the aetiology of malaria given to bad air or bad spirits, people armed themselves with charms and amulets with inscriptions to ward off the disease.

## **1.2 MALARIA INCIDENCE**

Malaria generally occurs in tropical and subtropical areas, where the vector can live and multiply. The Anopheles mosquito requires temperatures above 20°C (68°F) for its development. The mosquito does not thrive in non-endemic areas though the pathogen may be dispersed by infected travelers and vectors aboard aircraft. Malaria contracted in an endemic area, detected in a region non endemic for the disease after symptoms emerge is known as imported malaria (Ziegler et al., 1999). Imported malaria has been responsible for 918 cases and six deaths between 2001 and 2011 (Ziegler et al., 1999). Imported malaria transmission has reached alarming levels in some countries. In the era of malaria eradication, imported malaria cases are a potential threat to countries attempting elimination or working to prevent resurgence (Castellanos et al., 2015).

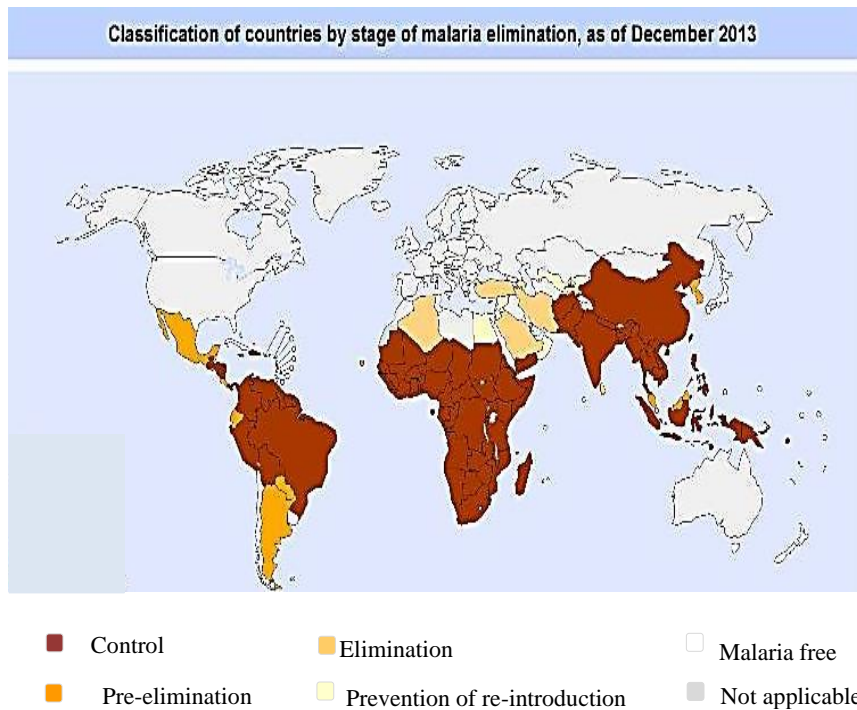
In the 1900s, Dichlorodiphenyltrichloroethane (DDT) was used to target the vector (Robertson, 2015), however, persistence in the ecosystem led to its discontinued use. Malaria still challenges the health sector. An estimate in 2010 indicated the deadliest countries per population were Burkina Faso, Mozambique and Mali (Murray et al., 2012). Geographic incidence of malaria may be altered by climate change, so regions clearly marked may show variation on other maps. Rise in temperature encourages increase in monthly potential transmission window (Sainz-Elipe et al., 2010; Caminade et al., 2014; Yu et al., 2015).

There are limits to the usefulness of modeling changes in future malaria distribution owing to anthropogenic climate change (Rogers and Randolph, 2000). This is because population and vector movement, technological development, vector and disease control, urbanization, and land use are not included (Tatem et al., 2008). Indeed, all future projections of malaria in a warmer world need to be put in the context of the observed global decline in the disease over the 20<sup>th</sup> century, mainly due to human intervention (Gething et al., 2010). Global mortality is on the decline with highest mortality in the tropics (WHO, 2014). Despite the efforts to reduce the high mortality rates, malaria continues to be a global problem (Jain et al., 2014).

The disease has been found in various animal species. *Plasmodium cephalophi* is responsible for antelope malaria (Bruce et al., 1913). *Plasmodium cyclopsi* infects bats (Landau and Chabaud, 1978). Anolis lizards of the eastern Caribbean Islands, two cryptic species of which have been identified, are affected by *Plasmodium mexicanum* (Schall and Staats, 1997). *Plasmodium relictum* is the parasite responsible for malaria in more than 419 avian species (Atkinson, 2008), while old world monkeys: Baboons and Macaques, and humans are affected by *Plasmodium knowlesi* (Singh and Daneshvar, 2013; Yakob et al., 2017).



With so many species of Plasmodium, the genus of malaria parasites thrives and the malaria elimination programme has produced a successful outcome in parts of the world (Figure 1.1).



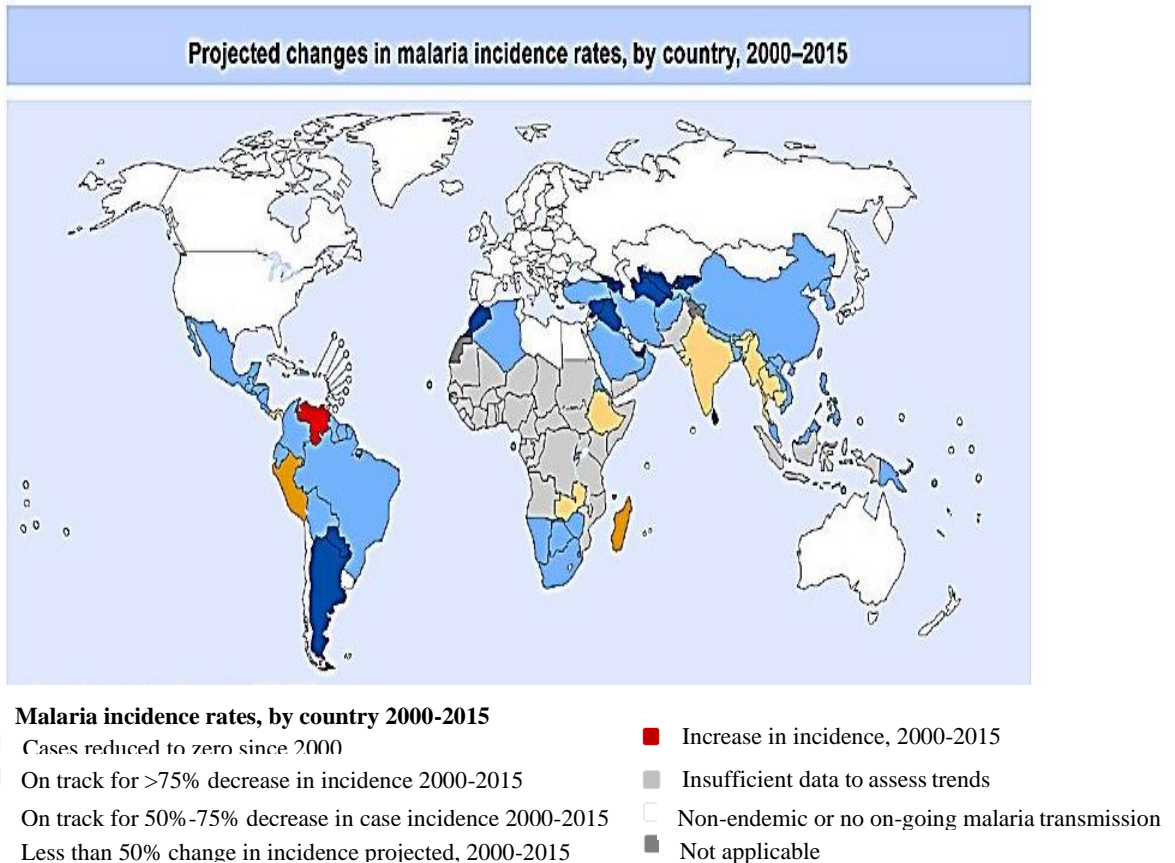
**Figure 1-1:** Countries by stage of malaria elimination (WHO, 2014). The boundaries and names shown and the destinations on this map do not imply the expression of any opinion whatsoever on the part of the World Health Organisation concerning the legal estate of any country, territory, city or area of its authorities, or concerning the delimitation of its frontiers or boundaries. Dotted and dashed lines on the maps represent approximate border use for which there may not yet be full agreement. Trends in global malaria incidence may show variation in regional and distribution factors in relation to intervention.

During the late 19<sup>th</sup> and early 20<sup>th</sup> centuries malaria was a major factor in the slow economic development of the American southern states (Humphreys, 2001; Worrall et al., 2005). Between 2000 and 2010 the incidence of malaria had fallen by 17% globally and by 33% in the African regions (WHO, 2011). There were 655,000 reported malaria deaths in 2010, of which 86% were of children under 5 years of age. In 2010, most of the malaria deaths occurred in Africa which had 91% of the global burden (WHO, 2011). It is estimated

that 50 million cases of malaria infection will emerge by 2100 (Odolini et al., 2012).

Malaria is not age-dependent or health status-related (Atoba and Adeyinka, 2013). In a study carried out on disabled members of the society, 41.3% of the population were found to suffer from malaria infection (Atoba and Adeyinka, 2013). According to estimates released in December 2014, there were about 198 million cases of malaria in 2013 (with an uncertainty range of 124 million to 283 million) and an estimated 584,000 deaths (with an uncertainty range of 367,000 to 755,000). In 2014, 13 countries reported zero cases and 6 countries reported <10 cases. Fastest decrease was seen in Eastern and Central Asia. With the effect of increasing global warmth, autochthonous malaria may occur. Malaria mortality rates have fallen by 47% globally since the year 2000, and 54% in the World Health Organization African Region (WHO, 2015).

In 2015, global malaria burden was high in sub-Saharan Africa (89% malaria cases and 91% of malaria deaths). Malaria is implicated in 60% of deaths worldwide and 65% of deaths in under-fives (WHO, 2015). It is further stated that in 2015, 97 countries had on-going malaria transmission and an estimated 3.2 billion people, nearly half the world's population were at risk of malaria. According to the malaria fact sheet (WHO, 2015), there has been a 37% decrease in malaria incidence globally since the year 2000, when the Millennium Development Goals (MDG) and projections had been made. Insufficient data in sub-Saharan Africa, however, still poses a challenge (Figure 1.2).



**Figure 1-2:** Projected changes in malaria incidence (WHO, 2015). The boundaries and names shown and the destinations on this map do not imply the expression of any opinion whatsoever on the part of the World Health Organisation concerning the legal estate of any country, territory, city or area of its authorities, or concerning the delimitation of its frontiers or boundaries. Dotted and dashed lines on the maps represent approximate border use for which there may not yet be full agreement. Trends in global malaria incidence may show variation in regional and distribution factors in relation to intervention.

The idea of malaria elimination was abandoned in the early 1970s however, interest in malaria eradication re-emerged as a long-term goal (WHO, 2011). Large-scale use of WHO-recommended strategies, currently available tools, strong national commitment, and coordinated efforts with partners were employed. In addition, modern control measures have been adopted such as vector control through insecticide spraying, use of bed nets, systematic early detection and treatment of cases (WHO, 2015). So far, seven countries have been certified by the WHO Director-General as having eliminated malaria:

United Arab Emirates (2007), Morocco (2010), Turkmenistan (2010), Armenia (2011), Maldives (2015), Sri Lanka (2016) and Kyrgyzstan (2016). This approach will enable more countries, particularly those where malaria transmission is low and unstable, to progress towards malaria elimination (WHO, 2015).

### 1.2.1 Malaria transmission

The name "mosquito" (formed by *mosca* and diminutive *ito*) is Spanish for "little fly". Females of most species are ectoparasites listed among arthropod phylum; class Insecta; Dipteran order, Nematocera sub-order; Culicomorpha infraorder; superfamily Culicoidea and family Culicidae. Malaria is transmitted by the nocturnal Anopheles female mosquito; a small flying insect weighing about 2.5 mg and which looks like a midge (Brown, 1993). Climatic conditions and survival of mosquitoes: rainfall pattern, temperature and humidity can affect mosquito behaviour (Noppadon et al., 2009). A blood-feeding mosquito is shown in Figure 1.3.



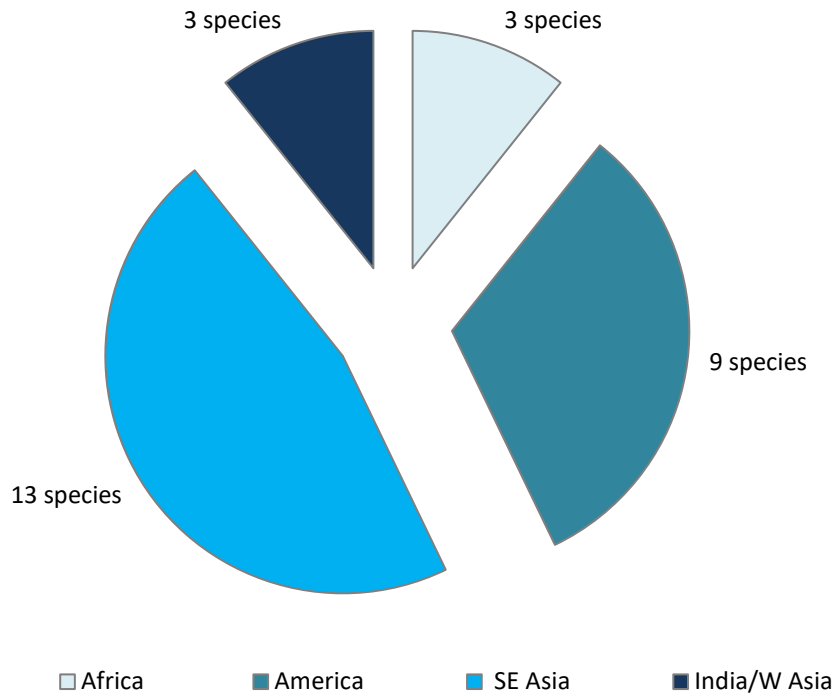
**Figure 1-3:** *A. gambiae* (Centres for Disease Control and Prevention, 1994).

The family Culicidae is divided into Anophelinae and Culicinae subfamilies. Some species of Culicidae help stabilize the ecosystem. These harmless

mosquito species feed on plant juices. Some species however feed on blood of animals, including humans causing an irritating bump.

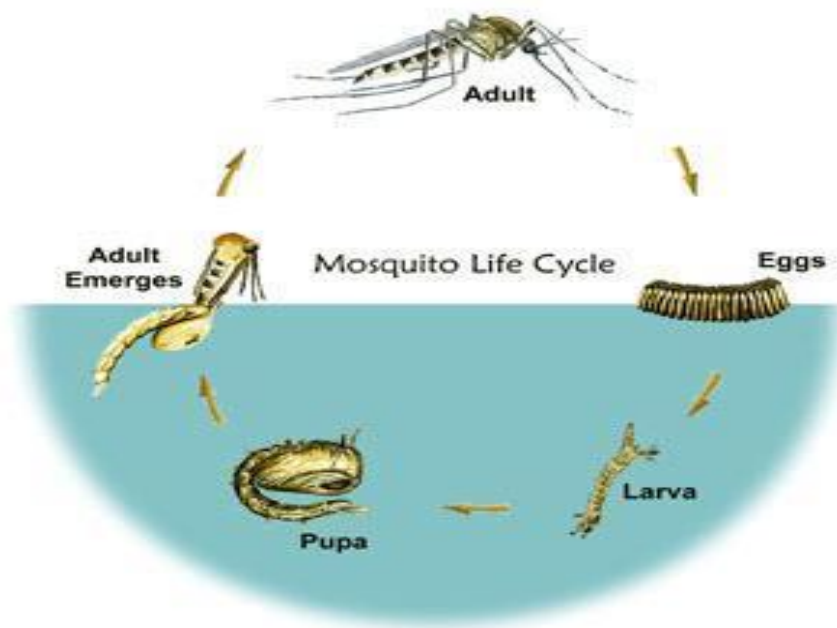
The infected malaria mosquito is the most common disease vector and transmits the organism when it feeds. The population at risk of infection has gone from being children and pregnant women (Ter Kuile et al., 2004) to male adults whose work exposes them to mosquitoes.

Pregnant women with low immunity are also affected as malaria causes high rates of miscarriage (up to 60% in *P. falciparum* infection) and maternal death rates of 10-50% in pregnant women in areas of high transmission (Ter Kuile et al., 2004; WHO, 2011). Mosquitoes can become agents for emerging zoonotic diseases when their habitats are disturbed by sudden deforestation (Wilcox and Ellis, 2006). In stable transmission areas, semi-immune HIV-infected pregnant women are also at risk of passing HIV infection to their newborns (WHO, 2011). In addition, international travelers from non-endemic areas and their children living in non-endemic areas, returning to their home countries are similarly at risk because of waning or absent immunity (WHO, 2011). With or without active immunity, the presence of the malaria mosquito is a major concern from dominant vectors spread across regions (Figure 1.4).



**Figure 1-4:** Dominant malaria vectors (Sinka et al., 2012). Malaria mosquitoes dominant in Africa are *A. arabiensis*, *A. fenestus* and *A. gambiae*. In the Americas there are nine dominant species: *A. albimanus*, *A. albitarsis*, *A. aquasalis*, *A. darlingi*, *A. freeborni*, *A. marajoara*, *A. nuneztovari*, *A. pseudopunctipennis* and *A. quadrimaculatus*. In South East Asia and the Pacific there are 13 known species: *A. koliensis*, *A. dirus*, *A. minimus*, *A. lesteri*, *A. sinensis*, *A. balabacensis*, *A. farauti*, *A. punctulatus*, *A. barbirostris*, *A. flavirostris*, *A. macularus* and *A. sundaicus*. In India / Western Asia there are 3 dominant malaria vectors: *Anopheles culicifacies*, *A. stephensi* and *A. fluviatilis*.

*Anopheles gambiae* is the best known vector of malaria infection in humans (Baker et al., 2011). The female adult mosquito mates once in her life. The eggs are laid in stagnant water collected in old tyres, boots, tin cans, tyre tracks, puddles, rice fields, hoof prints, ponds, storage containers or gutters (Figure 1.5).



**Figure 1-5:** Vector life cycle (American Mosquito Control Association, 2014).

To enable the development of her eggs, the mosquito obtains a rich protein source from a blood meal she obtains by piercing the skin of the host and lays approximately 100 eggs every 7 days. The eggs hatch within 12-14 days and the larvae emerge (AMCA, 2014). The larvae feed on organic material in the environment by creating a feeding current with their brush-like appendages. Mosquito larvae obtain oxygen via breathing tubes and develop into pupae within 10 days. The pupa is not a known voracious feeder but develops into a young adult mosquito which emerges from the pupa case after about 7 days for first blood meal and to begin the cycle of disease transmission. In many places, transmission is seasonal, with the peak during or just after the rainy season. Abdul-Ghani, 2014 reports that data on gametocytes and resistant genotypes of malaria parasite, detected by molecular techniques may be used to calculate the risk of resistant genotype transmission.

Vector disease transmission is aided by behaviour of the agent in search of food and breeding sites (Cotter et al., 2013; AMCA, 2014). Absence of suitable breeding sites interrupts developmental cycles and prevents malaria

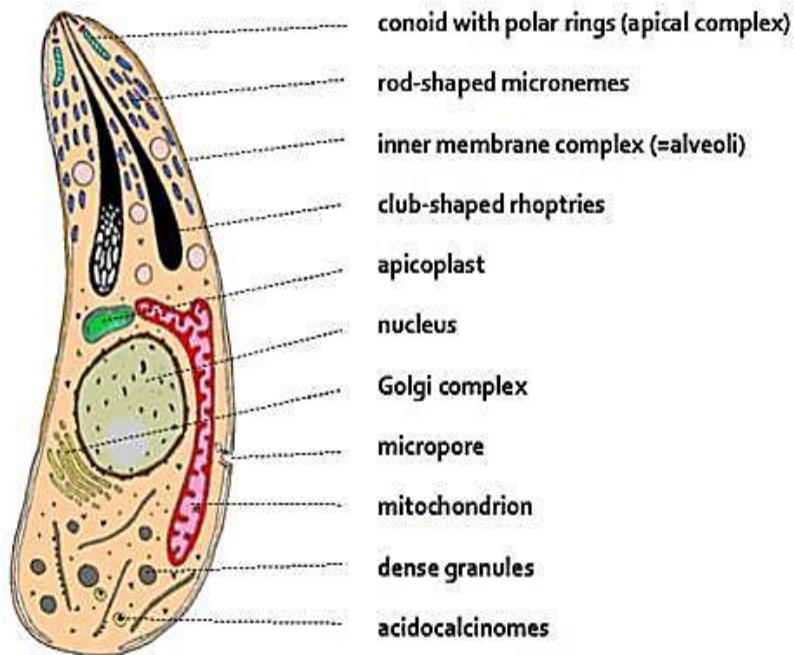
transmission. Nearly 30 of approximately 3,500 malaria vectors transmit the disease. The long lifespan and strong human-biting habit of the dominant African vector is the main reason why nearly 90% of the world's malaria cases are in Africa (WHO, 2015). In addition, different vectors can be associated with different parasite strains (Basilico et al., 2015; Kang et al., 2015).

Malaria epidemics can occur when climate and other conditions favour transmission where people have little or no immunity (WHO, 2015). Partial immunity is developed over years of exposure and reduces the risk of severe disease. Human immunity is important, especially among adults in moderate or intense transmission conditions. In areas with less transmission and low immunity, all age groups are at risk of disease from the bite of a parasitized mosquito (WHO, 2015).

### **1.2.2 The malaria parasite**

*Plasmodium falciparum* is of Protozoan kingdom, phylum Apicomplexa. It is animal-like and believed to have originated from the western ape (Liu et al., 2010). *Plasmodium falciparum* causes the most fatal of malaria infections (Baker et al., 2011). Apicomplexans comprise a diverse phylum with over 5,000 species. Seven genera affect man: *Cryptosporidium*, *Isospora*, *Cyclospora*, *Toxoplasma*, *Sarcocystis*, *Babesia* and *Plasmodium* (Wallach et al., 2012). The species do not possess locomotory organelles and exhibit a gliding motility though many species have flagellated gametes (Figure 1.6).





**Figure 1-6:** Apicomplexan parasite (Slapeta and Morin-Adeline, 2011).

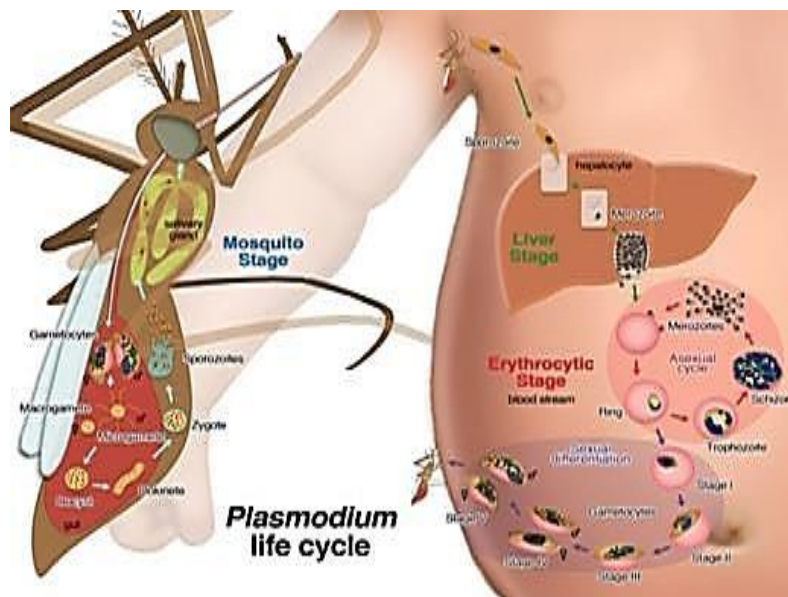
The polar ring at the cell's anterior gives rise to the microtubules running the length of the cell and form part of the inner membrane complex. The cell membrane comprises 3 layers impervious to biological and chemical substances. The plasma membrane surrounds the cell and cytosome interrupting the membrane's continuity. This structure is similar to the attachment point of cilia and flagella in other protists.

Molecular studies of the evolution of these parasites demonstrate that these parasites do not originate from a single parent (Krief et al., 2010). Group name was derived from the characteristic 'apical complex; the group was formerly called sporozoans, however, some do not sporulate and the names are interchangeable. Anterior of the parasite are secretory structures, flask-shaped rhoptries, small, oval micronemes and dense granules scattered in the cytoplasm or concentrated at the apex. Rhoptries are connected to the anterior end by channels while micronemes are located near the polar ring and aid contraction of the cell. Organelles located at one end of the parasite visible

under the electron microscope facilitate host cell invasion and parasite development in the vector.

### 1.2.3 Parasite development within the human body

The complex nature of the malaria parasite development involves development of sporozoites (Gr. *Sporos* for seeds) and merozoites (Gr. *Meros* meaning piece), trophozoites (Gr. *Trophes* food), and gametocytes (reproductive cells). Sporozoites invade hepatocytes about 45 minutes after a bite (Figure 1.7).



**Figure 1-7:** Plasmodium life cycle (University of California, 2013).

Reticulocyte-binding homologues are responsible for supporting red blood cell invasion. They act as binding agents enabling specific receptors adhere to the red blood cell (Arevalo-Herrera et al., 2012). Specific areas that mediate *PfPRH5* RBC specific interactions have been highlighted in the sequence of proteins. The trypsin-treated sensitive receptor prevents invasion by merozoites by up to 80% (Arevalo-Herrere et al., 2012). Developmental stages have different morphology and physiology; proteins and metabolic pathways enabling the parasite to resist the host immune system. Development continues within the

liver cells, which burst to release the merozoites. Some merozoites re-invade the liver cells while others develop into schizonts and then gametocytes. The cells are carried in the circulatory system until taken up during a mosquito blood meal.

#### 1.2.4 Plasmodium species variants

*P. vivax* species comprise two sub-types based on their amino acid constitution. They were identified in local Chinese populations, parts of South America like Brazil and Mexico, Peru, and in Papua New Guinea (Rich et al., 2009). Both *P. ovale* species are sympatric in Africa and Asia (Rich et al., 2009). *Plasmodium ovale* and *Plasmodium vivax* . variants are shown in Table 1.1.

**Table 1-1:** *Plasmodium* sp. variants (adopted from Kim et al., 2010).

<b><i>Plasmodium ovale</i></b>		<b>References</b>
<i>P. ovale</i> walliker (variant type)	<i>P. ovale</i> curtisi (classic type)	(Sutherland et al., 2010)
<b><i>Plasmodium vivax</i></b>		
VK210 dominant form	VK247 variant form	(Kim et al., 2010; Kim, 2012)

#### 1.2.5 Signs and symptoms of malaria

In general, the signs of malaria infection can be seen in the host within 15 days after a bite from an infected mosquito (Laloo et al., 2007). Malaria infection shows itself with an elevated body temperature, headache, sweats, chills and nausea, vomiting, muscle pain, dizziness, diarrhoea, generally feeling unwell and fatigue, dry cough and spleen enlargement. These symptoms are often mild and may not immediately be associated with malaria in non-endemic areas. Incubation period varies, depending on host immunity and parasite species. Clinical rhythmicity reflects in periodic fevers and chills recurring at approximately 48-hour intervals in tertian malaria (*P. vivax* or *P. ovale*) and 72-hours in quartan malaria (*P. malariae*). The 48-hour cycles in tertian malaria

may be modified in malignant tertian or falciparum malaria. Fever is associated with release of merozoites from red blood cells (RBCs) during erythrocytic schizogony, though the controlling mechanism for synchronous release is unknown (Lalloo et al., 2007). If the symptoms suggest malaria infection it is recommended to perform a confirmatory assessment (Moody, 2002; Lalloo et al., 2007).

Malaria can result in miscarriage and low birth weight, especially during first and second pregnancies. An estimated 200,000 infants die annually as a result of malaria infection during pregnancy (WHO, 2011; Singh et al., 2014). Glutathione peroxidase (GPx) is a catalyst and an indicator of platelet oxidative stress in *P. vivax* malaria and may be associated with the processes of malaria-induced thrombocytopenia, in which there is an abnormal number of thrombocytes or platelets (Joshi et al., 2014). Where severe thrombocytopenia occurs, attention should be drawn to the likelihood of an existing malaria infection (Joshi et al., 2014). *Plasmodium falciparum* parasite infections progress quickly and complications like renal failure and loss of consciousness can occur in severe cases.

#### **1.2.6 Cerebral malaria (CM)**

Cerebral malaria condition sometimes occurs in severe malaria attack when sequestered red blood cells breach blood–brain barrier (Renia et al., 2012). Mortality can be as high as 30% (Jain et al., 2014). Severity of CM cases are assessed using the Glasgow Coma Scale, a neurological assessment to monitor patient response in incidents of head injury or if patient is in intensive care. On a scale of zero to 15, a score of 3 is significant of deep unconsciousness. Convulsions are not uncommon and where treatment is inadequate, patients may develop organ failure.

### **1.3 TREATMENT OF MALARIA**

Malaria treatment depends on complication and if the patient is an expectant mother or young child (Lalloo et al., 2007). Lack of prompt or inadequate treatment and drug abuse have led to many malaria deaths. To reduce the

danger of misdiagnosis, it is recommended that before transfusing blood, donor blood be tested for *Plasmodium* parasites (Alii et al., 2010).

Chloroquine (4-Aminoquinolone) was the most widely used drug in most malaria endemic areas until the malaria parasite developed resistance to the drug orally (Lalloo et al., 2007). Mefloquine (Quinoline-methanols) may be combined with other anti malarials like primaquine. Mefloquine is known to affect the movement of haemoglobin and other products from the host cell to the food vacuole of the parasite and disrupts intraerythrocytic schizogonic stages, destroying hypnozoites in combination with primaquine absorbing rapidly when administered orally (Lalloo et al., 2007).

Halofantrine (Phenathrene-methanol) disrupts red blood cell schizogony in *Plasmodium falciparum* infection. It may be used to treat acute, uncomplicated, multi-resistant *P. falciparum* infection. Halofantrine may also be used in cases that are unresponsive to preventive chemotherapy, and where medical assistance is not immediately accessible (WHO, 2006).

Pyrimethamine (2, 4, diaminopyrimidine) hampers production and use of folate and inhibits the dihydrofolate reductase needed to produce tetrahydrofolate, a precursor in the parasite DNA synthesis (Figueiredo et al., 2008). They act on the red blood cell stages of *Plasmodium falciparum* parasites, not affecting sporozoites or hypnozoites. Resistant malaria forms can be treated with Sulphadoxine sometimes used as a malaria preventive drug in *P. falciparum* or *P.vivax* infections.

Sulphadoxine-pyrimethamine may cause serious skin reactions and blood dyscrasias, altering the blood components abnormally and so is no longer in use. Antibiotics like tetracycline and doxycycline are sometimes used to treat malaria when combined with pyrimethamine or quinine. The relationship between Chloroquine and Sulphadoxine-Pyrimethamine dosing is common (Figueiredo et al., 2008).

Artemisinin is the current drug of choice in *Plasmodium falciparum* infection. It is derived from the aromatic plant *Artemisia annua* commonly called, sweet Annie, annual wormwood, Qing hao (Chinese) which stands for blue-green Artemisia. It is an annual herb about 2 meters tall, used in Chinese traditional medicine and cosmetic industry. Artemisinin derivatives show quicker response to malaria infection than current drugs (White, 1997). Artemisinin low bioavailability prompted the production of its derivatives like Artesunate, Artemether, Artemether/Lumefantrine (Coartem), Dihydroartemisinin, Artelinic acid and Artemotil to enhance its efficacy. Malaria due to *P. vivax* and *P. falciparum* are now being treated worldwide with drugs containing artemisinin derivatives also called artemisinin-combination therapies (ACTs) as resistance to artemisinin was recorded in Southeast Asia, Cambodia in 2008 (Dondorp et al., 2009). Parasite resistance to artemisinin oral therapy is increasing rapidly and was reported in Thailand in 2012 (Abdin et al., 2003; Phyo et al., 2012). Imported malaria is also implicated in drug-resistant malaria species like *P. falciparum* and *P. vivax* (Nomura et al., 2001). *Plasmodium falciparum* multidrug resistance (*Pfmdr1*-N86Y) and *Plasmodium falciparum* chloroquine resistance transporter (*Pfcrt*-K76T) have also been studied as being responsible for drug resistance (Shrivastava et al., 2014).

### 1.3.1 Prevention of malaria

Malaria can be prevented using physical, biological and chemical methods. Prophylactic drugs interrupt the parasite life cycle. Travellers are administered antimalarial drugs like Paludrine prior to arrival in a malaria endemic area. To avoid mosquito bites, people wear light coloured clothing as blood sucking mosquitoes are attracted to dark colours. General body covering may not be practicable, however, in the approximate 37°C room temperature warmth of a typical tropical evening when certain kairomones emitted by humans enables the vector locate the host. Mosquito-repellent plants may also be used (Karunamoorthi et al., 2009). A major factor in malaria control lies in the behaviour of individuals. Mosquito repellent lotions may be applied, while the

use of insecticide-treated bed nets is encouraged (Figure 1.8). It is reported that 31% of households do not make use of the long-lasting insecticide treated bed nets (LLNTs) for the intended purpose of the malaria intervention programme (Araya et al., 2015).



**Figure 1-8:** Bed nets protect many from malaria (CDC, 2014).

While focusing on the mosquito and the interruption of its life cycle, introduction of ornamental fish like Guppies in ponds is a natural way of reducing the spread of malaria while providing a protein source for the fish. Likely breeding sites: empty containers and old tyres should however be cleared. In the process of vaccine development, there are currently no licensed, long-lasting vaccines against malaria or any other human parasite. One research vaccine against *P. falciparum*, known as RTS, S/AS01, is most advanced and is said to afford protection for a period of 12 months in early childhood (WHO, 2015). This vaccine has been evaluated in a large clinical trial in 7 countries in Africa and has been submitted to the European Medicines Agency under article 58 for regulatory review (Baker et al., 2011; WHO, 2015). A WHO recommendation for use will depend on the final results from the large clinical trial and a positive regulatory review (WHO, 2015). Malaria control challenges include

investigation of a suitable biomarker. Current malaria detection methods are discussed in section 1.5.

## **1.4 MALARIA BIOMARKERS**

Biomarkers are indicators of changes in cellular, biochemical, or molecular systems that can be determined in samples in response to a disease-causing organism or to a treatment (Murhandarwati et al., 2010). Biomarkers have gained recognition over the last 10 years due to their possible use as drug targets, also in the development of malaria detection techniques (Richards et al., 2013). In regions of high incidence, it has been observed that a lot of *Plasmodium falciparum* sufferers show malaria infection without indication of obvious symptoms. These cases have recorded a level as high as 53% (Richards et al., 2013). Biomarkers have also been used to evaluate therapeutic measures. The reaction may be chemical, disease-causing or biological (Richards et al., 2013).

Resistance to Artemisinin in the Menkong district, South East Asia has led scientists to believe that there are genetic biomarkers for malaria drug resistance. The genetic markers are responsible for the resistance of the World Health Organisation's recommended frontline treatment for malaria, artemisinin and artemisinin derivatives (Takala-Harrison, et al., 2013). Four Single Nucleotide Polymorphisms (SNPs) on chromosomes 10 (one), 13 (two), and 14 (one) were significantly associated with delayed parasite clearance. The two SNPs on chromosome 13 are in a region of the genome that appears to be under strong recent positive selection in Cambodia. Mutations found in the propeller region of the Kelch protein serve as molecular markers for artemisinin resistance (Ariey et al., 2013).

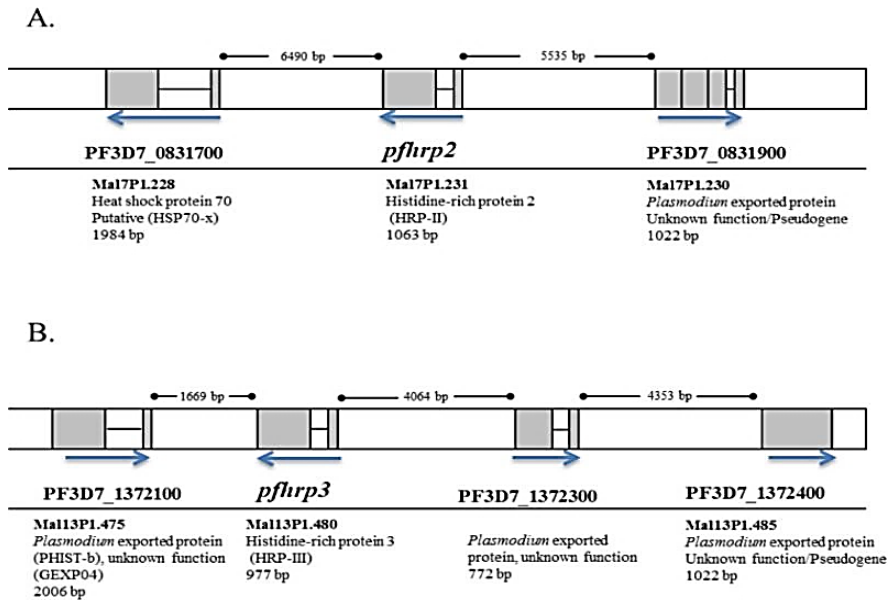


In addition to genetic biomarker resistance, more common are the protein biomarkers used in disease detection assays. There is no clear grouping for biomarkers however there are types of biomarker, according to their role (Jain et al., 2014). Type 0 biomarkers show the origin of a condition and indicate the relationship between the condition and the clinical result. Type 1 biomarkers usually show the natural result of a drug regime, and Type 2 biomarkers are like alternative markers and indicate the clinical point at which the patient shows some response to the treatment. The biomarkers that can predict the development and outcome of severe malaria may be clinically utilized for prognosis, diagnosis and disease management. There are molecules and functional entities which differ from the host counterpart as well as from those of other disease-causing organisms. Listed among the malaria biomarkers for disease detection are Parasite lactate dehydrogenase (pLDH), glutamate dehydrogenase (GDH), aldolase, hemozoin crystals and *Plasmodium falciparum* histidine rich protein 2 (*PfHRP 2*) (Leke et al., 1999; Jain, 2014) listed in Table 1.2.

**Table 1-2:** Malaria protein biomarkers.

Biomarker	Blood level	References
pLDH	4.9 ng mL <sup>-1</sup>	(Dzakah et al., 2014, Dirkzwager et al., 2015)
<i>PfHRP 2</i>	9.45 ng mL <sup>-1</sup>	(Ho Mei-Fong et al., 2014; Dzakah et al., 2014; Abdallah et al., 2015)
Aldolase	-	(Wanidworanun et al., 1999)
Glutamate dehydrogenase	-	(Werner et al., 2005)
Hemozoin	-	(Noland et al., 2003; Wilson et al., 2011)

Molecular sizes of some malaria proteins are shown in Figure 1.9.

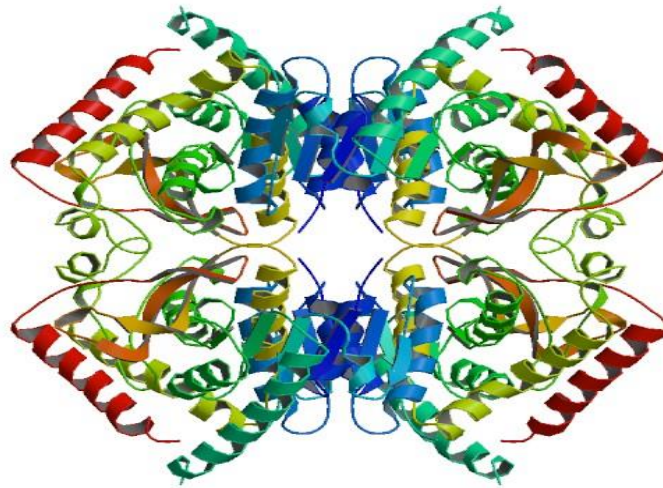


**Figure 1-9: Molecular sizes of some malaria proteins** (Akinyi et al., 2015).

Due to the highly polymorphic nature of *Pf*HRP 2 (Lynn et al., 1999; Desakorn et al., 2005; Verma et al., 2015) further research has studied cross-reactivity, presenting as false positive and false negative results in the field.

### 1.4.1 Parasite lactate dehydrogenase (pLDH)

Lactate dehydrogenase (LDH) is a biomarker found in the final stage of glycolysis in cells, muscles and tissues of organisms (Vander et al., 1981). Malaria parasite LDH is shown in Figure 1.10 (Read et al., 1999).



**Figure 1-10:** *Plasmodium falciparum* parasite LDH (Read et al., 1999).

*Plasmodium falciparum* produces pLDH in large amounts during intraerythrocytic stages; the parasite depends on anaerobic respiration for the formation of ATP from glucose, and the  $\text{NAD}^+$  is produced by conversion of pyruvate to lactate while the mitochondria add to the ATP pool (Frank and Hargreaves, 2003). *P. falciparum* LDH RNA expression level increases, with the highest point at 24 to 30 hours in the intraerythrocytic cycle. This expression is reduced to zero level in the schizont stage (Frank and Hargreaves, 2003).

Parasite LDH is a favourable candidate for antimalarial drug development as it possesses suitable characteristics. It regulates the production of Plasmodium ATP, possesses important amino acids at the active site as opposed to related organisms, and the Protein Data Bank (PDB) has several X-ray crystallographic features of pLDH complexed with compounds that are focal points in the designing of inhibitors. Studies reveal that gossypol and its derivatives working against the parasite enzyme pLDH concentrates on pLDH and not human LDH (Read et al., 1999).

#### 1.4.2 *P. falciparum* histidine rich proteins (*PfHRP*) 1, 2 and 3

Histidine is a basic amino acid found in many species and plays a variety of roles (Ge et al., 2006). *Plasmodium falciparum* produces a peculiar collection

of water soluble histidine rich proteins during the asexual red blood cell development. They are referred to as histidine rich proteins 1, 2, and 3 in the order of their discovery (Ge et al., 2006). HRP 2 comprises 34% histidine and 37% alanine, both of which are essential amino acids.

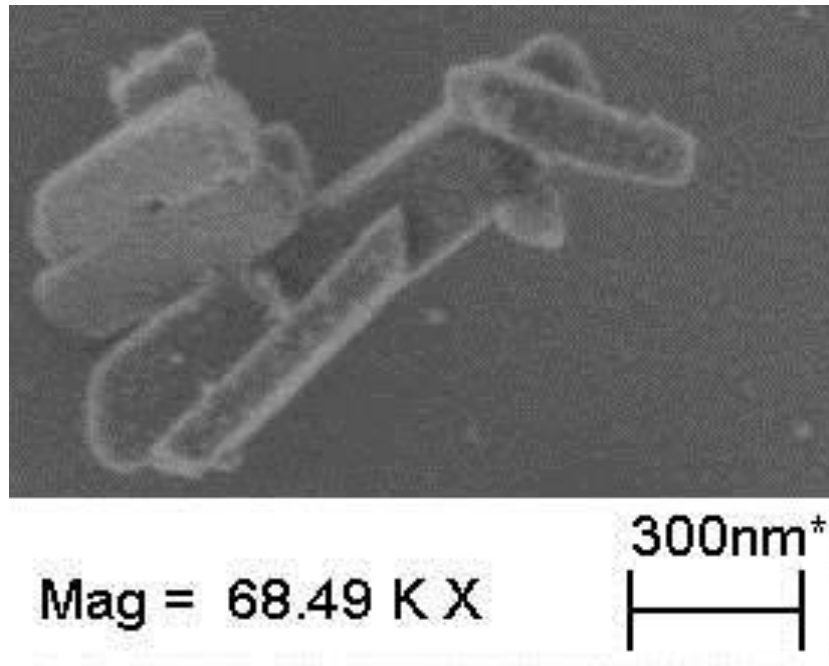
Histidine rich protein I (HRP 1) is also called Knob-Associated Histidine Rich Protein (KAHRP-1) is found in Knob<sup>+</sup> strains showing knob-like projections on the surface of the cell. HRP 1 assists cytoadherence of infected red blood cells to the venular endothelium and plays a partial role in the high parasitemia and hypoxia associated with *P. falciparum* (Zhao and Waite, 2006).

Histidine rich protein 2 (HRP 2) is particular to *Plasmodium falciparum* and is found in both Knob<sup>+</sup> and Knob<sup>-</sup> strains. HRP 2 is said to play several roles such as heme binding and heme detoxification by forming hemozoin (Karpen et al., 1992; Sullivan et al., 1996; Tjitra et al., 2001; Pandey et al., 2001; Ajumobi et al., 2015). HRP 2 also functions in the neutralization of bacterial toxin, Lipopolysaccharide (Ziegler et al., 1999; Accardo et al., 2007). This neutralizing ability of histidine rich protein 2 is said to have occurred in electrostatic interactions between histidines and the negatively charged phosphate groups of Lipopolysaccharide. It has been nominated as a model vaccine candidate against malaria. HRP 2 antigen is known to have multiple binding epitopes due to its repeat structure, unlike pLDH that has one antibody binding site (Gatton et al., 2015).

HRP 3 is also called Small Histidine-Alanine-Rich Protein (SHARP) is less available than the other two histidine rich proteins and is smallest.

### 1.4.3 Hemozoin

Hemozoin is a non-soluble, microcrystalline substance produced during the digestion of blood by *Plasmodium sp.* as well as other blood parasites. In the eighteenth century, it was shown that internal organs of malaria victims were an unusual colour (Pagola et al., 2000). Hemozoin structure is shown in Figure 1.11.



**Figure 1-11** Hemozoin crystal (Pisciota and Sullivan, 2002).

Haemoglobin digestion releases amino acids and free, toxic haem, known as ferriprotoporphyrin IX which is polymerized to hemozoin. Despite systematic research on the nature and properties of the hemozoin crystal (Noland et al., 2003; Wilson et al., 2011), the nucleation process is as yet unknown. There are reports about initiation of hemozoin formation occurring auto-catalytically. Hemozoin is a primary candidate in research towards the development of a malaria drug (Delahunty et al., 2014). Hemozoin crystals are however not suitable as a biomarker in field samples that may contain ring stage parasites less than 6 hours old (Delahunty et al., 2014).

#### 1.4.4 Aldolase

*Plasmodium falciparum* aldolase is a protein found mainly in the parasite cytoplasm as a potent and soluble component and is also reported to be related to the membrane fraction as an insoluble form (Knapp et al., 1990). Aldolase plays a prominent role in the parasite glycolytic pathway and is found in the host circulatory system during infection (Wanidworanun et al., 1999). The enzyme is a homotetrameric protein.(Fitch et al., 1999). Aldolase has been

recommended as a rapid test for monitoring response to therapy as it is sensitive only at high parasitaemia in sample (Maltha et al., 2010).

Aldolase has 61-68% sequence similarity to known eukaryotic aldolases (Dzakah et al., 2014). The aldolase genomic sequence comprises two exons separated by one intron. Research on the crystal structure of *Plasmodium* parasite aldolase has been studied at a resolution of 3 Å to determine the inhibitors that may be related to its structure (Dzakah et al., 2014). The enzyme sequence varies greatly from the host and may be used as a focal point for drug treatment. It was however reported that one aldolase gene occurs in *P. berghei*, *P. vinckei*, *P. chabaudi*, *P. yoelii* and *P. vivax*.

#### **1.4.5 Glutamate dehydrogenase (GDH)**

Glutamate dehydrogenases form a significant point of change in carbon and nitrogen metabolism. They are mostly related to ammonium assimilation (NADP-dependent GDHs) or glutamate catabolism (NAD-dependent GDHs). *Plasmodium falciparum* shows three GDH isozymes. GDH is not found in host red blood cell (Henze et al., 1998). PfGDH 1 is an NADP-dependent GDH, a homohexamer involved in the redox metabolism of the parasite (Frank and Hargreaves, 2003). Glutamate dehydrogenases show a unique N terminal residue extension that is absent in the mature human enzyme and noticeable during the red blood cell cycle (Werner et al., 2005).

#### **1.4.6 Serological markers for cerebral malaria (CM)**

There is noticeable variation in exosomes plasma levels of endothelial origin among Malawian children suffering from cerebral malaria (CM), severe malarial anaemia, and uncomplicated malaria caused by *Plasmodium falciparum* (Frasch et al., 2004). It had been reported that as yet there are no distinct biomarkers for CM, though research shows a significant association between chemokine interferon inducible proteins (CXCL10 and CXCL4) and the severity of CM; patients with CM have significantly higher levels of CXCL10 and CXCL4 (Werner, et al., 2005).

Micro particles are observed in the serum of malaria and diabetes patients (Jacobsen et al., 1994; Kassa et al., 2011), systemic lupus erythematosus (Wenish et al., 1997) acute coronary syndromes, and in severe trauma (Freyssinet, 2003). Exosomes, also called micro vesicles, are sections of plasma membrane shed by different types of cell under physiological stress. They have also been associated with pathophysiology (Casals-Pascualetal et al., 2008).

Fluorescence Activated Cell Sorting (FACS) micro particles from platelets may be a distinct marker in the routine follow-up since the levels of micro protein significantly increase during CM but reduce as soon as the patient is free of the disease. The serological biomarkers, however, are difficult to use reliably in diagnosing malaria in support of the malaria elimination goal in endemic areas (Cook et al., 2010, Mfonkeu et al., 2010).

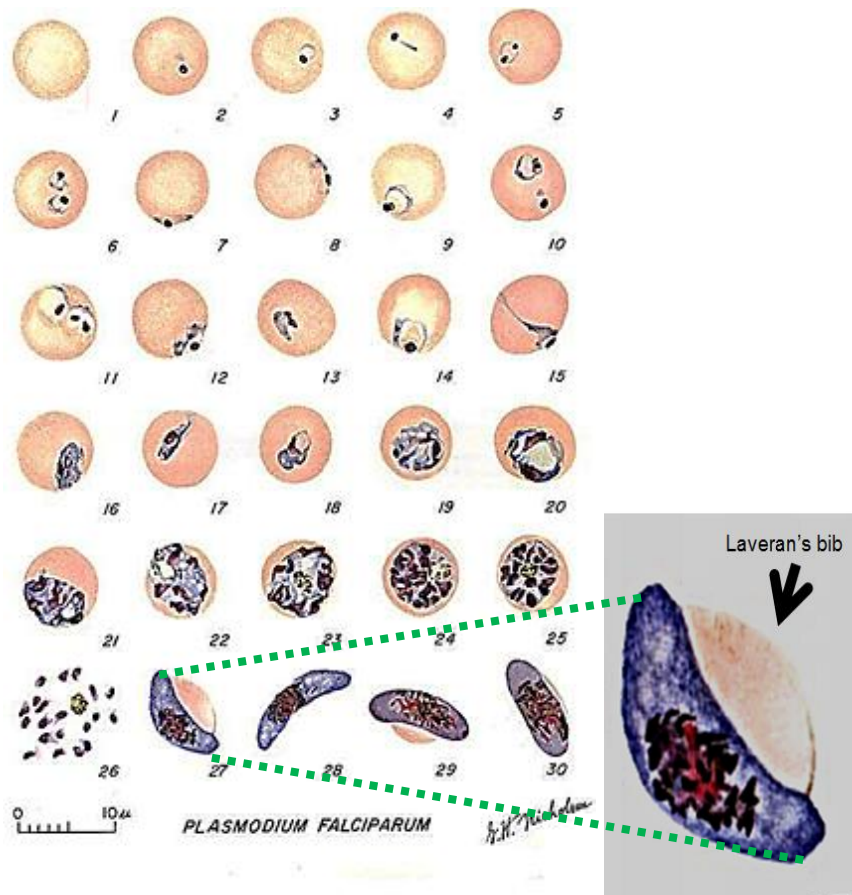
## **1.5 DETECTION OF MALARIA**

Malaria detection techniques vary from the gold standard microscopic examination of stained thick and thin blood smears, fluorescent microscopic techniques, serological tests using indirect antibody fluorescent test, immunochromatographic test, a range of spectroscopic methods, molecular and biosensing assays.

### **1.5.1 Peripheral blood smear (Malaria detection gold standard)**

The gold standard detection of malaria is carried out by light microscopic identification of the malaria parasite on a fixed, stained thin film of patient whole blood sample. Microscopic detection of malaria was first performed by Alphonse Laveran who identified *Plasmodium sp.* as the pathogen for malaria in around 1800 (Fleischer, 2004). The detection method adopted by Laveran was conducted directly on the blood of patients. Later, Dimitri Romanowsky tinted the organelles and cellular matrix of the organism in diseased red blood cells (Fleischer, 2004). For this to be possible, blue dye had to have 'matured' or have 'become 'stale', changing its physical and chemical appearance. A repeat

experiment was not attainable owing to the change that took place in the methylene blue dye. Several preparations and solution testing had to be performed for staining to be carried out satisfactorily. Giemsa's work described the new dye as azure B (trimethylthionine). The results were reproducible and sold as Giemsa solution for Romanowsky stain. Giemsa solution is still used today in the routine examination of stained blood films for malaria diagnosis (Fleischer, 2004). Thick and thin blood films prepared from peripheral blood of patients aid in identification and speciation of parasite by stage (Coatney et al., 1971). Thin film preparation with Giemsa stain sometimes reveals Laveran's 'bib' (Figure 1.12).



**Figure 1-12:** *P. falciparum* blood stages in thin blood smear (Coatney et al., 1971). Laveran's bib is known as the outline of the red blood cell and is not always visible in thin film preparations viewed under high magnification (100x objective) with oil immersion.

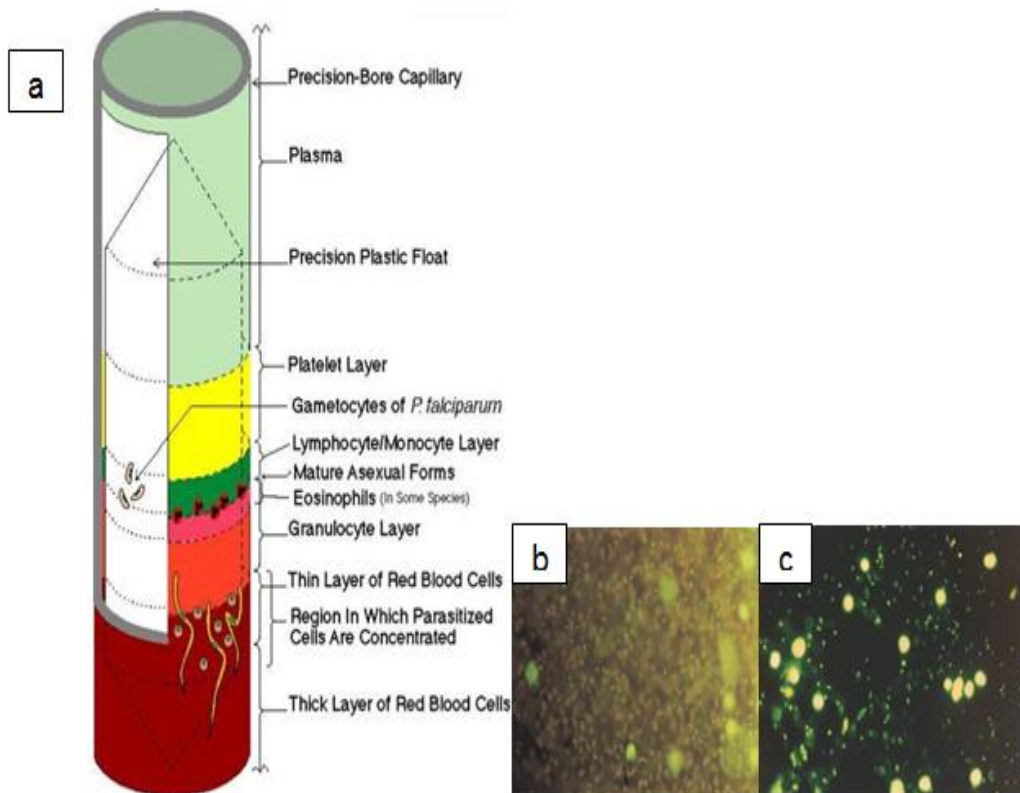


The high resolution of the image is achieved by viewing the image through a suitable objective lens. The lens is adjusted to make contact with the immersion oil applied to the film, thus eliminating the refractive index of air and glass as light passes through the lens. The light ray would normally bend as it traverses between media in dry mounts. The oil serves to direct the rays of light through the objective lens onto the sample.

Peripheral blood smear of patient samples is a reliable method for use by trained persons who have sound equipment to make accurate parasite identification (Bailey et al., 2013). This assay is known as the gold standard method for malaria diagnosis despite problems with its field accuracy, unacceptably high false-positive rates, and errors in species identification, leading to misdiagnosis, and its operator-dependence (Kifude et al., 2008; Herrera et al., 2014). Structural changes may take place in samples stored in Ethylenediaminetetracetic acid.

### **1.5.2 Quantitative buffy coat method (QBC)**

Quantitative buffy coat method is a quick method of detecting malaria infection. It is easy to use and more sensitive than the thick smear technique. QBC test was made usable by Becton and Dickenson Inc. for detecting malaria in 50-65 microliters of peripheral blood (Adeoye and Nga, 2007). Two fluorochromes have frequently been used to stain the parasitized cells: acridine orange (AO) and benzene thiocarboxypurine (BCP). Parasite DNA takes up the stain within the tube (Figure 1.13).

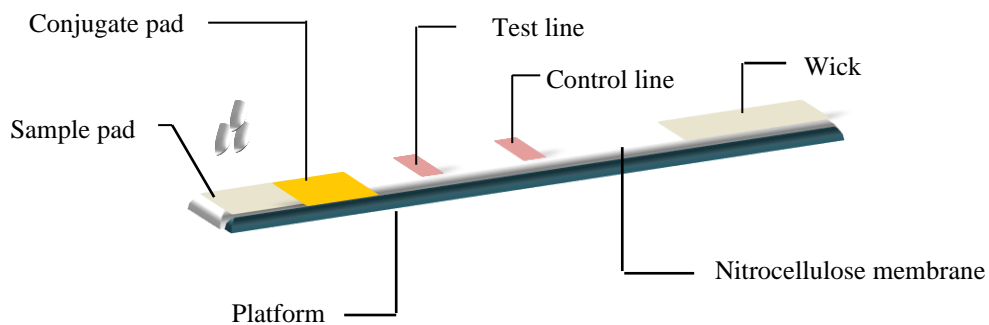


**Figure 1-13:** Quantitative buffy coat malaria detection (Kakkilaya, 2011). Quantitative buffy coat column (a) trophozoites of *P. falciparum* stained with AO (b) and BCP (c) in the QBC fluorescence method.

After the sample is introduced in the haematocrit tube a float is inserted and tube with contents centrifuged for 5 minutes at 12,000 rpm to obtain infected RBCs (iRBCs) in anticipated region of the QBC tube, below the (white blood cells) WBCs (Moody, 2002). The float occupies about 90% of the space in the tube so that cell layers are held down and made thicker. The parasites from the erythrocyte / leukocyte interface are examined under the standard white light of a microscope fitted with a UV microscope adapter. The tube is turned under the microscope to expose the parasites to the light. The parasites fluoresce as bright green or yellow dots in the midst of the uninfected RBCs.

### 1.5.3 Immunochromatographic tests (ICTs)

Immunochromatographic assays are devices made in dipstick or lateral flow designs that detect malaria antigens in small quantities of blood (2-50 microliters) (Kakkilaya, 2011). Such devices are fashioned to be amenable for field testing (Figure 1.14).



**Figure 1-14:** Schematic of lateral flow device (adopted from Innovabiosciences, 2017). The sample pad absorbs the applied sample which progresses to the conjugate pad. Conjugated pad carries immobilized antibody labelled with enzyme, gold nanoparticles or fluorescent dye. Primary antibody is immobilized on the test line. An antibody against the conjugate antibody is immobilized on the control line. The wick absorbs excess moisture at the end of the flow.

The surface of reaction is the zone where the antibody and antigen immobilization takes place in an embossed micro well and a detection zone. . The assay makes use of monoclonal antibodies labelled with a dye, fixed on the distal part of a strip for reaction with the parasite antigen. While running the test, blood and buffer is mixed with conjugated antibody and transported along the lines of localized antibody. Parasite antigen is attached which interacts with labelled antibody.

These devices are used in the diagnosis of malaria with highly specific results. The sensitivity of these devices relies on the species and number, viability and

difference in concentration of parasite antigen as well as the condition (storage  $\leq 30^{\circ}\text{C}$ ) (Kakkilaya, 2011). It also requires a skilled person to interpret the test results. Dipsticks are the simplest form. The nitrocellulose membrane provides a suitable medium for particle migration from one end of the strip to the other. As sample is applied, the antibody labelled with the conjugate immobilized on the conjugate pad interacts with the analyte in the sample and forms a complex. As migration continues, the complex reaches the test line where the primary antibody raised against the analyte interact with the sample / antibody / conjugate complex. As a result the analyte is sandwiched between the primary and conjugated antibodies. Intensity of the colour signal on the test line indicates the presence of the analyte while the control line with antibodies immobilized which are raised against conjugate antibody shows a colour signal to indicate that the strip is working normally. Cassettes and cards may also be used which tend to be more expensive.

Immunochromatographic devices have been used with varying measures of success. False negative results may be due to a number of factors including Lot no., product type, and storage temperature and testing conditions (Mubi, 2011). Many ICTs have been developed to detect *Plasmodium falciparum* HRP 2 and parasite lactate dehydrogenase or aldolase from all *Plasmodium sp.* Most of these ICTs have shown low sensitivity for the diagnosis of *P. vivax* and do not differentially detect *P. vivax* and *P. falciparum* or mixed infections. Others detect only *Plasmodium falciparum* through targeting the histidine-rich protein 2 (Bell et al., 2006) or all Plasmodium proteins such as lactate dehydrogenase (Iqbal et al., 2001). Some immunochromatographic malaria tests are listed in Table 1.3.

**Table 1-3: Immunochromatographic tests**

Test	Company	Biomarker	References
OptiMAL -IT	(DiaMed, Cressier, Switzerland)	pLDH	(Gilad, 2008; Kang et al., 2015)
Vistapan	(Mitra, New Delhi, India)	pLDH	(Fogg et al., 2008)
ParaHIT f	(Span Diagnostics)	HRP 2	(Guthmann, 2002)
Malar-Check	Cumberland diagnostics ltd)	HRP 2	(Avila et al., 2002)
Makromed	Dipstick (Makro Medical Pty. Ltd., Johannesburg, Republic of South Africa)	HRP 2	(Richardson et al., 2002; Singer et al., 2004)
ParaSight-F	(Becton Dickinson, USA)	HRP 2	(Shiff, 1993; Forney et al., 2001)
Paracheck Pf	(Orchid Biomedical Systems, Goa, India)	HRP 2	(Fogg et al., 2008; Guthmann, 2002)
BinaxNOW	Alere, UK	HRP 2 / pLDH	(DiMaio et al., 2012; Foster, 2014)
Carestart	(Access Bio, Princeton, NJ, USA)	HRP 2 / pLDH	(Maltha et al., 2011; Fogg et al., 2008)

These tests have been used successfully in conjunction with blood film microscopy to confirm diagnosis of malaria. Less accuracy may be observed, however in samples stored to wait for a competent person, handling a large number of samples or when the samples have to be transported for long distances due to the lack of adequate infrastructure (Maltha et al., 2010). Some malaria affected populations may be found in the interior of regions with difficult terrain.

The sensitivity and specificity of the CareStart Malaria test is comparable to the thick blood smear in diagnosis of malaria (Hailu and Kebede, 2014). It is therefore preferable to use the Pf / Pv Combo Test instead of microscopy in areas where microscopic diagnosis is limited. PfHRP 2 tests may show *P. falciparum* sensitivity > 90% in clinical cases (Forney et al., 2003). Some tests involve the use of serum-suspended parasite metabolites.

#### 1.5.4 Serological tests

Serological malaria tests are blood tests that detect specific malaria antibodies produced by the immune system (Corran et al., 2007). In the past 50 years, serological tests have been used to detect antibodies against malaria parasites (Moody, 2002). The serological test detects the antibody at some time in the preceding months up to a period of a few years assessing the infection status of a person who presents with malaria-related symptoms and whose blood is negative for malaria parasite. It may also be used for a patient who has previously undergone treatment and whose parasite load is uncertain (Corran et al., 2007).

These methods have their specific use as they are limited to the measurement of past exposure to the disease or to recognize disease biomarkers. The methods most commonly mentioned in literature to measure malarial antibody titres are Indirect Fluorescence Antibody Test (IFAT) and the Enzyme Linked Immunosorbent Assay (ELISA) (Forney et al., 2003; Bell et al., 2006; Merwyn, 2011; Thongdee et al., 2014).

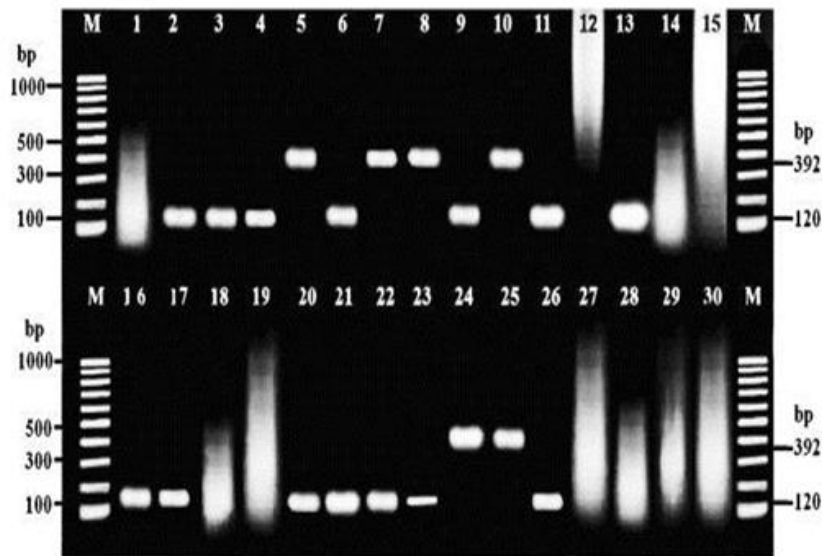
IFAT can be used to obtain information concerning the patient's history of malaria infection. These factors would immediately pose a serious challenge in low resource settings, many of which are the areas in need of malaria intervention (Merwyn, 2011; Thongdee et al., 2014).

ELISA on the other hand has shown higher sensitivity than the IFAT *Plasmodium falciparum* malaria detection (84% and 70.5% respectively). Both methods may be used for malaria detection in areas where the facilities are readily available. In rural sites, ELISA test has proven expensive in that it requires the use of expensive microtiter plates, is time-consuming, requires a steady supply of electricity to read the absorbance on the elaborate plate reader which is not easy to transport and which requires sufficient training to operate and interpret results (Thongdee et al., 2014).

### 1.5.5 Molecular tests

PCR (Polymerase chain reaction) and Loop Mediated Isothermal Amplification (LAMP) have shown great sensitivity and specificity, but require significant infrastructure and training, and are more expensive than the blood smear method (Demirev et al., 2002; Scholl et al., 2004; Maiera, 2011). LAMP focuses on carrying out molecular diagnostic procedure in field situations without the aid of highly specialized instruments (Notomi et al., 2000). The method involves the use of the enzyme DNA polymerase and has been applied successfully as a diagnostic tool for several diseases and is said to be a technique that can identify a sample with low copy number.

The primer-based interfaced enzyme propelled DNA amplification of selected genomic sequences is widely used for research and routine diagnosis of many diseases like hepatitis, cancer, leukemia and malaria. Due to its reliability, PCR is used as a major laboratory technique in studies involving DNA cloning, diseases of heredity, forensic studies, phylogeny, gene functional analysis, DNA sequencing, paternity testing, genetic fingerprinting and disease diagnosis. The PCR process amplifies the subject DNA using a heat stable enzyme known as the Taq polymerase to speed up the reaction to produce millions of copies of the template (McKeague and DeRosa, 2012; Baltzell et al., 2013; Iglesias, et al., 2014). PCR test involving DNA migration during agarose gel electrophoresis (Figure 1.15).



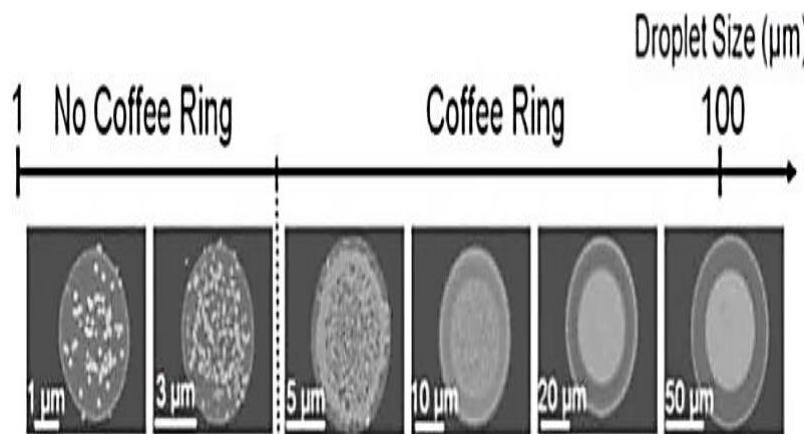
**Figure 1-15:** Diagnosis of malaria suspected blood samples (Ittarat et al., 2013). Diagnosis of malaria suspected blood samples (n=30) by the agarose gel electrophoresis. M is the ladder on the far left and right. Samples in lane 6, 9 and 20 were reported as negative by microscopic examination but showed a malaria positive DNA band at 120 bp (Ittarat et al., 2013).

Nucleic acid technology is not restricted to polymerase chain reaction and loop mediated isothermal amplification. DNA microarray may be used to determine the level of expression of a vast number of genes, the genetic constitution of several portions of the genome, for RNA analysis and for determining nucleic acid make up (Grubaugh et al., 2013). DNA microarray can be referred to as a DNA chip or DNA biochip and is a selection of sections of microscopic DNA adhered to a sturdy platform (Rathod et al., 2002). The method was first used in parasitological studies in which pre-synthesized DNA and DNA fragments comprise high density alignment of nucleic acids with high sensitivity. Though molecular methods are able to detect about 5 parasites per microliter of sample, molecular tests have their limitation in application in resource-sparse field conditions (Wang et al., 2015).



### 1.5.6 Coffee stain malaria detection

Coffee ring procedure for malaria detection is based on the principle of particle migration. A ring of coffee will evaporate so that the dissolved particles migrate to the periphery of the stain (University of California, 2010). This is an antibody-free format which relies on the outward flow of the liquid (Figure 1.16).



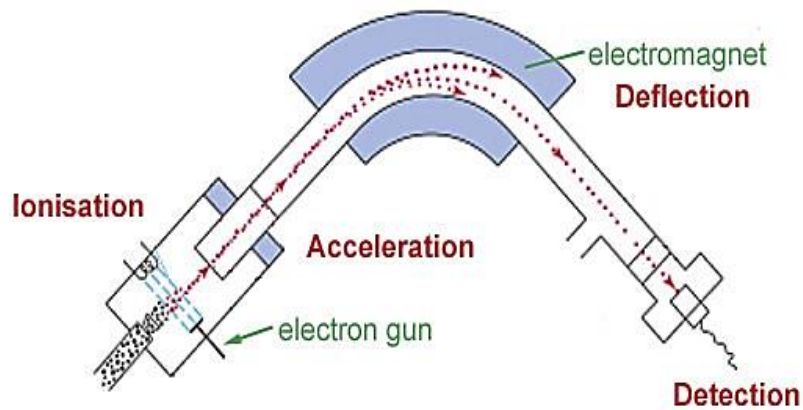
**Figure 1-16:** Coffee ring malaria detection (University of California, 2010).

Magnetic particles (250 nm in diameter) and non-magnetic particles (1 µm diameter) surface-modified with Ni Nitrilotriacetic acid [Ni (II) NTA], were shown to bind a poly-L-histidine target, a mimic of the malaria biomarker, *Pf*HRP 2 causing the formation of a sandwich. Non-reactive control particles (1 µm diameter) in solution were transported outward. Thus, the mimicked biomarker was detected. The assay however shows high background caused by non-target molecule (Gulka, 2015).

### 1.5.7 Laser desorption mass spectroscopy (LDMS)

Over the last few years, 'soft' ionization methods have extended the range of applications of mass spectrometry to biochemical, medical and environmental sciences (Karas and Bahir, 1986). Laser desorption is one of these techniques for identification and characterization of proteins (Mainini et al., 2013). Detection

is of particles of varying size occurs after the particles pass through an electron beam. The accelerated particles are then deflected according to size or ionic potential in fluids (Figure 1.17).



**Figure 1-17:** Schematic - Laser Desorption Mass Spectrometry (scienceaid.co.uk).

The LDMS hemozoin detection of *P. yoelii* infections at the middle and lowest dose of infected erythrocytes by as much as four days earlier than light microscopy (>0.1% parasitaemia threshold) demonstrates that LDMS can be used as a rapid screening tool to detect malaria infections in this mouse model. Laser desorption mass spectroscopy detection of haem in clinical *Plasmodium falciparum* samples is further evidence of the presence of sub-microscopic hemozoin in ring-stage parasites. These correspond to an average of 0.1, 0.3, 0.4-0.5 femtomoles per parasite, which suggests that LDMS, with sub-femtomole sensitivity for haem, can detect hemozoin from a single individual infected erythrocyte (Slomianny, 1990). Even though hemozoin is not visible under light microscopy in ring-stage parasites, electron micrographs depict recognizable haem crystals during this stage (Slomianny, 1990).

In a study conducted in pregnant women whose blood films test negative with microscopy, LDMS showed a sensitivity of 52% and a specificity of 92% compared with PCR. Malaria pigment (hemozoin) detection by LDMS was recently shown to be a sensitive (<10 parasites per  $\mu\text{L}$ ) technique for detecting

*Plasmodium falciparum* parasites cultured in human blood. LDMS technique is however not recommended as a malaria detection tool in mixed malaria infections, as the hemozoin available in the ring-stage parasites is less than in older, more mature-stage parasites (Scholl et al., 2004; Ter Kuile et al., 2004). LMDS is neither effective in parasite differentiation, and so it is to be supported by microscopy or ICTs for species recognition. LDMS is however useful for separating sample components according to mass and ionic potential (Scholl et al., 2004).

### 1.5.8 Flow Cytometry (FCM)

Flow cytometry is a simple, robust, and efficient method for the detection of physical and chemical properties in a fluid with labelled particles. As the fluid passes through one or more laser beams, thousands of particles are identified per second. FCM is based on immunochemistry and has found many uses in chemistry and parasitology for the analysis of blood infection by malaria parasites. Analysis of blood-stage development and determination of susceptibility to drugs by flow cytometry are reproducible and rapid. In the detection of blood-stage parasites, FCM appears to be sensitive and reproducible (Janse and Vianen, 1994).

Binding of human antibodies to the surface of erythrocytes infected with strains of *Plasmodium falciparum* can also be measured (Staalsoe et al., 1999). DNA-specific dyes are especially useful because the parasites multiply inside the red blood cell (RBC) population of the blood cells. As RBCs do not contain DNA, DNA-specific fluorescence from infected RBC can only be due to fluorescence of dyes bound to parasite DNA. Consequently, infected cells can be discriminated from non-infected cells based on their fluorescence intensity. In addition, because parasites multiply within the RBC by several mitotic divisions, the fluorescence intensity of stained parasites increases during development of the parasites. This can be analyzed by flow cytometry and used to determine the developmental stage of the parasite. The total DNA content of a parasite is 100-200 times less than that of nucleated blood cells. Therefore, the nucleated

blood cells can easily be distinguished from parasites on the basis of the difference in fluorescence intensity.

Hemozoin was used as the marker for detection in several studies from Africa and Asia. The amount of pigment found, particularly in neutrophils of malarious children, was a sensitive marker of progression toward the prognosis of severe malaria in children (Metzger et al., 1995; Phu et al., 1995; Amodu et al., 1988). Hemozoin within phagocytotes can be detected by depolarization of laser light, as cells pass through a flow-cytometer channel.

Flow cytometry method may provide a sensitivity of 49-98% of the studied population and a specificity of 82-97%, for malarial diagnosis (Grobusch et al., 2003; Padial et al., 2005) and is potentially useful for diagnosing clinically unsuspected malaria. The disadvantages are its labour intensiveness, the need for trained technicians, costly diagnostic equipment, and that false-positives may occur with other bacterial or viral infections.

### **1.5.9 Surface Enhanced Raman Spectroscopy (SERS)**

Raman spectroscopic methods are known to have a range of applications. Raman spectroscopy (RS) observes vibrational, rotational, and other low-frequency modes in a system, to provide a fingerprint by which molecules can be identified (Gardiner, 1989). Raman spectroscopy (RRS) on the other hand has been applied to monitor the effects of chloroquine (CQ) treatment on cultures of *Plasmodium falciparum* trophozoites (Webster et al., 2008). RRS has been reported to amplify the Raman signal of hemozoin in malaria parasite-infected blood cells by the close Raman shift matching between the laser source and electronic transition of hemozoin (Frosch et al., 2007; Wood et al., 2009; Park et al., 2010; Mauritz et al., 2010).

Raman spectrometry and Surface enhanced Raman spectrometry (SERS) have long been attempted for malaria detection. SERS effect has also been shown on a silver tip to enhance the Raman spectrum of hemozoin in infected cells via the augmented electromagnetic coupling between hematin and gold or silver

nanoparticles (Wood et al., 2011; Yeun and Liu, 2012; Hobro et al., 2013; Garrett et al., 2015). SERS is a highly sensitive optical spectroscopic detection technique based on the Raman signal enhancement from metallic (usually silver or gold) nano-structured substrates.

RS has been used to detect malaria in works focused on plasma detection (Hobro et al., 2013) while for SERS, the strategy is dominated by hemozoin detection (Wood et al., 2011; Yuen and Liu, 2012; Garret et al., 2015). RS techniques (with a sensitivity of 30 parasites / $\mu$ L) can be used in conjunction with confirmatory microscopy for parasite identification.

#### 1.5.10 Resonance imaging

Resonance imaging is one of the many medical techniques available for the visualization of parts of the body through the use of magnetic, radio and ultrasound waves: computer axial tomography, magnetic resonance imaging, near infra-red imaging, and nuclear resonance imaging. Resonance imaging is a welcome addition to the array of malaria detection methods. This development helps prevent misdiagnosis of cerebral malaria (CM), which often leads to treatment delay and mortality. Misdiagnosis of CM has been associated with 15-30% malaria deaths (Marsh and Snow, 1999). In mouse models, experimental cerebral malaria (ECM), optical imaging has been used to study the pathophysiology by infection with transgenic *P. berghei* expressing luciferase (Franke-Favard et al., 2005; Ploemen et al., 2009; Baptista et al., 2010). More recently, optical imaging methodologies have been developed for simple, safe and sensitive diagnosis and monitoring of tumors and other diseases (James and Gambhir, 2012; Mann et al., 2015) as well as intravital microscopy (Frevert et al., 2005; Baere et al., 2007; Cabrales et al., 2010; Pai et al., 2014; Nacer et al., 2014).

Malarial retinopathy consists of a set of retinal abnormalities, unique to severe malaria and common in children with cerebral malaria. Various conventional imaging methodologies, including magnetic resonance imaging have been

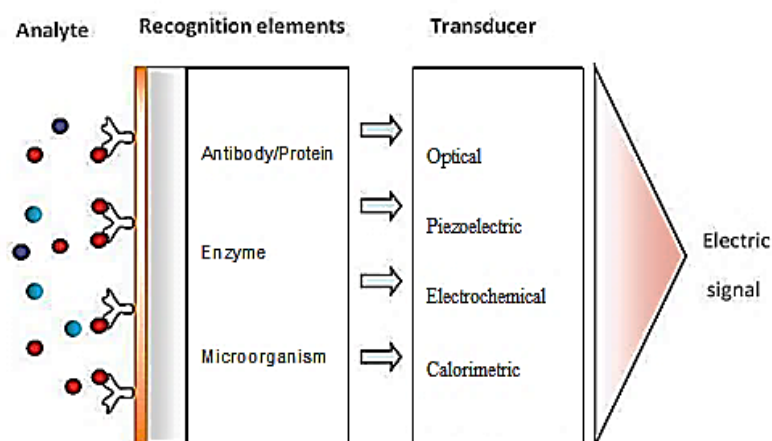
suggested in the observation of the retinal fundus for the diagnosis of cerebral malaria (Sugiyama et al., 2001; Patankar et al., 2002; Beare et al., 2007; Looareesuwan et al., 2009; Potchen et al., 2012; Zhao et al., 2015). Malarial retinopathy may be used for both prognostication, and triaging for optimum utilization of intensive care facilities (Joshi et al., 2016; Portnoy et al., 2016).

Near infrared (NIR) imaging and liposomes containing non-covalently bound indocyanine green (ICG), has been investigated as a tool for diagnosis and monitoring of cerebral therapy, looking at the optical fundus which may appear blanched. NIR is characterized by relatively deep tissue penetration and high signal to noise ratio, due to the low auto fluorescence and absorbance in its wavelength range (Franke-Favard et al., 2005; Frevert et al., 2005; Baer et al., 2007; Ploemen et al., 2009; Baptista et al., 2010; Cabrales et al., 2010; Luo et al., 2011; James and Gambhir, 2012; Nacer et al., 2014; Pai et al., 2014; Mann et al., 2015; Zhao et al., 2015).

ICG, on the other hand, a water soluble tricarbo-cyanine dye is the only US Food and Drug Administration (FDA) and European Medicines Agency-approved NIR molecule (Nguyen and Tsien, 2013). ICG is widely used for determination of cardiac output, hepatic function and liver blood flow, inspection of retinal and choroidal vessels (Dzurinko et al., 2004) and diagnosis of burn depth. These methods were only partially discriminative, and just a few MRI and PET units (expensive and technically complicated) are available in malaria endemic areas. Along with the available malaria detection methods are the more recent biosensor methods, bringing to bear on the focus of this research, to develop immunosensors for the highly sensitive and low cost detection of malaria.

## **1.6 BIOSENSORS**

A biosensor is defined as a bio-analytical device incorporating a molecular recognition entity associated with or integrated with a physicochemical transducer (Tothill, 2009) (Figure 1.18).



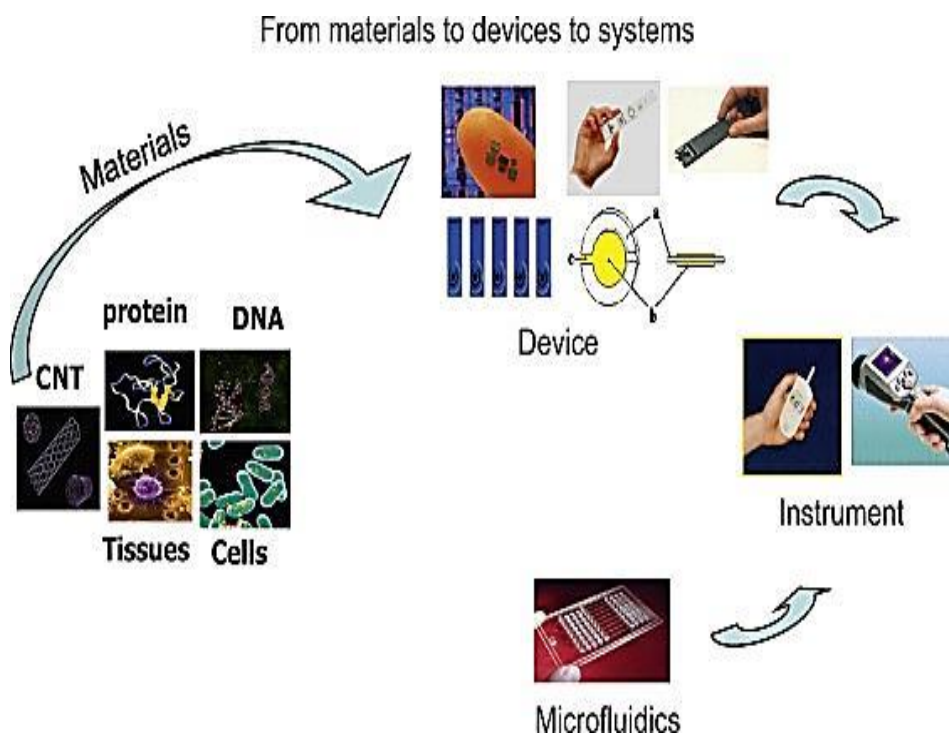
**Figure 1-18:** Schematic of a biosensor (Uludag, 2011).

According to Mistry et al., 2014, the development of the biosensor was first reported in the early 1960s by Clark Leland of Rochester, New York, who is known as the father of biosensors. He worked to develop the glucose sensor. The glucose enzyme electrode based on detection of hydrogen peroxide was tested. Later in 1973, the re-launch of the first commercial biosensor, YSI analyser was conducted in which a glucose sensor was used to measure glucose concentration in solution. Blood sugar levels of diabetes patients could be determined using these sensors.

There is a large market for biosensors of optical and chemical basis, a large proportion of which are screening devices (Eggins, 1996). Today's biosensor market is dominated by glucose biosensors; mass-produced enzyme electrodes for rapid self-diagnosis (Newman and Setford, 2006; Monosik et al., 2012). The devices are designed according to specification; some analytical devices are made up of more than one biosensor. Less frequently used biosensors are magnetic and thermometric biosensors.

Choice of the mediator was based on the fast enzymatic and reversible reaction. The mediator also possesses low  $O_2$  potential for regeneration and does not rely on pH. It would also be stable at either end of the redox event.

The devices made from electrical and chemical components are generally of low cost, easily transported and geared towards utilization in a vast array of medical, pharmaceutical, environmental and food processing industries (Eggins, 1996). They can be adapted for use in low resource settings and may be used by trained non-specialists in de-centralized locations for screening samples for target analyte (Figure 1.19).



**Figure 1-19:** Construction of biosensor assays (Tothill, 2009).

### 1.6.1 Biosensing receptors

Selection of the biosensing receptor is the main step in biosensor construction, followed by the transducer and finally fixing of the biological component to the transducer. The choice of bio-recognition component should be made such as to accommodate the recognition process that occurs between the recognition layer and the molecule under investigation (Aizawa et al., 1976). The affinity and avidity of the specific bonds maintain integrity of the sensor and affect



sensor sensitivity. Immobilization of the antibody on the transducer uses a well-known technique, enzyme immunoassay (EIA) (Aizawa et al., 1976) in a variety of formats. Enzyme immunoassay is discussed in greater detail in Chapter 3.

The immunoassays are regularly accompanied by labels to signal the occurrence of a chemical reaction. There is an extremely weak variation in potential from the antigen-antibody reaction (Yamamoto et al., 1978). The response of the transducer can be improved by provoking a chemical reaction. This involves the labelling to the biomolecule with an enzyme that is robust enough to withstand the redox processes of electrochemical detection; and which catalyzes the production of electrochemical species involved in the reaction. The specificity of the biosensor is then determined by the antibody and its sensitivity determined by the enzyme performing the chemical amplification (Yamamoto et al., 1978).

Finally, chemoreceptors in the form of cellular membranes can be excited by chemical stimuli which induce a conformational change in the chemoreceptors. These changes, and the functional modifications that result, are reversible and provide an interesting model for construction of biosensors (Thompson et al, 1986). Neuro-receptors can also be used in the detection of drugs, toxins and certain other substances (Wingard, 1987). This may involve one of a number of processes, such as bio catalysis, immunological coupling or chemoreception (Canh, 1993).

Enzymes are the most commonly used reagents, but many other biologicals and bio-mimics like antibodies, whole cells (including microbial, plant, and animal cells), subcellular organelles, tissue slices, lectins, and numerous synthetic molecules with affinity or catalytic properties similar to biologicals, extending to those obtained through parallel synthesis and imprinted polymers are used.

Examples of bio catalysis bio receptors are enzymes, microorganisms, tissues and organelles, animal and plant tissue and organelles such as lysosomes and

chloroplasts. In contrast to bio catalysis, immunological coupling does not involve liberation of reaction products or consumption of substrate. The working capacity of a biosensor with an enzyme as its recognition element relies on the method of its addition, hydrogen ion concentration, heat requirement and the process of its being fixed to the prepared substrate (Abdul Kadir and Tothill, 2010). This knowledge has proven useful in the development of immunosensors to evaluate the progress of disease conditions, for bacteria and virus assays or substance recognition (Sharma et al., 2008, Abdul Kadir and Tothill, 2010).

Each detection biomolecule is to be immobilized on the sensor surface for specific detection of analyte; the analyte will likely be in suitable medium with required pH for the specific assay. The biomolecules will be applied to the sensor surface by one of the 5 common immobilization methods: covalent, membrane entrapment, encapsulation (in which a porous encapsulation matrix (e.g. lipid bilayers) is formed around the biological material and helps in binding it to the sensor), adsorption or cross-linking. In most cases, adsorption is used when the loss of material to the modified sensor surface affects sensitivity and detection limit of the sensor. Apart from enzymes and antibodies, more sensitive single-stranded DNA can be used to develop immunosensors (Stadtherr et al., 2005).

Aptamers, artificial ligands based on nucleic acids are the same as monoclonal antibodies by virtue of property (specific interaction for specific binding), while withstanding deformation. To this end, those functional groups that are more suitable in sensing are used (Stadtherr et al., 2005). Various materials like carbon paste, pyrolytic graphite, glassy carbon, carbon fibre and carbon nanotubes have been used to immobilize the DNA of organisms. For standardized DNA base sequence, the complementary sequence can be produced then marked so as to visualize it. The compound hybridizes with respect to the strand under investigation while both strands are uncoiled. The marked strand is introduced then annealing takes place (Vo-Dinh and Cullum, 2000). Nucleic acid-based biosensors have an attraction between

complementary regions of aligned nucleotide sequences (Borgmann et al., 2011).

### **1.6.2 Transducers**

A transducer is the device that converts recognition signal events into electrical (often digital) signals-and can be electrochemical (amperometry, potentiometry, conductimetry / impedimetry), optical (colorimetric, fluorescence, luminescence, interferometry), calorimetric (thermistor), mass change (piezoelectric/acoustic wave) or magnetic in nature (Tothill and Turner, 2003). The information relayed to the transducer is generated from the interaction biomolecular moiety, giving the signal that the reaction has taken place. The choice of transducer is informed according to the reaction type, and the substances liberated or consumed during the reaction. The choice of transducer also depends on the intended application of the biosensor (Canh, 1993). Common transducer types include optical, piezoelectric and electrochemical platforms.

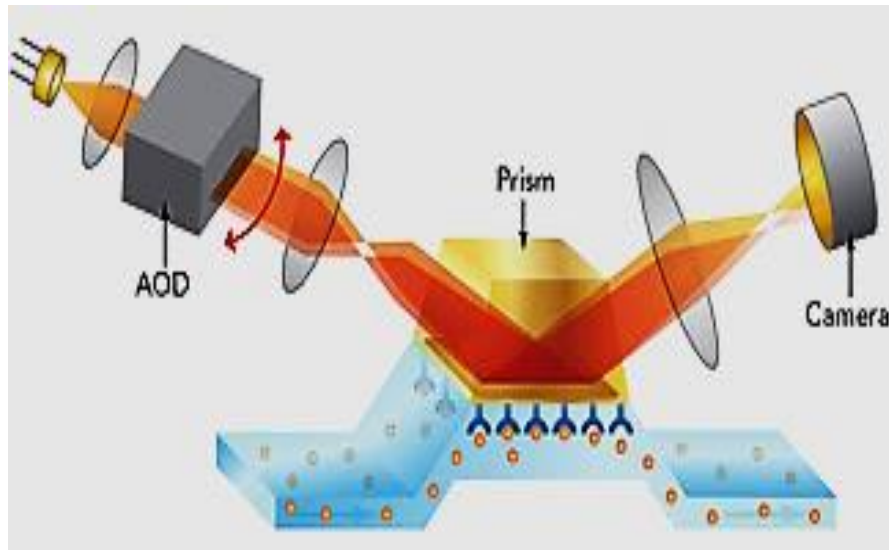
### **1.6.3 Optical biosensors**

Optical biosensors use the light in different configurations of the principal format to detect an analyte when surface polaritons are excited. Several optical sensors exist including resonant mirror, resonant waveguide grating and dual polarization interferometry sensors. Of the optical biosensors, surface plasmon resonance (SPR) is the most common. SPR is an optical based, label-free detection method utilizing a form of total internal reflection. Normally, when total internal reflection occurs, light traveling through an optically dense medium at an angle of incidence greater than the critical angle, is totally reflected when it reaches an interface with an optically less dense medium. Although the light is totally reflected, a component of the light, the evanescent wave, will penetrate the less dense medium by a distance approximately one wavelength of the incident light. If the light is monochromatic and p-polarized, and the interface between the two different media is coated with a thin metal film, the evanescent wave will, under certain conditions interact with the free oscillating electrons of the metal film.

When surface plasmon resonance occurs, light energy is lost to the metal film and the reflected light intensity is decreased. When all else is kept constant, the angle of the resonance phenomenon is dependent on the refractive index of the media close to the metal surface. Changes in this refractive index can then be characterized by monitoring the resonance angle over time.

In practice an SPR sensor is usually a gold coated glass slide. In biosensor applications, the binding of molecules to the sensor surface, or to molecules attached to the surface, changes the local refractive index and these changes are monitored over time. By measuring these changes in refractive index, information such as binding specificity, concentration of target molecules, kinetic rates, and affinity constants for molecular interactions can be determined.

Surface plasmon resonance was described by Otto (Otto, 1968) and made commercial by Biacore in the nineties (Daghestani and Day, 2010; Situ et al., 2010). The commercially available optical biosensors include surface plasmon resonance, resonant mirror, resonant waveguide grating, and dual polarization interferometric biosensors (Daghestani and Day, 2010). SPR was soon recognized for its versatility in a vast array of applications in research for analyte detection (Tothill, 2001; Pattnaik, 2005; Aubailly et al., 2011; Tothill, 2011; Suenaga, 2012). Optical biosensors offer real-time monitoring of interacting molecules and reduced interference of the label with analyte on simple user interface and significant limits of biomarker detection (Gulka et al., 2014). The prism configuration of an optical biosensor is shown (Figure 1.20).



**Figure 1-20:** Label – free SPR detection (Sierra sensors, 2014).

SPR chips work using a sensor chip which is gold-coated and connected to the optical system of the SPR machine and the reverse side related to the microfluidic system. The angle of incidence is altered to conform to the evanescent wave propagation rate of the surface plasmon polaritons.

The Surface Plasmon Wave (SPW) or Surface Plasmon Polariton (SPP) is an electromagnetic wave directed along the region between a dielectric and a metal. The propagation constant of a SPW,  $\beta$  can be expressed as:

$$\beta = \frac{\omega}{c} \sqrt{\epsilon_M \epsilon_D / \epsilon_M + \epsilon_D} \quad (1-1)$$

Where  $\omega$  is the angular frequency,  $c$  is the speed of light in a vacuum,  $\epsilon$  is the speed of light in a vacuum,  $\epsilon_D$  and  $\epsilon_M$  are dielectric functions of the dielectric metal.

SPR is used for malaria detection of merozoite surface protein-1 (Helg et al., 2003). It was further reported that competitive assays, like inhibition ELISA and SPR, which require only small amounts of reactant, are suitable alternative methods for the determination of relative binding avidities.

. In SPR the interaction of a biomolecule immobilized on the SPR chip surface with its counterpart in solution is monitored without any labelling of the biomolecules by using the interfacial refractive index changes associated with the affinity binding interactions (Myszka, 1999). A sigmoid binding curve can be viewed as a hybrid curve reflecting a transition from a low affinity state to a high affinity state (Nelson and Cox, 2005).

Measurements are taken as the refractive index changes when the analyte flows over the sensor surface. (Sikarwar et al., 2014). Variants to be determined include protein binding, association / dissociation kinetics and affinity constants (Sikarwar et al., 2014).

*Plasmodium falciparum* monoclonal antibody (MoabPf) and *Plasmodium falciparum* polyclonal antibody (PoabPf) of rHRP-II Ag were characterized in a label free and real time manner using a SPR gold chip.

The MoabPf may also find application in the effective and timely screening of malaria affected patients in pathology laboratories equipped with SPR system (Sikarwar et al., 2014). SPR technology in malaria detection requires skilled handling for effective use. Though some work has been carried out on malaria SPR immunosensors, the assay is not immediately adaptable to field conditions with low resource. There still exists the need for quick and user friendly instruments that can be transported easily and which are adaptable to field conditions (Lee et al., 2012; Jain et al., 2014). Other optical instruments for detection of biomolecules rely on changes in absorbance of a fluorescent molecule.

#### **1.6.4 Mass sensitive biosensors**

Piezoelectric devices have also been developed to measure changes on a sensor surface when an antibody interacts with a target in the sample (Luxton

and Kiely, 2009). The first conclusive demonstration of the piezoelectric effect was done by the Curies in the nineteenth century, showing a potential difference generated across two surfaces of a quartz crystal when pressure was applied (Tombelli, 2012). If the correct frequency is chosen for the electric field, the quartz crystal will oscillate at its resonant frequency. Resonant frequency depends on several factors including the angle at which the quartz crystal is cut. Piezoelectric quartz crystals have been used as microbalances since the pioneering work of G. Sauerbrey (Pang et al., 2006). The term Quartz Crystal Microbalance (QCM) was coined in the twentieth century. The Sauerbrey equation is used in the calculation of change in mass and is given by the equation:

$$\Delta f = \frac{-2f_0^2}{A\sqrt{\rho q \mu q}} \Delta m \quad (1-2)$$

Where  $\Delta f$  is the change in frequency,  $f_0$  is the frequency of oscillation and  $\Delta m$  is the alteration in mass. Shear modulus is given by  $\mu q$  and  $\rho q$  is the density of the quartz crystal. This relationship works in air but not in liquid. QCM has been used in the differential diagnosis of malaria (Ittarat et al., 2013) with the identification of two classes of bio-recognition processes: bio-affinity recognition and bio-metabolic recognition. A frequency shift at  $10 \text{ ng mL}^{-1}$  was detected of the  $10 \text{ }\mu\text{L}$  volume of sample. QCM detection of *P. vivax* and *P. falciparum* in blood is consistent with microscopy and immunochromatographic tests for 27 out of 30 samples (Ittarat et al., 2013). Differential diagnosis of *P. falciparum* from *P. vivax* is achieved with high accuracy and sensitivity, and is cost-effective. No cross-reaction with human DNA was reported (Ittarat et al., 2013).

As regards measurements in the presence of liquids, the directed relationship between mass and frequency shifts-microbalance interpretation as described by the Sauerbrey equation (Sauerbrey, 1959), is not always valid and the observed response is often significantly higher than theoretically expected.

The piezoelectric immunosensor is capable of detecting antigens in the picogram range with the potential to detect antigens in the fluids (Ittarat et al., 2013). The sensor surface may be bare or modified by a self-assembled layer; the enzyme or antigen thus immobilized on the self-assembled monolayer. The use of magnetic materials underneath the gold coating enhances detection. The sensor chip ensemble must be cleaned using an acid (to achieve successful layering for improved sensitivity) (Ittarat et al., 2013).

The QCM surface was constructed using a specific avidin–biotin interaction to immobilize the malaria oligonucleotide probe on quartz-silver electrode. Hybridization was assessed from shifts of the quartz oscillation frequencies due to surface mass changes. The malaria QCM potency in differential diagnosis of *P. falciparum* and *P. vivax* was evaluated and firstly reported (Ittarat et al., 2013).

The target fragments of either *P. falciparum* or *P. vivax* were amplified using three designed primers under optimized PCR condition. Then the amplified product was hybridized with the immobilized biotinylated probe and the quartz frequency shifts were measured. It was found that the new malaria QCM was sensitive, specific and stable after keeping at room temperature up to 2 months (Ittarat et al., 2013).

Clinical application was also evaluated and found that the malaria QCM could differentially identify *P. falciparum* and *P. vivax*. Using silver fabricated QCM is 10 times cheaper than the conventional gold fabricated QCM however; the silver fabricated QCM could not be reused nor re-probed (Chomean et al., 2010). It is possible to develop the malaria QCM whose sensor has two functioning sites, as a promising point-of-care testing method in malaria diagnosis (Ittarat et al., 2013). Some QCM biosensors are portable. .

### **1.6.5 Electrochemical biosensors**

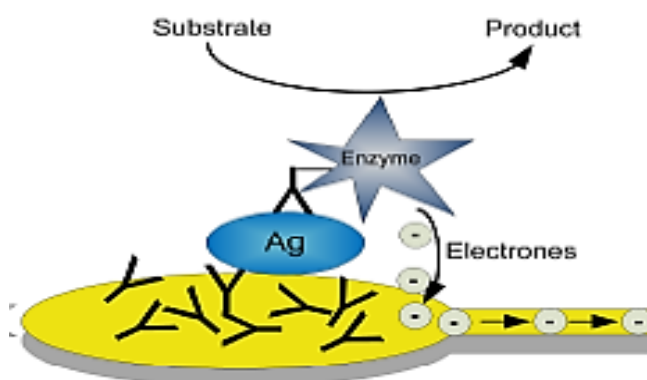
Electrochemical biosensors are used in point-of-care devices since they are portable, simple, easy to use, cost effective and in most cases disposable (Tothill, 2009). The electrochemical instruments used with the biosensors have



been miniaturized to small pocket size devices which make them applicable for home use or the doctor's surgery.

Electrochemical detection has been used to develop malaria biosensors, based on biological catalysis that produces or uses up electrons (Ronkainen et al., 2010; Sharma, 2010). The analyte under investigation takes part in the reaction that occurs on the surface of the working electrode. Such changes can be attributed to ionic strength, pH and redox reactions. The rate of flow of electrons is proportional to the concentration of the analyte at a fixed potential (Ronkainen et al., 2010).

Electrochemical techniques are suitable for coloured or turbid sample analysis which may produce false results in optical assays (Sharma et al., 2008). This technique is complementary to optical detection methods such as fluorescence, the most sensitive of the optical techniques. Since many analytes of interest are not strongly fluorescent and tagging a molecule with a fluorescent label is often labour-intensive, electrochemical transduction can be very useful. By combining the sensitivity of electrochemical measurements with the selectivity provided by bio-receptors, detection limits comparable to fluorescence biosensors are often achievable (Sharma et al., 2008). Electrochemical detection of protein markers is more widely used for cancer analysis (Tothill, 2009). Electrochemical biosensors can be grouped as amperometric, impedimetric or potentiometric with biomolecules attached to the sensor (Figure 1.21).



**Figure 1-21:** Schematic of an electrochemical immunosensor (Binder, 2014).

The capture antibody against the antigen is immobilized on the surface of the working electrode. The antigen to be detected interacts with the capture antibody while the detection antibody conjugated to the electroactive enzyme in turn interacts with the antigen. This is a common format in electrochemical assay.

During the development of biosensors it was determined that there are three known generations of biosensor, based on their construction (Eggins, 1996). The first generation of biosensors are the oxygen electrode-based sensors which use molecular oxygen as the oxidizing agent. The second generation biosensors are mediator-based sensors, used to replace oxygen with other oxidizing agents to remove electrons in a reversible reaction. Third generation biosensors are directly coupled enzyme-electrodes (Eggins, 1996). The agents used for this purpose were called mediators. One such mediator hexacyanoferrate (III),  $[\text{Fe}(\text{CN})_6]^{3-}$  was known formerly as ferricyanide.

#### **1.6.5.1 Amperometric biosensors**

Amperometric biosensors are often made by screen-printing the electrode pattern on a plastic substrate coated with a conduction polymer then attaching a biomolecule (Ronkainen et al., 2010).

In the early 80s, a group of scientists based at Cranfield and Oxford Universities (UK), realized that employing Redox couples, known as mediators, can eliminate many problems associated with electron transfer of the enzymes. This turned out to be in retrospect, a fore-runner of a glucose sensor (Cass et al., 1984). Mediators work as an electron shuttle between the redox centre of the enzyme and the electrode.

A typical screen-printed electrode consists of a chemically stable substrate on which is a printed working electrode (WE), reference electrode, (RE) and counter electrode (CE). The working electrode is the main electrode which

provides a platform for the analyte. The WE surface is incubated with the reagent by drop-wise addition of a pre-determined volume dissolved in a suitable buffer. Incubation time may vary depending on the assay.

The bio-material is then treated according to the assay format then the electrodes are scanned on application of a potential, via the leads. The loss and gain of electrons that occurs when the antigen and antibody interact is converted into a measureable signal at the solid liquid interphase.

Amperometric transducers rely on the nature and behaviour of the components such as conductivity and ionic affinity for the molecules in solution, and measure changes in current, while potentiometric biosensor measure voltage change and conductimetric biosensor quantify resistance.

Screen-printing is a very economically efficient method for the mass production and fabrication of microelectrode arrays. Though highly sensitive, the SPE surface on continued use will become fouled by products from redox processes and become less sensitive. Surface regeneration of an electrode coated with an antibody interferes with the complex and may damage the electrode surface. In addition, electrode surface regeneration may not also be practicable in time constrained formats.

Another challenge in the use of SPEs is their lack of reproducibility even though they bear the same Lot no. Recently, however, SPEs have been reported with appreciable reproducibility (Metters et al., 2012).

Surface modification, inter-electrode distance, ink composition, curing temperature, pre-treatment procedures and surface roughness must be taken into consideration (Pernia et al., 2009). All these factors dramatically enhance the voltammetric performance of these electrodes.

With particular reference to electrochemical transducers there is a range of electrodes available for a selection of reactions: some electrodes are pH sensitive, some are sensitive to anionic or cationic interaction while others are sensitive to the detection of gases.

Modifications can also be made by metal or metal oxide nanoparticles (gold nanoparticles). Carbon nanotubes may also be used as well as graphene diazonium chemistry modifications. Self-Assembled Monolayers (SAMs) form an integral part of investigating bio-molecular attachment on the surface of biosensors. Working electrode modification methods include polymerization using Polyaniline (PANI), in which the biomolecule becomes attached to the electrode surface via the polymer chains, producing an electrical charge thereby enhancing the surface structure and conductivity of the electrode.

The high performance SAM on a gold surface is reliant upon chip cleanliness, among other factors. The sulfhydryl group of the alkane is held onto the gold surface by a gold–sulphur bond. The oxidation achieved by the S-H bond and reduction by hydrogen removal transposes the alkyl chains of the thiol groups. A systematically arranged single layer forms via the Van der Waal's interaction between the chains. Orientation of samples on the surface of the sensor is as a result of the angle formed by the thiol groups.

Sol-gel based biosensors are relatively porous and chemically inert. They are simple to prepare, sensitive and biologically stable. Sharma et al., 2010 detected *Plasmodium falciparum* histidine rich protein 2 antibody using alumina sol-gel modified SPEs. The bare and modified electrodes were coated with 5  $\mu$ L of PfHRP2 protein dissolved in 0.1 M tris buffer. The developed immunosensor took less time to conduct the test than the conventional dot ELISA Sharma et al., (2010).

The most commonly utilized screen-printed electrodes (SPEs) are constructed of graphite and carbon black particles (Mettters et al., 2011). The amperometric immunosensors enable the detection of analytes at levels previously not achievable by high powered liquid chromatography. The detection of Plasmodium species by antigenic methods are as species specific as blood film microscopy (Azikiwe et al., 2012). Examples of biosensors for malaria detection are listed in Table 1.4.

**Table 1-4:** Biosensors for malaria detection.

Analyte	Assay principle	Range	Detection limit	References
<i>Pf</i> HRP 2	Photometric detection by laser light-scattering immunoassay	-	84 % sensitive compared to microscopy	(Mya et al., 2003)
<i>Pf</i> MSP	SPR	-	$3 \times 10^5/M$ ( $c=1$ ) lower; $3 \times 10^8/M$ ( $c=1000$ )	(Helg et al., 2003)
<i>Pf</i> HRP 2	SPR	-	5.6 pg mL <sup>-1</sup>	(Sikawar et al., 2014)
<i>P. falciparum</i> DNA	QCM	-	16 µg mL <sup>-1</sup>	(Ittarat et al., 2013)
ELECTROCHEMICAL				
<i>Pf</i> HRP 2	Carbon SPE modified with MWCN and Au/MWCN	-	8 ng mL <sup>-1</sup>	Sharma, et al., 2008
<i>Pf</i> HRP 2	Carbon SPE modified with AuNPs/Al <sub>2</sub> O <sub>3</sub> sol-gel	-	-	Sharma et al., 2010
<i>Pf</i> HRP 2	Graphite-epoxy composite magneto electrodes	-	0.36 ng mL <sup>-1</sup>	(de Sousa et al., 2011)
<i>Pf</i> HRP 2	Polydimethylsiloxane microfluidic chips	-	16 ng mL <sup>-1</sup>	(Lillehoj et al., 2013)
<i>Pf</i> HRP 2	Carbon nanofiber forest grown on glass microballons	0.01-10 ng mL <sup>-1</sup>	0.025 ng mL <sup>-1</sup>	Gikunoo et al., 2014)
<i>Pf</i> HRP 2	Mercaptopropylphosphonic acid functionalized copper doped zinc oxide nanofibers	10 ag mL <sup>-1</sup> -10µg mL <sup>-1</sup>	6.8 ag mL <sup>-1</sup>	(Brince et al., 2016)
<i>Pf</i> HRP 2	Low electrocatalytic indium tin oxide (ITO) on glass electrodes; APTES-glutaraldehyde modified	1pg mL <sup>-1</sup> -100 ng mL <sup>-1</sup>	2.2 pg mL <sup>-1</sup>	(Dutta et al., 2017)
Recombinat <i>Pv</i> LDH and <i>Pf</i> LDH Aptasensor	Colourimetric spectroscopy	-	1.25 and 2.94 pM respectively	(Lee et al., 2012)
Circumsporozoite protein (CSP)	Carbon SPE modified with EDC NHS, and layered with CNTs.	10-15 M	~6- 50 ng / mL	(Cardoso et al., 2017)

Of all the malaria detection methods, biosensors are the ones yet to be made commercial. Malaria detection methods and sensitivity are listed in Table 1.5.

**Table 1-5:** Some malaria detection methods.

Method	Detection limit (parasites / $\mu\text{L}$ )	Limitations	References
Peripheral blood smear (PBS)	5-10	Need skilled personnel and sound equipment	(Kakkilaya, 2011)
Quantitative buffy coat (QBC)	$\leq 15$	Requires adequate training	(Adeoye and Nga, 2007)
Immunochromatographic tests (ICTs)	50-100	False positives may occur with poor storage	(Hawkes, 2014)
Molecular tests	$\geq 1$	Expensive reagents	(Baltzell, 2013)
Serological tests	30-60	Detection of persistent biomarkers	(Cook et al., 2010; Mfonkeu et al., 2010; Merwyn, 2011)
Flow cytometry (FCM)	1	Labour intensive, costly	(Staalsoe et al., 1991)
Spectrophotometry	$\leq 1$	Heamozoin detection	(Slomianny, 1990; Yeun and Liu, 2012)
Biosensors	0.36 – 12 ( $\text{ng mL}^{-1}$ )	Most are expensive, not field applicable	(Sharma, 2008; Sikawar et al., 2014)

A similar three- electrode system has been used for malaria detection in this study, being the first use of DuPont SPGE in malaria detection to the best of my knowledge.

From the reviewed articles there is still the need to construct a combo of malaria sensitive test which is portable, cheap, time-saving and adaptable for field use on smart devices via suitable software to promote real time disease monitoring, presentation, evaluation and impact assessment.

### 1.7 Aims and objectives

Malaria antibodies are widely used in point-of-care diagnosis of malaria. However due to the limited sensitivity of some of the malaria detection methods, the need still remains for early detection of the disease in expectant mothers and children under the age of five. Advances in biosensor technology have provided simple, rapid and accurate testing systems to support existing technology in health care provision.

The aim of this study was to develop a test for malaria pathogen using a bio-sensing platform able to test for two malaria biomarkers, *P. falciparum* histidine rich protein 2 and parasite Lactate dehydrogenase. The two biomarkers were selected as the *PfHRP 2* is detected in species that causes the most lethal malaria cases while LDH is Pan-malaria and can be found in active infection cases. Furthermore, sensor surface chemistries were investigated. In the study, JD sensors provided by DuPont (Bristol, UK) were used along with an Autolab potentiostat (Metrohm, UK) for in vitro malaria detection in comparison with two commercial malaria test kits.

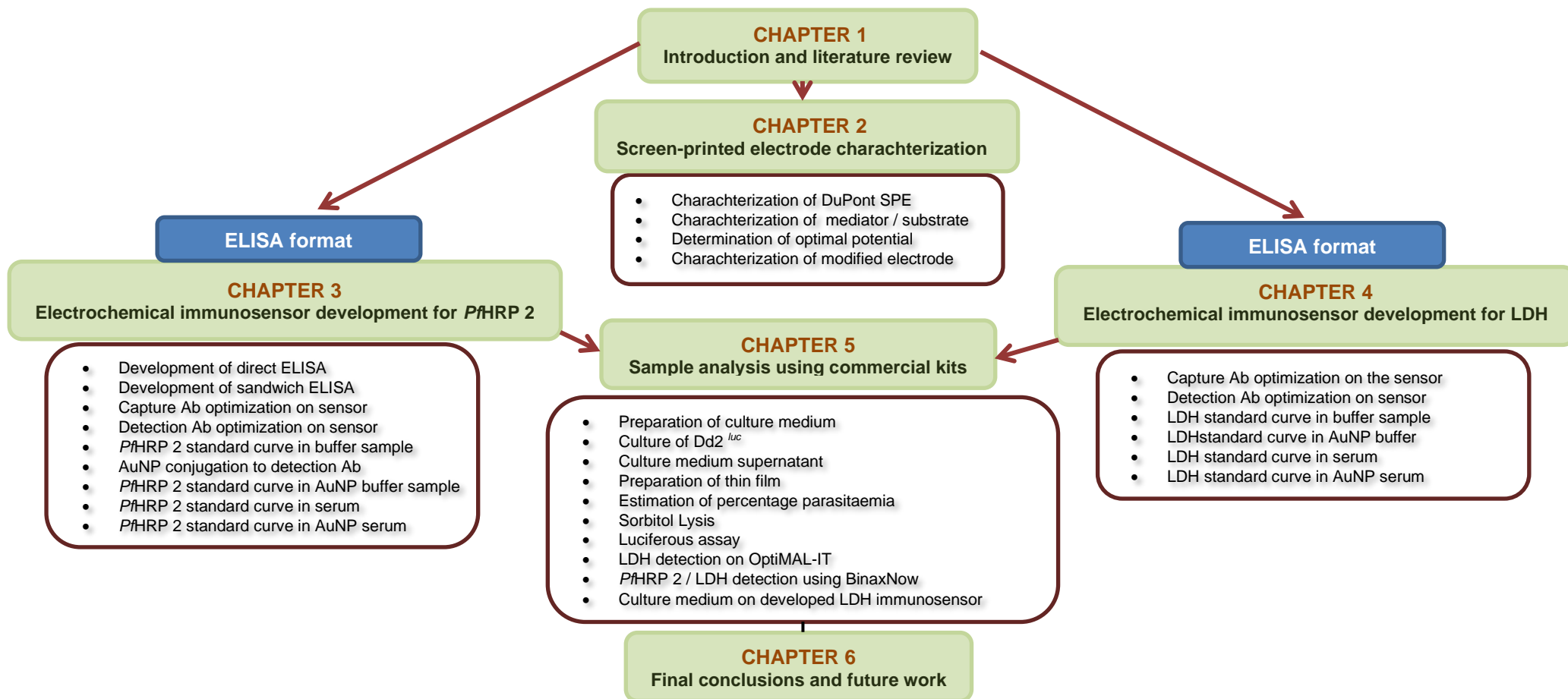
**Project objectives:**

1. Screen-printed electrode studies.
  - a. Characterization of JD 1 JD 2a and JD 2b in potassium ferricyanide.
  - b. Characterization of mediator / substrate.
  - c. Determination of optimal potential.
  - d. SEM and AFM of JD 2b bare sensor surface.
  - e. Characterization of SAM-modified electrode surface with ferricyanide.
  
2. Electrochemical immunosensor development for *PfHRP 2* detection.
  - a. Develop direct ELISA assay.
  - b. Develop sandwich ELISA assay.
  - c. Capture antibody optimization on JD 2b.
  - d. Detection antibody optimization on JD 2b.
  - e. SEM of assayed JD 2b.
  - f. DLS and TEM to determine AuNP particle size.
  - g. AuNP conjugation to detection antibody.
  - h. *PfHRP 2* standard curve in buffer sample.
  - i. *PfHRP 2* standard curve in AuNP buffer sample
  - j. *PfHRP 2* standard curve in serum sample.
  - k. *PfHRP 2* standard curve in AuNP serum sample.

3. Electrochemical immunosensor development for LDH detection.
  - a. Capture antibody optimization on JD 2b.
  - b. Detection antibody optimization on JD 2b.
  - c. LDH standard curve in buffer sample.
  - d. LDH standard curve in AuNP buffer sample.
  - e. LDH standard curve in serum sample.
  - f. LDH standard curve in AuNP serum sample.
  
4. Sample analysis using commercial malaria kits.
  - a. Preparation of culture medium.
  - b. Culture of *Plasmodium falciparum* Dd2<sup>luc</sup> clone.
  - c. Culture medium supernatant.
  - d. Preparation of malaria thin film.
  - e. Estimation of percentage parasitaemia.
  - f. Sorbitol Lysis for staging parasites.
  - g. Luciferase assay for viability curve.
  - h. LDH detection using OptiMAL-IT Malaria kit.
  - i. PfHRP 2 and LDH detection using BinaxNOW Malaria kit.
  - j. Immunosensor assay using culture medium supernatant compare to OptiMAL-IT.

The following flow chart shows the connection between the contributing parts of the research (Figure 1.22).





**Figure 1-22:** The flow chart shows relationship between the chapters during progress of this research to develop immunosensors for malaria detection.



## **CHAPTER TWO**

# **CHARACTERIZATION OF THE SCREEN-PRINTED ELECTRODES**



## 2 SCREEN-PRINTED ELECTRODE STUDIES

### 2.1 INTRODUCTION

Characterization of SPEs aids reproducibility of assay results and is the general method for assessing the working electrode active surface area and structure (Arya et al., 2007). Screen-printed electrode material may be of carbon, modified graphite or gold. Each of these materials has inherent characteristics, applicability and limitations. Electrode material is, therefore, responsible for its performance when a potential is applied and so the SPE is assessed (Arya et al., 2007). For the purpose of this work, potassium ferricyanide [ $K_3Fe(CN)_6$ ] was chosen as mediator to characterize the sensors. The redox reaction produces a cyclic voltammogram from software of Autolab potentiostat from which active surface area is calculated as a percentage. CV shape and size indicate scan rate and electromotive force sufficient to produce species consumption, and on the reverse sweep, re-oxidation of the mediator as the voltage passes the plateau (Davies and Higson, 2013). The shape is also an indication of shift of cathodic and anodic peak, descriptive of reversibility.

Optical surface characterization on the other hand reveals topography and elemental composition imaged by high power microscopy. Composition of electrode can affect performance at solid–liquid interphase during electrochemical reaction. According to the method of Binder, 2014, determination of working electrode suitable potential is achieved at uniform current measured against varied voltage in work conducted on DuPont JD 1 SPGEs. For the purpose of this research JD 2a and JD 2b of similar construct and varied batch and carbon inks are compared to JD 1 SPGE. This chapter describes DuPont JD SPGEs suitability for use in development of a malaria immunosensor.

## 2.2 MATERIALS

### 2.2.1 General chemicals and instrumentation

Potassium chloride and 3, 3', 5, 5' tetramethyl benzidine hydrochloride (TMB), hydrogen peroxide 30 % (w/w), potassium ferricyanide [ $K_3Fe(CN)_6$ ], phosphate citrate buffer tablets and plastic petri dishes were purchased from Sigma Aldrich (Dorset, UK). The vortex mixer model Genie 2 G-560E was purchased from Scientific Industries (Bohemia, USA) and electric pan balance (Mettler Toledo, UK).

Characterization of the surface of the electrodes was done using the Environmental Scanning Electron Microscope (Phillips, UK) and the Atomic Force Microscope (Digital Instruments, California). Curing of electrodes at 120°C was carried out in Carbolite oven, model PN 120 (200) (Hope, UK) while incubation at 37°C was carried out in a column oven (Shimadzu Corporation, Japan).

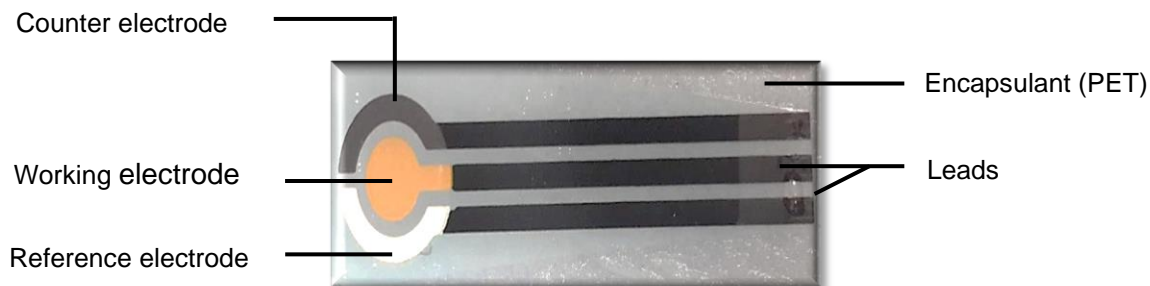
Electrochemical procedures were conducted using a computer controlled four channel Autolab electrochemical analyser multipotentiostat (Metrohm, Netherlands). The procedure allows the simultaneous detection of four sensors. Data capture was through the supplied GPES version 4.9 007 software installed onto a PC. Sensor edge connectors were from PalmSens (Provided by Alvatek, Gloucestershire, UK). Chronoamperometry on multi-mode GPES was selected from the menu and parameters set for the appropriate measurement.

Faraday cage was employed to reduce interference and Microsoft Excel was used to plot the curves. Photos were taken using Samsung Galaxy Note 3 SN-900.

### 2.2.2 Screen-printed electrodes

Three batches of JD SPGEs (designed by Cranfield University and produced by DuPont (Bristol, UK) were used in the study. The SPGEs comprise a gold working electrode (0.226 cm<sup>2</sup> planar area) as the anode, carbon counter to

balance three electrode system and Ag/AgCl reference electrode against which the current generated on the working electrode is compared. Electrodes were printed onto 125  $\mu\text{m}$  thick polyethylene terephthalate (PET) sheets (Figure 2.1).



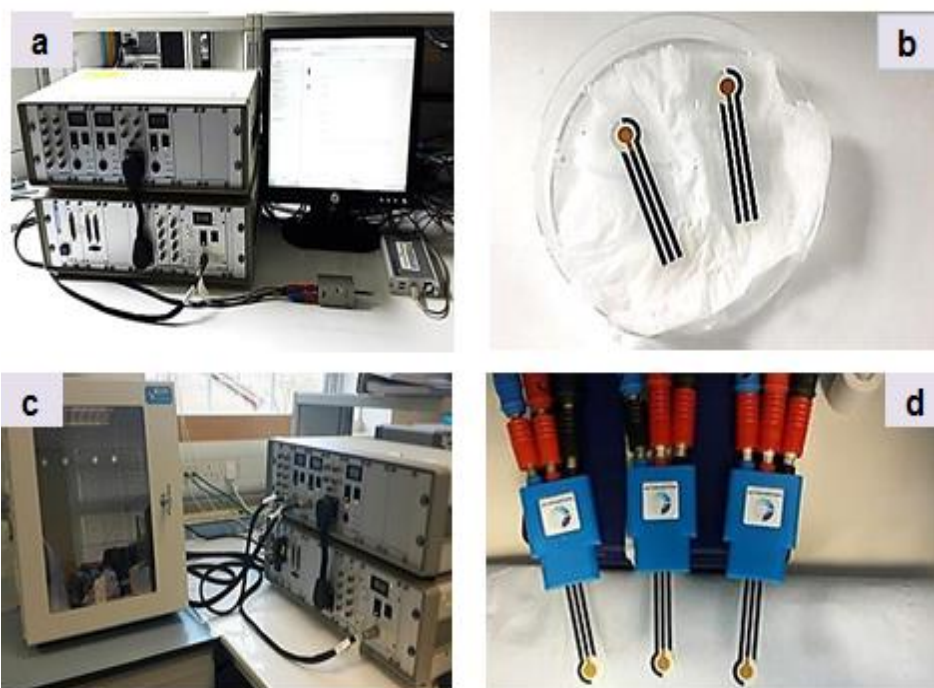
**Figure 2-1:** DuPont JD 2b SPGE is of similar construct to other batches. The JD 1 base carbon print (BQ 221) had been IR dried, the subsequent inks had been box-oven dried at 140°C for 30 minutes

The materials used in constructing the SPGEs are listed in Table 2.1.

**Table 2-1:** Batches of electrochemical screen-printed electrodes.

Batch	Carbon material	Gold	Ag/AgCl	Encapsulation	Year produced
JD 1	BQ 221	BQ 331	5880	5036	2010
JD 2a	BQ 226	BQ 331	5880	5036	2013
JD 2b	BQ 226	BQ 331	5880	5036	2015-2016

All batches of electrode were characterized connected to edge connector (Dropsens, Spain) (Figure 2.2).



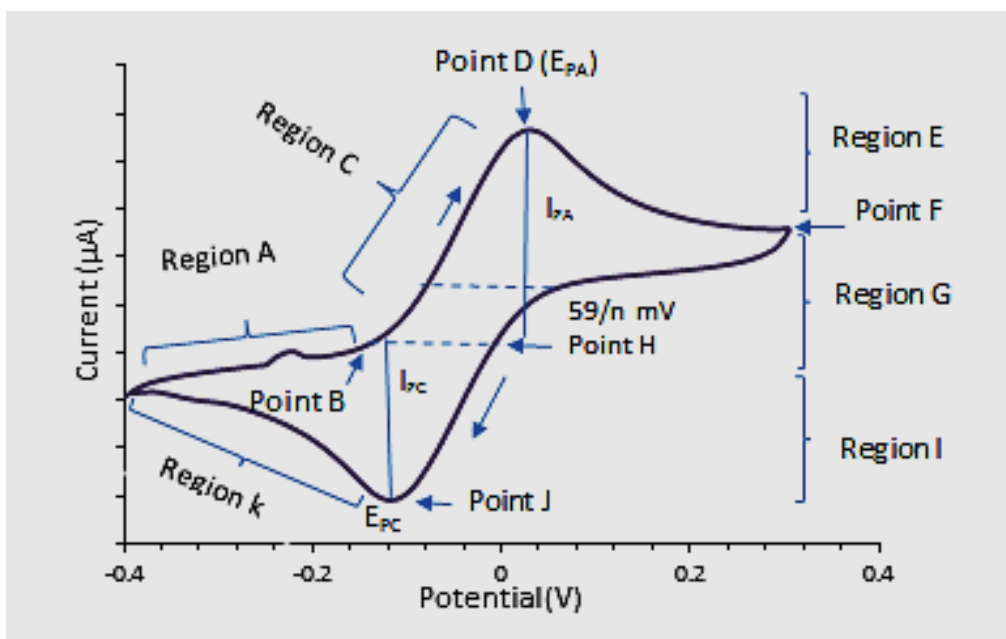
**Figure 2-2:** Electrochemical set-up with single channel Dropsens (Spain) edge connectors (a) SPE preparation (b) Faraday cage (c) to reduce interference and multichannel measurements using banana connectors (Palmsens, Netherlands) (d).

## 2.3 METHODS

### 2.3.1 Characterization measurements and data analysis

Cyclic voltammetry (CV) and chronoamperometry by GPES 4.9 007 were used to assess performance of JD 1, JD 2a and JD 2b SPGEs using potassium ferricyanide [ $K_4Fe(CN)_6$ ] (Figure 2.3).





**Figure 2-3:** Cyclic voltammogram redox curve during oxidation and reduction of electroactive species (adopted from Higson, 2003).

The potential is first swept from approximately -0.4 to +0.3 V versus Ag/AgCl. No current is observed between approximately -0.4 and -0.2 V in the absence of any electrochemical reaction occurring within this region (region A). At around -0.2 V, a cathodic current commences due to the oxidation of [Fe (CN)<sub>6</sub>]<sup>3-</sup> to [Fe (CN)<sub>6</sub>]<sup>4-</sup> (point B). The current increases as and the potential is increased due to the increased electron transfer rate (region C). [Fe (CN)<sub>6</sub>]<sup>3-</sup> is being consumed and its surface concentration decreases, causing a diffusion gradient between the surface of the electrode and bulk solution. When the surface concentration of [Fe(CN)<sub>6</sub>]<sup>3-</sup> approaches zero, the cathodic current peaks E<sub>PA</sub> (point D) and then falls as the diffusion gradient extends further into the solution (region E ).

The rate of mass transport to the working electrode now becomes rate limiting and the current now approaches a new equilibrium plateau until the direction of the potential sweep is reversed (point F). A reduction current is observed (region G), until the potential at which the peak cathodic current was observed is once more passed (point H). At this point the current momentarily passed

through zero.  $[\text{Fe}(\text{CN})_6^{4-}]$  begins to reduce (region I), and an ( anodic) current is seen, which again rises until in a similar manner the surface concentration of  $[\text{Fe}(\text{CN})_6^{4-}]$  approaches zero; a peak current  $E_{\text{PC}}$  is again observed (point J). The current once again decreases as the original potential is once more approached (region K).

Three electrode batches (Table 2.1) were investigated in this study using cyclic voltammetry and the electroactive mediator potassium ferricyanide  $[\text{K}_3\text{Fe}(\text{CN})_6]$  (Table 2.2).

**Table 2-2:** Scan parameters for potassium ferricyanide for SPGE characterization.

Step potential	0.01 V
First vertex potential	0.3 V
Second vertex potential	-0.4 V
Scan rate	10 $\text{mV s}^{-1}$ , 20 $\text{mV s}^{-1}$ , 50 $\text{mV s}^{-1}$ , 70 $\text{mV s}^{-1}$ and 100 $\text{mV s}^{-1}$
No. of scans	3

Volumes of 100  $\mu\text{L}$  of potassium ferricyanide (0.1, 0.5 and 1 mM) were applied to cover all three electrodes. SPGEs were then scanned between 10  $\text{mV s}^{-1}$  and 100  $\text{mV s}^{-1}$ . Step potential, first and second vertex potential remained constant. The average of three scans was used to determine WE surface activity using Randles Sevcik equation (Gosser, 1993; Bard and Faulkner, 2001).

$$I_p = 2.69 \cdot 10^5 \text{ A C } \sqrt{n^3 \text{ D V}} \quad (2-1)$$

where  $I_p$  is average of cathodic and anodic peaks followed by Randles Sevcik constant;  $A$  is the active surface area, bulk concentration  $C$  (mol / mL) of potassium ferricyanide is calculated at 1 mM, number of electrons  $n$  involved in

the redox reaction is 1; coefficient  $D$  of  $K_3Fe(CN)_6$  is  $7.6 \times 10^{-6} \text{ cm}^2 \text{ s}^{-1}$  (Morrin et al., 2007). The scan rate varies, where  $V$  was varied from  $10 \text{ mV s}^{-1}$  to  $100 \text{ mV s}^{-1}$  ( $n = 3$ ). Active surface area was calculated for JD 2b at  $20 \text{ mV s}^{-1}$ . From equation 2.1:

$$\begin{aligned}
 A_{\text{active}} &= \frac{I_p}{2.69 \cdot 10^5 \text{ C} \cdot \sqrt{n^3 DV}} \\
 &= \frac{\frac{13.70 + 18.93 \cdot 10^{-6}}{2}}{2.69 \cdot 10^5 \cdot 1 \cdot 10^{-6} \sqrt{1 \cdot 7.6 \cdot 10^{-6} \cdot 0.02}} \\
 &= \frac{16.32}{2.69 \cdot 10^5 \cdot 3.8987 \cdot 10^{-4}} \\
 &= \frac{16.32}{2.69 \cdot 10 \cdot 3.90} \\
 &= \frac{16.32}{104.91} \\
 A_{\text{active}} &= 0.1555 \text{ cm}^2
 \end{aligned}$$

Percentage activity of WE was obtained using:

$$A_{\text{active}} \% = \frac{A_{\text{active}}}{A_{\text{geometric}}} \cdot 100 \quad (2-2)$$

According to Binder (2014),  $A_{\text{geometric}}$  is obtained from diameter of working electrode as 5 mm, including rectangular gold surface below the main electrode, with length 'a' of 3 mm and width 'w' of 1 mm; geometric area is calculated at 0.226 cm<sup>2</sup>.

$$A_{\text{active}} \% = \frac{0.1555}{0.226} \cdot 100$$

$$A_{\text{active}} \% = 0.68\%$$

Above is the percentage WE surface area at 1 mM potassium ferricyanide and 20 mV s<sup>-1</sup> scan rate. Randles Sevcik equation governs quasi-reversible electrochemical processes (Kadara et al., 2009) and was again used for the calculation of active WE surface area ( $A_{\text{active}}$ ) at various scan rates on the SPGEs. Following electroactive surface area calculation, chronoamperometric determination for mediator / substrate complex, TMB/ H<sub>2</sub>O<sub>2</sub> was conducted in order to confirm the results.

### 2.3.2 Preparation of working buffer

To prepare working buffer, 0.05 M phosphate citrate buffer (pH 5.0) was added to 0.1 M KCl in a 1:1 ratio. The working buffer was used in preparation of substrate.

### 2.3.3 Preparation of H<sub>2</sub>O<sub>2</sub> (substrate)

To prepare the substrate solution, the working buffer (section 2.3.2) was then used to dilute a 30 % (v/v) hydrogen peroxide solution in a ratio of 1:10, resulting in a 3 % (v/v) hydrogen peroxide working buffer mix. The solution was prepared just before taking the readings, and placed in the dark.

### 2.3.4 TMB (mediator) solution preparation

TMB (3, 3', 5, 5'-Tetramethyl benzidine hydrochloride) was taken to be the mediator for this study. To prepare the solution, TMB (0.001g) was dissolved in 150 µL of de-ionized water (18.2 mΩ) in a 1.5 mL tube to give a final

concentration of 0.6 M. The solution was prepared just before taking the readings, and placed in the dark.

### **2.3.5 Preparation of TMB / H<sub>2</sub>O<sub>2</sub> (mediator / substrate) stock**

The preparation of the TMB/H<sub>2</sub>O<sub>2</sub> (mediator/substrate) was conducted when it was time to take the readings when assay had been completed on the SPGE. H<sub>2</sub>O<sub>2</sub> and TMB (prepared in sections 2.3.3 and 2.3.4) were added to the working buffer in 1.5 mL tubes. To produce 0.5 mL of the final substrate, 10 µL of the 3 % (w/w) hydrogen peroxide stock as well as 10 µL of the TMB-water stock was diluted in 480 µL of working buffer. This resulted in a final concentration of 4 mM TMB and 0.06 % H<sub>2</sub>O<sub>2</sub> in phosphate citrate-KCl buffer. To minimize the variations in the sensor signal due to poor reagent quality, a fresh TMB / H<sub>2</sub>O<sub>2</sub> mediator / substrate complex was mixed for every sensor batch or after 30 minutes of use.

### **2.3.6 Characterization of mediator / substrate system**

The TMB / H<sub>2</sub>O<sub>2</sub> system used is based on JD 1 SPGEs (Binder, 2014) however to assess its effect on JD 2b SPGE, investigation was conducted on electrode cured at 120°C for 30 minutes then rinsed twice in 1000 µL de-ionised water (18.2 mΩ) to remove impurities and dried in gentle nitrogen stream. The TMB / H<sub>2</sub>O<sub>2</sub> system for signal generation was characterized using cyclic voltammetry with a bandwidth ranging from -0.3 to 0.8 V at ambient temperature. Reagents were prepared in 0.05 M phosphate citrate buffer and 1 M KCl working buffer. The working volume comprised 10 µL of TMB solution (0.6 M) and 10 µL 1:10 (30%) hydrogen peroxide diluted in 480 µL of working buffer (1:1 KCl and 0.05 M phosphate citrate buffer, pH 5).

### **2.3.7 Chronoamperometric analysis to determine assay potential**

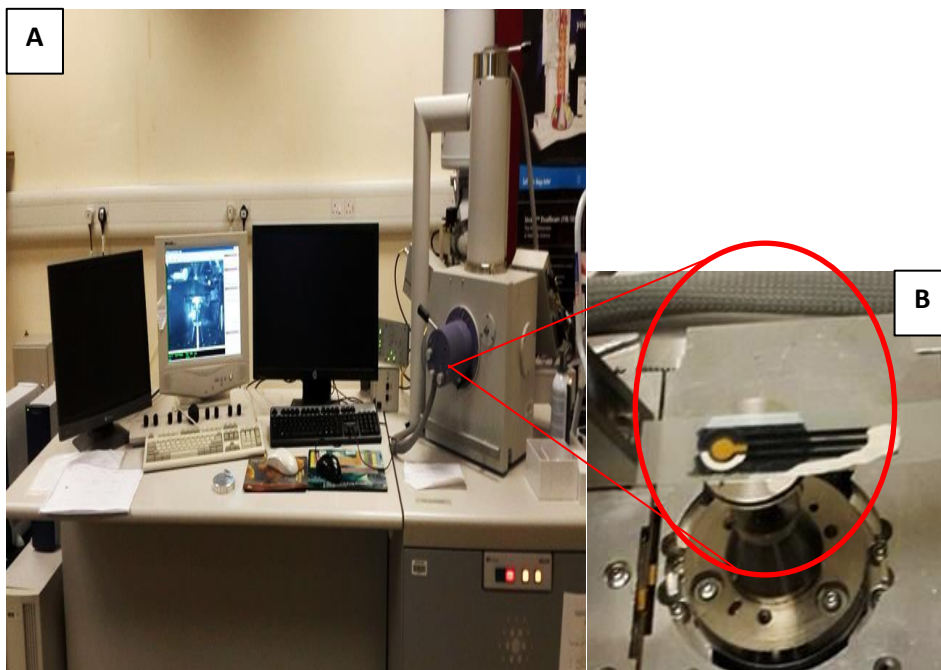
TMB was adopted as the suitable mediator in horse radish peroxidase conjugated affinity assay. Sensors were first heated at 120 °C for 30 minutes then rinsed with 1000 µL distilled water (18.2 Ω) to remove impurities and dried in gentle nitrogen stream. For this study, H<sub>2</sub>O<sub>2</sub> (adopted as the substrate). A

solution of TMB / H<sub>2</sub>O<sub>2</sub> (0.001g TMB in 150  $\mu$ L de-ionized water, 18.2 m $\Omega$ ) with 1: 10 H<sub>2</sub>O<sub>2</sub> in phosphate citrate buffer (0.05 M, pH 5) was added to 10  $\mu$ L monoclonal antibody, horse radish peroxidase conjugated.

The measurement was normalized by first obtaining baseline current of the TMB / H<sub>2</sub>O<sub>2</sub> system at each potential then injecting monoclonal antibody-HRP conjugated (10  $\mu$ g mL<sup>-1</sup>) at 100 s at ambient temperature between 18 °C and 25 °C. Results were calculated from 10 measurements before and after enzyme addition. Blank response was subtracted from the measurement to obtain the signal for the optimal current for the system. The optimal working potential was selected as the highest signal. Data was then copied to Microsoft Excel for presentation and compared with JD 1 from a previous study.

### **2.3.8 Characterization of the bare electrode surface**

To characterize the gold working electrode, scanning electron microscopy was used to obtain a visual image of the gold working surface. Prior to scanning sample preparation was conducted. The electrodes were thus heated, washed and dried as in section 2.3.7. The nitrogen dried screen-printed electrode was attached along the underside with adhesive tape to the platform. The vacuum having been created, an image was scanned via the introduction of a high power beam onto the sample. The image was captured from the excited particles from the working electrode. Images were captured at low and high magnification (Figure 2.4).



**Figure 2-4:** Scanning electron microscope (A) was used to generate an image of the gold working electrode surface, when an electron beam was incident on the mounted SPGE (B). An adhesive was used to stabilize the SPGE.

In order to determine elemental composition of the working electrode, the process was repeated using a fresh screen-printed electrode. The image scanned by the projection of an electron beam which interacts with the sample can be used to form a visual image showing lithographic pattern on the working electrode surface at 50x magnification.

During characterization, surface roughness, modification, inter-electrode distance, ink composition, curing temperature and pre-treatment procedures must be taken into consideration (Pernia et al., 2009).

Printing quality has improved in 2015 - 2016 batch of JD 2b. High surface area from the three dimensional ink granules has a direct association with the amount to bio-material in the stationary phase on the working electrode and is reported to have an improved performance (Noh and Tothill, 2009).

### **2.3.9 Characterization of modified electrode surface**

The redox behaviour of a reversible couple was used to assess the density and sensitivity of the monolayer (Bain et al., 1989). The formation of thiol monolayer on the gold surface was characterized using cyclic voltammetry analysis using 5 mM potassium ferricyanide solution in 0.1 M KCl. Surface modification of the SPGE was carried out (Salam and Tothill, 2009; Hayashi, et al., 2009).

Prior to characterization electrodes were cured in the oven at 120°C for 30 minutes and then dried with nitrogen stream. Following a method used by Salam and Tothill (2009), each electrode was then immersed in 5 mL of 11-mercaptoundecanoic acid, and 3, 3' dithiodipropionic acid (2 mM) overnight in the dark. The electrodes were washed in 1000  $\mu$ L of 95 % ethanol (twice) and then twice in 1000  $\mu$ L of deionized water (18.2 m $\Omega$ ). The electrodes were then dried in gentle nitrogen stream and scanned at 50 mV s<sup>-1</sup> using potassium ferricyanide (1 mM). Average of two sensors was used in the calculation of the active surface area percent. The results were compared with bare SPGE characterization at 50 mV s<sup>-1</sup>.

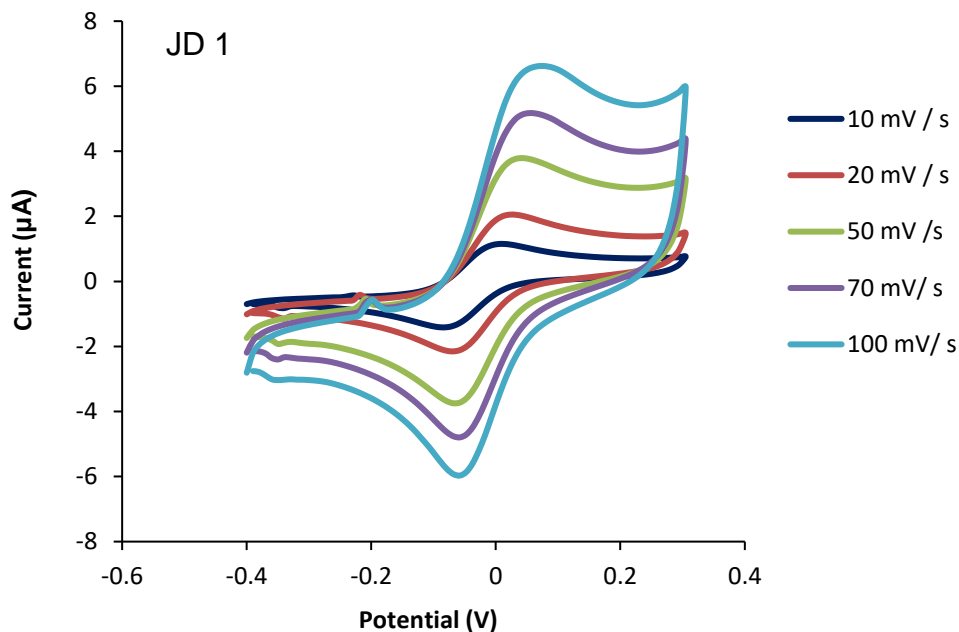
## **2.4 RESULTS AND DISCUSSION**

### **2.4.1 CV analysis of JD 1 SPGE against potassium ferricyanide**

Cyclic voltammetric analysis was used to characterize the working electrode surface using an electroactive marker, potassium ferricyanide. Electroactive markers can also evaluate sensor reproducibility. The electrochemical behaviour of potassium ferricyanide was tested at different scan rates such as 10 mV s<sup>-1</sup>, 20 mV s<sup>-1</sup>, 50 mV s<sup>-1</sup>, 70 mV s<sup>-1</sup> and 100 mV s<sup>-1</sup>. During a voltammetric scan, the potential applied to the working electrode becomes sufficiently positive and causes anodic current observed at that point. This will increase rapidly until the oxidized species falls to zero. Three batches of DuPont SPGE: JD 1, JD 2a and JD 2b electrodes were investigated (section 2.2.2; Table 2.1). Electrode suitability hinged on reversibility of reaction using potassium ferricyanide in potassium chloride as mediating electrolyte.



Characterization was therefore conducted on JD 1 with potassium ferricyanide concentrations 0.1 mM (Figure 2.5).



**Figure 2-5:** Cyclic voltammogram with 0.1 mM potassium ferricyanide on JD 1 at scan rates of 10, 20, 50, 70 and 100 mV s<sup>-1</sup> using 100 μL 0.1 mM potassium ferricyanide solution for the characterization of JD 1 SPGE. The graph represents the average of two scans per three sensors.

During reduction of the electrode immersed in solution, the potential is switched to negative values and the accumulated oxidized species on the electrode surface are reduced. Higher cathodic and anodic peak separation was observed at lower scan rate (Bard & Faulkner, 2012).

Cathodic and anodic peak current was employed to calculate active surface area of the working electrode. Randles-Sevcik equation averages the peak values while potential change  $\Delta E$  is the difference is potential which determines reversibility of the reaction. A anodic and cathodic peak separation,  $\Delta E$  of 0.059 V indicates that the electrochemical reaction is quasi-reversible (Table 2.3).

**Table 2-3:** Characterization of JD 1 SPGE using potassium ferricyanide (0.1 mM).

	10 mV s <sup>-1</sup>	20 mV s <sup>-1</sup>	50 mV s <sup>-1</sup>	70 mV s <sup>-1</sup>	100 mV s <sup>-1</sup>
<b>I<sub>PA</sub> (μA)<sup>a</sup></b>	1.16 ± 0.02	2.94 ± 0.03	3.79 ± 0.00	5.16 ± 0.02	6.59 ± 0.11
<b>E<sub>PA</sub> (V)<sup>b</sup></b>	0.00 ± 0.01	0.03 ± 0.01	0.04 ± 0.01	0.06 ± 0.00	0.07 ± 0.00
<b>I<sub>PC</sub> (μA)<sup>a</sup></b>	-1.71 ± 0.003	-2.2 ± 0.01	-3.73 ± 0.02	-4.78 ± 0.03	-5.93 ± 0.06
<b>E<sub>PC</sub> (V)<sup>b</sup></b>	-0.022 ± 0.004	-0.037 ± 0.01	-0.052 ± 0.00	-0.05 ± 0.00	-0.06 ± 0.00
<b>ΔE [V]<sup>c</sup></b>	0.024	0.067	0.92	0.11	0.13
<b>I<sub>PA</sub>/ I<sub>PC</sub><sup>d</sup></b>	-0.68	-0.131	-1.01	-1.07	-1.11
<b>A<sub>active</sub> (cm<sup>2</sup>)</b>	0.02	0.02	0.02	0.03	0.03
<b>A<sub>active</sub><sup>e</sup> (%)</b>	75	86	102	111	132

<sup>a</sup> I<sub>PC/A</sub>=Cathodic / anodic peak current

<sup>b</sup> E<sub>P C/A</sub> = Potential applied at the cathodic / anodic peak

<sup>c</sup> Peak distance ΔE = E<sub>PA</sub> – E<sub>PC</sub>

<sup>d</sup> Ratio between the cathodic and anodic peak current

<sup>e</sup> Ratio between the active area calculated by the Randles – Sevcik equation and the geometric surface.

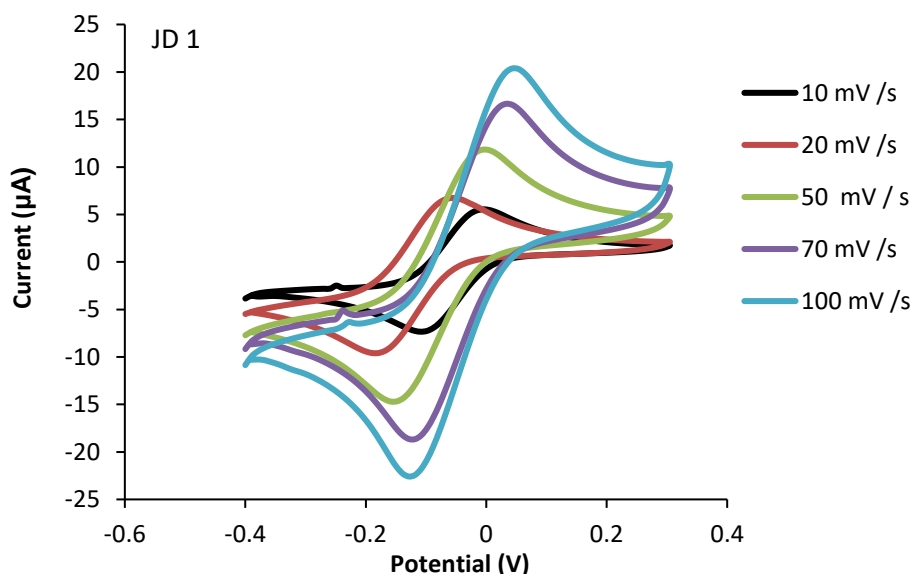
From Table 2.3 the I<sub>P C/A</sub> = Cathodic / anodic peak current, E<sub>P C/A</sub> = Potential applied at the cathodic / anodic peak, Peak distance ΔE = E<sub>PA</sub> – E<sub>PC</sub>; Ratio between the cathodic and anodic peak current e; Ratio between the active area calculated by the Randles–Sevcik equation and the geometric surface were calculated. These results show average of two scans vary with concentration and scan rate, in agreement with previous work (Binder, 2014) who used 50 mM potassium ferricyanide at a scan rate of 20 mV s<sup>-1</sup> and -0.4 V to 3.0 V band width.

As shown in Figure 2.5, gold working electrode performs well with peak to peak separation (ΔE<sub>p</sub> = E<sub>PA</sub> – E<sub>PC</sub>) at 20 mV s<sup>-1</sup> was found to be 100 mV, which indicates that the electrochemical reaction is quasi-reversible. The oxidation / reduction peaks showed variation when the lower scan rates are used. The ideal ΔE value for a perfectly reversible redox reaction of potassium ferricyanide is 56 to 59 mV and the ratio between the cathodic and anodic peak is 1 (Mueller and Adams, 1961; Arya et al; 2007). In practice however, the difference is

typically 100 mV and higher (Arya, 2007). It is reported that the redox reaction is less reversible with a higher concentration of potassium ferricyanide (Binder, 2014).

JD 1 SPGE was then investigated using 0.5 mM and then 1 mM potassium ferricyanide. Cyclic voltammetry has been described as the most versatile of electroanalytical techniques for the study of electroactive species and is often the first experiment performed in the study of a compound, biological material, or an electrode surface (Kissinger and Heineman, 1983).

The oxidation reaction was repeated to calculate active surface area of the working electrode. In order to achieve this investigation was then conducted by scanning JD 1 SPGE using 0.5 mM concentration of potassium ferricyanide (Figure 2.6).



**Figure 2-6:** Cyclic voltammogram JD 1 with potassium ferricyanide 0.5 mM at scan rates of 10, 20, 50, 70 and 100 mV s<sup>-1</sup> using 100 µL 0.5 mM potassium ferricyanide solution for the characterization of JD 1 SPGE. The graph represents the average of two scans per three sensors.

From Figure 2.6 there is a peak shift and the change in potential ( $\Delta E_p$ ) shows the reaction is quasi-reversible.

Cyclic voltammetry consists of cycling the potential of an electrode in unstirred solution, measuring the resulting current. The potential of the working electrode is controlled against a reference electrode. The controlling potential applied between the electrodes is regarded as the excitation signal which sweeps the potential of the electrode between two values. One of the electrodes probes the solution, while the other serves as a reference. The reference electrode has a constant and reproducible potential which is independent of its environment. The potential of the probe electrode is the potential at the interface of the solid and liquid phases. From Figure 2.6 values were used to generate the table and performance of the electrode using 0.5 mM potassium ferricyanide was determined (Table 2.4).

**Table 2-4:** Characterization of JD 1 SPGE using potassium ferricyanide (0.5 mM).

	10 mV s <sup>-1</sup>	20 mV s <sup>-1</sup>	50 mV s <sup>-1</sup>	70 mV s <sup>-1</sup>	100 mV s <sup>-1</sup>
<b>I<sub>PA</sub> (μA)<sup>a</sup></b>	5.53± 0.01	6.87± 0.19	12.0± 0.28	16.8± 0.23	18.5± 2.63
<b>E<sub>PA</sub> (V)<sup>b</sup></b>	0.025± 0.001	-0.1± 0.07	-0.010 ± 0.01	-0.00 ± 0.00	0.04± 0.03
<b>I<sub>PC</sub> (μA)<sup>a</sup></b>	-7.32± 0.03	-9.55±13.62	14.7± 20.12	-18.6± 0.04	-20.6± 2.79
<b>E<sub>PC</sub> (V)<sup>b</sup></b>	-0.62± 5.65	-0.2± 0.25	-0.15 ± 0.01	-0.12± 0.00	-0.12± 0.01
<b>ΔE (V)<sup>c</sup></b>	-0.595	.1	1.65	0.12	0.16
<b>I<sub>PA</sub>/ I<sub>PC</sub><sup>d</sup></b>	-0.76	-0.72	0.85	-0.90	-0.89
<b>A<sub>active</sub> (cm<sup>2</sup>)</b>	0.09	0.08	0.81	0.09	0.05
<b>A<sub>active</sub> (%)<sup>e</sup></b>	77	69	60.2	79.6	47

<sup>a</sup> I<sub>PC/A</sub>=Cathodic / anodic peak current

<sup>b</sup> E<sub>P C/A</sub> = Potential applied at the cathodic / anodic peak

<sup>c</sup> Peak distance ΔE = E<sub>PA</sub> – E<sub>PC</sub>

<sup>d</sup> Ratio between the cathodic and anodic peak current

<sup>e</sup> Ratio between the active area calculated by the Randles – Sevcik equation and the geometric surface.

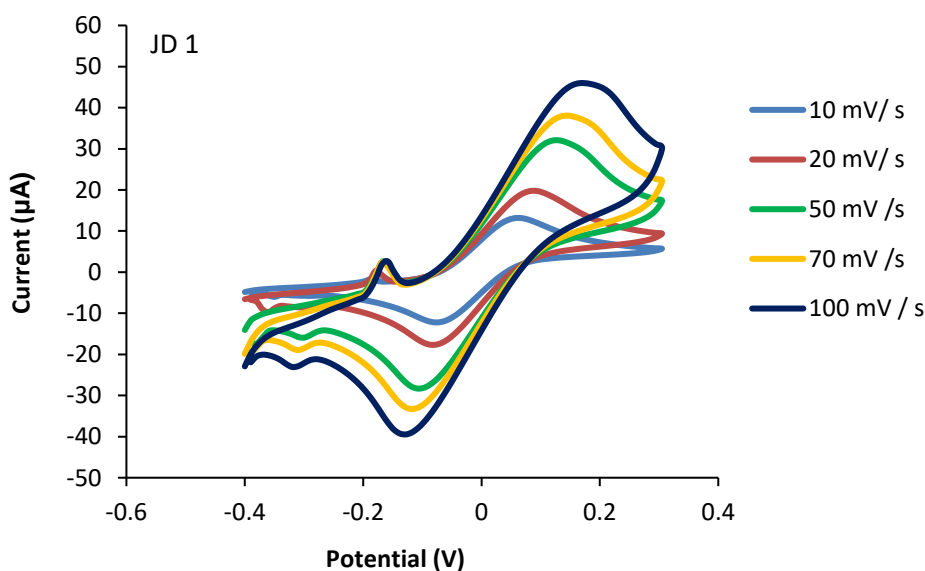
As expected, calculation of active surface area equilibrium of the redox reaction must be achieved (Tables 2.3 and 2.4) when the rates of oxidation and reduction are equal, and the composition of the solution surrounding the electrode is constant. The equilibrium potential is given by Nernst Law:

$$E = E_0 + \frac{RT}{nF} \ln \frac{[ox]}{[red]} \quad (2-3)$$

Where  $E_0$  is the equilibrium potential,  $R$  the perfect gas constant,  $T$  temperature constant,  $F$  faraday constant where  $[ox]$  and  $[red]$  represent concentrations of oxidized and reduced forms. This law is only valid for very dilute solutions (Canh, 1991). In the one electrode reaction, ferricyanide is reduced and re-oxidized:



In the one electrode reaction, ferricyanide oxidation produces a shift of cathodic and anodic peaks at different scan rates. According to the results in Table 2.3 and 2.4,  $\Delta E$  is similar at  $20 \text{ mV s}^{-1}$ . In order to make further investigate the JD 1 electrodes produced in 2010, a concentration of  $1 \text{ mM}$  was used to characterize the electrode surface (Figure 2.7).



**Figure 2-7:** Cyclic voltammogram with  $1 \text{ mM}$  potassium ferricyanide on JD 1 at scan rates of  $10, 20, 50, 70$  and  $100 \text{ mV s}^{-1}$  using  $100 \mu\text{L}$   $1 \text{ mM}$  potassium ferricyanide solution for the characterization of JD 1 SPGE. The graph represents the average of two scans per three sensors.

As with in Figures 2.5 and 2.6, results show a quasi-reversible curve at scan rate  $20 \text{ mV s}^{-1}$  with  $1 \text{ mM}$  potassium ferricyanide scanned from  $-0.4$  to  $3 \text{ V}$ . From the results of the peak search the performance of the electrode was calculated (Table 2.5).

**Table 2-5:** Characterization of JD 1 SPGE using potassium ferricyanide ( $1 \text{ mM}$ ).

	$10 \text{ mV s}^{-1}$	$20 \text{ mV s}^{-1}$	$50 \text{ mV s}^{-1}$	$70 \text{ mV s}^{-1}$	$100 \text{ mV s}^{-1}$
$I_{PA} (\mu\text{A})^a$	$13.30 \pm 0.14$	$19.88 \pm 0.18$	$32.1 \pm 0.01$	$38.14 \pm 0.00$	$48.00 \pm 0.00$
$E_{PA} (\text{V})^b$	$0.064 \pm 0.00$	$0.09 \pm 0.01$	$0.13 \pm 0.00$	$0.15 \pm 0.22$	$0.16 \pm 0.00$
$I_{PC} (\mu\text{A})^a$	$-12.3 \pm 0.11$	$-18.4 \pm 1.48$	$-28.3 \pm 0.03$	$-33.3 \pm 66.6$	$-39.5 \pm 0.31$
$E_{PC} (\text{V})^b$	$-0.08 \pm 0.00$	$-0.08 \pm 0.11$	$-0.10 \pm 0.00$	$-0.21 \pm 0.11$	$-0.21 \pm 0.02$
$\Delta E (\text{V})^c$	0.14	0.17	0.23	0.36	0.37
$I_{PA} / I_{PC}^d$	-1.08	-1.14	-1.13	-1.15	-1.21
$A_{\text{active}} (\text{cm}^2)$	0.17	0.18	0.18	0.18	0.11
$A_{\text{active}} (\%)^e$	76.3	78.9	80.1	80.5	46.7

<sup>a</sup>  $I_{PC/A}$  = Cathodic / anodic peak current

<sup>b</sup>  $E_{P C/A}$  = Potential applied at the cathodic / anodic peak

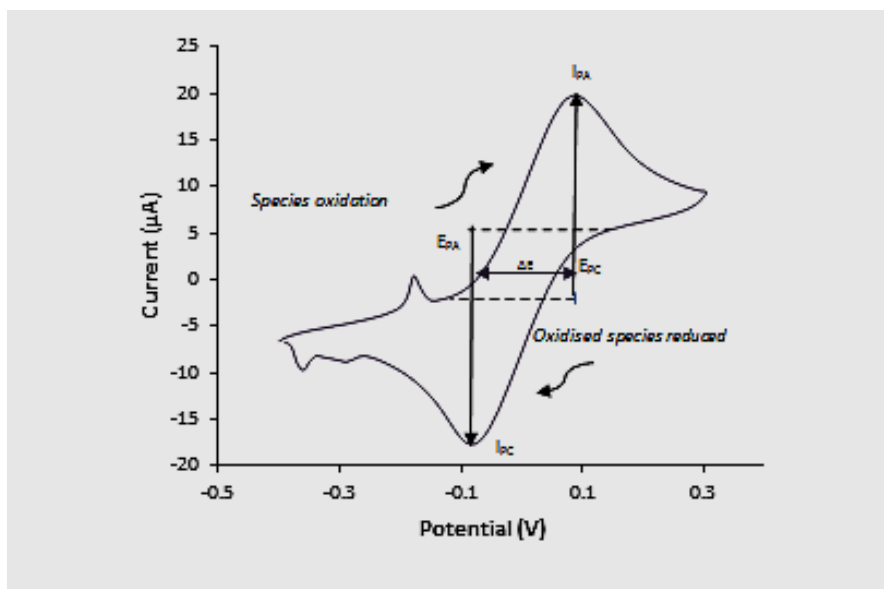
<sup>c</sup> Peak distance  $\Delta E = E_{PA} - E_{PC}$

<sup>d</sup> Ratio between the cathodic and anodic peak current

<sup>e</sup> Ratio between the active area calculated by the Randles – Sevcik equation and the geometric surface.

JD 1 electrodes showed overall good performance and quasi-reversibility when the distance between the cathodic and anodic peaks was measured.

According to experimental conditions, diffusion, convection and migration transport processes are found to be significant (Fisher, 1996). Diffusion electron transfer occurs across solid / liquid interphase in unstirred media used in characterization of SPGE batches. A JD 1 electrode was used to show the direction of species oxidation and reduction when the potential difference was applied (Figure 2.8).



**Figure 2-8:** Generalized peak measurements for JD 1 SPGE (1 mM) with indicated parameters for the calculation of active surface area.

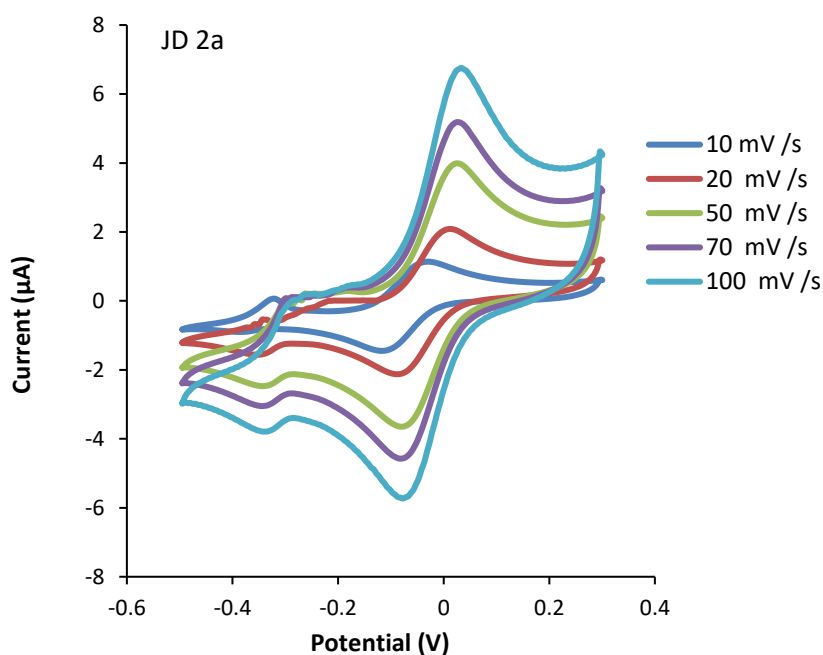
Cyclic voltammogram for the JD1 (2010) gold screen-printed electrode using a 1 mM potassium ferricyanide solution in 1 M KCl at a scan rate of 20 mV s<sup>-1</sup> (Binder, 2014). The peak establishes at the point of species consumption, affected by rate of electron transfer controlled through relatively small increments in potential.  $I_{P C/A}$  = Cathodic / anodic peak current;  $E_{P C/A}$  = Peak current at the cathode / anode;  $\Delta E = E_{PA} - E_{PC}$  produced values approximate to the ideal for a reversible reaction (0.059 V). The reactions from JD 1 characterization using concentrations of potassium ferricyanide all showed stability of the batch since production date of 2010. The results also suggest the suitability of JD 1 for use in developing an affinity sensor.

#### 2.4.2 CV analysis of JD 2a SPGE against potassium ferricyanide

Having investigated the performance of JD 1 SPGEs, a batch produced in 2013 (JD 2a) were characterized using 0.1, 0.5 and 1 mM concentrations of

potassium ferricyanide in order to establish similarities or differences in the quality and performance of the electrodes.

JD 2a batch construct differed from JD 1 in the carbon counter electrode ink print quality (section 2.2.2; Table 2.1). The results show a quasi-reversible curve with clear peak separation at varied scan rates ranging from 10 to 100  $\text{mV s}^{-1}$  (Figure 2.9).



**Figure 2-9:** Cyclic voltammogram with 0.1 mM potassium ferricyanide on JD 2a at scan rates of 10, 20, 50, 70 and 100  $\text{mV s}^{-1}$  using 100  $\mu\text{L}$  0.1 mM potassium ferricyanide solution for the characterization of JD 2a SPGE. The graph represents the average of two scans per three sensors.

Following a peak search, the values obtained from the cyclic voltammogram were used to calculate the difference in peak height and the activity of the working electrode. The results also shed light on the effect of counter electrode print quality on general performance of the JD SPGE (Table 2.6).



**Table 2-6:** Characterization of JD 2a SPGE using potassium ferricyanide (0.1 mM).

	10 mV s <sup>-1</sup>	20 mV s <sup>-1</sup>	50 mV s <sup>-1</sup>	70 mV s <sup>-1</sup>	100 mV s <sup>-1</sup>
<b>I<sub>PA</sub> (μA)<sup>a</sup></b>	1.138± 0.00	1.444± 0.07	3.211± 0.00	5.280± 0.32	6.857±0.00
<b>E<sub>PA</sub> (V)<sup>b</sup></b>	-0.-17± 0.00	-0.042± 0.00	-0.04± 0.07	-0.024± 0.04	0.032± 0.01
<b>I<sub>PC</sub> (μA)<sup>a</sup></b>	-1.43± 0.6	-1.88± 0.00	-3.210± 0.00	-3.985± 0.1	— 5.733±0.00
<b>E<sub>PC</sub> (V)<sup>b</sup></b>	-0.057± 0.1	-0.143± 0.00	-0.092± 0.00	-0.024± 0.01	-0.072± 0.02
<b>ΔE (V)<sup>c</sup></b>	0.041	0.10	0.052	-0.04	-0.023
<b>I<sub>PA</sub>/ I<sub>PC</sub><sup>d</sup></b>	0.0118	-0.77	-1.00	1-1.32	-1.195
<b>A<sub>active</sub> (cm<sup>2</sup>)</b>	0.17	0.15	0.173	0.23	0.27
<b>A<sub>active</sub> (%)<sup>e</sup></b>	77	67.54	77	103	118.7

<sup>a</sup> I<sub>PC/A</sub>=Cathodic / anodic peak current

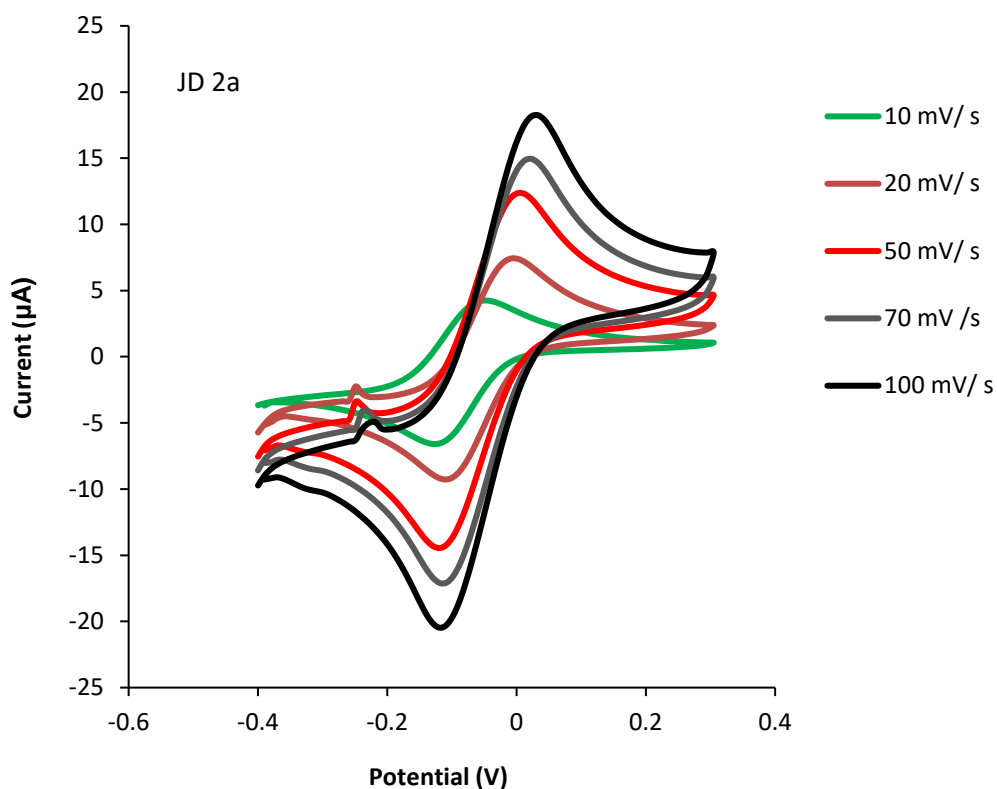
<sup>b</sup> E<sub>P C/A</sub> = Potential applied at the cathodic / anodic peak

<sup>c</sup> Peak distance ΔE = E<sub>PA</sub> – E<sub>PC</sub>

<sup>d</sup> Ratio between the cathodic and anodic peak current

<sup>e</sup> Ratio between the active area calculated by the Randles – Sevcik equation and the geometric surface.

Results from Table 2.6 show the I<sub>P C/A</sub> = Cathodic / anodic peak current, E<sub>P C/A</sub> = Potential applied at the cathodic / anodic peak, Peak distance ΔE = E<sub>PA</sub> – E<sub>PC</sub>; Ratio between the cathodic and anodic peak current e; Randles–Sevcik equation was used to calculate percentage activity of the gold working electrode. These results show average of two scans. The rate of electron transfer can be seen to vary according to scan rate. The JD 2a batch shows similarity to the earlier JD 1 batch in the quasi-reversibility at 0.1 mM (Figure 2.10).



**Figure 2-10:** Cyclic voltammogram with 0.5 mM potassium ferricyanide on JD 2a at scan rates of 10, 20, 50, 70 and 100  $\text{mV s}^{-1}$  using 100  $\mu\text{L}$  0.5 mM potassium ferricyanide solution for the characterization of JD 2a SPGE. The graph represents the average of two scans per three sensors.

Concentration using DuPont sensor type JD 2a SPGE scanned at 10, 20, 50, 70 and 100  $\text{mV s}^{-1}$ . With increase in potassium ferricyanide concentration, JD 2a showed slight variation in cathodic peak.

Investigation of the JD 2a electrode at 0.5 mM concentration of potassium ferricyanide gave produced the results from which the active surface area of the electrode was calculated (Table 2.7).

**Table 2-7:** Characterization of JD 2a SPGE using potassium ferricyanide (0.5 mM).

	10 mV s <sup>-1</sup>	20 mV s <sup>-1</sup>	50 mV s <sup>-1</sup>	70 mV s <sup>-1</sup>	100 mV s <sup>-1</sup>
<b>I<sub>PA</sub> (μA)<sup>a</sup></b>	4.53±0.39	7.50±0.09	12.1±0.01	15.09±0.20	18.41±0.22
<b>E<sub>PA</sub> (V)<sup>b</sup></b>	-0.04±0.01	-0.01±0.01	0.02±0.00	0.02±0.00	0.03±0.00
<b>I<sub>PC</sub> (μA)<sup>a</sup></b>	-6.65±0.07	-9.25±0.02	-15.89±11.2	-17.04±0.12	-20.40±0.12
<b>E<sub>PC</sub> (V)<sup>b</sup></b>	-0.13±0.00	-0.11±0.00	-0.12±0.00	-0.12±0.00	-0.15±0.17
<b>ΔE (V)<sup>c</sup></b>	0.09	0.11	0.13	0.14	0.12
<b>I<sub>PA</sub>/I<sub>PC</sub><sup>d</sup></b>	-0.68	-0.81	-0.78	-0.89	-0.90
<b>A<sub>active</sub> (cm<sup>2</sup>)</b>	0.07	0.08	0.08	0.08	0.08
<b>A<sub>active</sub> (%)<sup>e</sup></b>	64.6	70.6	70.8	71.6	73.4

<sup>a</sup> I<sub>PC/A</sub>=Cathodic / anodic peak current

<sup>b</sup> E<sub>P C/A</sub> = Potential applied at the cathodic / anodic peak

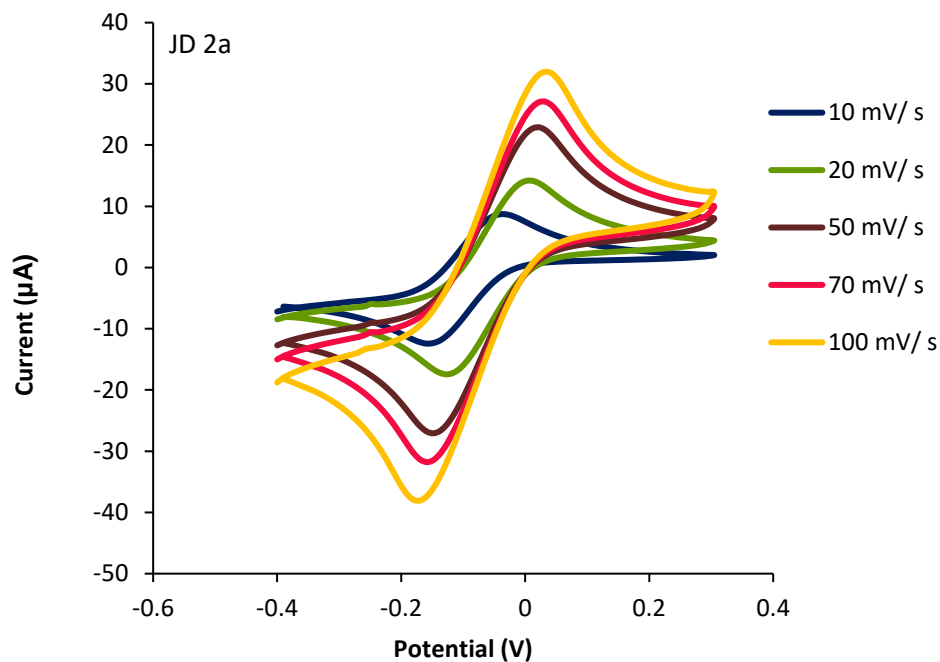
<sup>c</sup> Peak distance ΔE = E<sub>PA</sub> – E<sub>PC</sub>

<sup>d</sup> Ratio between the cathodic and anodic peak current

<sup>e</sup> Ratio between the active area calculated by the Randles – Sevcik equation and the geometric surface.

Results from Table 2.7 show the I<sub>P C/A</sub> = Cathodic / anodic peak current, E<sub>P C/A</sub> = Potential applied at the cathodic / anodic peak, Peak distance ΔE = E<sub>PA</sub> – E<sub>PC</sub>; Ratio between the cathodic and anodic peak current e; Randles–Sevcik equation was used to calculate percentage activity of the gold working electrode. These results show average of two scans. The rate of electron transfer can be seen to vary according to scan rate. The JD 2a batch shows similarity to the earlier JD 1 batch in the quasi-reversibility at 0.5 mM.

To make a comparison between the results, a concentration of 1 mM potassium ferricyanide was used to characterize JD 2a. Results show little variation compared with 0.1 and 0.5 mM using JD 2a at scan rates of 10, 20, 50, 70 and 100 mV s<sup>-1</sup>. The standard deviation shows limit of error between average two scans (Figure 2.11).



**Figure 2-11:** Cyclic voltammogram with 1 mM potassium ferricyanide on JD 2a at scan rates of 10, 20, 50, 70 and 100  $\text{mV s}^{-1}$  using 100  $\mu\text{L}$  1 mM potassium ferricyanide solution for the characterization of JD 2a SPGE. The graph represents the average of two scans per three sensors.

Scan rates of 10, 20, 50, 70 and 100  $\text{mV s}^{-1}$  using 1 mM potassium ferricyanide. Graph was plotted with average measurement of two scans per three sensors (Table 2.8).

**Table 2-8:** Characterization of JD 2a SPGE using potassium ferricyanide (1 mM).

	10 mV s <sup>-1</sup>	20 mV s <sup>-1</sup>	50 mV s <sup>-1</sup>	70 mV s <sup>-1</sup>	100 mV s <sup>-1</sup>
I <sub>PA</sub> (μA) <sup>a</sup>	9.09± 0.51	14.41± 0.32	26.09± 3.96	27.27± 0.30	32.29± 0.43
E <sub>PA</sub> (V) <sup>b</sup>	-0.04± 0.01	0.00± 0.001	0.02± 0.00	0.03± 0.01	0.03± 0.01
I <sub>PC</sub> (μA) <sup>a</sup>	-12.7± 0.37	-17.4± 0.01	-28.94± 38.2± 38.2	-31.71± 0.12	-37.7± 0.24
E <sub>PC</sub> (V) <sup>b</sup>	-0.16± 0.001	-0.13± 0.01	-0.15± 0.00	-0.16± 0.001	-0.17± 0.00
ΔE (V) <sup>c</sup>	0.12	0.13	0.17	0.19	0.2
I <sub>PA</sub> / I <sub>PC</sub> <sup>d</sup>	-0.72	-0.83	1.09	0.86	-0.85
A <sub>active</sub> (cm <sup>2</sup> )	0.13	0.15	0.15	0.15	0.15
A <sub>active</sub> (%) <sup>e</sup>	57.1	66.8	66.81	66.37	65.9

<sup>a</sup> I<sub>PC/A</sub>=Cathodic / anodic peak current

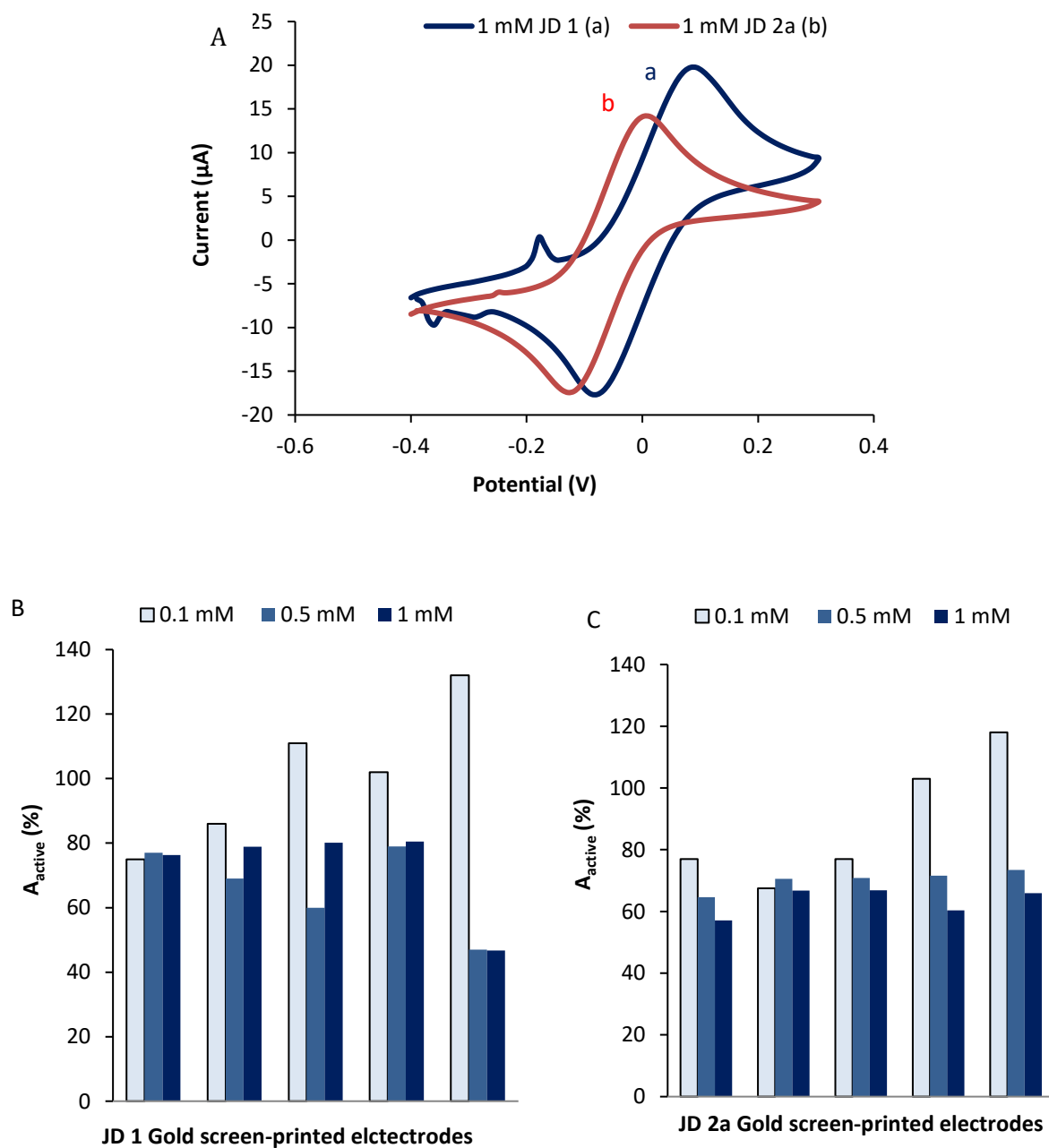
<sup>b</sup> E<sub>P C/A</sub> = Potential applied at the cathodic / anodic peak

<sup>c</sup> Peak distance ΔE = E<sub>PA</sub> – E<sub>PC</sub>

<sup>d</sup> Ratio between the cathodic and anodic peak current

<sup>e</sup> Ratio between the active area calculated by the Randles – Sevcik equation and the geometric surface.

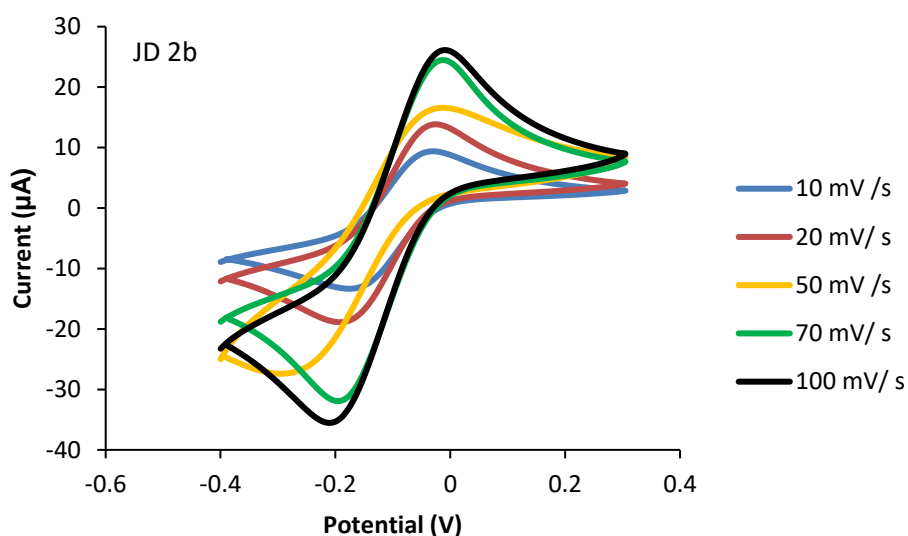
To visually assess peak shift between JD 1 and JD 2a SPGE during characterization with potassium ferricyanide (1 mM) at 20 mV s<sup>-1</sup> CV overlay. A<sub>active</sub> % was compared at 0.1, 0.5 and 1 mM (Figure 2.12).



**Figure 2-12:** Cyclic voltammograms of JD 1 and JD 2a overlay (A); potassium ferricyanide concentrations JD 1 (B) and JD 2a (C) SPGEs. Percentage active area taken between 10 - 100  $\text{mV s}^{-1}$  ( $n = 5$ ). Higher signal in JD 1 while 20  $\text{mV s}^{-1}$  is the best scan rate.

### 2.4.3 CV analysis of JD 2b SPGE against potassium ferricyanide

JD 2b, produced in 2015 (Table 2.1) was characterized with 1 mM potassium ferricyanide. The electrode had the same configuration and material as JD 2a; however the assessment was carried out in order to confirm the relative performance of the JD electrodes as the last batch of electrodes received from DuPont (Figure 2.13).



**Figure 2-13:** Cyclic voltammogram with 1 mM potassium ferricyanide on JD 2b at scan rates of 10, 20, 50, 70 and 100 mV s<sup>-1</sup> using 100 μL 1 mM potassium ferricyanide solution for the characterization of JD 2b SPGE. The graph represents the average of two scans per three sensors.

Results from the peak search JD 2b batch showed expected peak separation and shift with change in potential (Table 2.9).

**Table 2-9:** Characterization of JD 2b SPGE using potassium ferricyanide (1 mM).

	10 mV s <sup>-1</sup>	20 mV s <sup>-1</sup>	50 mV s <sup>-1</sup>	70 mV s <sup>-1</sup>	100 mV s <sup>-1</sup>
I <sub>PA</sub> (μA) <sup>a</sup>	9.39± 0.90	13.70± 1.12	18.81±2.15	25.15± 1.19	27± 4.03
E <sub>PA</sub> (V) <sup>b</sup>	-0.03± 0.01	-0.03±0.01	-0.02±0.01	-0.01±0.01	-0.02±0.01
I <sub>PC</sub> (μA) <sup>a</sup>	-13.5± 0.22	-18.93	-27.7±0.99	-35.5±0.91	-35.29±0.07
E <sub>PC</sub> (V) <sup>b</sup>	-0.17±0.02	-0.20±0.02	-0.20±0.02	-0.21±0.01	-0.21±0.02
ΔE (V) <sup>c</sup>	0.14	0.17	0.18	0.2	0.11
I <sub>PA</sub> / I <sub>PC</sub> <sup>d</sup>	-0.70	-0.72	-0.68	-0.74	-0.78
A <sub>active</sub> (cm <sup>2</sup> )	0.15	0.16	0.17	0.16	0.07
A <sub>active</sub> (%) <sup>e</sup>	68.2	68.80	76.73	69.6	30.0

<sup>a</sup> I<sub>PC/A</sub>=Cathodic / anodic peak current

<sup>b</sup> E<sub>P C/A</sub> = Potential applied at the cathodic / anodic peak

<sup>c</sup> Peak distance ΔE = E<sub>PA</sub> – E<sub>PC</sub>

<sup>d</sup> Ratio between the cathodic and anodic peak current

<sup>e</sup> Ratio between the active area calculated by the Randles – Sevcik equation and the geometric surface.

The rate of electron transfer is affected by the speed of the scan. Using this value to calculate active area of the working electrode, the percentage value is low as a result of speed in scan rate. The scan rate most suited to the JD sensors in this study is 20 mV s<sup>-1</sup>, confirming a previous study conducted on similar SPGE (Binder, 2014). For use in assay development, the JD 2b is suitable and chosen as the latest batch.

#### 2.4.4 Data comparison of the three electrodes

The JD 1, JD 2a and JD 2b results were compared according to Peak search (Table 2.10) and percentage activity per scan rate (Figure 2.14). From the characterization experiments it is clear that the sensors are stable for a long time (up to seven years) as JD 1 shows very good performance.



**Table 2-10:** Comparison of three JD batches at 20 mV s<sup>-1</sup> (1 mM).

	JD 1	JD 2 a	JD 2 b
<b>I<sub>PA</sub> (μA)</b> <sup>a</sup>	19.88±0.18	14.41±0.32	13.70±1.12
<b>E<sub>PA</sub> (V)</b> <sup>b</sup>	0.09±0.01	0.004±0.001	-0.03±0.01
<b>I<sub>PC</sub> (μA)</b> <sup>a</sup>	-18.43±1.48	-17.43±0.01	-18.93±0.67
<b>E<sub>PC</sub> (v)</b> <sup>b</sup>	-0.108±0.00	-0.13±0.01	-0.20±0.02
<b>ΔE (V)</b> <sup>c</sup>	0.17	0.13	0.17
<b>I<sub>PA</sub> / I<sub>PC</sub></b> <sup>d</sup>	-1.14	-0.83	-0.72
<b>A<sub>active</sub></b>	0.18	0.15	0.16
<b>A<sub>active</sub> (%)</b> <sup>e</sup>	78.9	66.8	68.8

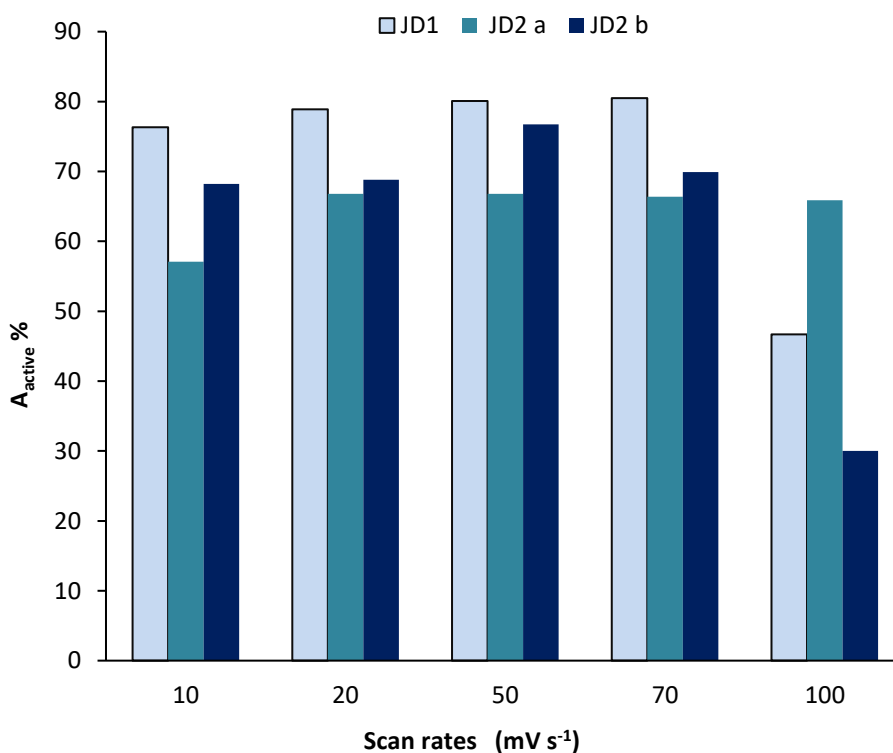
<sup>a</sup> I<sub>PC/A</sub>=Cathodic / anodic peak current

<sup>b</sup> E<sub>P C/A</sub> = Potential applied at the cathodic / anodic peak

<sup>c</sup> Peak distance ΔE = E<sub>PA</sub> – E<sub>PC</sub>

<sup>d</sup> Ratio between the cathodic and anodic peak current

<sup>e</sup> Ratio between the active area calculated by the Randles -Sevcik equation and the geometric surface.

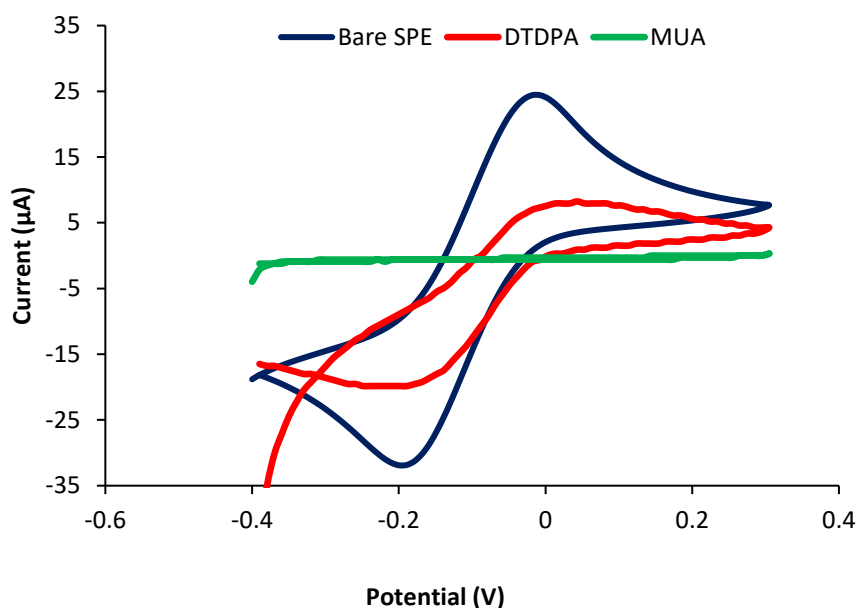


**Figure 2-14:** Profile of performance of JD 1, JD 2a and JD 2b gold working electrodes at scan rates of 10-100 mV s<sup>-1</sup>. The average of two scans was used to compute these results.

However, JD 2b batches showing greater similarity between batches, while JD 1 batch shows higher signal response. JD 2b produced in 2015-2016 was more available and was therefore used in further work on malaria immunosensor development prior to which evaluation of the mediator / substrate system was conducted.

#### **2.4.1 CV analysis of modified JD 2b SPGE against potassium ferricyanide**

Self-assembled monolayers (SAM) of organic molecules are molecular assemblies formed spontaneously on surfaces by adsorption and are organized into more or less large ordered domains (Love et al., 2005). Such a SAM consists of a head group, tail and functional end group. Common head groups include thiols, silanes and phosphonates. Long-chain alkane thiols (11-Mercaptoundecanoic acid) produce more ordered self-assembled monolayers (SAMs) than those with shorter chains (Dithiodipropionic Acid). The thiol groups chemically adsorb onto the gold surface by the formation of a thiolate bond. Attractive Van der Waals forces between the alkyl thiol chains enhance the stability and orders of the self-assembled monolayer (Bain et al., 1989). Thiol deposition and bare SPGE characterization were compared to make selection of the suitable immobilization method (Figure 2.15).



**Figure 2-15:** Cyclic voltammogram with 1 mM potassium ferricyanide on JD 2b. Percentage active area of gold working electrode after deposition of the thiol monolayer on the SPGE JD 2b using potassium ferricyanide 1 mM at 50 mV s<sup>-1</sup> scan rate. Average of two scans was used.

The calculation of active area based on Randles-Sevcik equation was used to assess performance of the gold surface after adsorption of the thiol monolayer. A percentage of non-active area towards the geometric area suggests the successful deposition of monolayer on gold sensor (Table 2.11).

**Table 2-11:** Effect of surface chemistry modification

	$I_{PC}$ ( $\mu A$ )	$A_{geometric}$ ( $cm^2$ )	Aactive %	% Inactive
Bare SPE	$-33.36 \pm 0.03$	0.226	76.73	23.27
3,3'-dithiodipropionic acid (DTDPA)	$-23.27 \pm 0.01$	0.226	29.29	70.71
11-mercaptoundecanoic acid (MUA)	-	0.226	-	-

According to these results, adsorption is the recommended immobilization method for bioreagents on the SPGE surface. The thiols block mass transfer process thus not allowing electron transfer on the working electrode surface and produce a low peak height. Highest peak average height is seen in the bare SPGEs as a result of the high activity recorded.

With the MUA, there were no visible peaks to show the redox reaction. Two SPGEs were scanned at  $50 \text{ mV s}^{-1}$  using potassium ferricyanide as the mediator and 1 M KCl as the supporting electrolyte and the average taken for calculation of the active surface area.

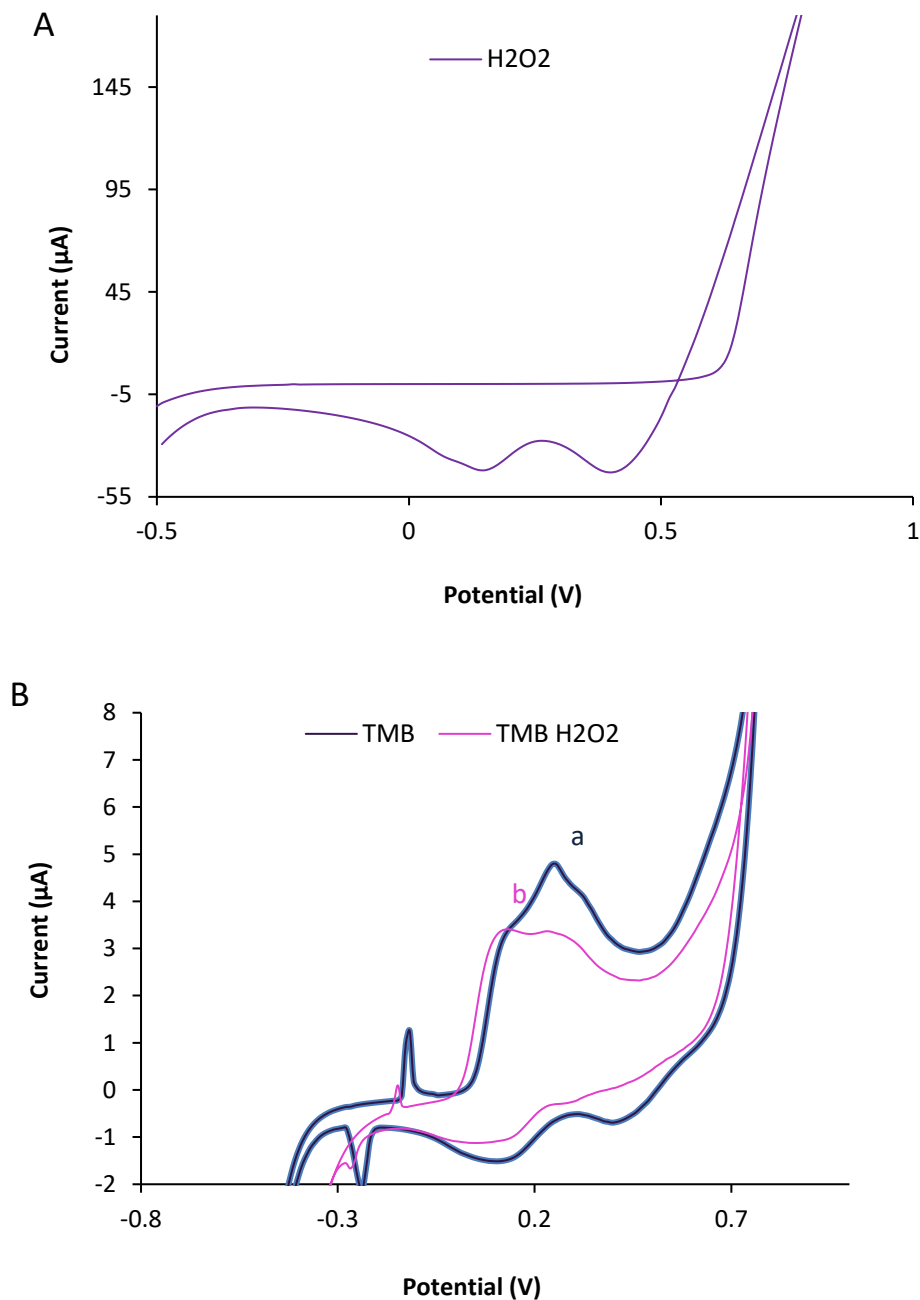
The bare SPGE had the highest available area for the reaction to take place on while the modified electrodes showed the lowest response showing the blocking of the electrode and hindrance to the transport of electrons during the oxidation and reduction of mediator.

As expected, monolayer coating on gold electrode surface normally used to provide an effective coupling with biosensing component on the transducer surface and reduce non-specific binding. It is therefore important to test the integrity and properties of such layered structure on gold surface when considering suitable immobilization methods.

Covalent bonding methods will however not be used in the development of the immunosensor due to low active surface area compared to active surface area of the bare SPGE.

#### **2.4.2 TMB / H<sub>2</sub>O<sub>2</sub> System**

With advent of the second generation of biosensors, hydrogen peroxide became the oxidizing agent (Eggins, 1996). H<sub>2</sub>O<sub>2</sub> is a strong oxidising agent that works well, with the mediator, TMB in a system suited to detecting activity of horse radish peroxidase conjugated biomolecules. The characterization was conducted according to a previous method (Binder, 2014) described in section 2.3.6. Results show H<sub>2</sub>O<sub>2</sub> alone (Figure 2.16 A) and with TMB (2.16 B).



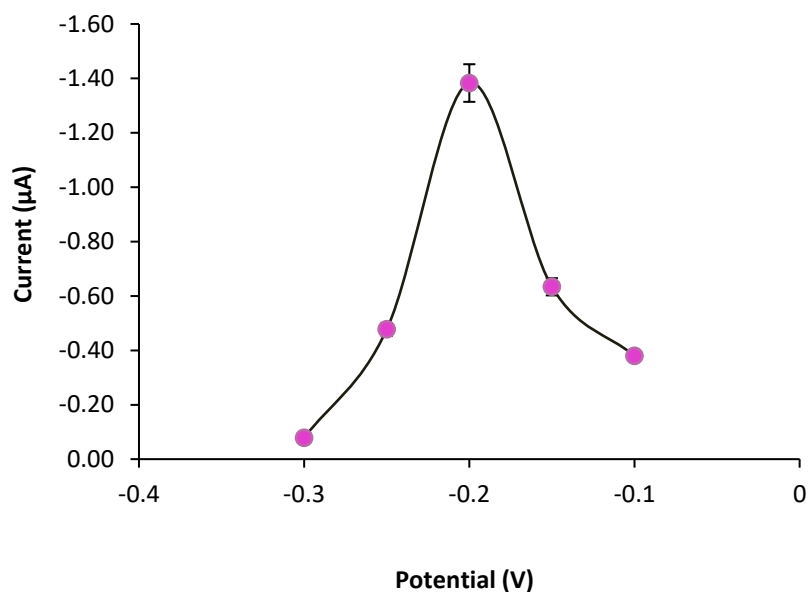
**Figure 2-16:** Characterization CV of H<sub>2</sub>O<sub>2</sub> (A) and TMB / H<sub>2</sub>O<sub>2</sub> system on JD 2b (B). The TMB / H<sub>2</sub>O<sub>2</sub> system for signal generation was characterized using cyclic voltammetry with a bandwidth ranging from -0.3 to 0.8 V at ambient temperature. The 100 μL working solution comprised 10 μL of TMB solution (0.6 M) and 10 μL 1:10 (30%) hydrogen peroxide diluted in 480 μL of working buffer (1:1 KCl and 0.05 M phosphate citrate buffer, pH 5).

The scan rate was constant at 20 mV s<sup>-1</sup> during the scan. Oxidizing agent alone gives a higher peak than in solution with TMB. During electrolysis, working electrode acts as an anode or cathode, according to the analyte. When using

H<sub>2</sub>O<sub>2</sub> as an oxidising agent, the gold working electrode is an anode, polarized to a positive potential. H<sub>2</sub>O<sub>2</sub> acts to transport electrons to the substrate. In contrast, when oxygen is monitored, working electrode is polarized to a negative potential. The applied step potential is reliant upon the material the electrode is fabricated from (Wollenberger, 2008). It follows that for every biosensor set up, the step potential for chronoamperometric measurements must be analysed in order to determine the optimal potential for the assay.

### **2.4.3 Confirmation of suitable potential for the JD 2b electrode**

Amperometry is the determination of the intensity of current crossing an electrochemical cell under an imposed potential. This intensity is a function of the concentration of the electrochemically active species in the sample. Different step potentials ranging from -0.3 to -0.1 V confirmed HRP / TMB-H<sub>2</sub>O<sub>2</sub> system for best signal to noise ratio as described in section 2.3.6. With enzyme addition, the current at which this potential was obtained was -1.4  $\mu$ A (Figure 2.17).



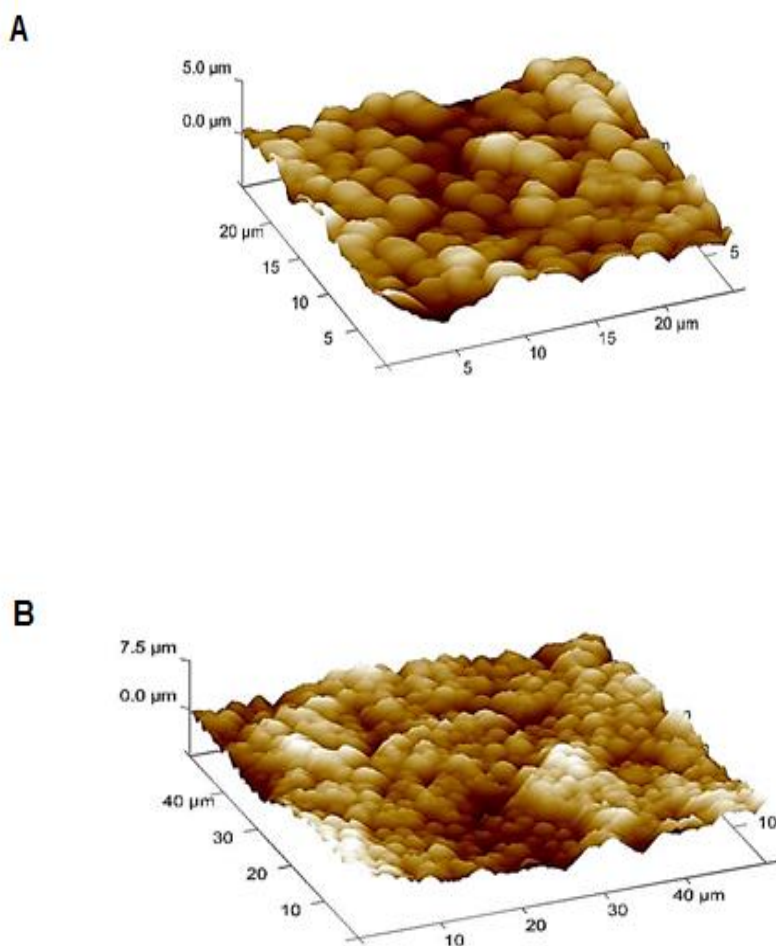
**Figure 2-17:** Determination of a suitable potential. The measurement was normalized by first obtaining baseline current of the TMB / H<sub>2</sub>O<sub>2</sub> system at each potential then injecting monoclonal antibody-HRP conjugated (10 µg mL<sup>-1</sup>) at 100 s. at ambient temperature between 18°C and 25°C. Results were calculated from 10 measurements before and after enzyme addition. Blank response subtracted from the measurement produced the signal for the optimal current for the system as -1.4 µA.

The experiment was conducted as described in section 2.4.3. Following the initial baseline signal of the TMB–H<sub>2</sub>O<sub>2</sub> system and injection of HRP - conjugated monoclonal antibody (10 µg mL<sup>-1</sup>), results were calculated from 10 measurements before and after enzyme addition. Blank response subtracted from the measurement yielded the optimal current for the TMB / H<sub>2</sub>O<sub>2</sub> – HRP system. From the results shown in Figure 2.17, optimum potential (-0.2 V) was used for further experiments.

#### 2.4.4 Atomic Force Microscopy

Electrode surface construct is a major factor in the performance it exhibits in analytical work (Arya et al., 2007). The surface of the working electrode is therefore studied prior to assay development to establish an understanding of its structure to discuss performance in assay development (Davies et al., 1988). In order to obtain an image which shows the surface roughness of the gold working electrode (diameter 5 mm), the atomic force microscope Digital

Instruments (NY, USA) was used to visualize the surface of the bare SPGE in two measurements (25 and 50)  $\mu$  to show the topography of the gold working electrode (Figure 2.18).



**Figure 2-18:** AFM image of bare JD 2b SPGE at 25  $\mu$ m (A) and 50  $\mu$ m (B). Images show the uneven surface of the gold working electrode prior to antibody immobilization.

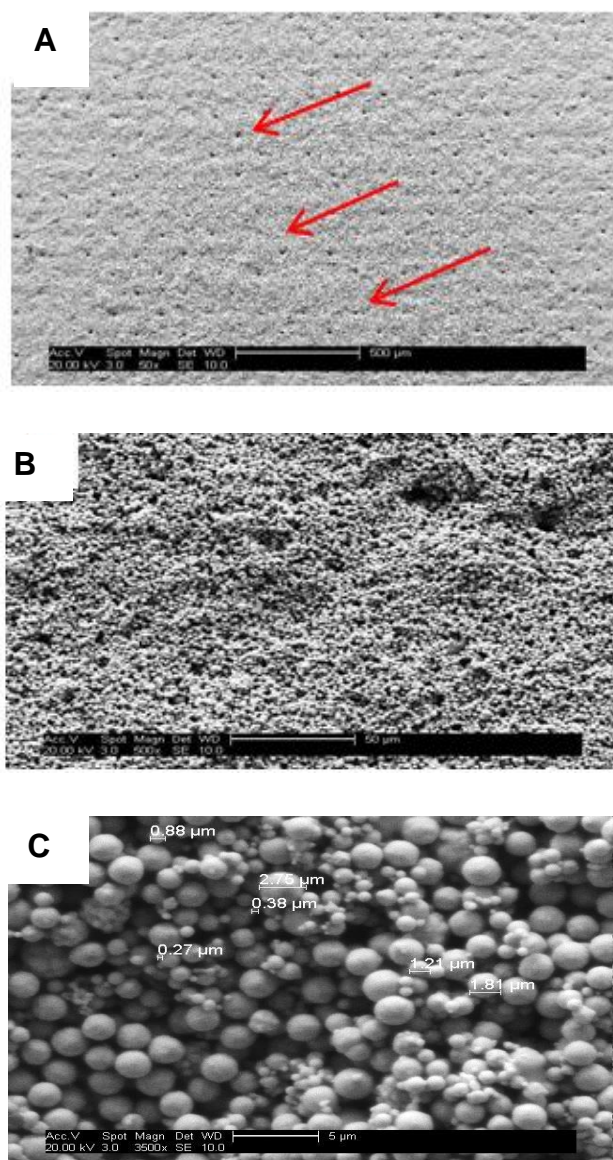
### 2.4.5 Scanning Electron Microscopy

Scanning electron microscopy is a tool used to visualize the surface structure of a dry sample in a vacuum (Todokoro and Ezumi, 1999). The SEM (Phillips, UK)



was used to obtain an image of the surface of the bare working electrode. SEM of JD SPGE shows a homogenous distribution of gold ink with round ink granules, producing a maximized surface area.

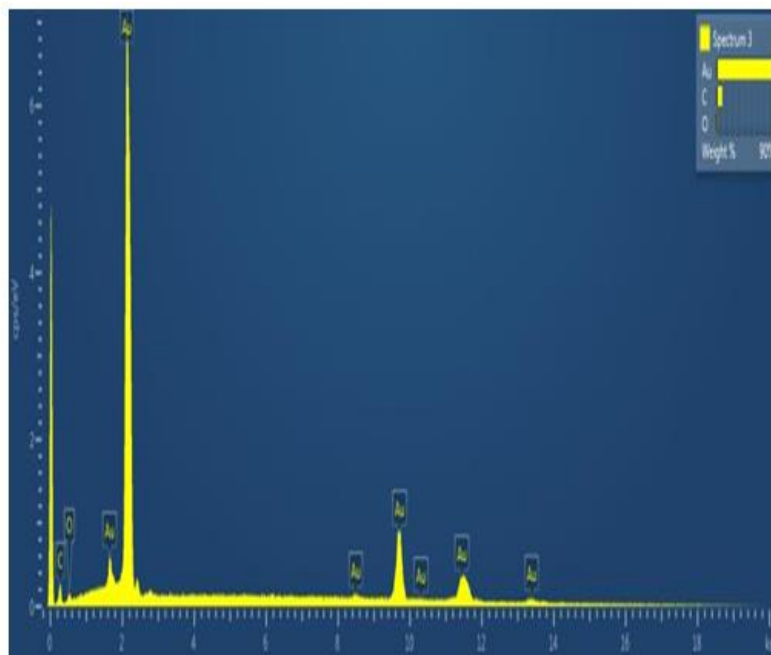
(Figure 2.19).



**Figure 2-19:** SEM of JD 2b bare SPGE 50x magnification (A) enlarged to 500x (B) and 3,500x magnification (C). Arrows show lithographic pattern.

### 2.4.6 Electron Emission Spectrum of the Bare SPGE

Emitted electrons evaluate composition of the element on the SPGE. The working electrode was analysed at a working distance of 10.3 mm (Figure 2.20).



**Figure 2-20:** Elemental composition of bare SPGE using electron emission spectrum. The average of three scans showed 89.14 % gold, 9.28 % carbon and 1.59 % oxygen.

The electron emission spectrum was obtained using the Environmental Scanning Electron Microscope to determine the elemental presence on the SPGE. The image was obtained after the three electrode system was cured in an oven at 120°C for 30 minutes. The sample was prepped by cutting off the ethylene substrate around the leads and applying an adhesive beneath to stabilize the sample on the stage.

## 2.5 CONCLUSIONS

This chapter describes the successful characterization of three batches of JD gold screen-printed electrodes for use in the development of vector-borne malaria rapid, low cost, highly sensitive immunosensor. DuPont screen-printed electrodes show quasi-reversibility with potassium ferricyanide 0.1, 0.5 and 1

mM. The highest 1 mM concentration of potassium ferricyanide is recommended for optimizations involving gold screen-printed electrode at a band width of -0.4 to 3 V.

All batches of electrode demonstrate stability in active percentage working area within a range of production dates. This characteristic is essential if low cost screen-printed electrodes are to be utilised over a period of time. Cost of production can be controlled by dark storage to prevent possible oxidation of the Ag Ag/Cl reference electrode. Gold working electrode and Ag/AgCl reference electrode are not adversely affected by the strong oxidizing agent in KCl supporting electrolyte.

TMB / H<sub>2</sub>O<sub>2</sub> as the mediator / substrate system is confirmed a suitable medium for electron transfer in redox reaction. The system will therefore be suitable for use in detection of low current signals during biomolecular oxidation on the anode. The working electrode surface texture is potentially suitable for direct immobilization of the primary biomolecule due to the large surface area provided by the granular gold seen by AFM at 25 and 50 nm. The high proportion of gold ink on the screen-printed electrode reduces non-specific binding and increases sensor sensitivity. This comprehensive study highlights great potential of SPGE for malaria immunosensor development. The SPGE was used to continue the work in optimization experiments.



## **CHAPTER THREE**

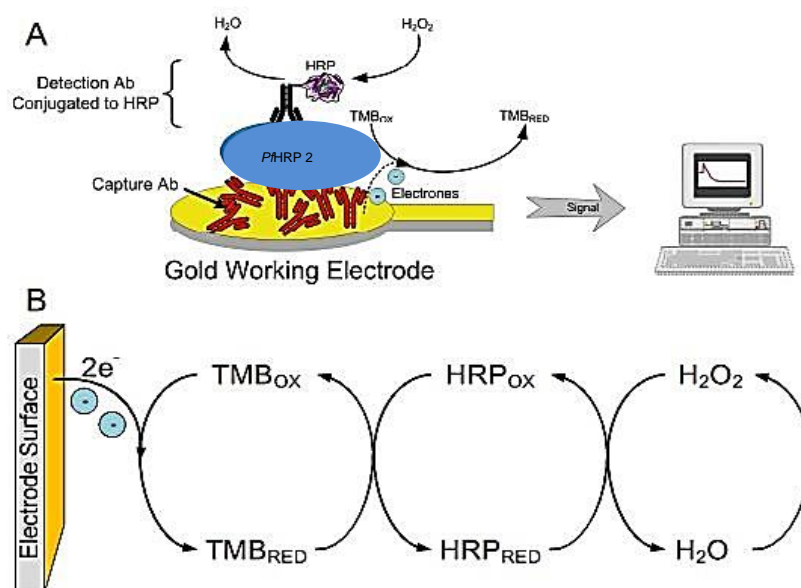
### **DEVELOPMENT OF *Plasmodium falciparum* HISTIDINE RICH PROTEIN 2 IMMUNOSENSOR**



### 3 ELECTROCHEMICAL IMMUNOSENSOR FOR P<sup>h</sup>HRP 2

#### 3.1 INTRODUCTION

Electrochemical immunosensors are effective mechanisms for evaluating affinity assays because they are reliable, show good reproducibility and high sensitivity (Iqbal et al., 2002; Tothill, 2003; Davies et al., 2007; Sharma et al., 2008; Tothill, 2009; Sharma et al., 2010; Wan et al., 2013; Mistry et al., 2014 ). Most electrochemical immunosensors rely on enzymes to catalyse reaction of substrate such that electrons are either produced or utilized in a redox reaction. Electroactive region of many enzymes are found within their structure, affecting electron transfer (Figure 3.1).



**Figure 3-1:** Working principle of the immunosensor with HRP as the electroactive species (adapted from Binder, 2014).

Electron transfer may also be affected by surface immobilization or orientation of the molecule (Newman and Turner, 2007). Redox couples, mediators act as transporters between redox centre and enzyme (Cass et al., 1984) however some enzymes or redox proteins overcome steric insulation of the protein

matrix. With electrodes, bio catalytic transformation of the enzyme is stimulated to drive the substrate nearer the enzyme's active site for non-mediated electron transfer (Arya et al., 2007). The most common examples of the enzymes employed in amperometric detection are glucose oxidase, lactate oxidase and alkaline phosphatase (Arya et al., 2007).

DNA-based electrochemical sensors have also been developed. Various materials like carbon paste, pyrolytic graphite, glassy carbon, carbon fibre and carbon nanotubes have been used to immobilize the DNA of organisms (Vo-Dinh and Cullum, 2000; McKeague and DeRosa, 2012). Nucleic acid-based biosensors have an acquired attraction that exists between complementary regions of aligned nucleotide sequences (Stadtherr et al., 2005; Borgmann et al., 2011). The most commonly utilized screen-printed electrodes (SPEs) are constructed of graphite and carbon black particles (Meters et al., 2011). Research-based immunosensors for parasitic infection, *Salmonella typhimurium*, *Campylobacter jejuni*, *Escherichia. coli*, *Staphylococcus aureus*, Enterococcus species, Botyllium toxin and malaria proteins have been reported (Iqbal et al., 2002).

In this study, horseradish peroxidase (HRP) as a conjugate on the detection antibody was used as the enzyme label. TMB / H<sub>2</sub>O<sub>2</sub> (mediator / substrate) complex was used as the electroactive substance for signal generation. TMB provides a safe and sensitive substrate for HRP when compared with O-phenylenediamine (OPD) (Fanjul-Bolado et al., 2005). The assessment of reaction relies on consumption of electrochemical species. Several researchers have proposed biosensor and bioelectronics designs using feature phones for portable healthcare diagnostics outside well-resource laboratories (Martinez et al., 2008, Breslauer et al., 2009; Tseng et al., 2010).

*Pf*HRP 2 has a histidine and alanine-rich composition with repetitive epitopes. Multiple B-cell epitopes arranged in tandem repeats of AHHAAD interspersed with AHH and AHHA allow easy detection by an antigen capture assay (Taylor and Voller, 1993; Sharma et al., 2008; Azikiwe et al., 2012; Perraut et al., 2014). *Pf*HRP 2 is synthesized by asexual and early sexual stages of the parasite and



exported through the erythrocyte cytoplasm and surface membrane to accumulate in the extracellular plasma (Kifude et al, 1986). Blood levels for *Pf*HRP 2 are  $\sim 9.45 \text{ ng mL}^{-1}$  (Ho et al., 2014, Dzakah et al., 2014; Abdallah et al., 2015). *Pf*HRP 2 has a long half-life and persists in the circulation for up to 3 weeks after parasite clearance, reducing its utility for active infection diagnosis but increasing its potential as a serological marker of infection history (Dondorp et al., 2005).

ELISA analysers are widely used in clinical diagnostics (Mistry et al., 2014). There still remains however, the need for species-specific, reliable and cheap yet highly sensitive detection methods suitable for use by non specialists (Munge et al., 2010; Sharma et al., 2010). ELISA assay with increased sensitivity is achieved by nanomaterials: magnetic nanoparticles, carbon nanotubes, photonic crystals, quantum dots and gold nanoparticles (AuNP). When proteins and enzymes are adsorbed onto gold nanoparticles, their bioactivity is retained. AuNP are often cited in literature due to their unique properties: large surface area and excellent biocompatibility (Bharathi and Nogami, 2001).

This chapter directs efforts at development of sandwich ELISA in buffer and serum on screen-printed electrodes, enhanced with gold nanoparticle-conjugated antibodies raised against *Pf*HRP 2 and evaluation of their immunosensing performance in amperometric detection.

## **3.2 MATERIALS**

### **3.2.1 General chemicals and instrumentation**

Potassium chloride (pH 7.4), 3,3',5,5'-tetramethyl benzidine hydrochloride (TMB), sodium carbonate, sodium bicarbonate, sodium acetate (0.2 M), hydrogen peroxide 30 % (w/w), phosphate citrate buffer tablets, plastic petri dishes, human serum (P2918) and colloidal gold (40 nm) were purchased from Sigma (Dorset, UK). Albumin from bovine serum (BSA), phosphate buffered saline tablets (PBS, 0.01 M phosphate buffer, 0.137 M sodium chloride and

0.0027 M potassium chloride, pH 7.4), Tween-20 and sulphuric acid (H<sub>2</sub>SO<sub>4</sub>, 95-98 %), 1-step Ultra TMB-ELISA was purchased from Thermo Fischer Scientific (MA, U.S.A.). Double-distilled ultrapure water produced by a Millipore Direct-Q® 3 UV (Millipore; Molsheim, France). Milk blocking solution concentrate was purchased from KPL (Gaithersburg, USA).

Human monoclonal capture antibody (*Plasmodium falciparum* HCA 160), detection antibody (horse radish peroxidase-conjugated *Plasmodium falciparum* HCA 159 P) and *Plasmodium falciparum* recombinant protein (PIP001) were purchased from AbDSerotec, now Bio-Rad (Kidlington, UK).

JD 2b Gold screen-printed Electrodes (SPGE) consisting of gold working electrode, carbon counter and silver–silver chloride pseudo-reference electrode were fabricated using a procedure similar to that described by Noh and Tothill (2006), and printed using the screen-printing facilities at DuPont (DuPont Microcircuit Materials, Bristol, UK). Three electrode batches JD1, JD 2a and JD 2b was characterized (Chapter 2). Curing of electrodes was carried out in Carbolite oven, model PN 120 (200) (Hope, UK) while incubation at 37°C was carried out in a column oven (Shimadzu Corporation, Japan). Electrochemical procedures were conducted using a computer-controlled four channel Autolab electrochemical analyser multipotentiostat (Metrohm, The Netherlands) connected to an adapter (DropSens, Spain). USB box connecting the setup of equipment and General Purpose Electrochemical Software (GPES) version 4.9.007 were used. On multi-mode GPES, chronoamperometry was selected from the menu and parameters set for the appropriate measurement. Faraday cage was employed to reduce interference and Microsoft Excel was used to modify the curves.

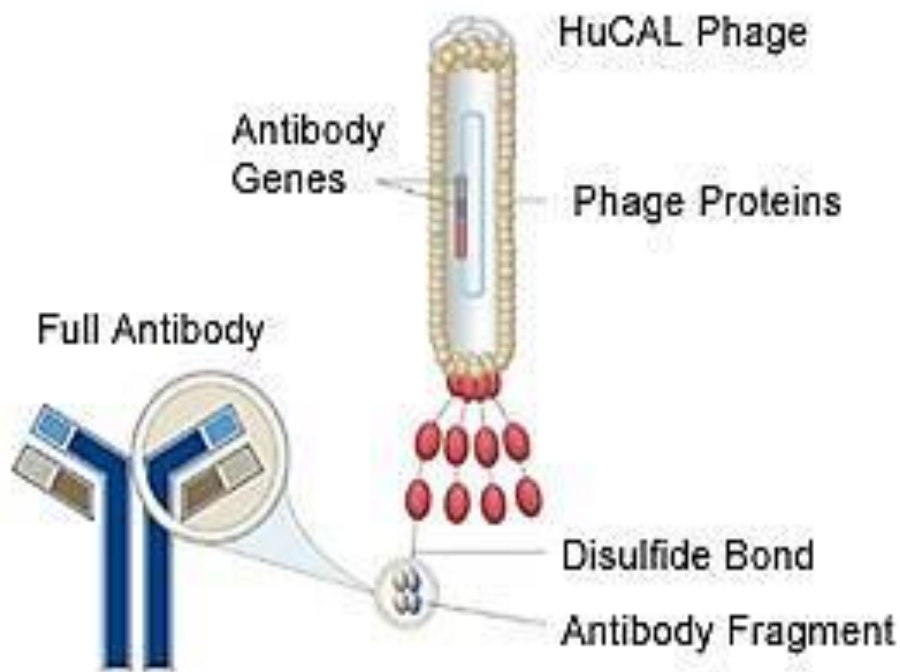
Zetasizer nano-s was obtained from Malvern Instruments (Malvern, UK). Electric pan balance (Mettler Toledo, UK) was used for buffer preparation. The vortex mixer model Genie 2 G-560E was purchased from Scientific Industries (Bohemia, USA). Centrifugation of samples was performed in Microfuge

Beckman (Alkonbury, UK). Transmission electron microscope, Phillips CM-20 (London, UK) was used to determine gold nanoparticle size. Absorbance measurements for ELISA were performed using varioskans plate reader while centrifugation was conducted in Heraeus Fresco 21 centrifuge obtained from Thermo Scientific (Waltham, U.S.A.). Microtiter plates, MaxiSorp (Nunc Immuno), were purchased from Thermo Fischer Scientific (Milton Keynes, UK). Incubation at 37°C was performed under a controlled environment provided by an incubator / shaker model iEMS 1415 (Labsystem, Helsinki, Finland).

### **3.3 METHODS**

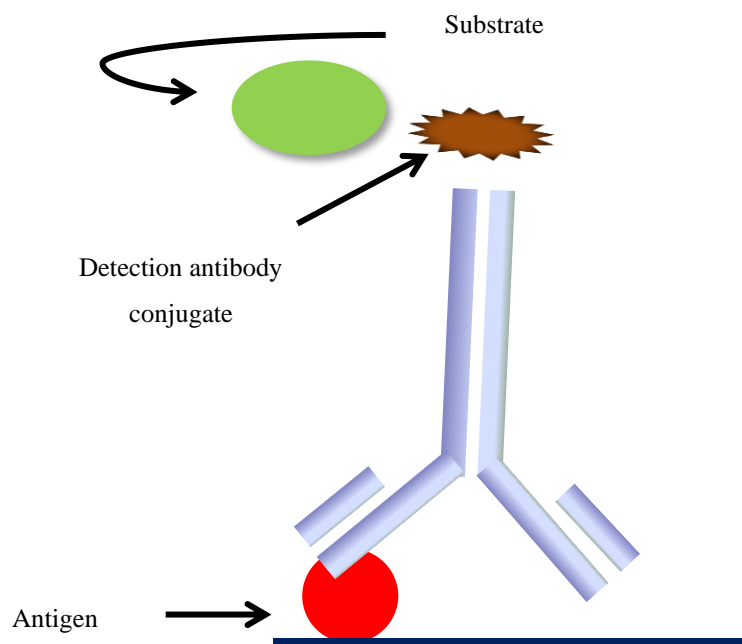
#### **3.3.1 Direct ELISA Assay**

Commercial monoclonal antibodies raised from phage display techniques (Zeitlin et al., 1999) using human combinatorial antibody library (HuCAL) with variable terminal amino acid sequences (Borman, 2000; Mahajan and Gupta, 2010; Perkel, 2012) for guided selection (Bio-Rad, 2016) were used (Figure 3.2).



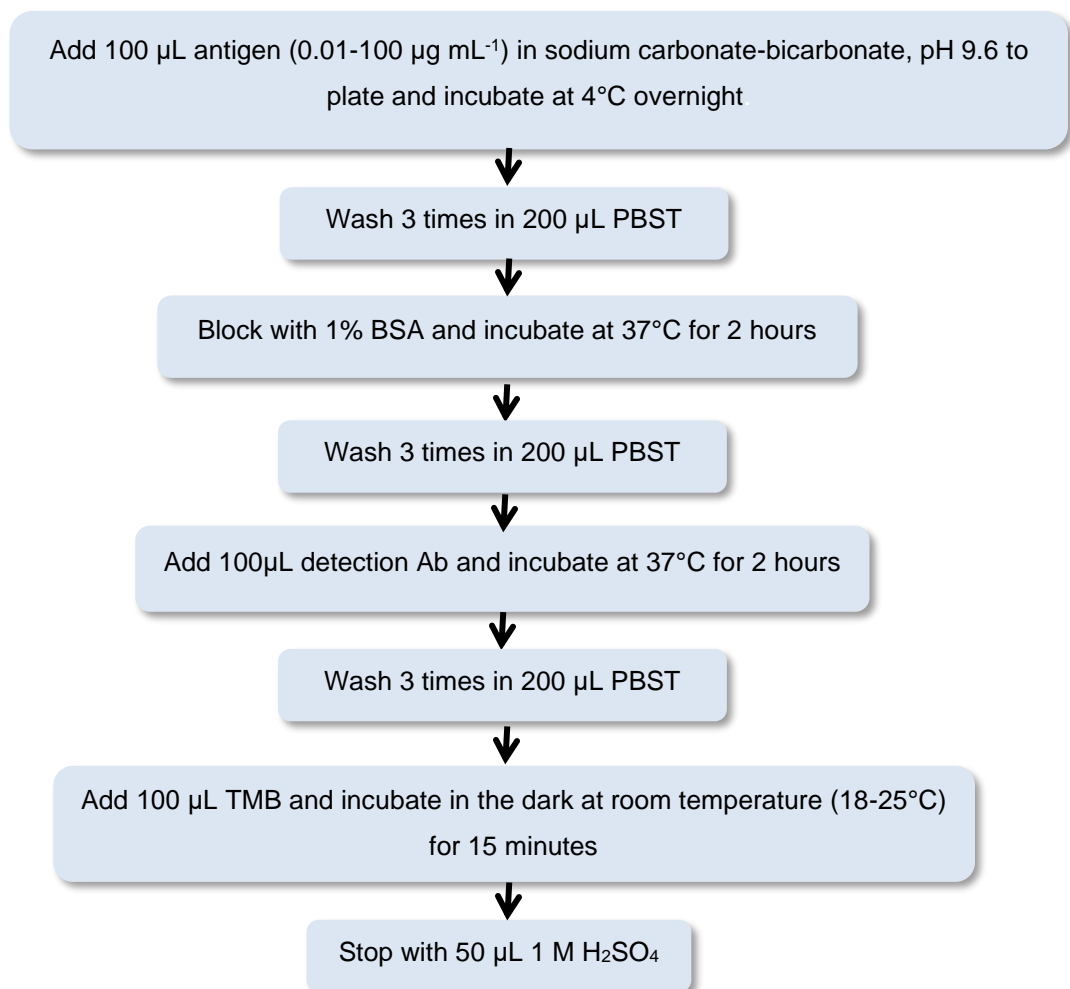
**Figure 3-2:** Human combinatorial antibody library (Bio-Rad, 2016). Fab region recombinant conjugates are generated through the use of viral proteins, removing the need to use animals in antibody generation.

Adsorption was used in this test for the attachment of the antigen on the plate surface was followed by addition of detection antibody conjugated with the enzyme. Specific recognition event between antibody and antigen was determined. The reactions were conducted in triplicate. Bio-Rad general ELISA protocol was adapted by changing quantity of blocking solution from 150  $\mu\text{L}$  to 100  $\mu\text{L}$  in ELISA detection of *Pf*HRP 2 antigen (Figure 3.3).



**Figure 3-3:** Schematic of a direct ELISA (adopted from Abcam.com, 2016). The antigen is first immobilized on the platform.

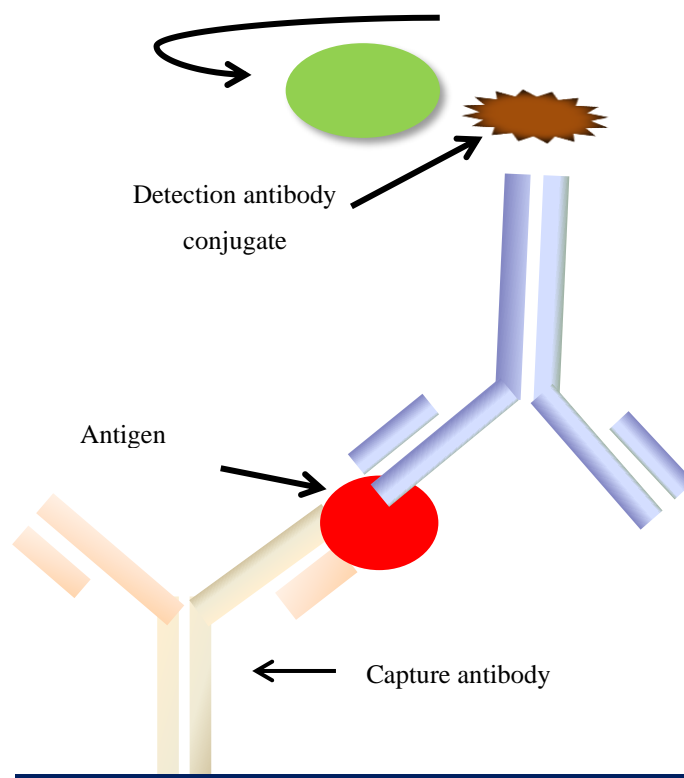
*Pf*HRP 2 recombinant protein (PIP001) was serially diluted in 0.1 M sodium carbonate-bicarbonate buffer (pH 9.6) producing  $100 \mu\text{g mL}^{-1}$ ,  $10 \mu\text{g mL}^{-1}$ ,  $1 \mu\text{g mL}^{-1}$ ,  $0.1 \mu\text{g mL}^{-1}$ ,  $0.01 \mu\text{g mL}^{-1}$ . The plate was washed 3 times with  $200 \mu\text{L}$  0.01 M PBST (phosphate buffered saline with 0.05 % Tween-20). Vacant spots on the plate were blocked with  $100 \mu\text{L}$  1% BSA and incubated at  $37^\circ\text{C}$  for 2 hours in ELISA plate incubator/shaker model iEMS 1415 (Labsystem, Helsinki, Finland). Wash step was repeated. A concentration of  $10 \mu\text{g mL}^{-1}$  detection antibody conjugated to horse radish peroxidase ( $100 \mu\text{L}$ ) was added to the wells and the plate incubated at  $37^\circ\text{C}$  for 2 hours. Wash step was repeated. A  $100 \mu\text{L}$  volume of 1-step Ultra TMB-ELISA was added to the wells and incubated at ambient temperature ( $18\text{-}25^\circ\text{C}$ ) for 15 minutes. The reaction was stopped using  $50 \mu\text{L}$  of 1 M  $\text{H}_2\text{SO}_4$ . Plate was then read at 450 nm wavelength using Varioskan plate reader (Thermo scientific, U.S.A.)(Figure 3.4).



**Figure 3-4:** Direct ELISA assay flow chart.

### 3.3.2 Sandwich assay

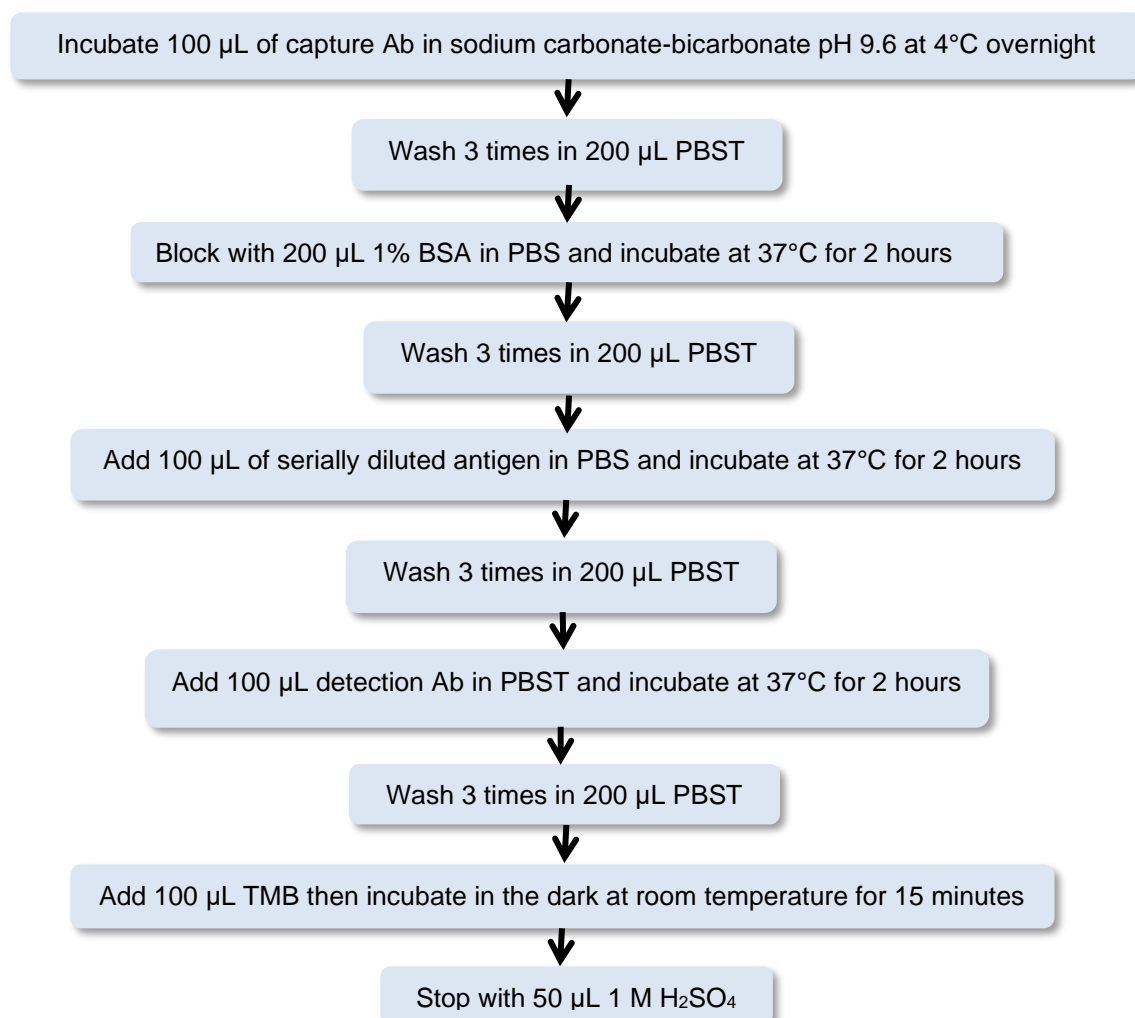
Sandwich ELISA development involves immobilization of the capture antibody on the platform. The antigen attaches via two epitopes between capture and detection antibodies (Figure 3.5).



**Figure 3-5:** Schematic sandwich ELISA format (adopted from Abcam.com, 2016). The capture antibody is immobilized first.

A 100  $\mu\text{L}$  of *Pf*HRP 2 capture antibody (HCA 160) original concentration 500  $\mu\text{g mL}^{-1}$  was dissolved in 900  $\mu\text{L}$  of 1 M sodium carbonate-bicarbonate buffer (pH 9.6) to give a concentration of 50  $\mu\text{g mL}^{-1}$ . A volume of 100  $\mu\text{L}$  of the capture antibody solution was added to microtitre plate wells in triplicate. Antigen concentrations 0.01  $\mu\text{g mL}^{-1}$ , 0.1  $\mu\text{g mL}^{-1}$ , 1  $\mu\text{g mL}^{-1}$ , 10  $\mu\text{g mL}^{-1}$  and 100  $\mu\text{g mL}^{-1}$  of *Pf*HRP2 recombinant protein (PIP001) were serially diluted in PBS (0.01 M). A 200  $\mu\text{L}$  volume of PBST, 0.01 M, pH, 7.4, Tween (0.05 v/v) was used to reduce non specific binding. A concentration of 20  $\mu\text{g mL}^{-1}$  detection antibody conjugated to horse radish peroxidase (100  $\mu\text{L}$ ) was added to the wells and the plate incubated at 37°C for 2 hours. Wash step was repeated. A 100  $\mu\text{L}$  volume of 1-step Ultra TMB-ELISA was added to the wells and incubated at ambient temperature (18-25°C) for 15 minutes. The reaction was stopped using 50  $\mu\text{L}$  of 1 M  $\text{H}_2\text{SO}_4$ . Plate was then read at 450 nm wavelength using

Varioskan plate reader (Thermo scientific, U.S.A.). Summary of the process is in Figure 3.6.



**Figure 3-6:** Sandwich assay flow chart.

### 3.3.3 Capture antibody optimization (HCA 160) on JD 2b sensor.

Prior to the immobilization, sensors were cured at 120 °C in an oven [Carbolite, model PN 120 (200), Hope, UK] for 30 min at 120 °C. The surface was gently washed with 1000 μL PBST (0.05 v/v) pH 7.4, followed by 1000 μL ultra-pure water (18.2 mΩ) and dried in gentle nitrogen stream. To obtain a saturated surface with an optimal amount of immobilized antibodies, the working electrode was coated with 20 μL P<sub>1</sub>HRP 2 capture antibody with concentrations of 10, 20 and 30 μg mL<sup>-1</sup> using sodium carbonate-bicarbonate buffer (1 M, pH 9.6). Capture antibody was incubated at 4°C overnight. A volume of 100 μL 1:10



milk protein concentrate (KPL Inc., Gaithersburg, USA) was used to cover all three electrodes to reduce non-specific binding and incubated for 1 hour at 37 °C in a column oven Shimadzu Corporation (Kyoto, Japan) according to the method of Binder (2014). The wash step was repeated after which 30  $\mu\text{g mL}^{-1}$  *Pf*HRP 2 antigen (PIP001) original concentration 1000  $\mu\text{g mL}^{-1}$  was prepared in 1:10 milk protein concentrate (KPL Inc., Gaithersburg, USA). A 20  $\mu\text{L}$  volume was dropped on the working electrode and incubated for 1 hour at 37°C. The purified detection antibody with horse radish peroxidase conjugated (HCA 159 P) original concentration 100  $\mu\text{g mL}^{-1}$  was diluted to a working strength of 30  $\mu\text{g mL}^{-1}$  in 1:40 milk concentrate / PBS (0.01 M, pH 7.4) and incubated for 1 hour at 37 °C. A volume of 20  $\mu\text{L}$  dropped on the working electrode and incubated for 1 hour at 37°C.

Before starting the amperometric measurement, 100  $\mu\text{L}$  of the TMB /  $\text{H}_2\text{O}_2$  (mediator / substrate) were dropped on the sensor surface covering all three electrodes (Chapter 2, section 2.3.6). After dropping the substrate on the electrode, the pipette tip was changed to avoid contamination of the TMB / $\text{H}_2\text{O}_2$  stock with mobilized HRP from the sensor surface. Care was also taken not to touch the treated SPGE.

#### **3.3.4 Detection antibody optimization on JD 2b SPGE**

The procedure was repeated as in section 3.3.3. A 20  $\mu\text{L}$  volume of *Pf*HRP 2 capture antibody (20  $\mu\text{g mL}^{-1}$ ) in sodium carbonate-bicarbonate buffer (1 M, pH 9.6), was immobilized on the working electrode. After each incubation and washing, 20  $\mu\text{g mL}^{-1}$  *Pf*HRP 2 antigen was prepared in 1: 10 milk / PBS and 20  $\mu\text{L}$  was dropped on the working electrode. In order to determine concentration of detection antibody effect on recognition event, purified detection antibody was diluted to working strengths of 10, 20 and 30  $\mu\text{g mL}^{-1}$  in 1: 40 milk PBS. The optimal detection antibody concentration was used in the antigen titre.

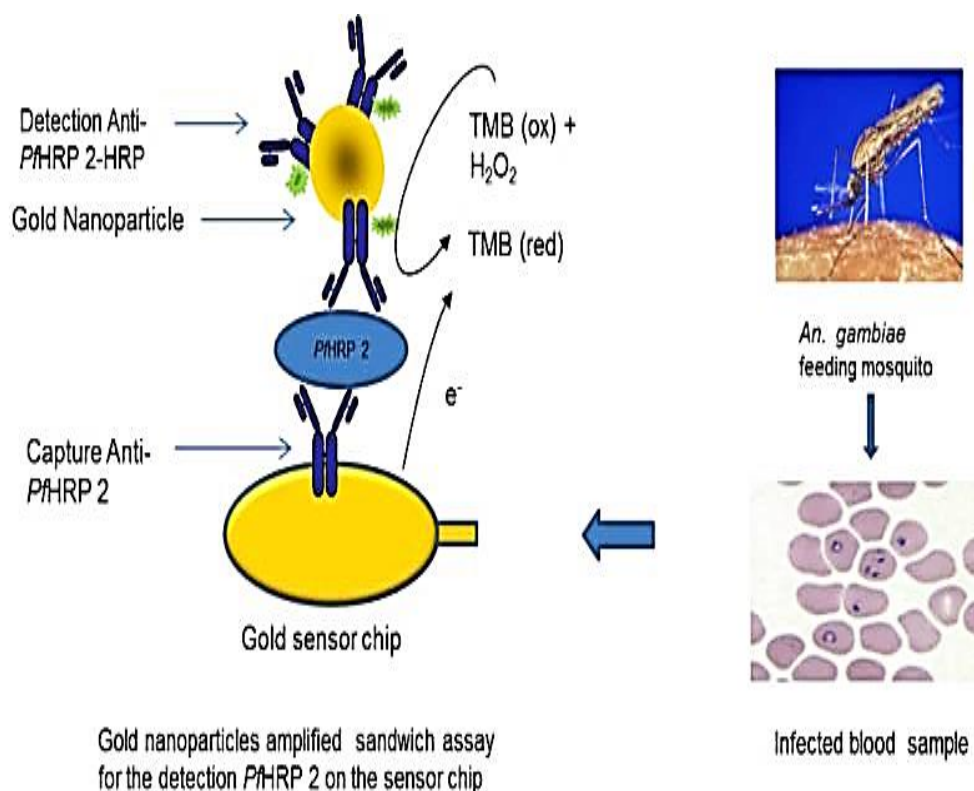
#### **3.3.5 Standard curve for *Pf*HRP 2 antigen (PIP001) in buffer**

To determine lowest detectable concentration of *Pf*HRP 2 antigen, 20  $\mu\text{L}$  *Pf*HRP 2 capture antibody with a concentration of 20  $\mu\text{g mL}^{-1}$  in sodium carbonate-bicarbonate buffer (1 M, pH 9.6), was immobilized on the working electrode.

After incubation, washing, and blocking, concentrations of 0, 2, 16, 20, 40, 64, 80 and 100 ng mL<sup>-1</sup> *PfHRP 2* antigen was prepared 1:10 milk / PBS (0.01 M) and 20 µL of the antigen solution was dropped on the working electrode. The detection antibody (*PfHRP 2*) was diluted to a working strength of 20 µg mL<sup>-1</sup> in PBST. Low detection limit (LOD) of antigen was calculated as (3 x SD of the blank measurement) + (average blank measurement) and interpolated in GraphPad prism (version 5). The curve was plotted using Microsoft Excel.

### 3.3.6 Signal enhancement using gold nanoparticles

AuNP (40 nm) were used in this research. Horse radish peroxidase is oxidized and then reduced when an electric current is applied at a fixed potential (-0.2 V) and signal enhancement occurs with binding of HRP-conjugated reporter protein to gold particles (Figure 3.7).



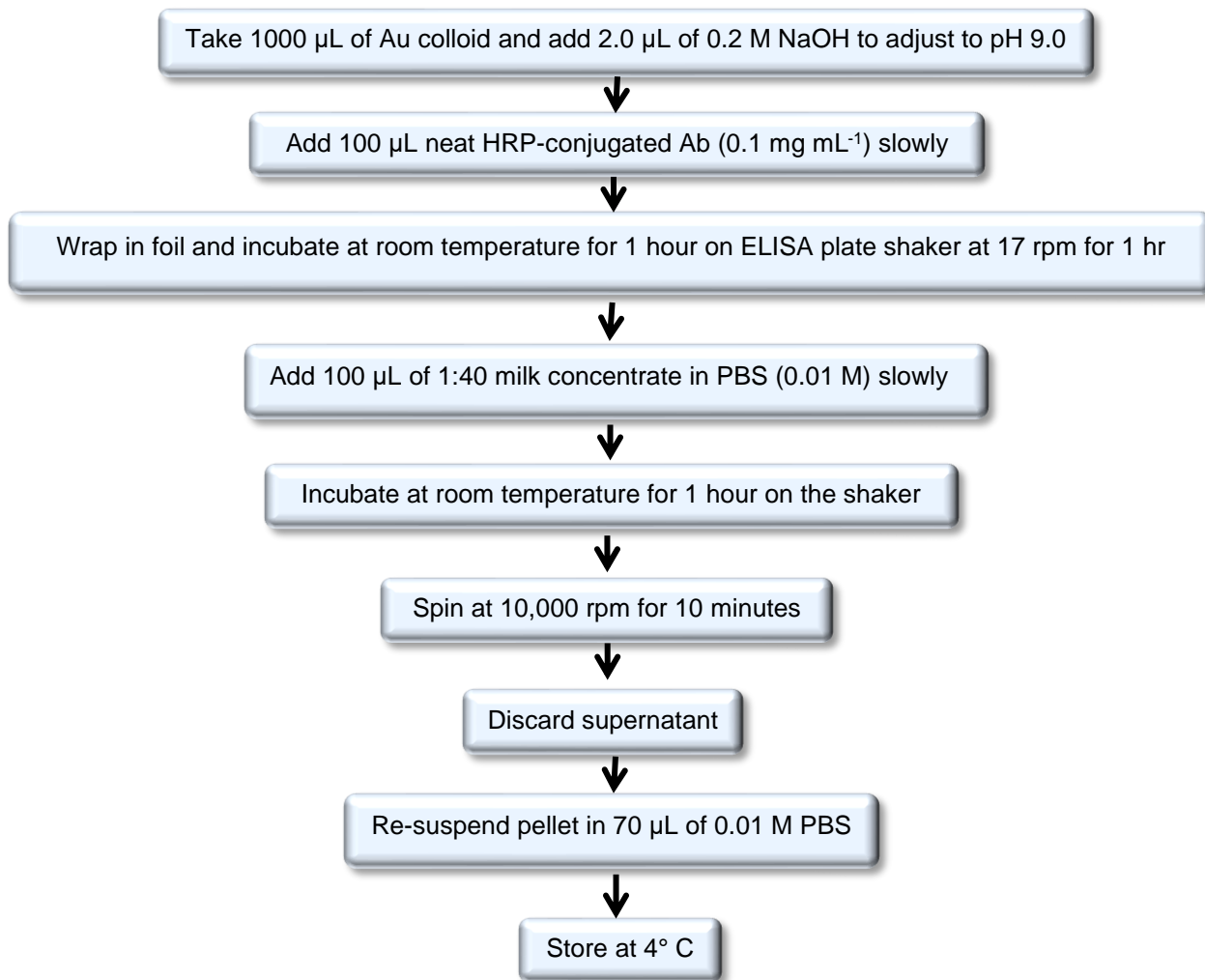
**Figure 3-7:** AuNP detection of malaria antigen. Malaria mosquito transmits the Plasmodium parasite. The parasite produces the soluble biomarkers during red blood cell stages of its development. These biomarkers have been detected in sandwich assay format on the DuPont SPGE using horse radish peroxidase as the enzyme label on detection antibody. On application of current at optimal potential, a signal is

measured in  $\mu\text{A}$ , proportional to the amount of target analyte present in sample. The enhanced assay makes use of gold nanoparticles to enhance the signal.

To confirm size and polydispersity index (PDI) of commercial colloidal AuNP (40 nm), a 100  $\mu\text{L}$  volume AuNP was taken in 1000  $\mu\text{L}$  PBS. Particles were dispersed by sonication using SONIC 6MX; James Products Europe (Dorset, UK) for 1 minute at 37 KHz at 40% power (24°C). Readings were taken using Zetasizer nano -s.

### **3.3.7 AuNP conjugation to detection antibody (HCA 159 P)**

Conjugation of the colloidal gold to the reporter protein was carried out according to the modified method of Salam and Tothill (2009) excluding add-in enzyme. A 1000  $\mu\text{L}$  quantity of gold colloid was taken in a 2 mL tube and 2  $\mu\text{L}$  0.2 M NaOH was added, adjusting pH to 9.0. A 100  $\mu\text{L}$  volume of neat (0.1 mg  $\text{mL}^{-1}$ ) detection antibody (HCA 159 P) was added slowly. The tube containing mixture was wrapped in foil and incubated on ELISA plate incubator/shaker model iEMS 1415 LabSystem (Helsinki, Finland) at 16-17 rpm, at room temperature (18-25°C) in the dark for 1 hour. Blocking buffer (100  $\mu\text{L}$ ) 1:40 milk in PBS (0.01 M) was added. The tube was incubated as again on ELISA plate incubator / shaker. Centrifugation was at 10,000 rpm for 10 minutes (4°C) in Heraeus Fresco 21 centrifuge Thermo Scientific (Waltham, U.S.A) for 1 hour. Supernatant was discarded and pellet re-suspended in 70  $\mu\text{L}$  PBS (0.01 M). Stock AuNP conjugated to detection antibody was stored at 4°C (Figure 3.8). NaCl (2.5 M) and the Au-conjugated Ab were mixed 1:1 proportion to test for conjugation. A pink colour should be seen as opposed to purple colour if conjugation is not successful. Further investigation of the binding affinity of the sandwich pair for the antigen was carried out. For this work, free horse radish peroxidase was not added.



**Figure 3-8:** Flow diagram of AuNP conjugation to detection antibody (HCA 159 P).

### 3.3.8 *Pf*HRP 2 detection limit using AuNP

To determine assay sensitivity, *Pf*HRP 2 capture antibody with a concentration of 20 µg mL<sup>-1</sup> in sodium carbonate-bicarbonate buffer (1 M, pH 9.6), was immobilized on the WE according to method in section 3.3.3. Antigen concentrations were however assayed at 0.05 ng mL<sup>-1</sup>, 0.1 ng mL<sup>-1</sup>, 0.2 ng mL<sup>-1</sup>, 0.3 ng mL<sup>-1</sup>, 0.4 ng mL<sup>-1</sup> and 0.5 ng mL<sup>-1</sup>. To detect the antigen, in amplified assay, 20 µL of AuNP- detection antibody stock (1:10) in PBS (0.01 M) was dropped on the sensor (Figure 3.8). Lowest detection of antigen was calculated

as (3 x SD of the blank measurement) + (average of the blank measurement) interpolated in GraphPad prism (version 5). The curve was plotted using Microsoft Excel.

### 3.3.9 Blocking agent

Milk concentrate, KPL (Gaithersburg, USA) in PBS 0.01 M (1:40) was used as blocking agent during the assay development on SPGE, to block the unoccupied spaces on the working electrode surface. A 1000  $\mu\text{L}$  quantity of gold colloid was taken in a 1.5 mL tube and 0.2 M NaOH was added, adjusting the pH to 9.0. The process was adopted from Salam and Tothill (2009).

### 3.3.10 *Pf*HRP 2 detection in 100% spiked serum

To obtain the limit of detection for commercial serum spiked with the antigen, the assay was conducted according to the method used in section 3.3.3. Using 100% serum as the matrix for dilution of the antigen, 20  $\mu\text{L}$  *Pf*HRP 2 capture antibody with a concentration of 20  $\mu\text{g mL}^{-1}$  in sodium carbonate-bicarbonate buffer (1 M, pH 9.6), was immobilized on the working electrode at 4°C overnight. After incubation, washing, and blocking, serial dilution of 0, 2, 16, 20, 40, 64, 80, 100  $\text{ng mL}^{-1}$  in 100% serum, was used in sandwich assay with 0.02  $\text{mg mL}^{-1}$  of the capture antibody HCA 160 used in sandwich assay. A concentration of 0.02  $\text{mg mL}^{-1}$  detection antibody (HCA 159 P) in 1:40 milk / PBS was used on the working electrode. Lowest detection of antigen was calculated as (3 x SD of the blank measurement) + (average blank measurement) and interpolated in GraphPad prism (version 5). The curve was plotted using Microsoft Excel.

### 3.3.11 *Pf*HRP 2 detection using AuNP in 100% serum

To determine assay sensitivity, *Pf*HRP 2 capture antibody with a concentration of 20  $\mu\text{g mL}^{-1}$  in sodium carbonate-bicarbonate buffer (1 M, pH 9.6), was immobilized on the working electrode according to method in section 3.3.5. The range for antigen detection was 0.05  $\text{ng mL}^{-1}$ , 0.1  $\text{ng mL}^{-1}$ , 0.2  $\text{ng mL}^{-1}$ , 0.3  $\text{ng mL}^{-1}$  0.4  $\text{ng mL}^{-1}$  and 0.5  $\text{ng mL}^{-1}$ . A 20  $\mu\text{L}$  volume of 1:10 AuNP conjugated

to detection antibody (section 3.3.7, Figure 3.8) was used on the working electrode to enhance the assay. Lowest detection of antigen was calculated as in section 3.3.10.

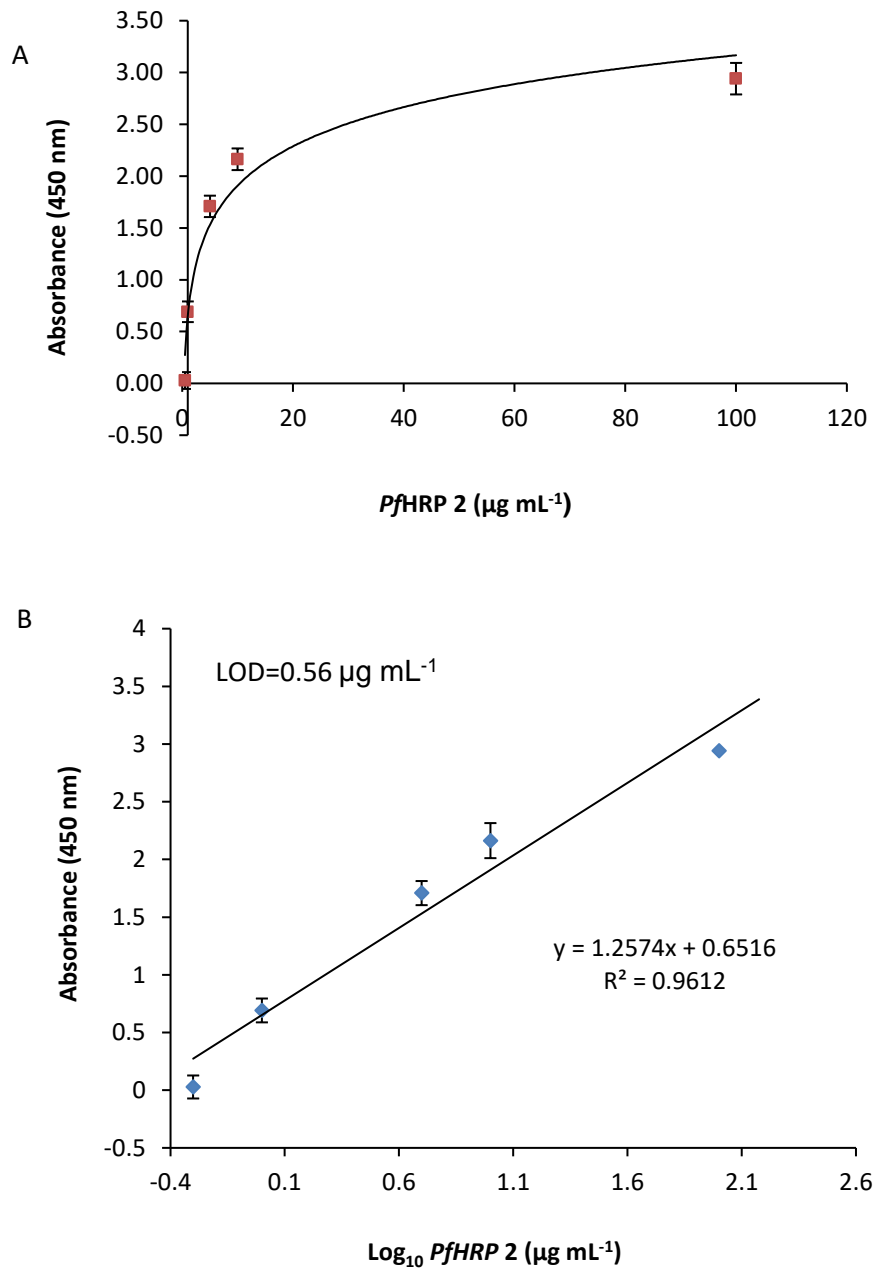
### 3.4 RESULTS AND DISCUSSION

#### 3.4.1 Direct ELISA

ELISA is an established method used to optimize antigen-antibody reactions used in this work. Commercial HuCAL antibodies were used to recognize recombinant PfHRP 2 (PIP 001) in heterogeneous direct and sandwich assays using polystyrene microtiter plates. The choice of plate depends on colour of the samples (Wang et al., 2015). Colourless samples are more easily assessed for colour change in transparent plates. Average and standard deviation about the mean were plotted in Microsoft Excel based on the general formula below:

$$s = \sqrt{\frac{\sum[(x-\bar{x})^2]}{n-1}} \text{ Standard Deviation} \quad (3-1)$$

Where  $x$  is each individual value,  $\bar{x}$  is the average of all values and  $n$  is the number of values (Figure 3.9). The enzyme system reacts rapidly with high substrate turnover rates and the resultant signal is strong and exhibits good performance (Parker and Tothill, 2009).



**Figure 3-9:** Direct ELISA standard curve (A) and linear regression (B) obtained from Log concentration. Standard curve of the direct ELISA format with HuCAL antibody HCA 159 P conjugated to enzyme horse radish peroxidase (20 µg mL<sup>-1</sup>) as detection reagent (n=3).

Measurements were taken after stopping the reaction and plotted against various PfHRP 2 concentrations. Limit of detection was calculated by 3 x SD control + average control interpolated in GrapPad prism (version 5) and

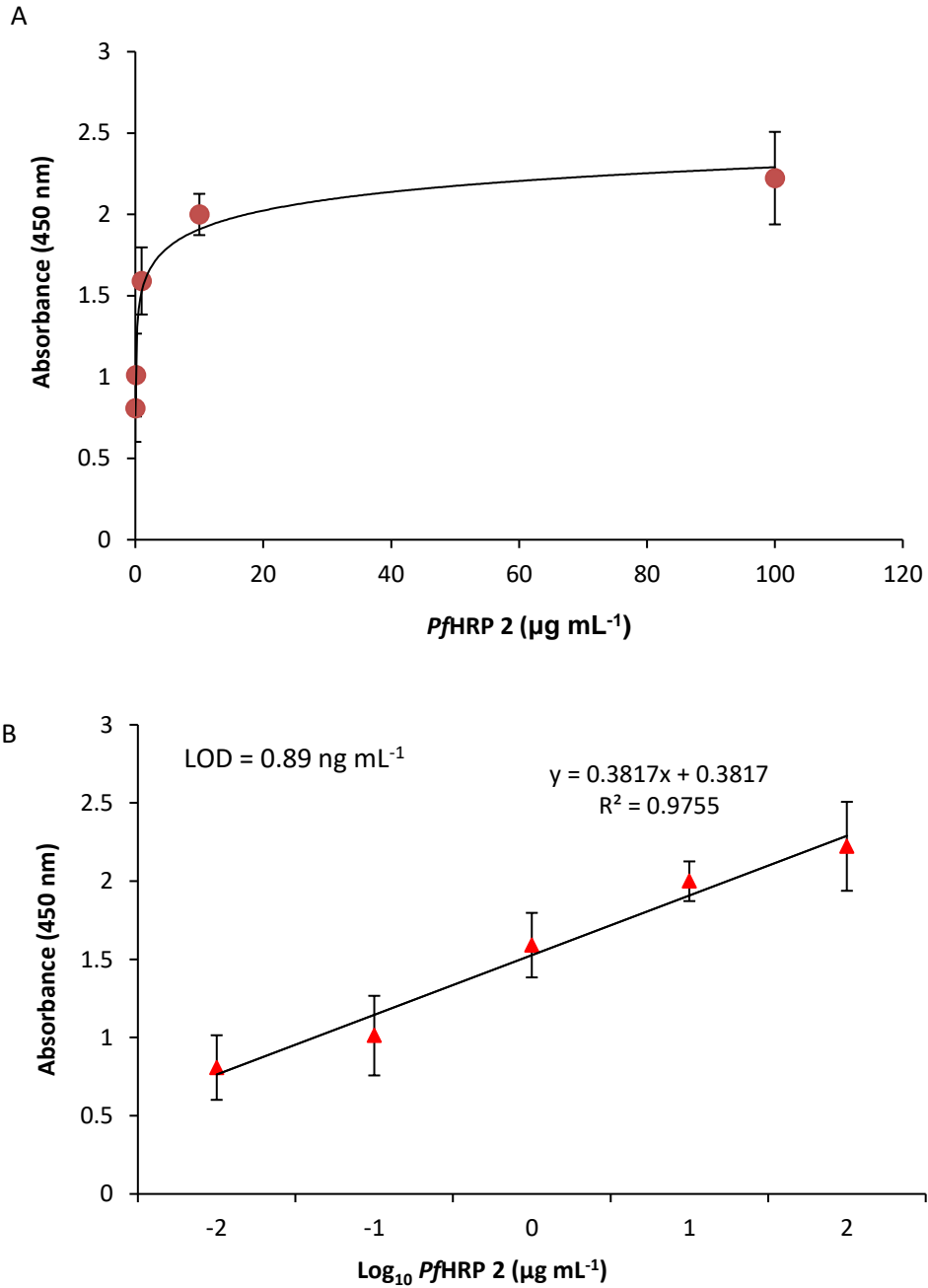
presented in Microsoft Excel. LOD was found to be  $0.56 \mu\text{g mL}^{-1}$ . Coefficient of correlation  $R^2 = 0.9612$  indicated how well the data fit the linear regression statistical model when plotting the difference between measurement and background signal.

Antibody production for ELISA reliably assesses and detects malaria antigen-antibody responses in multiplex platforms, homogenous or heterogeneous systems (de Souza Castilho et al., 2011; Lee et al., 2012; Grabias et al., 2014). Heterogeneous systems were employed in direct and sandwich assay to determine interaction event of the HuCAL proteins. When used in ELISA assays bio-molecular recognition event involves protein immobilization. The most commonly used immobilization techniques for biosensor construction are physical adsorption (Nanduri et al., 1997), covalent binding (Schuhmann et al., 1991); matrix entrapment (Rechnitz, 1986; Berg et al., 1989; Gupta and Chaudhury 2007) inter molecular cross-linking (Nenkova et al., 2010) and membrane entrapment (Scouten et al., 1995; Pancrazio et al., 1998; Sharma et al., 2003). Adsorption can be performed on materials as diverse as steel (Hasselberger et al., 1974; Charles et al., 1975), titanium (Nakabayashi et al., 1985), cellulose (Emery et al., 1972) and polystyrene (van Oss and Singer, 1966; Morrissey and Han, 1978; Ulbrich et al., 1991). Lower surface loading implies a decreased initial sensitivity relative to a sensor with covalent immobilization; desorption would further reduce the sensitivity over time. The direct assay proved the affinity of the antibody used for the analyte.

### 3.4.2 Sandwich ELISA

To determine affinity of paired HuCAL antibodies for *Pf*HRP 2 antigen sandwich ELISA was conducted (Figure 3.10).





**Figure 3-10:** Sandwich ELISA standard curve using paired antibodies (A) and linear regression obtained from Log values (B). Standard curve of the sandwich ELISA format with HuCAL antibody HCA 160 as capture antibody and HCA 159 P conjugated to horse radish peroxidase (20  $\mu\text{g mL}^{-1}$ ) as detection reagent. LOD = 0.89  $\mu\text{g mL}^{-1}$ . Coefficient of correlation  $R^2 = 0.9755$  (n=3).

Results show a higher analytical sensitivity in sandwich assay when plotting the difference between measurement and background signal (Table 3.1).

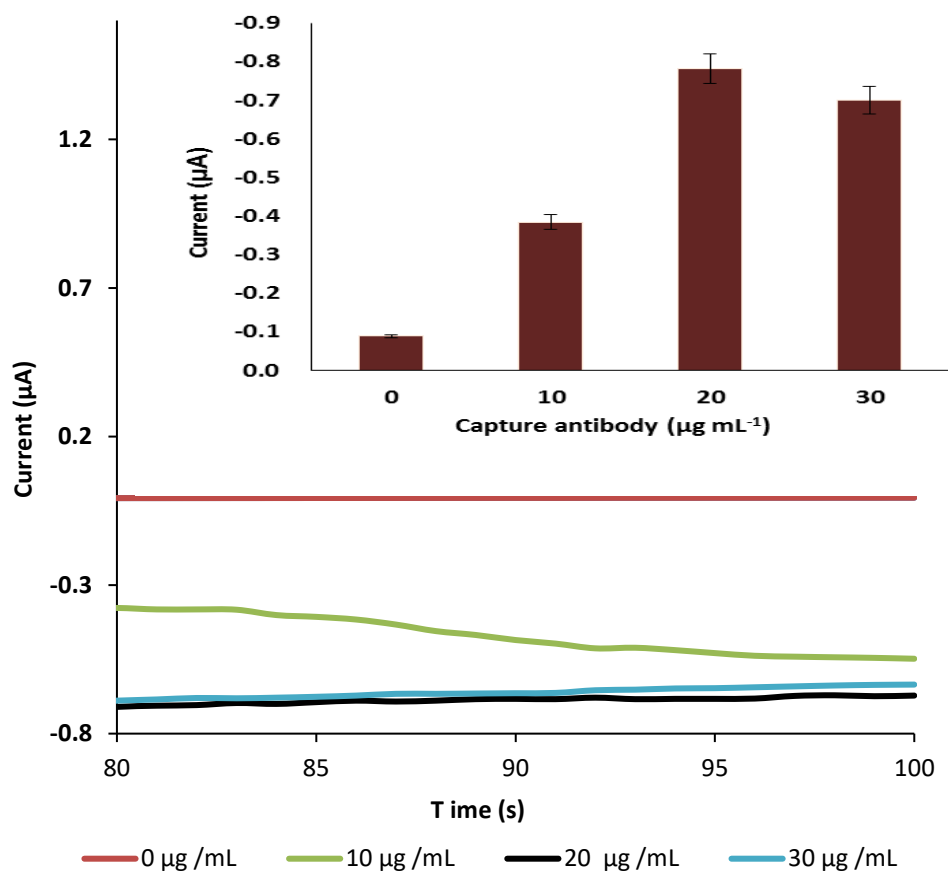
**Table 3-1:** Direct and Sandwich ELISA

	<b>LOD (<math>\mu\text{g mL}^{-1}</math>)</b>	<b>R<sup>2</sup></b>
Direct ELISA	0.56	0.9612
Sandwich ELISA	0.89	0.9755

Even though both direct and sandwich ELISA formats demonstrated good response, the sandwich ELISA was selected as the sandwich assay is known to be highly sensitive. Immunosensor development was therefore progressed with using the sandwich assay format. Work on the immunosensor began with optimization of the capture antibody by adsorption on the screen-printed electrode.

#### **3.4.3 Capture antibody (HCA 160) optimization on SPGE**

Capture antibody optimization was investigated as described in section 3.3.3. *Pf*HRP 2 antigen (PIP001) and detection antibody conjugated to horse radish peroxidase (HCA 159 P) concentrations were kept constant at  $30 \mu\text{g mL}^{-1}$  while concentration of capture antibody was varied as  $10 \mu\text{g mL}^{-1}$ ,  $20 \mu\text{g mL}^{-1}$  and  $30 \mu\text{g mL}^{-1}$  (Figure 3.11). Signal is average of three sensors per concentration (embedded graph).



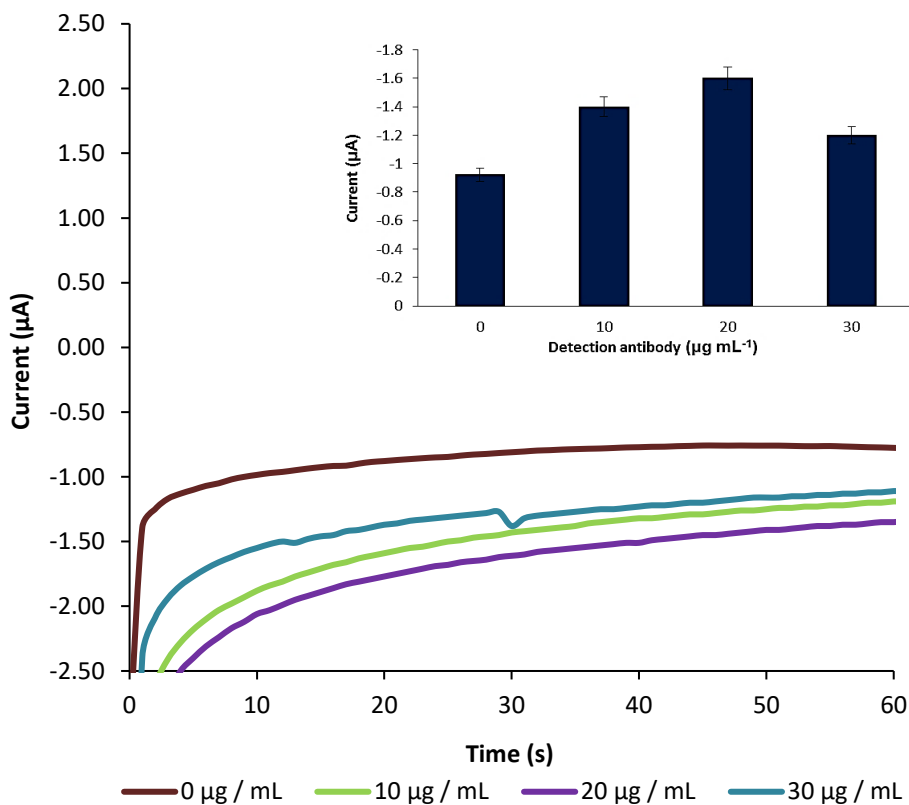
**Figure 3-11:** *PfHRP 2* Capture antibody optimization on JD 2b sensor. Capture antibody optimization was conducted by immobilizing 10, 20 and 30  $\mu\text{g mL}^{-1}$  of the capture antibody (HCA 160) in sodium carbonate-bicarbonate, pH 9.6, overnight. Antigen concentration of 30  $\mu\text{g mL}^{-1}$  was applied after the wash and block steps. Antigen detection was carried out by applying detection antibody (30  $\mu\text{g mL}^{-1}$ ) (n=3).

As expected, signal increased with capture antibody concentration until saturation at 20  $\mu\text{g mL}^{-1}$ . The results show greater stability and saturation of capture antibody at 20  $\mu\text{g mL}^{-1}$  suggesting the suitability of this concentration to be used in further studies. The graph was plotted so as to show clear separation.

#### 3.4.4 Detection antibody (HCA 159 P) optimization on SPGE

To determine optimal detection antibody concentration, the capture antibody (HCA 160) concentration was constant at 20  $\mu\text{g mL}^{-1}$ ; antigen concentration was maintained at 30  $\mu\text{g mL}^{-1}$  while detection antibody (HCA 159 P) was optimized at 10, 20 and 30  $\mu\text{g mL}^{-1}$  in 1: 40 milk PBS. The embedded graph

shows the average signal from each measurement of three sensors (Figure 3.12).



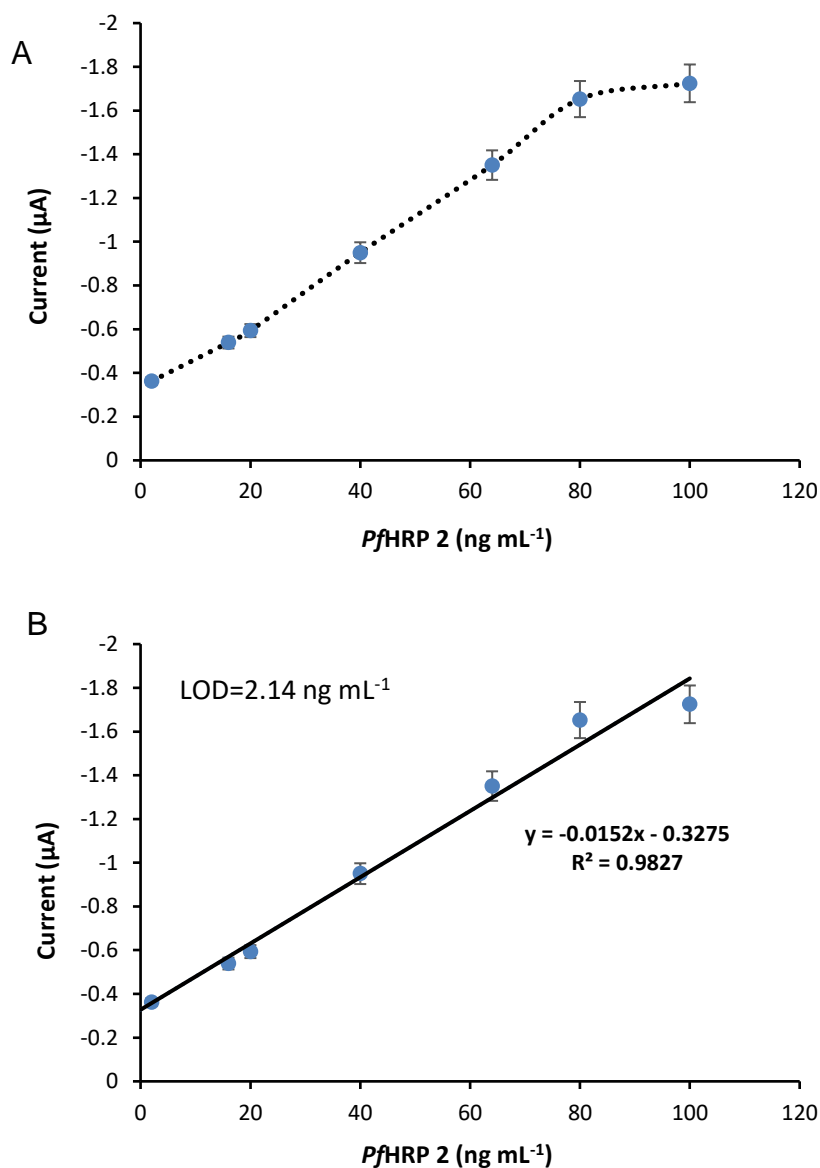
**Figure 3-12:** Detection antibody optimization on JD 2b. Optimization of the detection antibody was carried out using 20 µg mL<sup>-1</sup> of the capture Ab in buffer on the electrode. Incubation was carried out overnight at 4°C. Antigen detection was carried out with 30 µg mL<sup>-1</sup> antigen in dissolved in PBS (0.01 M, pH 7.4). The detection antibody was used in concentrations of 10, 20 and 30 µg mL<sup>-1</sup>.

Capture antibody was first incubated overnight at 4°C and the method conducted as in section 3.3.3. The detection antibody (HCA 159 P) showed the highest current on reaching saturation at 20 µg mL<sup>-1</sup> concentration, implying suitability for use in investigating *Pf*HRP 2 (PIP001) antigen for calibration of the standard curve.

### 3.4.5 *Pf*HRP 2 standard curve in buffer samples

After accomplishing the optimization process, a standard curve was created by testing the biosensor response to *Pf*HRP 2 concentrations ranging from 0, 2, 16, 20, 40, 64, 80 and 100 ng mL<sup>-1</sup>. The optimization concentrations guided choice of range in addition to known properties of the biomarker. *Pf*HRP 2 is has multiple binding sites; however the hydrophobic alanine is oriented towards the centre of the protein structure while the polar histidine is oriented towards the outside of the structure.

The assay was performed as described in section 3.3.3 with a capture antibody concentration of 20 µg mL<sup>-1</sup>. Signal was obtained using horseradish peroxidase conjugated antibody (20 µg mL<sup>-1</sup>). After reading, the current was normalized by subtracting the blank reading and plotted against *Pf*HRP 2 concentration. Linear regression was used to correlate the data. Limit of detection (LOD) was then calculated by 3 x standard deviation of control reading plus average of the control. Value was interpolated in GrapPad prism (version 5) and presented in Microsoft Excel (Figure 3.13).



**Figure 3-13:** Calibration curve of the chronoamperometric response of *PfHRP 2* detection in buffer. The lower limit of detection of the immunosensor was assayed using the optimized capture and detection antibodies. The standard curve showed a response that is linear with a long linear range. The range of the assay was determined by the low limit of detection sought. Average of three sensors was used.

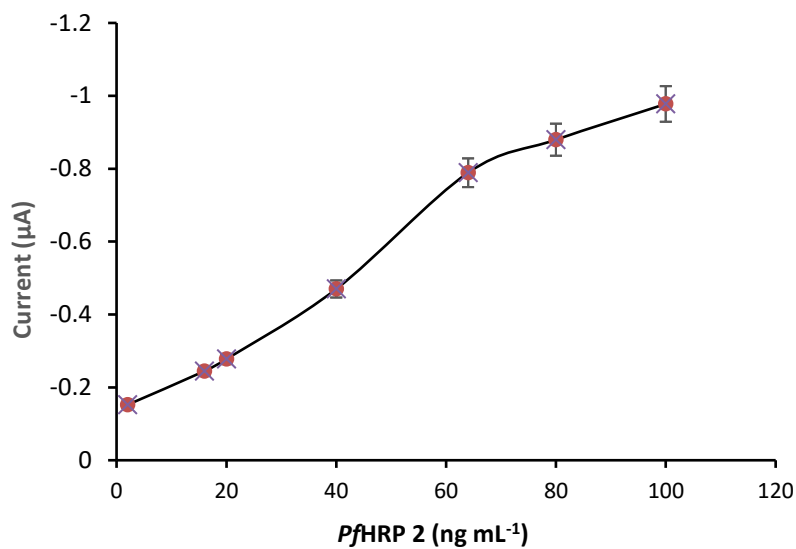
The assay was conducted as described in section 3.3.3 From the data, LOD was found to be  $2.14 \text{ ng mL}^{-1}$  while correlation coefficient ( $R^2$ ) of 0.9827 was observed in buffer matrix.

The protein shows a long linear range. A steady amperometric was not attainable as the detection fluctuated throughout the curve at a range of reading. In addition, the tandem repeats of alanine and histidine in the structure of the polypeptide make for ready detection of the antigen (Lillehoj, 2016). Multiple binding epitopes of this protein also give rise to the signalling peculiarities of *PfHRP 2* in this study.

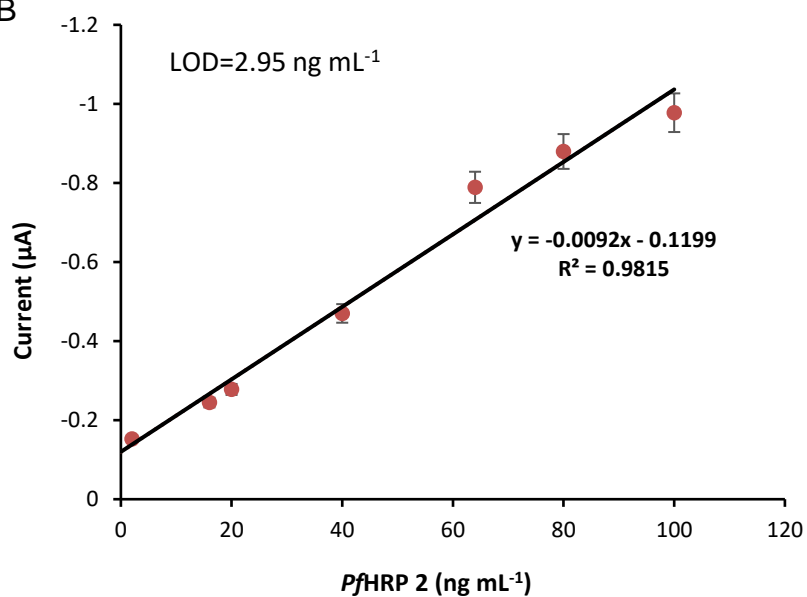
#### **3.4.6 *PfHRP 2* standard curve in serum samples**

In order to assess the effect of the matrix on the assay, the assay was repeated in 100 % serum using the same concentration as in section 3.4.5. Capture antibody immobilization was carried out at 4°C and the assay was conducted as in section 3.4.5. Normalization of the measurements was again carried out by subtracting the background signal from the measurements. The signal was measured using spiked serum samples. With calculation of limit of detection as earlier described, the limit of detection in 100 % commercial serum was found to be 2.95 ng mL<sup>-1</sup> (Figure 3.14).

A



B



**Figure 3-14:** Calibration curve of the chronoamperometric response of *PfHRP 2* detection in commercial serum (A) and linear regression (B). A 100% concentration of commercial serum was used to dilute recombinant *PfHRP 2* to a concentration of 1 – 100 ng mL<sup>-1</sup>. Correlation coefficient and R<sup>2</sup> value of 0.9815 serum matrix was observed from the formula generated by the data in Excel. Average of three sensors was used to plot the curve.



The analytical range was adopted to accommodate the blood levels of the biomarker and also the detection capability of the developed immunoassay (Lillejoh, 2011).

It was found that lower signals occurred in serum samples. The change is due to hampering of the transport of materials by the serum proteins which partially block the electrode surface. Hence as the analyte undergoes oxidation at the anode, the signal is reduced by the matrix effect of the commercial serum.

*Plasmodium falciparum* parasite is found in the red blood cells and the histidine rich proteins it produces are found expressed at the surface of the red blood cells. The antigen may also be found in serum along with other endogenous proteins. Although serum typically contains a vast number of different proteins, some are specific to blood while others are secreted into blood from tissues and organs. Serum does not contain red blood cells nor white blood cells or even fibrinogen (Thrift et al, 1986). Several types of reagent can help in reducing non-specific binding such as detergents, salts, proteins and polymers. The method was conducted as in section 3.3.3 using 100% serum as the matrix for dilution of the antigen. A serial dilution of 0, 2, 16, 20, 40, 64, 80, 100 ng mL<sup>-1</sup> was used in sandwich assay with 0.02 mg mL<sup>-1</sup> of the capture antibody HCA 160 and 0.02 mg mL<sup>-1</sup> detection antibody HCA 159 P on the working electrode.

These results show the sensor to be suitable for detection of *Plasmodium falciparum* histidine rich protein 2 (*PfHRP 2*). As previously indicated, blood level is ~9.45 ng mL<sup>-1</sup> (Ho, et al., 2014, Dzakah et al., 2014; Abdallah et al., 2015).

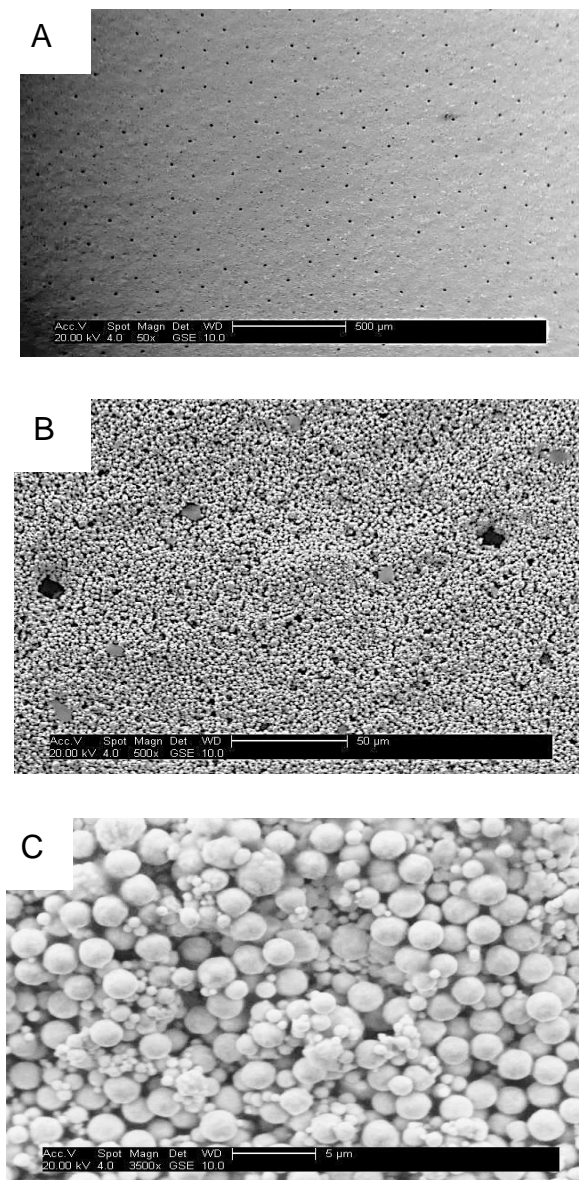
To increase the sensitivity, the detection antibody-HRP was attached to gold nanoparticles and used in the sandwich assay. Several experiments were conducted to achieve the best results before a calibration curve was repeated with serial dilution of the antigen in buffer and 100 % serum matrices. The developed *PfHRP 2* immunosensor is as sensitive as in buffer assay, in agreement with Sharma et al., 2011.

### **3.4.7 Scanning electron microscopy of SPGE JD 2b assay**

The structure of the sensor determines the performance of the sensor as the surface is the platform for the immunoassay. Microscopic techniques like scanning electron microscopy (SEM), scanning tunnelling microscopy and transmission electron microscopy (TEM) contribute to the surface structure characterization (Davies et al., 1998).

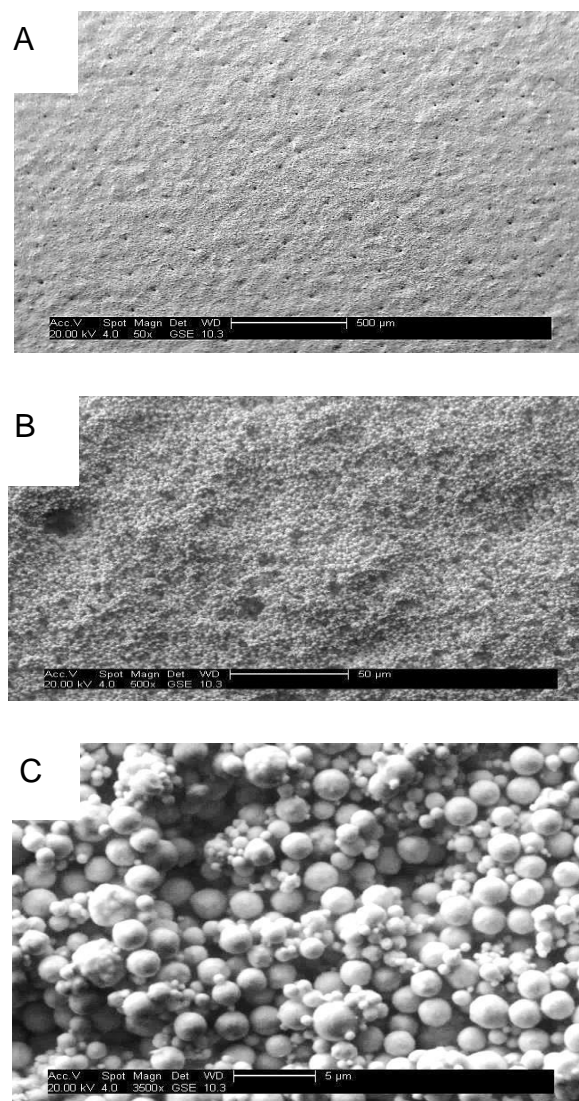
Scanning electron micrograph of JD SPGE shows a homogenous distribution of the gold ink with round ink granules, producing a maximized area between the big sized ink particles. High surface area resulting from the three dimensional ink granules has a direct impact on the maximum amount of biomaterial immobilized on the working electrode and was reported to improve assay performance (Noh and Tothill, 2006).

The scanning electron microscope (Phillips, UK) was used to obtain an image of the surface of the working electrode. The structure of the working electrode during sandwich assay was visualized in order to make a comparison between the different stages of the assay regarding the working electrode surface. The surface of the working electrode measures about 5 mm in diameter. In order to obtain a visual image of the treated SPGE, SEM of the sensor surface was taken to show lithographic structure of the working electrode. At 50x, 500x and 3,500x magnification surface roughness of the gold particles is visible, showing the ditches approximately 10 - 50 nm deep after each step of assay. Figure 3.15 shows the sensor surface after the capture antibody immobilization.



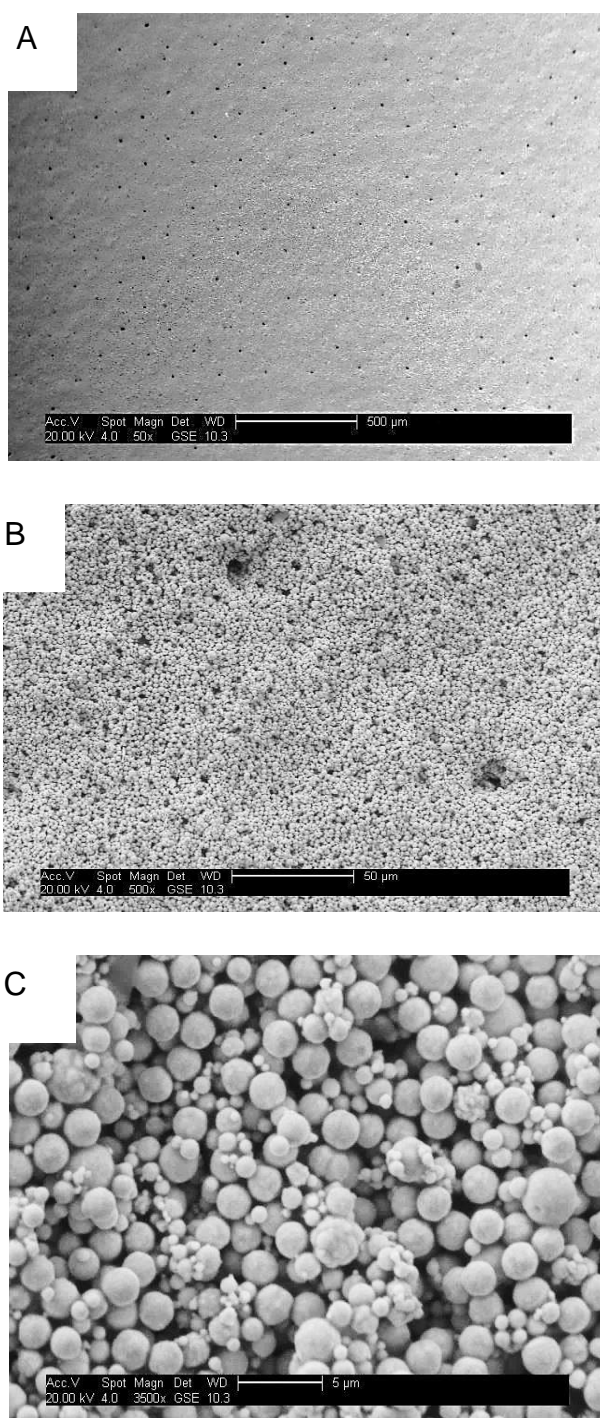
**Figure 3-15:** Capture antibody immobilization on the SPGE at 50x magnification (A) and enlarged to 500x (B) and 3,500x magnification (C).

*Pf*HRP 2 antigen was then added (10 μL) in a 100 ng mL<sup>-1</sup> concentration and then incubated at 37°C for 1 hour followed by washing two times with 1 mL 0.01 M PBST (0.05 v/v) (Figure 3.16).



**Figure 3-16:** *P*HRP 2 antigen added following the immobilization step. The three electrodes were blocked using 100  $\mu$ L of a 1:10 solution of milk concentrate in 0.01 M PBS and incubated at 37°C for 1 hour. SEM of JD 2 SPGE treated with capture antibody, blocking buffer and antigenic interaction at 50x magnification (A) and enlarged to 500x (B) and 3,500x magnification (C).

The increasingly compact working electrode surface is again imaged (Figure 3.17).



**Figure 3-17:** Sandwich assay for *P/HRP 2* immobilized on SPGE. The final step in the sandwich format was applied using 10  $\mu\text{L}$  of 0.02  $\text{mg mL}^{-1}$  of the *P/HRP 2* horse radish peroxidase-conjugated detection antibody. Incubation at 37°C for 1 hour was followed by washing two times with 1 mL 0.01 M PBST (0.05 v/v). Detection antibody interaction at 50x magnification (A), enlarged to 500x (B) and 3,500x magnification (C).

Immobilizing proteins on the working electrode affects the resolution of the SEM images, as they inhibit the current flow of the scanning electrons. A gold coating to increase the conductivity and the resolution was not practicable as the 20 nm layer covered the gold particles in the same manner. The gold nanoparticles are visible as bright dots. The imaging software of the SEM comprises a measuring mode which calculates the length of the magnified objects. This function was used to identify the gold particles on the working electrode, by estimating the diameter of the particles.

#### **3.4.8 Signal amplification using gold nanoparticles**

Gold nanoparticles (AuNPs) generally possess excellent catalytic activity and offer a hospitable environment for the biomolecules (Bharathi et al., 2001). AuNP, magnetic nanoparticles, carbon nanotubes, quantum dots, polymeric crystals are among nanotechnology enhancing materials increasing diagnostic sensitivity to the nanoscale (Jain, 2003; Munge et al., 2010).

With the results from the bare SPGE assay, effort was focused on the amplification of sensitivity and the improvement of the signal generated by the transport of electrons in the recombinant protein from the surface of the electrode through the supporting electrolyte. Electrochemical studies have revealed that AuNPs enhance electrode conductivity and improve the detection limit (Song et al., 2003; Stoeva et al., 2006; Salam and Tothill, 2009).

#### **3.4.9 Dynamic light scattering for the particle size determination of colloidal gold**

The commercial gold nanoparticle was obtained at (40 nm) size however as a confirmation, the gold nanoparticles were analysed in the Zetasizer nano-s to assess the particle size using 100  $\mu$ L of AuNP in 1000  $\mu$ L of PBS. The mixture was sonicated for 1 minute to facilitate dispersion and the cuvette loaded.

Using exposure to a beam of light, the average peak was found at 51.76 nm and light scattering angle of 173° (Table 3.2).

**Table 3-2:** Physical properties of the gold nanoparticles

Average (nm)	SD	PDI	Temperature	Scattering angle
51.76	0.42	0.14	25°C	173°

Gold nanoparticles show a range of colours that vary with particle size and dispersion. Using seven scans, the results showed a average of 51.76 nm in particle size. To begin investigations using the gold nanoparticles it was necessary to conjugate the particles to the detection antibody.

#### **3.4.10 Conjugation of AuNP to HRP- conjugated detection antibody**

Conjugation of AuNP to the detection antibody is a technique used to increase the amperometric signal and sensitivity of the assay. The assay sensitivity is enhanced as the gold particles increase the surface area available for antigen interaction following successful conjugation of the colloid to the reporter protein. The solution remains clear when tested 1:1 with NaCl (2.5 M). This test with NaCl verifies the conjugation of colloidal gold to reporter protein as the AuNP-conjugated antibody showed no flocculation. The successfully conjugated AuNP / detection antibody is then stored at 4°C. AuNP were conjugated to horse radish peroxidase-conjugated detection antibody and diluted 1:10 in PBS before use (Figure 3.18).



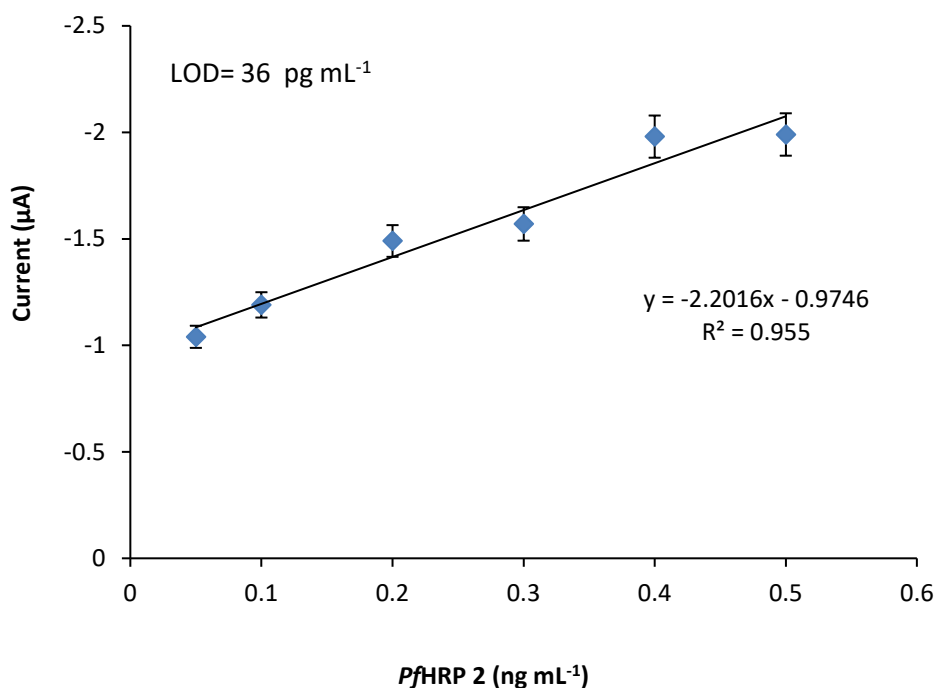
**Figure 3-18:** AuNP in working concentration (A) and stock dilution (B).

After having conjugated the gold nanoparticles to the detection antibody, the assay was again conducted to assess the enhancement capability of the conjugated detection antibody.

#### 3.4.11 *Pf*HRP 2 standard curve in buffer samples with AuNPs

Amplification of the signal is effected using AuNP. The AuNP assay showed a signal when plotted against the developed immunoassay which failed to give an appropriate signal. Sandwich assay was conducted with 1:10 (detection antibody conjugated to AuNP) stock dilutions (Figure 3.19). Chronoamperometric response of sandwich ELISA format with monoclonal HuCAL antibody (HCA 160) as capture reagent and detection antibody labelled with horse radish peroxidase (HCA 159 P) conjugated to 40 nm gold particles. Measurement were taken after 100 s at a potential of -200 mV and plotted against various concentrations. The graph shows the averaged signal of three sensors for each concentration; the error bars represent the standard error about the mean (n=3).





**Figure 3-19:** Linear regression of the chronoamperometric response of *PfHRP 2* detection in buffer, enhanced with gold nanoparticles. Concentrations of recombinant *PfHRP 2* (0.05 – 0.5 ng mL<sup>-1</sup>) were diluted in PBS (0.01 M). Correlation coefficient, R<sup>2</sup> value of 0.955 was observed from the formula generated by the data in Excel. Average of three sensors was used to plot the curve.

From the above data, Limit of detection 0.036 ng mL<sup>-1</sup> was obtained in the amplified buffer assay while R<sup>2</sup> value of 0.955. The AuNP results gave good sensitivity and limit of detection without the use of additional free enzyme (horse radish peroxidase) to load the particles. The best AuNP conjugate stock diluted used was 1:10 in PBS and also blocking with milk proteins.

In addition, the developed gold nanoparticle enhanced malaria electrochemical immunosensor is more sensitive than electrochemical magnetic particle enhanced immunoassay (de Souza et al., 2011).

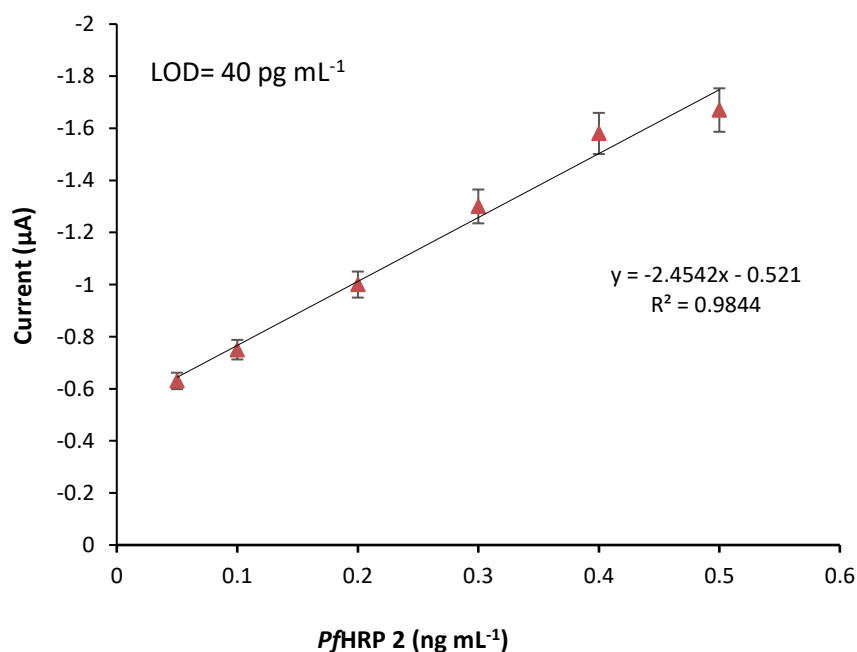
The capture and detection antibody concentrations were taken at 0.02 mg mL<sup>-1</sup> for the detection of *Plasmodium falciparum* histidine rich protein 2 antigen. With the 1:10 dilution, it was possible to obtain a signal at lower concentration of analyte implying that the AuNP amplification was successful. The linear regression curve generated the equation of best fit in Microsoft excel. LOD

was calculated as (3 x SD blank measurement) + (average blank measurement) and interpolated in GraphPad prism (version 5).

### 3.4.12 *Pf*HRP 2 standard curve in serum samples with AuNPs

Gold nanoparticle enhancement of the detection antibody gives a signal at low concentrations not detectable by the un-enhanced assay (Salam and Tothill, 2009). With the limit of detection obtained for both the assays, an attempt was made to detect lower concentrations of the analyte. A comparison between the original assay and the AuNP-enhanced assay was conducted for the detection of *Plasmodium falciparum* antigen using 1:10 AuNP / Ab stock dilution and HCA 159 P antibody detection.

Buffer assays yielded good results however, the serum assays were used to compare the effect of serum proteins on the developed assay. The large surface area and affinity of gold for proteins allows for the attachment of the enzyme to the enzyme label (horse radish peroxidase)(Figure 3.20).



**Figure 3-20:** Linear regression of the chronoamperometric response of *Pf*HRP 2 detection in serum, enhanced with gold nanoparticles. Concentrations of recombinant *Pf*HRP 2 (0.05 – 0.5 ng mL<sup>-1</sup>) were diluted in 100% commercial serum. R<sup>2</sup> value of 0.9844 was obtained. Average of three sensors was used to plot the curve.

From the above data, Limit of detection  $0.04 \text{ ng mL}^{-1}$  was obtained in the amplified buffer assay while  $R^2$  value of 0.9844. LOD was calculated as  $(3 \times \text{SD blank measurement}) + (\text{average blank measurement})$  and interpolated in GraphPad prism (version 5). Signal of serum matrix is similar to the buffer assay (Lee et al., 2006). The working capacity of a biosensor with an enzyme as its recognition element relies on the method of its addition, hydrogen ion concentration, heat requirement and the process of its being fixed to the prepared substrate (Ronkainen et al., 2010). This knowledge has proven useful in the development of immunosensors to evaluate the progress of disease conditions, for bacteria and virus assays or substance recognition (Sharma et al., 2008, Abdul Kadir and Tothill, 2010).

### **3.5 CONCLUSIONS**

The results will be used in future experiments using sandwich ELISA format. The direct and sandwich ELISA immunoassays demonstrate utility of commercial HuCAL monoclonal capture antibody (HCA 160) and horse radish peroxidase conjugated detection antibody (HCA 159P) paired antibodies in detection of recombinant *Pf*HRP 2 antigen (PIP001).

As a tool for assay optimization, the antibodies are accurate, however the cost of reagents may be reduced in further experiments by using samples from *Plasmodium falciparum* culture media containing dissolved antigenic biomarker, *Pf*HRP 2. The highly selective sandwich ELISA format involving two antigenic epitopes is recommended for further investigation on the gold screen-printed electrode. Affinity of gold for proteins makes the SPGE sensor a promising tool for malaria diagnosis. Gold working electrodes are not as prone to non-specific binding as graphene working electrodes, though graphene may be cheaper than gold ink. Milk concentrate in PBS is adopted from a previous study as the blocking reagent, which reduces non-specific binding on the electrode surface.

The immunosensor assay successfully quantified recombinant protein in various amounts in standard curve with a long linear range relying on tandem amino acids in its structure.

**Table 3-3:** Sensitivity of histidine rich protein 2 curves

Sample	LOD (ng mL <sup>-1</sup> )	Equation	R <sup>2</sup>
<i>Pf</i> HRP 2 buffer	2.14	y= -0.0152x -0.3275	0.9827
<i>Pf</i> HRP 2 100% serum	2.95	y= -0.0084x -0.124	0.99
AuNP <i>Pf</i> HRP 2 buffer	0.036	y= -2.2016x -0.9746	0.955
AuNP <i>Pf</i> HRP 2 100% serum	0.04	y= -2.4542x -0.521	0.9844

Electrochemical measurements produced a 2.14 ng mL<sup>-1</sup> detection limit in unenhanced assay, which is better than the ELISA assay developed in this work. An amplified signal is also achieved on the immunosensor with AuNPs conjugated to the detection antibody. Higher chronoamperometric separation occurs in relation to enzyme attachment on gold nanoparticles. The large surface area of the 40 nm gold nanoparticles increases the response. Signal amplification using gold nanoparticles gave LOD of 0.036 ng mL<sup>-1</sup> while serum assay LOD is 0.04 ng mL<sup>-1</sup>. The results are similar.

The first malaria DuPont SPGE biosensor developed in this work detects *Pf*HRP 2 antigen in the picogram range. The method is adaptable for use in appropriate mobile technology application with the potential for use in remote, resource deprived settings. The developed immunosensor offers a highly sensitive, reliable, easy to use, portable and low cost method of detecting species specific *Plasmodium falciparum* histidine rich protein 2.

## **CHAPTER FOUR**

### **DEVELOPMENT OF Plasmodium L- LACTATE DEHYDROGENASE IMMUNOSENSOR**



## 4 ELECTROCHEMICAL IMMUNOSENSOR FOR L-LDH

### 4.1 INTRODUCTION

Electrochemical immunosensors are significant analytical tools for monitoring antibody-antigen interaction because of their simplicity, high sensitivity and good reproducibility (Darain et al., 2003).

Protozoal LDHs display some major structural and kinetic differences compared to their mammalian counterparts that may be exploited to develop selective drugs and detection systems for malaria (Hurdoyal et al., 2010; Jain, 2014). Another striking difference of pLDH from other dehydrogenases is its substrate specificity. These structural differences are exploited during antimalarial drug design and selective detection of pLDH for malaria diagnosis. Recent studies have shown a direct correlation between blood levels of pLDH and response to therapy (Dondorp et al., 2005). Even though these molecules are released into plasma, their binding characteristics and clearance rates vary. The enzyme does not however, persist in the blood after treatment, and its absence serves as an indication of the success of treatment (Iqbal et al., 2004). For parasite LDH detection, monoclonal antibodies are used to capture the parasite enzyme (Piper et al., 1999).

Immunosensors are relatively recent in malaria detection. The most widely used technique for malaria detection, microscopy, is unable to consistently provide reliable results in uncomplicated malaria, certain cerebral malaria presentations, and malaria during pregnancy (Leke et al., 1999). Therefore, more rapid, accurate and diagnostic methods for malaria are required in the form of point of care diagnostics. Detection relies on attachment of the horse radish peroxidase-conjugated reporter protein to the parasite antigen. Signal generated can be enhanced by nanomaterials conjugated to the detection antibody. Gold nanoparticles have been used in the field of catalysis (Layek et al., 2011; Statakis and Layek et al., 2012; Layek and Nandi, 2013) and biosensors (Pingarron et al., 2008; Hutter and Maysinger, 2013).

Point-of-care (POC) diagnostics offer great potential to detect and monitor infectious diseases at resource limited settings. In addition, disposability renders POC diagnostics attractive to end users by preventing exposure to bio-hazardous waste and can be adapted via blue-tooth connection to a smart device. The smartphone connects to the analyser so that the dynamics of the reaction produce an empirical signal (Mya et al., 2003). Furthermore, results directly linked to “the cloud” through available mobile technology (and archiving of information) could be geographically decoupled from the site of testing.

To enable electrochemical measurements and communication in any setting, useful technology must be able to perform complete electrochemical analysis while remaining low in cost, simple to operate, and as independent of infrastructure as possible. The technology must also be compatible with any generation of mobile telecommunications technology, including the low-end phones and 2G networks that continue to dominate communications in much of the developing world (Nemiroski et al., 2014; Solon, 2014).

In this chapter, an electrochemical immunosensor detecting sub-microscopic levels of Pan-malaria antigen (parasite L- Lactate dehydrogenase) has been developed with sandwich format in buffer and serum assays. The sensor signal was enhanced with gold nanoparticle-conjugated to horse radish peroxidase. The novel DuPont SPGE immunosensors developed in this work for sub-microscopic, quantitative malaria detection have adaptive potential for field use in remote settings on a portable, battery-operated potentiostat coupled to smart phone and iPad (Figure 4. 1).





**Figure 4-1:** PStouch application (A) useful for analysing and up-loading data from remote locations, and DropSens hand-held potentiostat (B).

## 4.2 MATERIALS

### 4.2.1 General chemicals and instrumentation

General chemicals and instrumentation remain the same as in Chapter 3 in this thesis. For the development of L-LDH immunosensor HuCAL monoclonal capture antibody (*Plasmodium falciparum* HCA 158), and detection antibody (horse radish peroxidase-conjugated *Plasmodium falciparum* HCA 157 P) were purchased from AbDSerotec, now Bio-Rad, (Kidlington, UK) while recombinant *P. falciparum* L-LDH (CSB-EP632935PLS) was purchased from 2B Scientific (Oxford, UK). Colloidal gold (40 nm) was purchased from BBI solutions (Cardiff, UK). Transmission electron microscope (CM-20) was from Phillips (Essex, UK).

## 4.3 METHODS

### 4.3.1 Parasite L-LDH capture antibody (HCA 158) optimization

Capture antibody optimization was carried out using HuCAL parasite L-LDH, a ubiquitous enzyme detectable in serum during active infection. To control cost of HuCAL reagents, ELISA assay (Chapter 3) optimization was omitted and blocking reagents were adopted from the previous work. The most suitable

concentration for the assay was obtained by optimization in which the capture antibody (HCA 158) was immobilized on the working electrode (section 3.3.3).

Prior to the immobilization of antibodies, the sensors were cured at 120°C. The electrodes were then washed two times in 1000  $\mu\text{L}$  de-ionized water (18.2 m $\Omega$ ) and dried in gentle nitrogen stream. Working electrode was coated with 20  $\mu\text{L}$  pLDH capture antibody (HCA 158) at concentrations of 2.5  $\mu\text{g mL}^{-1}$ , 10  $\mu\text{g mL}^{-1}$  and 20  $\mu\text{g mL}^{-1}$  using sodium carbonate-bicarbonate buffer (1 M, pH 9.6), according to manufacturer's recommendation.

After each incubation step, the surface was washed two times using 1000  $\mu\text{L}$  PBST (phosphate buffered saline with 0.05 % Tween - 20) and two times with 1000  $\mu\text{L}$  de ionized water then dried in gentle nitrogen stream. The sensor surface free of antibody was blocked using milk protein concentrate (KPL Inc., Gaithersburg, USA) diluted 1:10 milk concentrate / PBS buffer (0.01 M, pH 7.4.) to reduce non-specific binding. A volume of 100  $\mu\text{L}$  blocking buffer was applied on all three electrodes. The assay was incubated for 1 hour at 37°C.

After repeating wash step, 30  $\mu\text{g mL}^{-1}$  of recombinant L-LDH was prepared in 1:10 milk PBS then 20  $\mu\text{L}$  was dropped on the working electrode and incubated for 1 hour at 37°C. Wash step was again repeated to remove unbound material with 1000  $\mu\text{L}$  PBST (0.05 v/v) followed by 1000  $\mu\text{L}$  de-ionized water (18.2 m $\Omega$ ).

The purified detection antibody HCA 157 P was diluted to a working strength of 30  $\mu\text{g mL}^{-1}$  in 1:40 milk concentrate / PBST (0.05 v/v). A 20  $\mu\text{L}$  volume was applied to the working electrode and incubated for 1 hour at 37°C. For signal detection using TMB / H<sub>2</sub>O<sub>2</sub> (mediator / substrate) complex, a stock of working buffer was prepared by adding 0.05 M phosphate citrate buffer (pH 5.0) to 0.01 M KCl in equal volumes (Chapter 2, section 2.3.5).

The final mediator / substrate complex was constituted just before application and the electrochemical measurement was taken. Before starting the amperometric measurement, 100  $\mu\text{L}$  of the TMB / H<sub>2</sub>O<sub>2</sub> complex were dropped on the sensor surface covering all three electrodes. Pipette tip was changed

to avoid contamination of the TMB / H<sub>2</sub>O<sub>2</sub> stock with horse radish peroxidase from the sensor surface.

#### 4.3.2 Parasite L-LDH detection antibody (HCA 157 P) optimization

For optimization of detection antibody, the procedure in Chapter 3, section 3.3.4 was adopted using the best concentration of capture antibody obtained at saturation. The sensors were cured at 120°C. The electrodes were then washed two times in 1000 µL de-ionized water (18.2 mΩ) and dried in gentle nitrogen stream. A 20 µL volume of parasite L-LDH capture antibody (10 µg mL<sup>-1</sup>) in sodium carbonate-bicarbonate buffer (1 M, pH 9.6) was immobilized on the WE overnight at 4°C. The electrodes were then washed two times using 1000 µL PBST (phosphate buffered saline with 0.05 % Tween - 20) and two times with 1000 µL de-ionized water (18.2 mΩ) then dried in gentle nitrogen stream. A 30 µg mL<sup>-1</sup> parasite L-LDH recombinant antigen (CSB-EP632935PLS) supplied by 2B Scientific (Oxford, UK) was prepared in 1: 10 milk concentrate / PBS buffer (0.01 M, pH 7.4).

A 20 µL volume was dropped on the working electrode and incubated at 37°C for 1 hour and the wash step repeated. In order to determine the effect of concentration of detection antibody on recognition event of parasite L-LDH antigen (CSB-EP632935PLS), the purified detection antibody (HCA 157 P) was diluted to working strengths of 10, 20 and 30 µg mL<sup>-1</sup> in PBST. A 20 µL volume was dropped on the working electrode and incubated for 1 hour at 37°C. Amperometric detection was conducted using TMB / H<sub>2</sub>O<sub>2</sub> complex and optimum detection antibody concentration was used in the antigen titre.

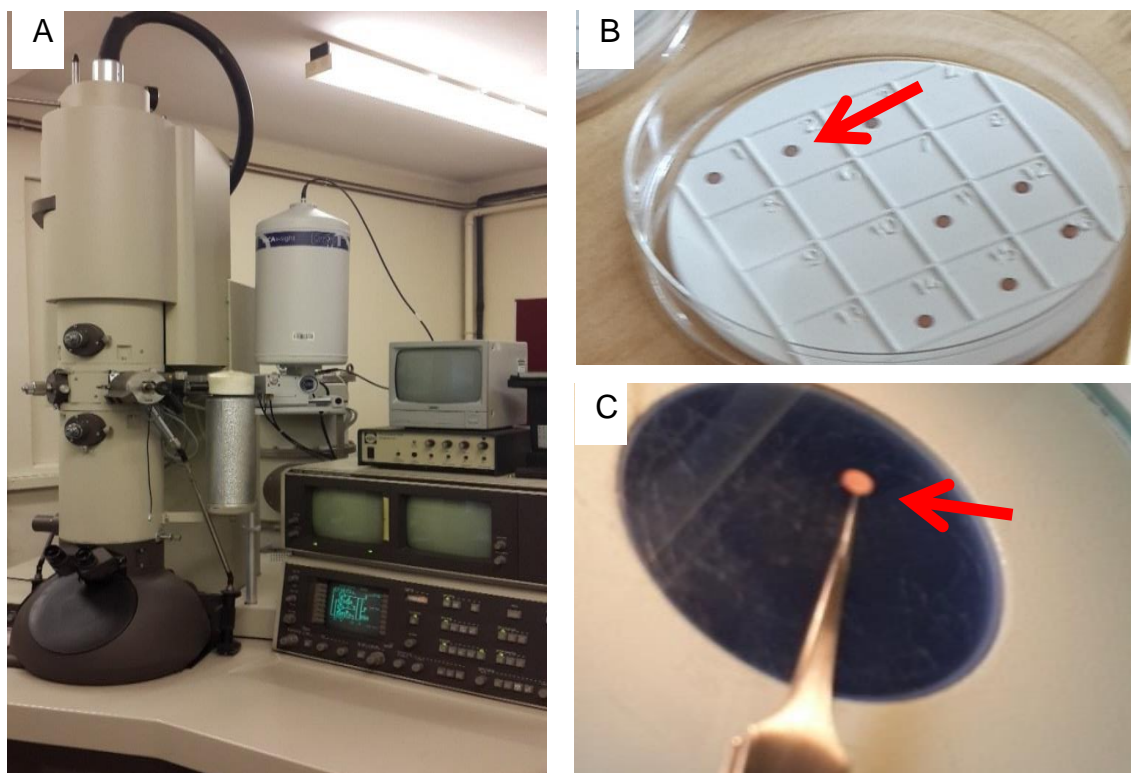
#### 4.3.3 LOD recombinant L-LDH (CSB-EP632935PLS) detection in buffer

To determine detection limit of SPGE for recombinant *P. falciparum* parasite L-LDH detection, 20 µL of 10 µg mL<sup>-1</sup> parasite L-LDH capture antibody (HCA 158) in sodium carbonate-bicarbonate buffer (1 M, pH 9.6) was immobilized on the working electrode and incubated overnight at 4°C (section 4.3.2). After incubation, washing, and blocking steps, recombinant L-LDH (CSB-

EP632935PLS ) was serially diluted in 1 in 10 milk /PBS (0.01 M) from 100,000 ng mL<sup>-1</sup> (100 µg mL<sup>-1</sup>) to 1 ng mL<sup>-1</sup>. A 20 µL volume was dropped on the working electrode and incubated at 37°C for 1 hour. The wash step was repeated and the detection antibody (HCA 157 P) was diluted to a working strength of 10 µg mL<sup>-1</sup> in 1: 40 milk concentrate / PBS 0.01 M). Lowest detection of antigen (LOD) was calculated as (3 x SD blank measurement) + (average blank measurement) and interpolated in GraphPad prism (version 5). The curve was plotted using Microsoft Excel.

#### 4.3.4 Transmission electron microscopy of gold nanoparticles

Particle size is essential in nanoparticle work. Large surface area of the gold nanoparticles achieves higher sensitivity in assays. A visual confirmation of the BBI gold nanoparticle was obtained by transmission electron microscopy (TEM) Phillips CM-20 (Essex, UK) (Figure 4.2).

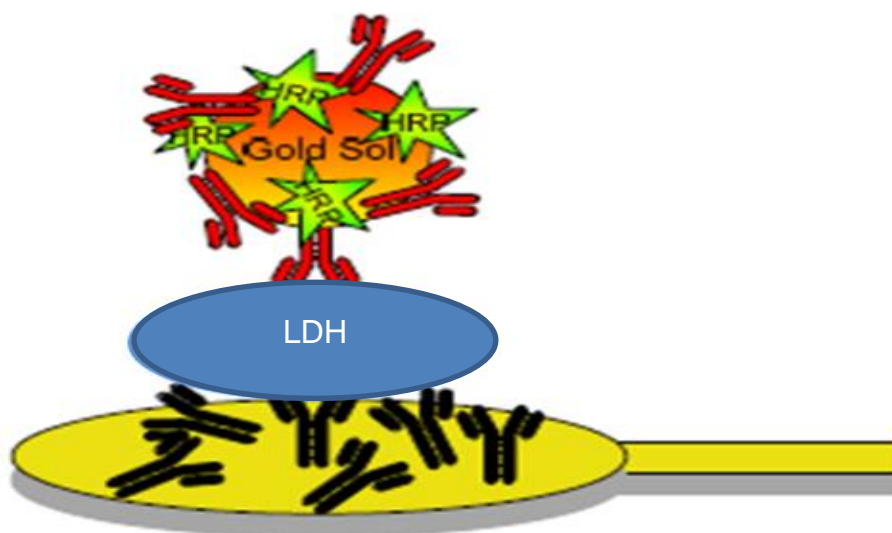


**Figure 4-2:** TEM set up (A) mesh (B) and AuNP droplet (C). A 20 µL drop of BBI gold colloid was applied to the mesh. The particle was air dried on the mesh before microscopic examination.

#### 4.3.5 Conjugation of AuNP to reporter protein (HCA 157 P)

Gold nanoparticles were conjugated to the detection antibody (HCA 157 P) as in Chapter 3 (section 3.3.8.) according to the modified method of Salam and Tothill (2009). A 1000  $\mu\text{L}$  volume of gold colloid (BBI solutions) was taken in a 2 mL tube and 2  $\mu\text{L}$  0.2 M NaOH was added, adjusting pH to 9.0. A 100  $\mu\text{L}$  volume of neat 0.1 mg mL<sup>-1</sup> detection antibody (HCA 157P) was added slowly; the mixture was shaken at room temperature for 1 hour on the ELISA plate shaker (16-17 rpm) in the dark. Blocking buffer (100  $\mu\text{L}$ ) 1:40 milk in PBS (0.01 M) was added. The tube was incubated on ELISA plate shaker incubator / shaker model iEMS 1415 Labsystem, (Helsinki, Finland) at (18-25°C) for 1 hour in the dark. Centrifugation was at 10,000 rpm for 10 minutes (4°C) in Heraeus Fresco 21 centrifuge (Thermo scientific, U.S.A).

The supernatant was discarded and pellet re-suspended in 70  $\mu\text{L}$  PBS (0.01 M; pH 7.4). Stock AuNP-conjugated to detection antibody was stored at 4°C. AuNP stock was diluted (1:10) in PBS (0.01 M) for use in sandwich assay signal enhancement (Figure 4.3).



**Figure 4-3:** Schematic sandwich ELISA with HRP and antibody-labelled gold nanoparticles on SPGE.

#### **4.3.6 Detection of L-LDH in spiked serum**

Parasite LDH is expressed at high levels during asexual stage or blood stage in all four malaria parasites (Sherman, 1979). Lactate dehydrogenase also correlates with the number of parasites present in the plasma of infected patients (Piper, 1999). To assess the electrochemical response in serum matrix, the assay was conducted as in section 4.3.3 using 100% commercial Human serum (P2918) from Sigma (Dorset, UK). A serial dilution of L-LDH recombinant protein recombinant L-LDH (CSB-EP632935PLS ) 1000, 100, 10 , 1 and 0.1 ng mL<sup>-1</sup> was used in sandwich assay with 0.01 mg mL<sup>-1</sup> of the capture antibody (HCA 158) and 0.01 mg mL<sup>-1</sup> detection antibody HCA 157 P on the working electrode.

Amperometric measurements were taken using Autolab potentiostat (Metrohm, The Netherlands) connected to an adapter (DropSens, Spain). USB box connecting the setup of equipment and General Purpose Electrochemical Software (GPES) version 4.9.007 were used (n=3).

#### **4.3.7 LOD spiked serum L-LDH AuNP-enhanced detection**

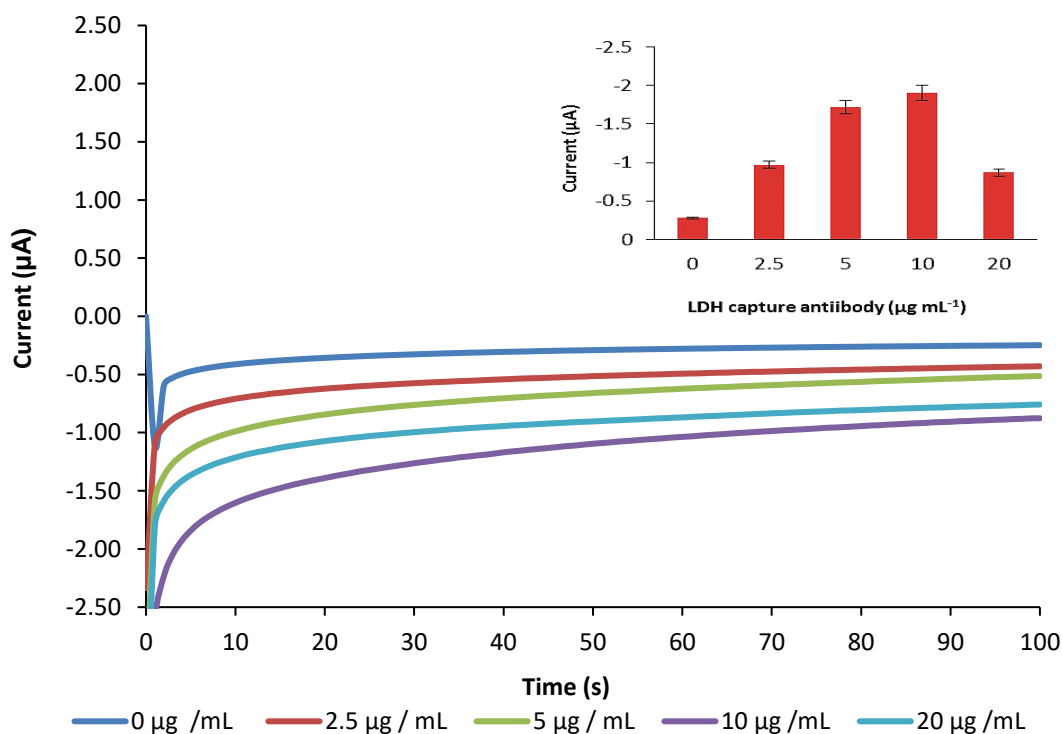
AuNP enhanced assay for detection of parasite L-Lactate dehydrogenase was conducted according to section 4.3.6 using 100% serum as the matrix for dilution of the antigen. A serial dilution of 1000, 100, 10 , 1 and 0.1 ng mL<sup>-1</sup> recombinant L-LDH was used in sandwich assay with 0.01 mg mL<sup>-1</sup> of capture antibody (HCA 158) and 1:10 AuNP detection antibody (HCA 157 P) stock / PBS (0.01 M) on the SPGE working electrode. Current generated was measured (n=3).

### **4.4 RESULTS AND DISCUSSION**

#### **4.4.1 Capture antibody (HCA 158) optimization on SPGE**

Sandwich assay was conducted on the SPGE according to the method in section 4.3.1. Recombinant protein L-Lactate dehydrogenase (CSB-

EP632935PLS) and detection antibody conjugated to horse radish peroxidase (HCA 157 P) concentrations were kept constant at  $30 \mu\text{g mL}^{-1}$  while concentration of capture antibody (HCA 158) was varied as  $2.5 \mu\text{g mL}^{-1}$ ,  $5 \mu\text{g mL}^{-1}$ ,  $10 \mu\text{g mL}^{-1}$  and  $20 \mu\text{g mL}^{-1}$  (Figure 4.4). Signal is average of three sensors per concentration (embedded graph).

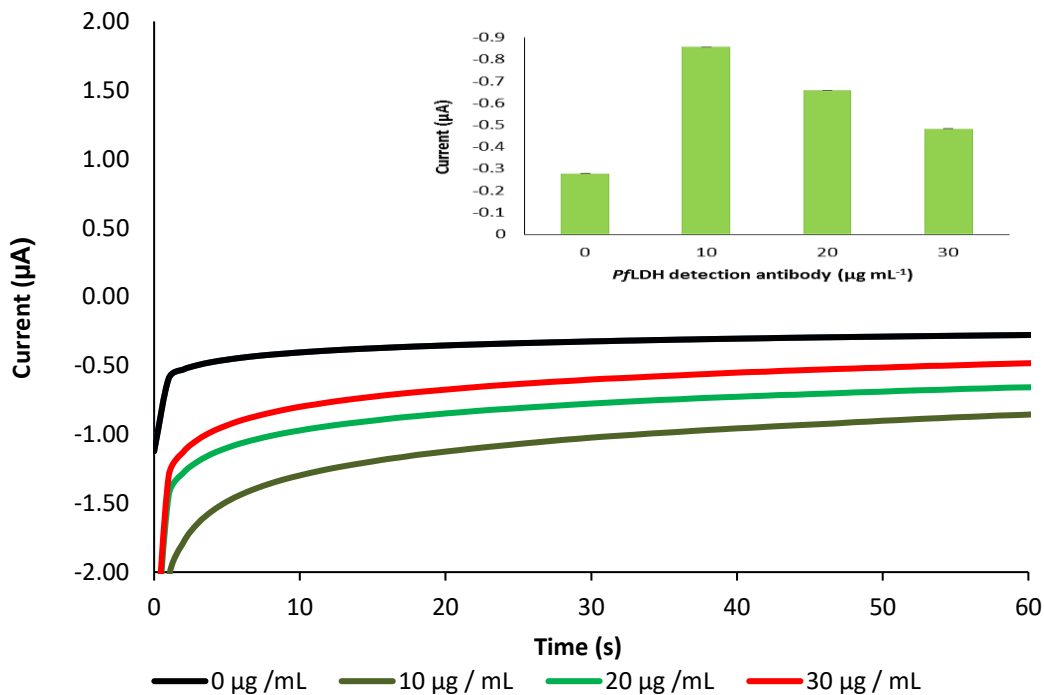


**Figure 4-4:** Amperometric measurements for *PflDH* capture antibody optimization. Capture antibody concentration assayed were  $2.5$ ,  $5$ ,  $10$  and  $20 \mu\text{g mL}^{-1}$  in sandwich format. Detection of the LDH analyte is evident in the profile of averages of 3 sensors used.

Capture antibody optimization shows an increase in signal until saturation at  $10 \mu\text{g mL}^{-1}$ . This implies that  $10 \mu\text{g mL}^{-1}$  is the optimal concentration for the assay. Having established that  $10 \mu\text{g mL}^{-1}$  is suitable as the optimal capture antibody concentration, the detection antibody was optimized using  $10 \mu\text{g mL}^{-1}$  capture antibodies on all the electrodes including the blanks in duplicate.

#### 4.4.2 Detection antibody (HCA 157 P) optimization on SPGE

To determine the most suitable horse radish peroxidase-conjugated detection antibody concentration for the assay, sandwich procedure was conducted as in section 4.3.3 and scanned for amperometric signal (Figure 4.5).



**Figure 4-5:** Amperometric measurements for *Pf*LDH detection antibody optimization. A  $10 \mu\text{g mL}^{-1}$  capture antibody (HCA 158) and  $30 \mu\text{g mL}^{-1}$  recombinant L-LDH concentrations were used. The detection antibody (HCA 157 P) was however diluted in 1: 40 milk PBS to working concentrations of 10, 20 and  $30 \mu\text{g mL}^{-1}$ . Detection antibody (HCA 159 P) showed saturation at  $10 \mu\text{g mL}^{-1}$  concentration, and best signal response for the assay confirming capture antibody optimization. Average of three sensors was used to show profile (embedded plot).

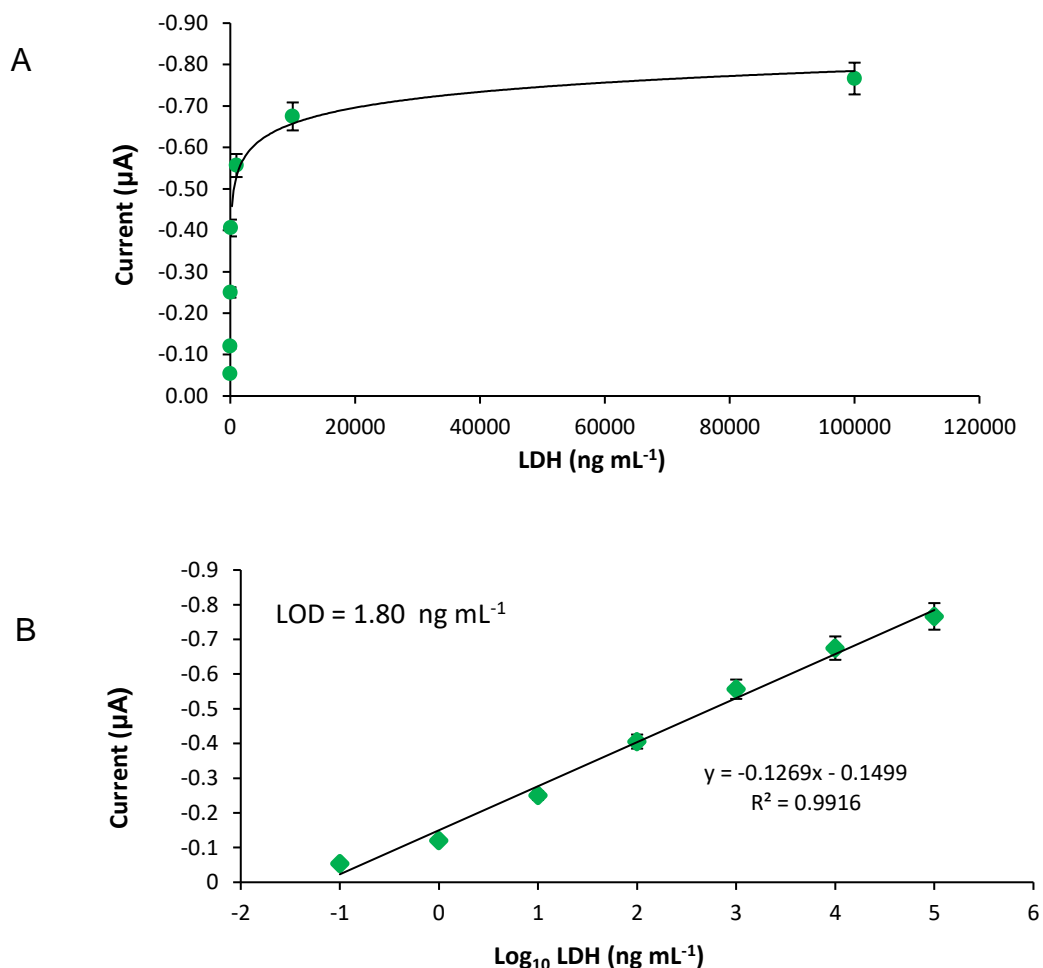
In the electrochemical detection of LDH, concentrations above  $10 \mu\text{g mL}^{-1}$  were also optimized. Early saturation at around  $10 \mu\text{g mL}^{-1}$  was observed for the detection antibody optimal concentration for use in the assay.

#### 4.4.3 L-LDH standard curve in buffer samples

Following optimization of the capture and detection antibodies, standard curve was obtained by testing the immunosensor response to *Pf*L-LDH (CSB-EP632935PLS) concentrations ranging from 1, 10, 100, 1 000, 10, 000 and 100, 000  $\text{ng mL}^{-1}$ . The assay was performed as described in section 4.3.3 with capture and detection antibody concentrations kept constant at  $10 \mu\text{g mL}^{-1}$ . The assay was run in triplicate for all the measurements. After measurements were taken, blank reading was subtracted from the signal and plotted against *Pf* L-LDH concentration. The average of three sensors was used to determine the



lowest detectable analyte concentration, calculated as blank reading plus three times its standard deviation. The value was interpolated in GrapPad prism (version 5) and plotted in Microsoft Excel (Figure 4.6).

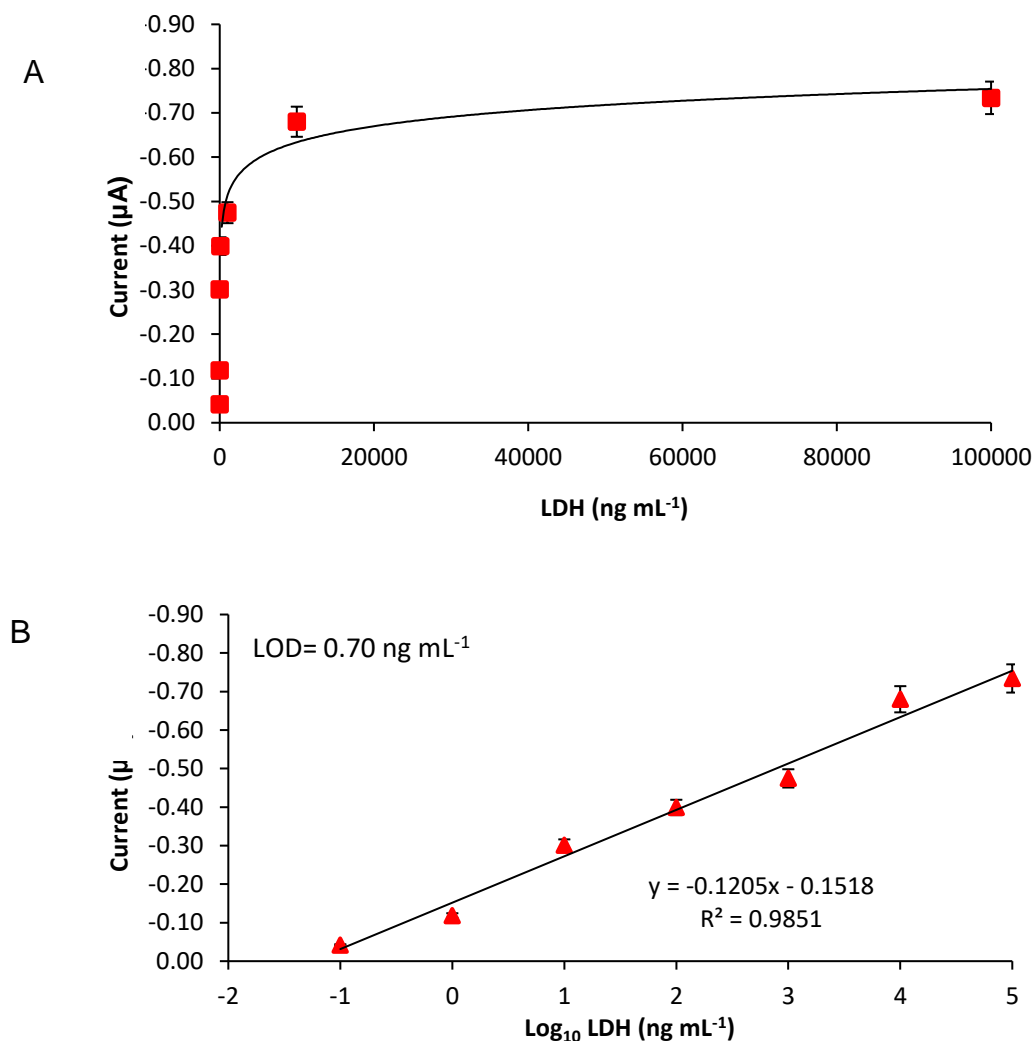


**Figure 4-6:** Standard curve of the chronoamperometric signal of L-LDH detection in buffer (A) and linear regression (B). The range was from 0.1, 1, 10, 100, 1000, 10000 and 100,000  $\text{ng mL}^{-1}$ . The lower limit of detection of the immunosensor showed a response that is linear with a long linear range. Correlation coefficient  $R^2$  value of 0.9916 was observed in buffer matrix. Limit of detection was  $1.80 \text{ ng mL}^{-1}$ , using an average of three sensors.

Limit of detection was calculated as previously using 3 x standard deviation of the blank plus the average value of the blank, interpolated in the independent variables with GraphPad prism (version 5). Following the experiment to determine antigen recognition in standard curve using buffer matrix, a separate investigation was conducted to determine the response in 100% commercial serum matrix.

#### 4.4.4 L-LDH standard curve in serum samples

The assay was conducted as in section 4.4.3 using 100% serum as the sample matrix to test for interference with amperometric detection and to verify detection limit of the buffer assay (Figure 4.7).



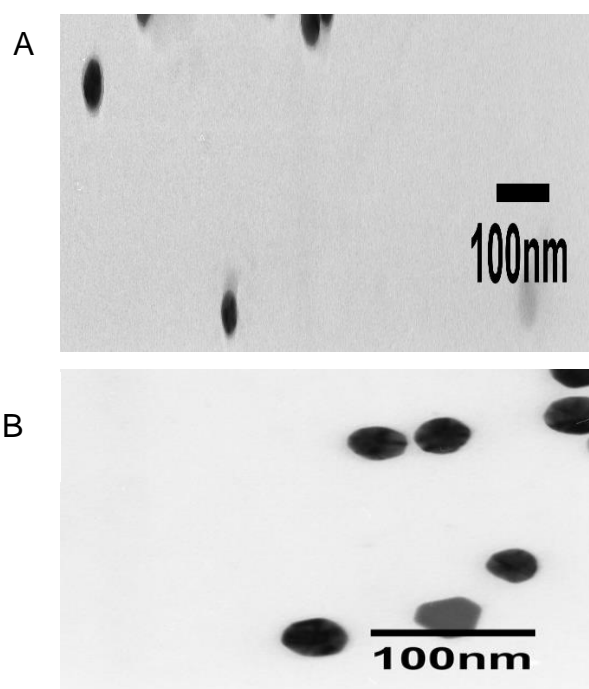
**Figure 4-7:** Standard curve of the chronoamperometric signal of L-LDH detection in serum (A) and linear regression (B). The range was from 0.1, 1, 10, 100, 1000, 10,000 and 100,000  $\text{ng mL}^{-1}$ . The lower limit of the immunosensor in this assay shows response as per available antigen. Correlation coefficient and  $R^2$  value of 0.9851 was observed, while limit of detection was 0.70  $\text{ng mL}^{-1}$  in spiked serum.

As expected, the serum assay was not much variant from the buffer assay. This is encouraging as it shows the high and accurate sensitivity of the immunosensor with regard to sample matrices.

Blood levels of pLDH are  $\sim 4.9 \text{ ng mL}^{-1}$  (Dzakah et al., 2014; Dirkzwager et al., 2015). With recent studies showing a direct correlation between blood levels of pLDH and response to therapy (Druilhe et al., 2001), it follows that parasite clearance is responsible for a drop in antigenic blood levels. Improper diagnosis and treatment may also result in drug abuse and unexpected side effects (Evans et al., 2004).

#### 4.4.5 Conjugation of AuNP to detection antibody (HCA 157 P)

Commercial AuNP (40 nm) purchased from BBI was conjugated to horse radish peroxidase detection antibody (HCA 157 P) as described in section 3.3.8. The particle size was visually estimated before and after conjugation with AuNPs using transmission electron microscopy (Figure 4.8).



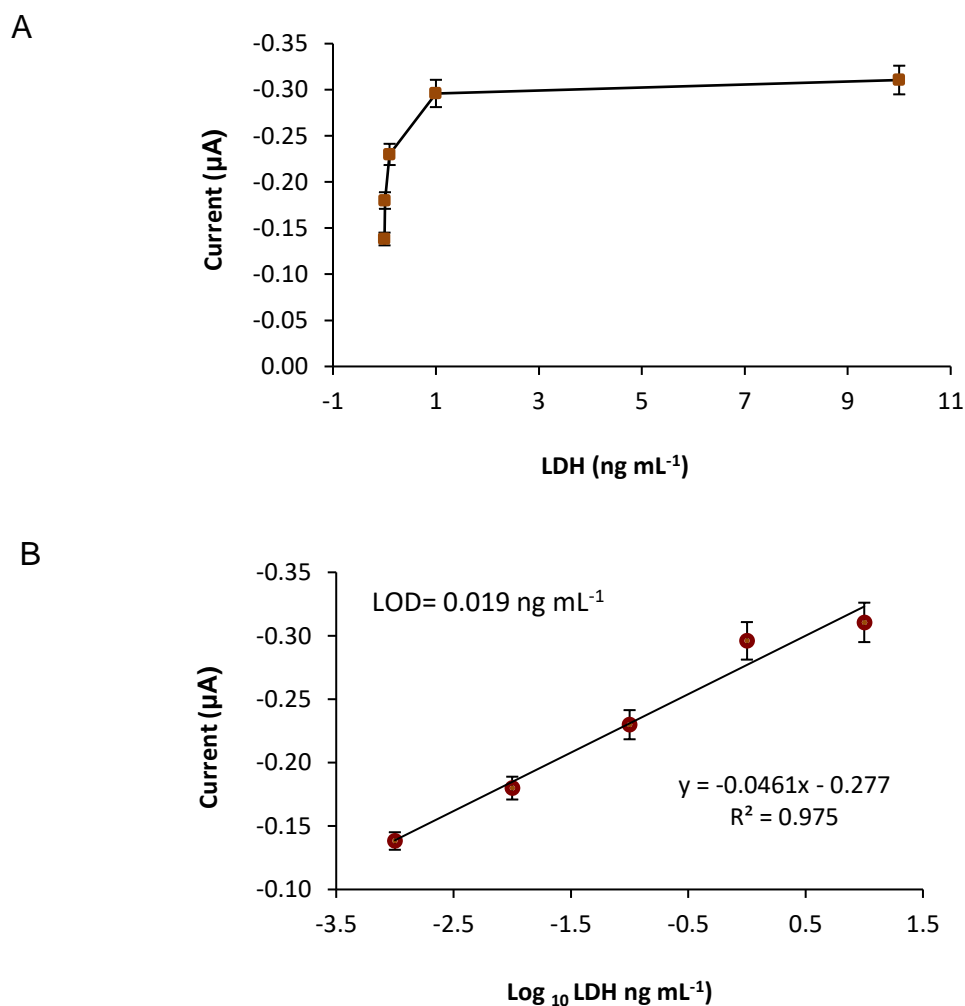
**Figure 4-8:** TEM AuNP before (A) and after (B) antibody conjugation. Nanoparticle sizes range between 1 and 100 nm. The size of commercial gold nanoparticles was determined by transmission electron microscopy.

With a 100 nm scale bar for comparison, the gold nanoparticles were found to be approximately 40 nm in size prior to conjugation to the detection antibody. Conjugation of BBI gold nanoparticle to horse radish peroxidase conjugated detection antibody was therefore as successful as the Sigma AuNP (section

3.4.10, Figure 3.18) as solution of AuNP- antibody stock diluted (1:1) with 2.5 M NaCl was clear. The addition of NaCl causes flocculation if the conjugation of AuNP to detection antibody is unsuccessful.

#### 4.4.6 LDH standard curve in buffer samples with AuNPs

As carried out in Chapter three (section 3.4.11), gold nanoparticles (40 nm) have been used to amplify the signal generated in affinity assay. The AuNP assay showed a lower signal range than the unenhanced assay in buffer matrix (Figure 4.9).

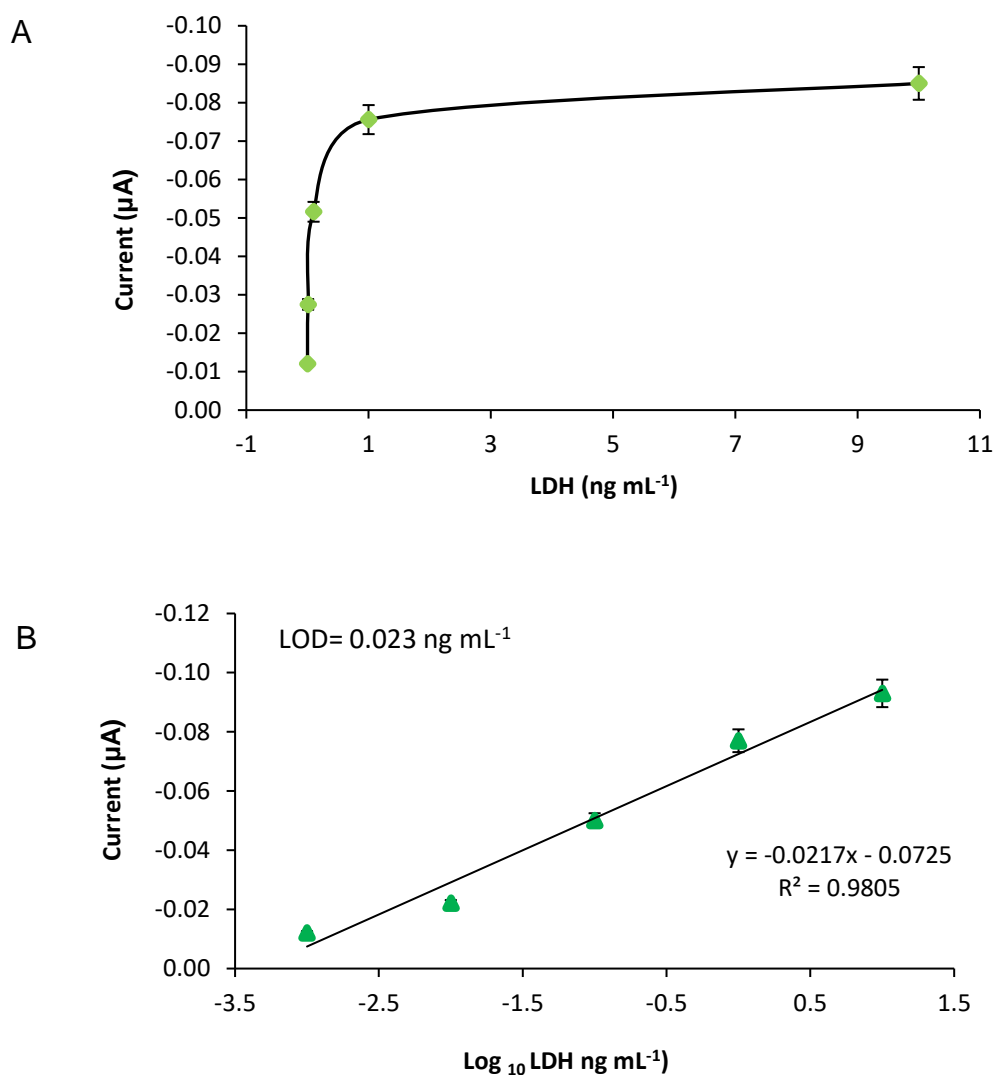


**Figure 4-9:** Calibration curve of the enhanced chronoamperometric response of LDH detection in buffer (A) and linear regression (B) using 1: 10 AuNP stock dilution used. Independent variable range was taken to be 0.001, 0.01, 0.1, 1 and 10 ng mL<sup>-1</sup> with the logarithm of the values plotted in the linear regression curve. Limit of detection was 0.019 ng mL<sup>-1</sup> and correlation coefficient ( $R^2$ ) 0.975. Average of three sensors was used to plot the curve.

The investigation carried out with AuNP signal enhancement in buffer matrix is successful and therefore compared to commercial serum in order to investigate the effect of the matrix on the detection of the analyte.

#### 4.4.7 LDH standard curve in serum samples with AuNPs

Further investigation has been carried out to assess the effect of serum matrix on signal enhancement using gold nanoparticles (40 nm) as in section 4.4.6 (Figure 4.10).



**Figure 4-10:** LDH AuNP enhanced assay standard curves (A) and linear regression (B) in 100 % serum matrix. A 100% concentration of commercial serum was used to dilute recombinant LDH to a concentration of 0.001, 0.01, 0.1, 1 and 10  $\text{ng mL}^{-1}$ . Limit of detection  $0.023 \text{ ng mL}^{-1}$  while  $R^2$  value of 0.9805.

The capture and detection antibody concentrations were taken at 0.10  $\mu\text{g mL}^{-1}$  for the detection of LDH antigen. The limit of detection for the assay was determined using the 3x the standard deviation of the blank average plus the blank average. The signal amplification was successful when compared with the unenhanced assays (Table 4.1).

**Table 4-1: Parasite L-Lactate dehydrogenase standard curves**

Sample	LOD ( $\text{ng mL}^{-1}$ )	Equation	R <sup>2</sup>
LDH buffer	1.80	$y = -0.1269x - 0.1499$	0.9916
LDH 100% serum	0.70	$y = -0.1205x - 0.1518$	0.9851
AuNP LDH buffer	0.019	$y = -0.0461x - 0.277$	0.975
AuNP LDH 100% serum	0.023	$y = -0.0217x - 0.0725$	0.9805

The sensor showed good performance in electrochemical assay, and low limit of detection. Other non commercialized, electrochemical malaria immunosensors from previous research were compared against the developed HPR 2 and LDH enhanced immunosensor assays (Table 4.2).

**Table 4-2:** Comparison with some malaria electrochemical immunosensor assay detection limit

Immunosensor	LOD	References
Magnetic nanoparticle	0.3 $\text{ng mL}^{-1}$	(de Souza et al., 2011)
Carbon nanofibre	0.025 $\text{ng mL}^{-1}$	(Ginkunoo et al., 2014)
DEA buffer assay	60 $\text{ng mL}^{-1}$	(Sharma et al., 2011)
PBS buffer assay	1 pM	(Lee et al., 2012)
AuNP HRP 2	36 $\text{pg mL}^{-1}$	This work
AuNP LDH	19 $\text{pg mL}^{-1}$	This work

The values from this work represent sensitivity of immunosensors in gold nanoparticle-enhanced buffer assay. Notably, the magnetic nanoparticle

immunosensor (deSouza et al., 2011) and the carbon nanofiber immunosensor (Giknoo et al., 2014) exhibit comparable sensitivity to the developed gold nanoparticle assays. The developed gold nanoparticle assays have the added advantage of low production cost and lower toxicity than both the electromagnetic nanoparticle assay and the carbon nanofiber assay.

## 4.5 CONCLUSIONS

L-LDH immunosensor for pan-malaria antigen has been successfully developed using HuCAL monoclonal capture antibody (*Plasmodium falciparum* HCA 158), detection antibody (horse radish peroxidase-conjugated *Plasmodium falciparum* HCA 157 P) and recombinant *P. falciparum* L-LDH (CSB-EP632935PLS) in sandwich assay. The assay is more sensitive than microscopy which is the gold standard, detecting all malaria antigens in buffer and serum in the picogram range. The signal is amplified in gold nanoparticle assay.

Matrix effect is not significant in the assay, a good indication that the limit of detection with field samples will be within the range detectable with the developed immunosensor. When using the developed immunosensors, with adequate mobile network, real time monitoring, evaluation and impact assessment can be conducted.

In the next chapter, the assay will be compared with the immunochromatographic assay which is a POC device already in use in the field for detecting malaria. This assay has potential for adoption as part of a conjugated smart device to simultaneously consult with laboratory while sample analysis takes place in the field.

The second malaria DuPont SPGE biosensor developed in this work detects malaria parasite LDH. As with *PfHRP 2*, the method is adaptable and can be used in combo for more rapid, specific detection of malaria.





**CHAPTER FIVE**  
**SAMPLE ANALYSIS AGAINST COMMERCIAL KITS**



## 5 SAMPLE ANALYSIS USING COMMERCIAL KITS

### 5.1 INTRODUCTION

Since introduction in the 90s, malaria immunochromatographic tests (ICTs) have undergone much improvement (Iqbal et al., 2002; Maltha et al., 2010). Initially two-band tests were used, comprising a control line and a parasite species-specific band. Later, a three-band ICT was developed which detects both biomarkers, PfHRP 2 and LDH, and a control line. Some strengths and weaknesses of ICTs are listed in Table 5.1.

**Table 5-1: Advantages and disadvantages of Immunochromatographic tests**

Advantage	Disadvantage	Reference
Some tests can detect different parasites such as <i>P.ovale</i> , <i>P. malariae</i> and <i>P. vivax</i>	Some tests detect PfHRP 2 only	(WHO, 2000; WHO, 2004)
Dipstick cassette or card format easy to use	Qualitative result, unpredictable sensitivity in the field caused by high temperature, humidity	Gaye et al., 1998; Ricci et al., 2000; Iqbal et al., 2001; Coleman, et al., 2002; Craig et al., 2002; Mason et al., 2002; WHO, 2003)
Simple to perform and interpret do not require electricity	Potential for misdiagnosis due to biomarker persistence for 1-3 weeks	(WHO, 2000)
Fewer requirements for personnel training	Malaria antigens have different characteristics affecting suitability	(WHO, 2000; WHO, 2004)

Current detection of malaria parasite typically depends on commercial immunochromatographic tests (ICTs) in dipstick and cassette format. Lateral flow technology is a popular platform because of its low development cost and ease of use (Zhou et al., 2014). Some antibody-based immunochromatographic tests detect all Plasmodium proteins such as lactate dehydrogenase (Iqbal et al., 2001; Jain et al., 2014). These tests have been used successfully in conjunction with blood film microscopy to confirm diagnosis of malaria with varying sensitivity (Table 5.2).

**Table 5-2:** Comparative sensitivity of some immunochromatographic tests

Test	Analyte	Sensitivity (%)	Reference	Website
Acon (Acon Labs, SanDiego, CA, USA)	HRP 2	94	Mawili-Mboumba et al., 2010	www.aconlabs.com
Parabank (Orchid/Zephyr, Goa, India)	LDH	84.7		www.tulipgroup.com/Zephyr
Vistapan (Mitra, New Delhi, India)	LDH	91.9	Fogg et al., 2008	www.jmitra.co.in
CareStart (Access Bio, Princeton, NJ, USA)	LDH / HRP 2	95.6		http://www.accessbio.net/eng/products
PALUTOP+4(ALL.DIAG, Strasbourg, France)	LDH / HRP 2	95.4		www.alldiag.com
OptimMAL-IT (DiaMed, Cressier, Switzerland)	LDH	75.8	Rakotnirina et al., 2008	www.bio-rad.com
ParaHIT-f Diagnostics	(Span HRP 2	87.5	Singh et al., 2005	www.span.co.in
ParaSight -F Dickinson, USA)	(Becton HRP 2	95	Forney et al., 2001	www.bd.com
Makromed (Makro Medical Pty. Ltd., Johannesburg, Republic of South Africa)	Dipstick HRP 2	97	Richardson et al., 2002	www.makro-med.com
Malar-Check test(Cumberland diagnostics ltd)	<i>Pf</i> HRP 2	97.4	Avila et al., 2002	www.cumberland-diagnostics.com
Paracheck Pf Biomedical Systems, Goa, India)	(Orchid HRP 2	91.7	de Oliveira et al., 2009	www.tulipgroup.com

The sensitivity and specificity of CareStart Malaria test is comparable to the thick blood smear in diagnosis of malaria. Less accuracy may occur in stored samples (Maltha et al., 2010).

ICTs are commonly used for malaria detection in whole blood samples containing the water soluble malaria biomarker (Moody, 2002). With reports of insufficient data for projection of malaria incidence (WHO, 2015), this research will progress and contribute in screening of sub-microscopic malaria in sub-

Saharan Africa. Several recent reports have described biosensor assays detecting and differentiating malaria biomarkers (Sharma, 2008; Ittarat, 2013). As yet, there is no commercial malaria biosensor that meets the diagnostic requirement of infected individuals in endemic and remote areas. Sub-microscopic detection offered by biosensors demands further investigation in low cost, easy to use, portable and disposable format. With a view to meeting this need, JD 2b screen-printed electrodes, have been utilized in the construction of two highly sensitive immunosensors, with signal enhanced using gold nanoparticles.

Work in this chapter involves samples of *Plasmodium falciparum* Dd2<sup>luc</sup> culture medium supernatant containing water soluble malaria biomarkers, PfHRP 2 and LDH. The samples were used to investigate sensitivity of the qualitative BinaxNOW Malaria and OptiMAL-IT commercial kits in comparison to the quantitative, developed LDH electrochemical immunosensor.

## **5.2 MATERIALS**

### **5.2.1 General chemicals and instrumentation**

Chemicals and instrumentation for cell culture were obtained through collaboration with scientists from Keele University (Staffordshire, UK); malaria parasite culture medium from Roswell Park Memorial Institute (RPMI) 1640 Lot no. RNBF4698. HEPES buffer, glucose solution, NaOH, glutamine solution, 1000x hypoxanthine solution, pooled human serum, Albumax-II, BSD and gentamycin sulphate solution were from Sigma (Dorset, UK).

Microbial safety cabinet NuAire DH Autoflow (ON, Canada), while 20 % Giemsa stain, 100% methanol, 70% alcohol, 5% sorbitol, pipettes, culture flasks, 96 well plates and pH test Strips Lot 010B164786, passive lysis buffer and luciferase substrate (luciferin) were purchased from Sigma (St.Louis, USA). Microfilter (0.45 µm) syringe-driven filter unit was purchased from Millipore (Dublin, Ireland), 1% Oxygen / 3% CO<sub>2</sub> / N<sub>2</sub> gas BOC (Surrey, UK), light microscope, immersion oil and microscope slides were purchased from Olympus (Essex, UK), centrifuge U-320R (Boeco, Germany) blow drier

(Phillips, UK) and GloMax luminometer was purchased from Promega (Madison, USA). Stainless steel hand counter was also used (such as are available from miniscience.com)

OptiMAL-IT malaria dip stick kit (containing dipstick, buffer ampoule, reaction and wash wells, and Pasteur pipette) and positive control were purchased from Bio-Rad (Oxford, UK), while BinaxNOW Malaria test kit (lateral flow device and wash buffer) was purchased from Alere (Bedford, UK). Fume cupboard was from Kottermann (Zurich, Switzerland) while, autoclave was purchased from Priorclave (London, UK). As before, screen-printed electrodes as, JD 2b, described in Chapter 2 were obtained from DuPont (Bristol, UK).

## **5.3 METHODS**

### **5.3.1 Preparation of the culture medium**

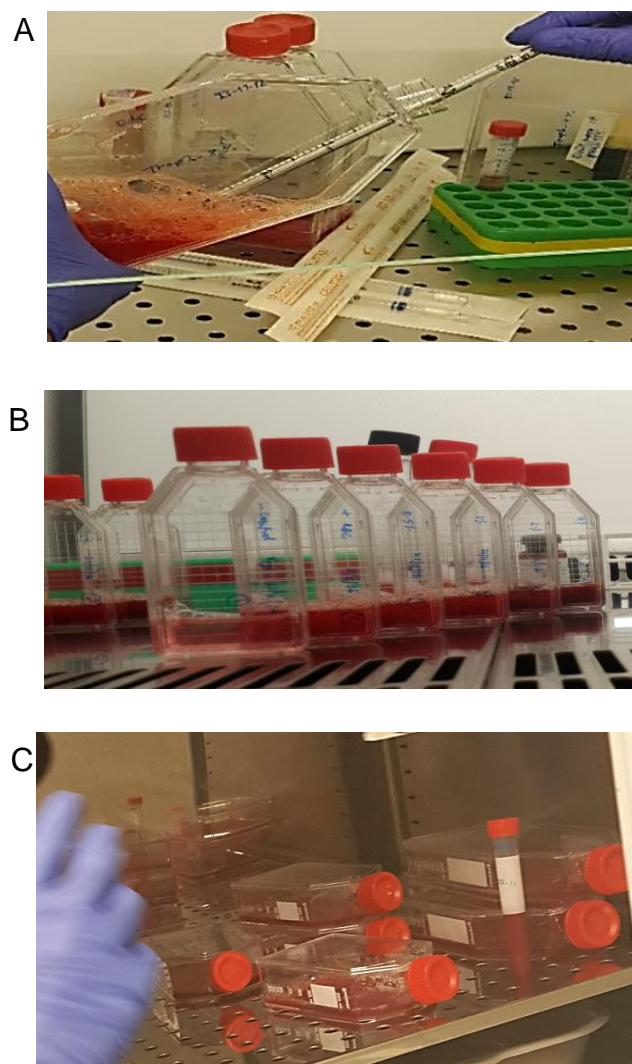
The media preparation and *in vitro* culture of *P. falciparum* cells was conducted in level 3 laboratory in Keele University in the group of Professor Paul Horrocks. For over 40 years, Roswell park memorial institute (RPMI) 1640 medium has been commonly used for *in vitro* parasite culture preparation (Desai, 2013). RPMI medium contains major cations and anions based on values in human blood of glucose, amino acids and key vitamins; serving as energy source for cell metabolism. The medium supports synthesis of proteins, nucleic acids and lipids (Desai, 2013).

A 500 mL volume of RPMI 1640 medium was taken in a tissue culture bottle and supplemented with 1 M HEPES buffer (18.75 mL), 45% glucose solution (2 mL), 1 M NaOH (2.5 mL), 200 mM glutamine solution (5 mL), 1000x hypoxanthine solution (0.1 M solution in NaOH) (500  $\mu$ L), pooled human serum (20 mL) 5% Albumax-II (20 mL) BSD (125  $\mu$ L), 10 mg mL<sup>-1</sup> gentamycin sulphate solution (1.25 mL) and 8% v/v human serum ) at the desired haematocrit in an atmosphere of 1% Oxygen / 3% CO<sub>2</sub> / N<sub>2</sub> ; in a modified method according to Hasenkamp et al., 2011. 1000x stock solution of

hypoxanthine (50 mM) can be prepared by dissolving 680 mg in water and then adding a few drops of NaOH to bring to pH 9.0, before making up to 100 mL. Stock is filter sterilized and stored at 4°C.

### 5.3.2 Culture of Dd2<sup>luc</sup> in RPMI medium

Dd2<sup>luc</sup> is a transgenic *Plasmodium falciparum* clone expressing luciferase under the control of *Pfpcna* flanking sequences (Wong et al., 2011). To begin, the microbiological cabinet was swabbed with 100% methanol. Dd2<sup>luc</sup> was cultured *in vitro* using standard continuous culture conditions. To the medium prepared (section 5.3.1) RPMI medium were prepared in tissue culture flasks to mimicked human physiology, using a parasitaemia of 0.5%, 1%, 2% and 4% early trophozoites and 0.5%, 1%, 2% and 4% mixed stage cultures in a second group (Figure 5.1). Both groups had culture media (plain and containing uninfected RBC) as control. Following inoculation, the samples were incubated at 37°C for 48 hrs.



**Figure 5-1:** Preparation of culture. Following inoculation, the samples were gassed to mimic physiological conditions of human internal environment (A). When the two groups were sufficiently gassed (foamy), as in (B), they were incubated at 37°C(C).

For *in vitro* Plasmodium cell culture, the physiological conditions of the human host environment are produced to support the parasite. When the parasite encounters the host cell, the parasitophorous vacuole isolates the parasite from the cell cytoplasm (Haldar and Mohandas, 2009; Bosch et al., 2012; Yap et al., 2014). The parasite takes in haemoglobin. As development continues, the parasite increases in number within the erythrocyte. It also enhances the beginning and sustenance of electrochemical ion gradients. In addition, early destruction of the infected red blood cell is prevented by the copious amounts of



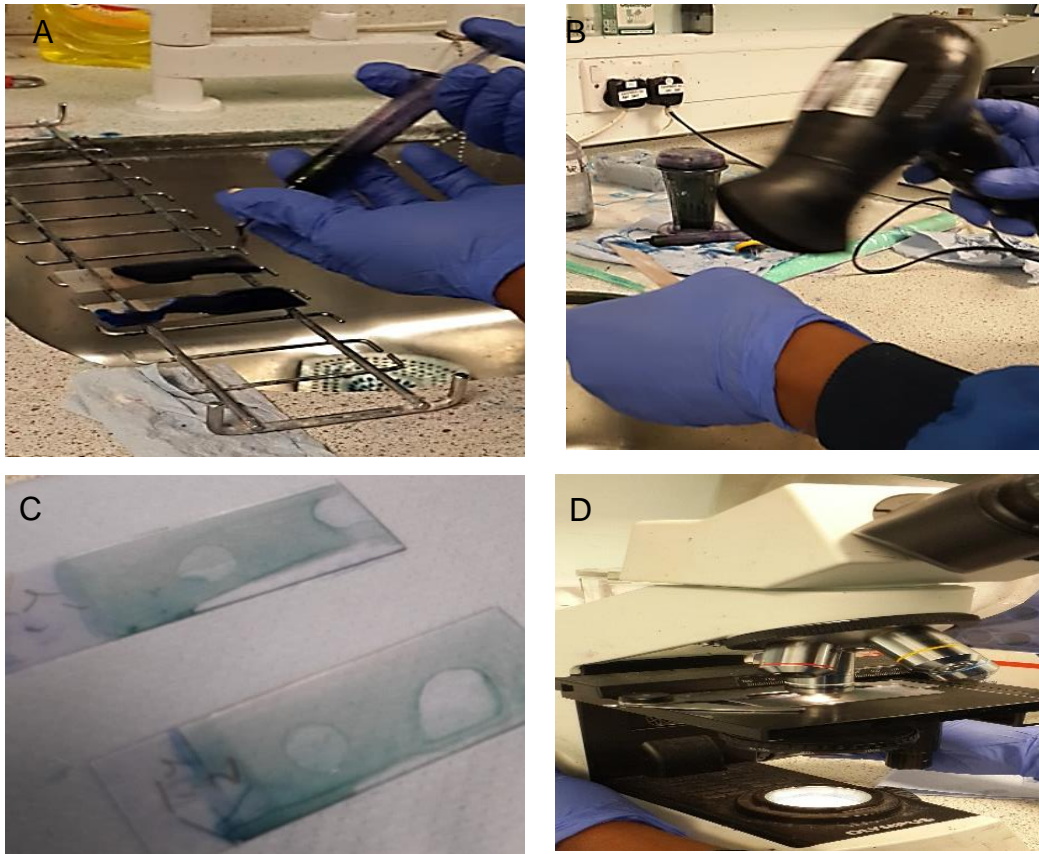
haemoglobin that the parasite takes in, utilizes, detoxifies and removes from the infected red blood cell thus ensuring osmotic stability (Haldar and Mohandas, 2009). The stage at which the asexual form of the parasite in the red blood cell develops into the sexual form of the parasite is however a process that is little explained (Akhouayri et al., 2013).

### **5.3.3 Culture medium supernatant of Dd2<sup>luc</sup> (in RPMI)**

To conduct investigations on the biomarker, the supernatant was obtained from the tissue culture flask. The cultured cells were then collected into a falcon tube. The tube was spun at 3,500 rpm for 5 minutes at room temperature (18-25°C). The supernatant now devoid of Plasmodial cells (6% parasitaemia) was separated from the pellet and stored in aliquots of 1 mL to be used in immunoassay.

### **5.3.4 Preparation of malaria thin film**

After 48 hr incubation, Plasmodium parasite must have gone through asexual developmental stages (Coatney et al., 1971). To observe the parasites by microscopy, the culture was removed from incubation at 37°C between 26-38 hours in order to target the trophozoites (Silamut, 2000). The medium was aspirated using a pipette. A drop (~20 µL) of the sediment of cultured parasites was transferred to a clean, dry microscope slide. The film was made by spreading the drop on the slide. The film was gently blow dried. The film was fixed for 1 minute using methanol and washed in tap water. Giemsa stain (20%) was filtered using syringe-attached microfilter (0.45 µm) to remove particles. The filtered stain was applied to cover the dry film and allowed to stain for 10 minutes (Figure 5.2). The slide was then washed in tap water and gently blow dried. Once dry, the film was immersed in oil and observed using 100x objective lens. Oil immersion is a technique used to increase the resolving power of a microscope. This is achieved by immersing both the objective lens and the specimen in a transparent oil of high refractive index, thereby increasing the numerical aperture of the objective lens.



**Figure 5-2:** Preparation of malaria thin film. Preparation of the thin film involved Giemsa staining (A) gently drying (B) stained film (C) microscopic examination (D).

Giemsa stain is commonly used for routine examination of blood films for malaria diagnosis (Fleischer, 2004; Redd et al., 2006). The number of visible parasites should be reported especially where the infection is due to *P. falciparum*. The limitations that may occur when using this method are reflected in false positives and false negatives. In addition, the specific parasite identification poses a challenge as the stages appear to be the same in mixed infections. Debris sometimes takes on the form of parasites and is erroneously counted as parasites. *P. knowlesi* infection has also been misdiagnosed. *P. knowlesi* is reported to produce the same symptoms as *P. falciparum*.

In light microscopy, oil immersion is a technique used to increase the resolving power of a microscope. This is achieved by immersing both the objective lens and the specimen in a transparent oil of high refractive index, thereby increasing the numerical aperture of the objective lens.

### 5.3.5 Estimation of percentage parasitaemia

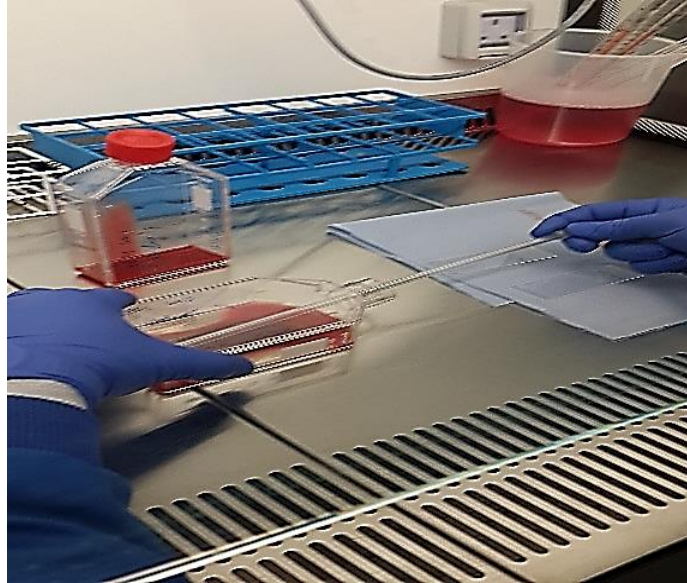
The number of parasitized cells was then counted using a mechanical cell counter (such as available on miniscience .com). Percentage parasitaemia was obtained using the equation:

$$\% \text{ parasitaemia} = \frac{\text{Average 10 parasitized}}{\text{Average 3 parasitized + non parasitized}} \times 100 \quad (5-1)$$

Where the average of 10 counted fields of parasitized cells is divided by the average of 3 counted fields of the total visible cells i.e. parasitized and non-parasitized cells. Malaria parasitaemia is reported using the World Health Organisation method of counting the number of parasites per microliter (/  $\mu\text{L}$ ) of blood instead of percentage parasitaemia (WHO, 2006). An alternative method recommended by the WHO involves the comparison of the number of parasites in a **thick blood film** with the white blood cell count (Bowers et al., 2009).

### 5.3.6 Sorbitol lysis to obtain developmental stage parasites

In malaria drug efficacy experiments it is often required to separate the developmental stages (in a process commonly known as staging) to observe their reaction to drug exposure. For this experiment the samples were synchronised at 0 h and also at 48 hr incubation at 37°C. Synchronization lyses infected red blood cells within the culture at a specific stage in their *in – vitro* development such that only parasites of the same developmental stage remain in the culture medium. In order to separate the parasite stages, 5% sorbitol (five times the pellet) was added to the pellet and incubated at 37°C for five minutes. The pellet was then centrifuged at 1,800 rpm for 5 minutes. Following incubation, the supernatant was aspirated (Figure 5.3) and pellet re-suspended in RPMI 1640 culture medium and then transferred to a sterile tissue culture flask. The medium was gassed in 1% Oxygen / 3% CO<sub>2</sub> / N<sub>2</sub> and incubated for 48 hrs at 37°C.

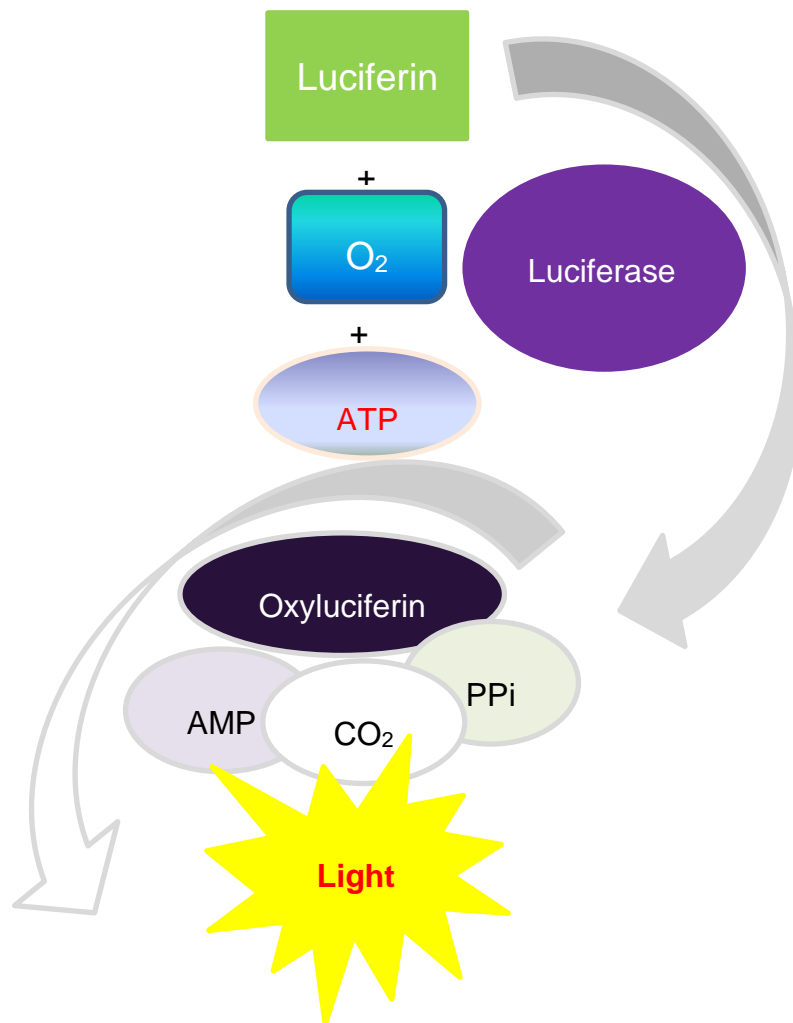


**Figure 5-3:** Aspiration of the supernatant. After incubation, the surface layer above was aspirated (removed) to leave the cell sediment in the bottom of the tissue culture flask. The growth of the cells was then determined in luciferase assay.

### 5.3.7 Luciferase assay

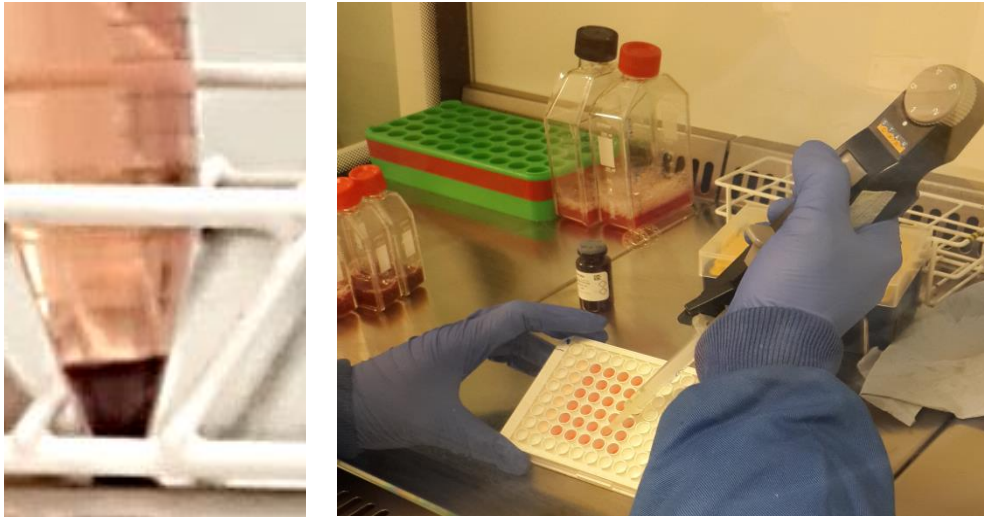
The luciferase enzyme belongs to a group of oxidative enzymes which allow the organism to bio luminesce, for example, the firefly. Organisms which bio luminesces are known to exhibit this behavioural trait in response to competition for food, mates, communication, camouflage and self-defence.

Luciferase assay is a commonly used reporter assay for quantitative, sensitive gene expression in organisms. As the reaction is energy efficient it serves as an effective reporter assay. A schematic is shown in Figure 5.4.



**Figure 5-4:** Schematic of luciferase reporter assay. Light emission is brought about by a reaction in which luciferin is converted to oxyluciferin by luciferase, with some of the energy of conversion produced as light.

In order to determine viability of the culture, luciferase assay was conducted on the cultured Dd2<sup>luc</sup> cells. Following culture of the parasites, luciferase assay was performed at 0 h and again at 48 hr (Hasenkamp, 2011). For cell-based assays, a host cell is engineered to express a reporter gene (Burrows et al., 2011). Samples were prepared as described in section 5.3.1 following which a 10 µL volume of passive lysis buffer was added to 40 µL of *P. falciparum* cells and 50 µL of luciferase substrate (luciferin) run in triplicate (Figure 5.5).

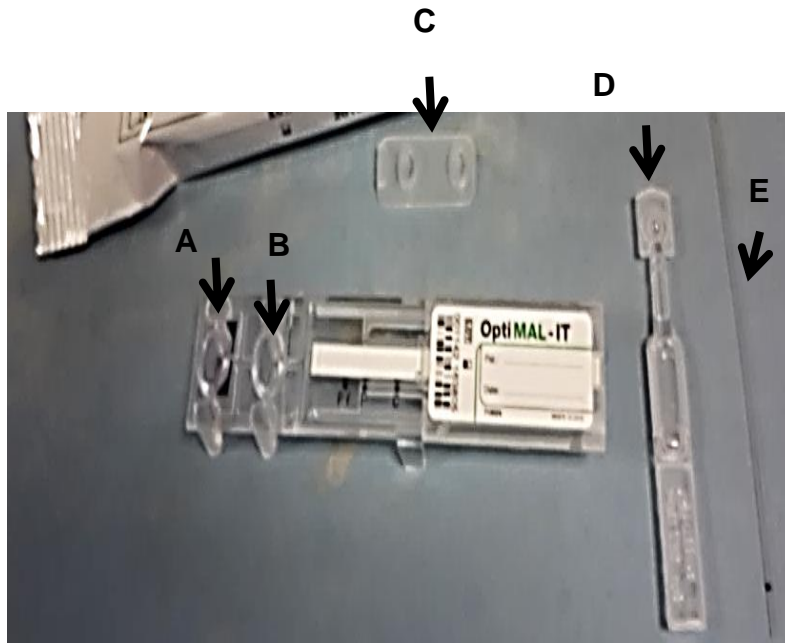


**Figure 5-5:** Pellet obtained before sorbitol lysis and luciferase assay. Synchronized and asynchronous pellets were used for luciferase assay to determine cell growth. The luciferin (50  $\mu$ L) was added to 10 $\mu$ L passive lysis buffer and then 40  $\mu$ L of *P. falciparum* cells was added. Samples were prepared in triplicate in a 96 -well microtitre plate.

The assay was run in the GloMax Luminometer to measure Relative Luminescence Units (RLU). The average of three readings was plotted in Microsoft Excel along with standard deviation. The readings represent trophozoite viability as the luciferase gene is expressed.

### 5.3.8 LDH detection using OptiMAL-IT Malaria kit

OptiMAL-IT is an immunochromatographic test, using monoclonal antibodies against the metabolic enzyme pLDH (parasite lactate dehydrogenase) of the Plasmodium sp. The kit purchased from Bio-Rad (UK) contains sachet of the test device with all its components (Figure 5.6).



**Figure 5-6:** OptiMAL-IT test. Contents include reaction well (A) wash well (B) well cover (C) buffer ampoule (D) and pipette (E).

OptiMAL-IT detects LDH produced by both asexual and sexual forms of the parasite. There is no cross reactivity with the human LDH or rheumatoid factor.

### 5.3.8.1 LDH recombinant detection in 100% serum on OptiMAL-IT

OptiMAL-IT is a commercially available for ICT for malaria detection. Each test in dipstick format is ready to use. To determine the detection of recombinant LDH in 100% serum, buffer ampoule was torn open and 1 drop (20  $\mu\text{L}$ ) was added to the conjugate well already coated with LDH antibody, and 4 drops (80  $\mu\text{L}$ ) were added to the wash well. The device was then allowed to stand for one minute. A concentration of 100  $\mu\text{g mL}^{-1}$  (20  $\mu\text{L}$ ) recombinant LDH in 100% serum was drawn up using the pipette. The entire volume was added to the conjugate well. Following the addition of the samples, contents of the well were stirred gently with the spatula end of the pipette and allowed to stand for 1 minute. The pipette was discarded and the device pulled open. The wells were then replaced on the work bench and the dip stick stood in the conjugate well supported by the holders beside the wells such that the dip stick end reached the bottom of the conjugate well and was allowed to stand for 10 minutes so the sample / conjugate mixture was completely soaked up.

The dipstick was transferred to the wash well and allowed to stand for 10 minutes so that the reaction was completely cleared of spiked serum leaving the control band clearly visible. The dipstick was removed and clicked back in the clear plastic piece. The wells were then covered and broken off along with the two legs from the clear plastic piece and placed in autoclavable bag. The reaction was read immediately and again after 60 minutes.

Test validity was determined using the internal control band. In another test, neat recombinant (LDH)  $0.8 \text{ mg mL}^{-1}$  in serum was applied to the reaction well and the test conducted as described to compare the results.

#### **5.3.8.2 LDH detection using positive control on OptiMAL-IT**

Since the neat LDH was negative after testing it was decided to apply the positive control of recombinant LDH from Bio-Rad (Oxford, UK). The positive control was reconstituted by adding 1 drop of buffer from the optimal-IT kit and left to stand for 1 minute. The reconstituted positive control was then aspirated ( $\sim 20 \mu\text{L}$ ) and added to the reaction well of the optiMAL-IT dipstick test. The LDH positive control was then assayed in immunochromatographic test in the same method as was conducted in section 5.3.8.1.

#### **5.3.8.3 LDH detection using culture medium supernatant on OptiMAL-IT**

To determine the sensitivity of the test on Dd2<sup>luc</sup> culture medium supernatant (section 5.3.2), the process in section 5.3.8.1 was conducted on the dipstick assay, using  $20 \mu\text{L}$  of 3-fold serially culture medium supernatant.

#### **5.3.8.4 LDH detection using culture medium supernatant on biosensor**

Immunoassay for the detection of LDH was carried out as in (Chapter 4) using a  $20 \mu\text{L}$  volume of 6% parasitaemia Dd2<sup>luc</sup> culture medium supernatant from a previous culture. The culture medium supernatant was aspirated from the tissue culture flasks according to the method in section 5.3.3. The sample containing soluble *Plasmodium falciparum* biomarkers PfHRP 2 and LDH was then serially diluted 3-fold and used in the electrochemical immunoassay.



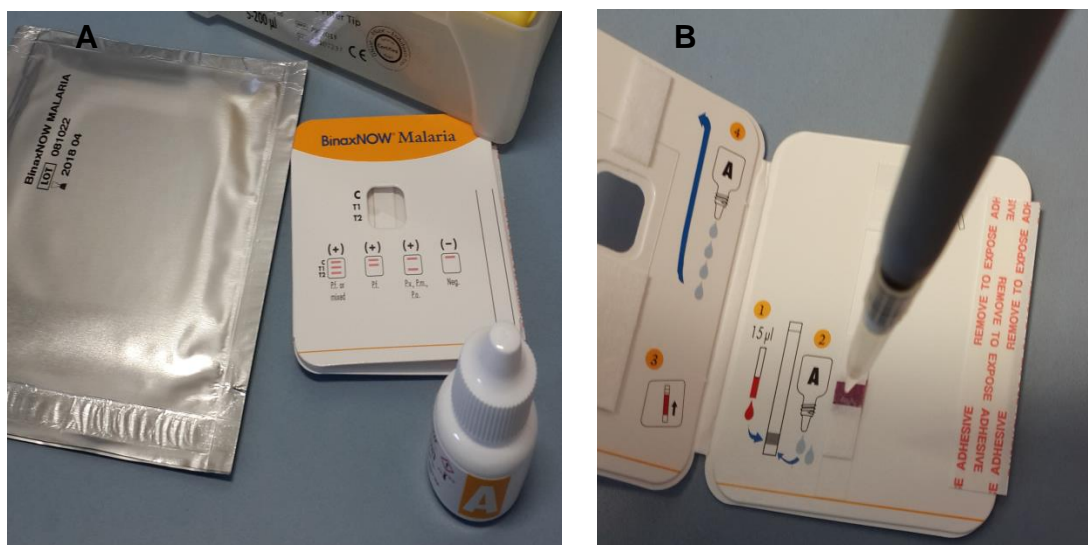
### **5.3.9 PfHRP 2 and LDH detection using BinaxNOW Malaria kit**

BinaxNOW Malaria is another *in vitro* immunochromatographic assay using monoclonal antibody (MoAb) for the quantitative detection of Plasmodium antigens circulating in human venous and capillary ethylenediaminetetraacetic acid (EDTA) whole blood of individuals with signs and symptoms of malaria infection.

The combo kit for LDH and PfHRP 2 malaria detection allows for the differentiation of *P. falciparum* from other less virulent species. The kit was investigated for sensitivity of the test on culture medium supernatant, according to manufacturer's insert.

#### **5.3.9.1 PfHRP 2 / LDH detection using culture supernatant on BinaxNOW**

Having established the detection of the biomarker using the commercial kit and immunosensor, a further investigation was carried out using the BinaxNOW Malaria kit. The samples were brought from -20°C to room temperature (18-25°C). The device was opened and the pipette primed twice. A volume of 15 µL of the asynchronous and synchronous culture medium supernatant (0%, 0.5% and 4%) were applied to the bottom half of the purple reaction pad (Figure 5.7).



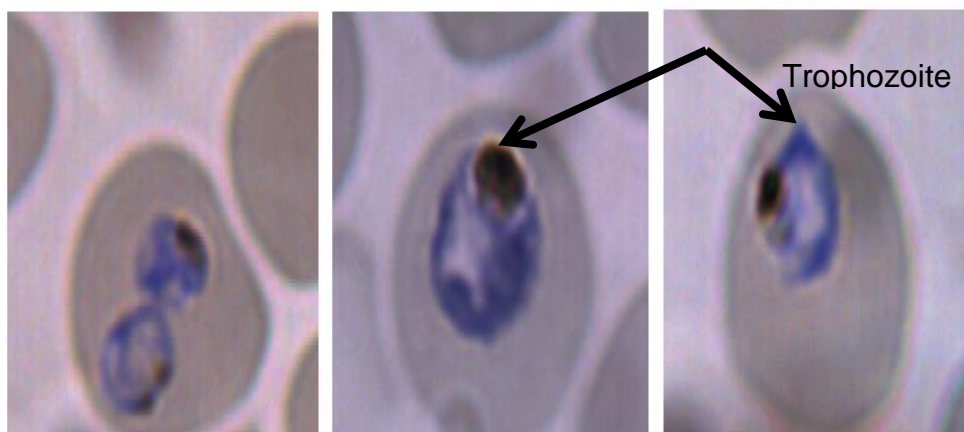
**Figure 5-7:** Contents of BinxNOW Malaria kit (A) and application of sample (B). Buffer A can be added to the sample pad to increase the flow rate if after 1 minute the sample is yet to reach the end of the strip.

Two free-falling drops (~40  $\mu\text{L}$ ) of Reagent A were added vertically to the white pad below the purple pad. The sample was allowed to run until it almost touched the absorbent pad at the top of the strip. Just before the sample reached and base of the white absorbent pad, four (4) free-falling drops of Reagent A were applied to the pad. When the sample just reached the base of the absorbent pad, the adhesive strip was removed then the device was closed. From closing, the reaction was timed for 15 minutes. The result was read through the viewing window.

## 5.4 RESULTS AND DISCUSSION

### 5.4.1 Estimation of percentage parasitaemia of *P. falciparum*

Percentage parasitaemia is the method by which malaria infection was made. The infected red blood cells show brown pigmented cytoplasm typically seen in mid-stage trophozoites (Figure 5.8). Counting of red blood cells infected with parasites of *Plasmodium falciparum* is essential and the percentage parasitaemia should always be reported as this has implications for prognosis and the pattern of treatment employed (NEQAS UK, 2013).



**Figure 5-8:** *Plasmodium falciparum* trophozoite in RBC. Following the Giemsa staining of the thin film, ~20  $\mu$ L of immersion oil is placed in the centre of the film. Thus the cells are viewed at high resolution with the exclusion of refraction as light travels from air to liquid medium.

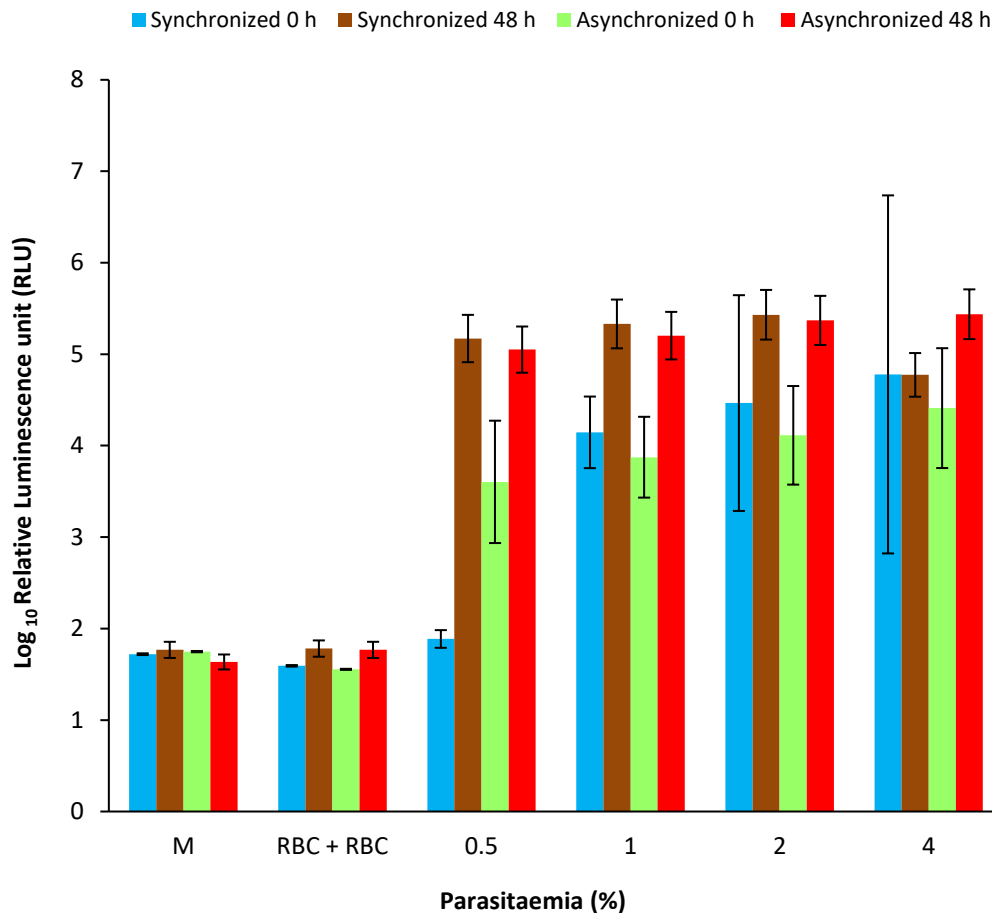
The stained cells are clearly visible under the light microscope enhanced by immersion oil under 100x objective lens. During microscopy, it is usual to observe Plasmodium cells at various stages of development. The stages range from tiny rings (0-6 h) through to gametocytes formation.

Levels of parasitaemia are not necessarily correlative with the progression of the disease, particularly when the parasite is able to adhere to blood vessel walls. Therefore, more sensitive, low-tech diagnostic tools need to be developed in order to detect low levels of parasitaemia in the field (Redd et al., 2006). Parasitaemia due to malaria infection has been reported to have a threshold of 2,500 parasites per microliter (Mwangi et al., 2005). Immunochromatographic tests may be used to complement microscopy in low resource areas (Bailey et al., 2013).

#### 5.4.1 Luciferase assay

Luciferase assay was conducted to determine the viability of the Dd2<sup>luc</sup> culture by testing for luciferase expression in cultured samples, according to the method described in section 5.3.7. Both groups of synchronized and asynchronized trophozoite samples with parasitaemia ranging from 0.5 - 4%

showed positive growth when compared to the control. The control contained no parasites. Two controls were used namely: RPMI medium only (M) and RPMI + uninfected red blood cells (RBC) (Figure 5.9).



**Figure 5-9:** Relative light unit for luciferase expression at the start and end of incubation during *Plasmodium falciparum* Dd2<sup>luc</sup> cell culture viability test. Synchronized and asynchronous samples were tested for cell growth by luciferase expression. Asynchronous samples contain all stages of parasite development while synchronous samples contain parasites at same developmental stage assayed at 0 hour incubation time. Both control samples are constant against 0.5%, 1%, 2% and 4% parasitaemia. Control for the experiment comprised neat culture medium RPMI 1640 referred to as 'M' and neat medium + uninfected red blood cells, referred to as 'RBC' (n=3).

Since the transgenic strain, Dd2<sup>luc</sup> expresses luciferase in the trophozoite stage, all the samples showed luminescence response. Luciferase assays have been used widely in high throughput screening for drug candidates (Hasenkamp et al., 2011) and to observe cell growth.

Bioluminescence is characterized by the use of a bioluminescent compound, luciferin and firefly luciferase. Luminescent reactions are measured in relative light units (RLU) that are typically proportionate to the amount of analyte present in a sample. A decline in cell culture growth is expected to occur as soon as depletion of nutrients occurs as a result of the cells competing for available resources in order to develop to the next stage of parasite development. A guide to parasite development in stages over a 48 hour period is shown in Figure 5.10.



0-6 hours = tiny rings  
 6-16 hours = small rings  
 16-26 hours = large rings  
 26-30 hours = early trophozoites

30-34 hours = mid trophozoites  
 34-38 hours = late trophozoites  
 38-44 hours = schizonts  
 44-48 hours = schizonts

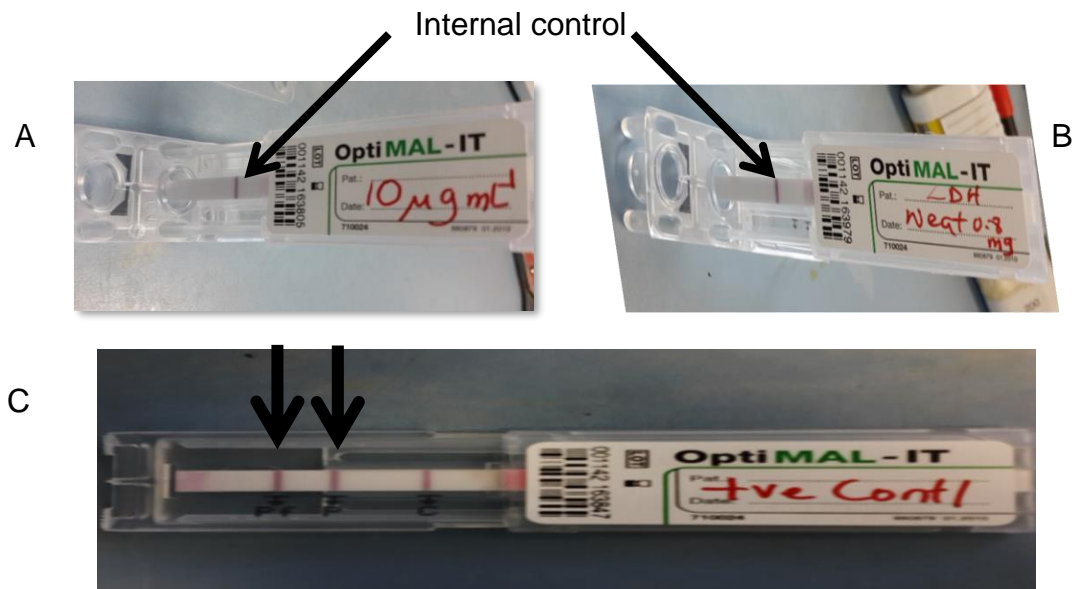
**Figure 5-10:** Chart staging *Plasmodium falciparum* cultured cells (Silamut, 2000). Trophozoite stage of parasite development is just prior to vegetative reproduction by schizogony. It is at this stage that sorbitol lysis was conducted to destroy other stage cells and obtain a synchronized culture. Box contains trophozoites of the age range used in the research.

With culture medium supernatant of known parasitaemia, the samples were then tested on OptiMAL immunochromatographic dipstick, for comparison with recombinant LDH.

#### 5.4.2 LDH detection using OptiMAL-IT Malatia dipstick kit

The dipstick and lateral flow assays are sensitive to small volumes (2–50  $\mu\text{L}$ ) of malaria antigens in blood (Kakkilaya, 2011). Some work has been reported on the use of monoclonal antibodies in conjunction with colloidal gold in an immunochromatographic assay for *Plasmodium falciparum* malaria detection showing 86.6% sensitivity and 96.4% specificity in the population (Lee et al., 2006). The sensitivity of these devices relies on the species and number, the viability and difference in amount of parasite antigen as well as the condition (storage  $\leq 30^\circ\text{C}$ ) of the device and the efficacy of the method (Bell et al., 2006; Kakkilaya, 2011).

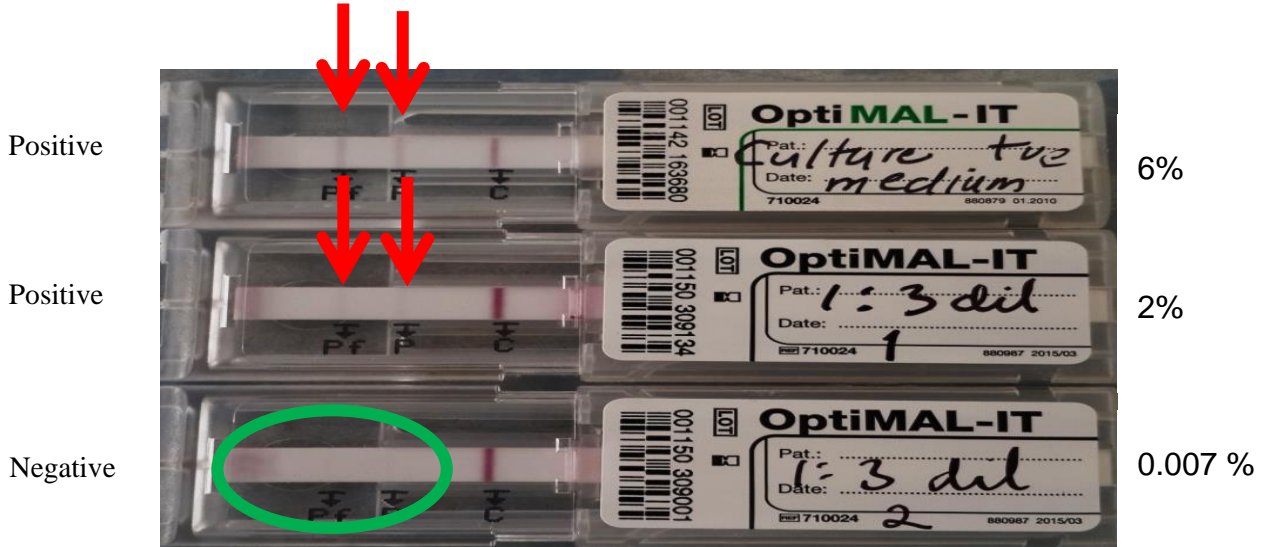
The test carried out in this research using recombinant LDH showed negative results while the culture medium supernatant showed a progressively lighter band with serial dilution of the sample (Figure 5.11).



**Figure 5-11:** OptiMAL-IT dip stick assay with recombinant LDH. Concentrations of recombinant LDH in 100% serum ( $10 \mu\text{g mL}^{-1}$ ) (A) and neat recombinant protein ( $0.8 \text{mg mL}^{-1}$ ) showing negative control band (B). Internal control confirms test validity. The results also confirm kit manufacturer's assertion that the test kit is only positive when

live parasites are present in the sample. This was further confirmed in the results of the LDH positive control assay (C).

Following the assay of LDH recombinant protein on OptiMAL-IT dipstick assay, a comparison was made with Dd2<sup>luc</sup> culture medium supernatant to assess the validity of the results. The culture medium supernatant was diluted 3-fold in blank RPMI 1640 medium from 6% parasitaemia and tested until no band was seen (Figure 5.12).



**Figure 5-12:** OptiMAL-IT dip stick assay. Arrows show internal control negative band. OptiMAL-IT dip stick assay with 3-fold dilution of Dd2<sup>luc</sup> culture medium supernatant. No band in dilution number two.

From the results, the OptiMAL-IT dipstick test failed to detect lactate dehydrogenase in culture medium supernatant from Dd2<sup>luc</sup> at 0.007 % parasitaemia.

According to Hawkes et al., 2014, the pLDH antigen on three-band immunochromatographic tests increases the specificity for malaria parasitaemia and may differentiate acute infection from recently treated infection.

It has been reported that ICTs show a decrease in sensitivity (88%) for *Plasmodium falciparum* when the parasite load descends below 50 per  $\mu\text{L}$  (Sharma et al., 2010). It is however preferable to use the Pf / Pv Combo Test

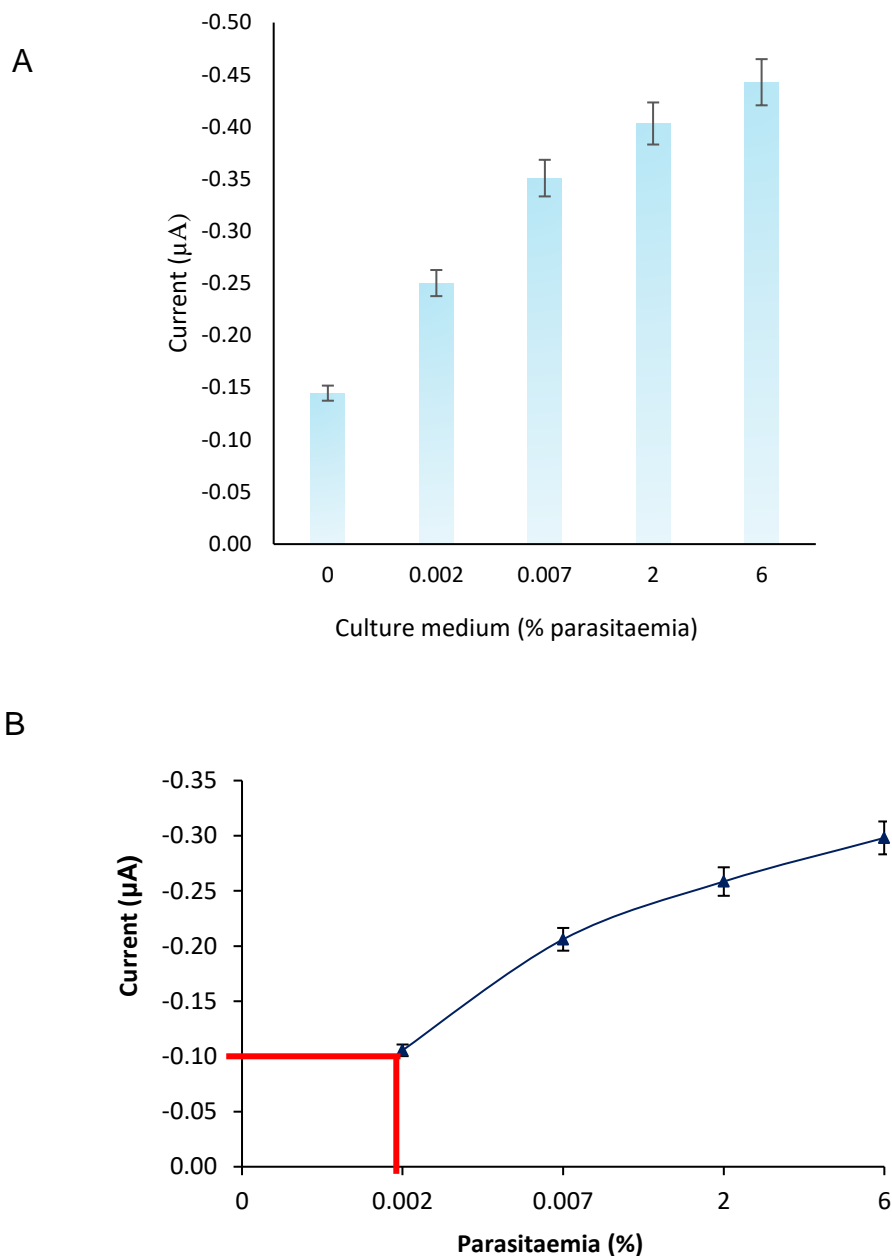
instead of microscopy in areas where microscopic diagnosis is limited (Hailu and Kebede, 2014).

The samples tested on the OptiMAL-IT test were then tested for comparative sensitivity using the developed immunosensor for Pan-malaria amperometric detection. The methods were the same as those in Chapter 4, section 4.3.3.

#### **5.4.3 LDH detection on immunosensor using culture supernatant**

The JD 2b gold screen-printed electrode (SPGE) immunosensor developed in this work has successfully detected pan malaria antigen LDH in the sample, Dd2<sup>luc</sup> culture medium supernatant. Amperometric signal using culture medium supernatant shows similar results to the signals obtained in LDH detection (section 4.3.3) (Figure 5.13).





**Figure 5-13:** Amperometric signal for LDH detection in culture medium supernatant (A). A concentration of  $10 \mu\text{g mL}^{-1}$  capture antibody was immobilized on the working electrode. For analyte detection, a concentration of  $10 \mu\text{g mL}^{-1}$  detection antibody with horse radish peroxidase conjugated was immobilized on the working electrode. The 6% parasitaemia was diluted in blank RPMI 1640 culture medium supernatant. The diluted sample was beyond the detection limit of the OptiMAL-IT malaria dipstick test. The graph was plotted minus the zero value of background from the observed measurements without gold nanoparticle signal enhancement on immunosensor (B). Red lines show smallest measurement obtained at lowest parasitaemia.

Results of culture supernatant in immunosensor assay show signal detection in the region of failure of the OptiaMAL -IT. The range of amperometric signal

reflects the change in the analyte concentration. Smallest signal is at **-0.11  $\mu\text{A}$** . This value was obtained from the difference of the background of blank RPMI 1640 culture medium from the measurement.

Comparison of signals from developed assays, show similarity (Table 5.3). Least amperometric signal on each of the curves representing different sample matrices of both enhanced and unenhanced assays has been compared to the LDH immunosensor detection using Dd2<sup>luc</sup> culture medium supernatant.

**Table 5-3: Amperometric signal of LDH immunosensor assay**

Assay sample	Current ( $\mu\text{A}$ )	LDH concentration ( $\text{ng mL}^{-1}$ )
Buffer assay	-0.12 $\pm$ 0.00	1
AuNP buffer	-0.14 $\pm$ 0.03	0.001
Serum assay	-0.09 $\pm$ 0.00	1
AuNP serum	-0.002 $\pm$ 0.00	0.001
*CMS Dd2 <sup>luc</sup>	-0.10 $\pm$ 0.01	~1

\*Culture medium supernatant

AuNP current was the lowest. In this investigation, culture medium supernatant was not examined in AuNP-enhanced assay due to the sensors running out. From the table, however, the corresponding antigen concentration (1  $\text{ng mL}^{-1}$ ) of CMS Dd2<sup>luc</sup> in relation to the signal is seen in unenhanced assay. The results imply that the immunosensor can be used in detection of non-species malaria and may be used to detect lactate dehydrogenase, an enzyme common to all malaria parasites.

A report from previous work states electrochemically-based measurement process does not perturb the chemical composition of the culture medium (Pemberton, et al., 2014). The results are in agreement with some reports stating amperometric immunosensors are more sensitive and specific than some immunochromatographic test kits (Sharma et al., 2008). This work was

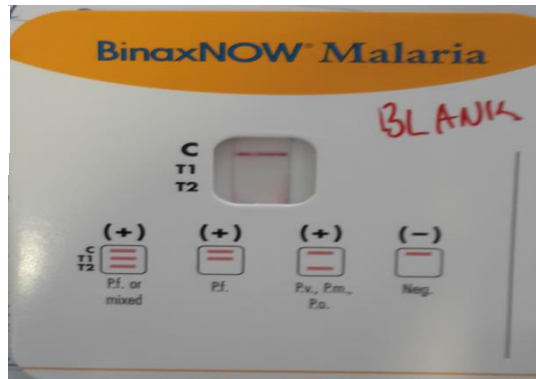
however conducted on DuPont gold screen-printed electrodes and tested on biomarker dissolved in medium from in vitro culture of *Plasmodium falciparum*. Malaria culture supernatant containing the biomarkers parasite Lactate dehydrogenase is used in the assay as sample containing live parasites is known to be more sensitive on the ICT than the recombinant protein as already indicated by the manufacturer.

According to OptiMAL-IT kit manufacturer, the kit can detect parasitaemia levels of 0.001-0.002 % (50-100 parasites per  $\mu\text{L}$  of blood). The variation in sensitivity may be affected by dilution used as opposed to the direct supernatant obtained from a culture of specified parasitaemia. Also, it is not clear if the values are for staged parasites.

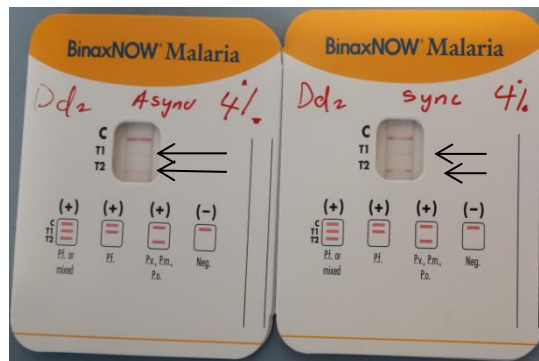
#### **5.4.4 BinaxNOW Malaria on ICT**

Culture supernatant 0.5% and 4% were detected by the BinaxNOW Malaria ICT. The results aid to confirm earlier detection using diluted medium (section 5.4.3) (Figure 5.14).

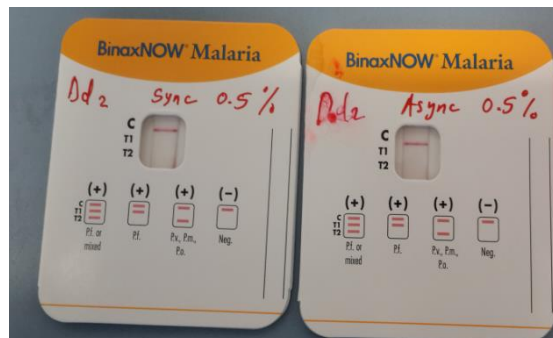
A  
Blank medium (Control)



B  
Positive



C  
Negative



T1 = positive *P. falciparum* T2 = positive *P. vivax*, *P. malariae*, *P. ovale* or mixed

**Figure 5-14:** BinaxNOW Malaria kit for PfHRP 2 and LDH detection. The blank (A) showed internal control line validation of the test. The antigens were however not detected in the samples. Synchronized samples of (B) showed negative low parasitaemia and positive PfHRP 2 / LDH high parasitaemia (C). Asynchronized and synchronized low parasitaemia samples however failed to detect both HRP 2 and LDH malaria biomarkers in culture medium supernatant. The immunoassay however detected LDH in less than 5% parasitaemia (section 5.4.3).

BinaxNow Malaria kit is sensitive to both histidine rich protein 2 and lactate dehydrogenase malaria biomarkers. *Plasmodium falciparum* histidine rich protein 2 is known to be polymorphic and is prone to genetic diversity which affects the reliability of some immunochromatographic assays (Baker et al.,

2005). In addition the kit has the limitation that it cannot distinguish between a single species and a mixed infection.

Abba et al., 2014 also reported that immunochromatographic tests have been designed to detect *P. vivax* specifically. On the other hand, Grigg et al., 2014 reported that combining two immunochromatographic tests was an accurate method for some malaria species with low sensitivity while PoAb-based immunoassays show greater sensitivity to false positives than Moab-based assays (Sousa et al., 2014).

The methods for detecting malaria researched in this work are comparative in sensitivity and can be used to support other methods in the detection of malaria (Table 5.4).

**Table 5-4:** Methods compared in this research for detection of malaria

Detection method	Sample type	Quantity (µL)	Sensitivity	Ag detection	Test duration (mins)
Thin film	* CMS	50 - 60	1 parasite per field	-	30 - 45
OptiMAL –IT	Spiked serum CMS	20	0.007 (% parasitaemia)	Colourimetric	20
BinaxNOW Malaria ICT	CMS	15	4 (% parasitaemia)	Colourimetric	15
LDH immunosensor	CMS	20	<1 parasite	Amperometric	120
<i>Pf</i> HRP immunosensor	2 CMS	20	<1 parasite	Amperometric	120

\*Culture medium supernatant (CMS)

## 5.5 CONCLUSIONS

This research has successfully developed two immunoassays to detect malaria biomarkers. The water soluble biomarkers *Plasmodium falciparum* histidine rich protein 2 and lactate dehydrogenase are detectable on both the immunoassays with nanogram level sensitivity in gold nanoparticle enhanced assay. The confirmation of sensitivity of the assays has been compared in buffer, commercial serum and culture medium supernatant. In addition, the

immunoassay for lactate dehydrogenase detection has been compared to the sensitivity for two commercial malaria test kits, OptiMAL-IT and BinaxNOW Malaria immunochromatographic tests.

These results imply that the developed Pan-malaria immunosensor is more sensitive. SPGE used in this work is stable over a 7 year period and is recommended for further work in the investigation of malaria biomarkers detection. The developed sensors are also recommended for field trial using blood samples in comparison to the culture medium supernatant and ICTs.

Both the immunosensors have similar steep, linear range. Amperometric detection at low concentration (nanogram range) however displays higher background and less curve separation than analyte high concentration (microgram range).

Both immunosensors have not been optimized for cross-reactivity and time, though they are not as rapid as the ICTs (15-20 minute assays). This immunosensor currently takes 2 hours to conduct as assay. Having established sensitivity and reliability, we can now focus on the time optimization of immobilization and incubation temperatures, this time can be shortened. It will take some more investigation to develop the immunosensor until becomes a stand-alone POC device for easy detection of malaria.

**CHAPTER SIX**  
**FINAL CONCLUSIONS AND FUTURE WORK**





## 6 FINAL CONCLUSIONS AND FUTURE WORK

### 6.1 Overview

Malaria is a globally importance parasitic disease. Approximately 50% of the global population is at risk of malaria. Sub-Saharan Africa carries a disproportionately high share of the global malaria burden. In 2015, the region was home to 90% of malaria cases and 92% of malaria deaths.

This study successfully developed two electrochemical malaria immunosensors against *Plasmodium falciparum* histidine rich protein 2 and parasite L- Lactate dehydrogenase biomarkers. The focus of the research was to provide highly specific malaria detection to reduce malaria incidence in areas where malaria tests are either expensive or not readily available. Malaria-related morbidity and mortality, especially in children under age 5 and pregnant mothers. Both biomarkers were investigated on the highly sensitive screen-printed gold electrodes designed by Cranfield University in combination with an enzymatic electrochemical signal generating system.

The immunosensor showed high performance through a wide range of antigen concentrations with a limit of detection that is suitable to detect pre-symptomatic malaria infection and offering significant advantage over other commercial detection methods for malaria such as ELISA kits and ICTs.

Prior to the red blood cell phase there is little or no indication of infection by the host and no symptoms to describe. The pre-erythrocytic phase maintains a single, one-way process in comparison to the red blood cell phase that is a cyclic process. The merozoites that form in the hepatocyte are found in merosomes, produced by the host cell vesicles. The merosomes aid the passage of the merozoites as they leave the liver and prevent their being encapsulated by Kupffer cells. These merozoites enter the circulation via the vesicles of the lungs. The sporozoites of *Plasmodium vivax* and *Plasmodium ovale* however have been found to remain in a state of dormancy for several months in the liver. These hypnozoites develop into schizonts after a period of

inactivity. It has been suggested that these hypnozoites may have a varying genetic composition from the sporozoites that produce febrile malaria disease without this latent phase. They have been associated with repeated clinical manifestation in patients (Collins, 2007).

## **6.2 ELECTROCHEMICAL IMMUNOSENSORS**

With both malaria antigen and antibodies being very expensive, care had to be taken in designing the experiments to achieve optimized results. Chronoamperometric results HRP 2 in buffer based on capture and detection antibody optimization results is recommended at higher and broad range for significant separation.

This work establishes the detection of the predominant ring-infected erythrocytes of *P. falciparum* by LDMS. The field and hospital use of LDMS will require further study in larger clinical trials using more carefully designed assay protocols that scan sufficient blood to meet a targeted sensitivity and probability of detection. A potential role may be as a screening tool of large populations before more time- and labor-intensive diagnostics are used.

The current development of miniature, field-portable MS systems may make this LDMS method more widely available. Although the LDMS instrument costs are expensive, the protocol we have developed is simple-to-perform, rapid, and requires no consumables other than water and a lancet for obtaining the droplet of blood (ter Kuile et al, 2004).

When the ruptured infected erythrocyte releases merozoites, the residual body containing parasite membranes surrounding hemozoin is released into the circulation. Hemozoin and/or the residual body containing hemozoin can be ingested by circulating neutrophils or monocytes. Immunochromatographic tests can detect sequestered parasites in pregnant patients through circulating antigens, as the schizont rupture of the infected erythrocytes in placental tissues releases *P. falciparum* aldolase, HRP II, or lactate dehydrogenase into

the plasma. In addition to that contained inside circulating erythrocytes. Therefore, like the immunochromatographic tests, LDMS has the capability to detect the molecular remnants of previous generations of *P. falciparum* parasites, in addition to the intact intraerythrocytic ring-stage parasites in the blood sample (Ter Kuile et al, 2004). Ginsburg and others have measured the hemozoin content of ring-, trophozoite-, and schizont-stage parasites to be approximately 1, 3, and 4–5 micromoles per parasites, respectively (Sullivan, 2002). These correspond to an average of 0.1, 0.3, 0.4–0.5 femtomoles per parasite, which suggests that LDMS, with subfemtomole sensitivity for heme, can detect hemozoin from a single infected erythrocyte.

LDMS may be useful for rapidly screening many samples for infection, and subsequently using microscopy or dipsticks to speciate those samples that are positive (Duffy and Fried, 2005).

Laser desorption mass spectrometry is able to detect heme from hemozoin, the breakdown product of hemoglobin that is commonly referred to as parasite pigment. Importantly, heme from hemozoin yields a spectral signature that is distinct from that of heme from normal hemoglobin, allowing LDMS to discriminate infected from uninfected red blood cells (Demirev et al, 2002, Scholl et al., 2004).

This consideration is paramount in ensuring correct diagnosis is made and appropriate management administered. Sample components are separated according to mass and ionic potential. A single erythrocyte harboring late stage trophozoites can produce more than 1 fmol of heme as hemozoin crystals.

The immunoassays achieved a detection level in the nanogram range, 1.80 ng mL<sup>-1</sup> in LDH buffer assay and 0.7 ng mL<sup>-1</sup> in LDH serum assay. Sensitivity of 0.019 ng mL<sup>-1</sup> was achieved with gold nanoparticle assay in buffer while, 0.023 ng mL<sup>-1</sup> was achieved in AuNP enhanced assay conducted in commercial serum matrix.

*Pf*HRP 2 immunosensors on the other hand achieved a sensitivity of 2.14 ng mL<sup>-1</sup> in buffer and 2.95 ng mL<sup>-1</sup> in serum, while 0.036 ng mL<sup>-1</sup> in buffer and 0.04 ng mL<sup>-1</sup> were achieved in serum enhanced assays.

### **6.3 MALARIA IMMUNOCHROMATOGRAPHIC KITS**

There still exists the need for quick and user friendly instruments that can be transported easily and which are adaptable to field conditions (Lee et al., 2012).

### **6.4 LIMITATIONS**

The malaria immunosensors with immobilized antibodies on the surface of the screen-printed electrode is a highly sensitive format with a limit of detection comparable to other commercially available detection methods, and more sensitive than the lateral flow immunochromatographic assay. However, it is a multistep procedure which requires the operator to add solutions on the sensor surface at different stages of the assay, thus requires numerous incubation and washing steps, which will result in an assay requiring up to 2 hours. In respect to reproducibility, the enzyme conjugate requires evaluation over a period of 6-12 months.

The major obstacle in assessment of stability of immobilized antibody on the electrode surface over a period of at least 6 months was the limited time for the original research and the eventual short supply of DuPont SPGEs.

In view of current market trends, the malaria electrochemical immunosensor is a promising detection method for active and past malaria infection. This research had investigated the practical application of the malaria immunosensor however, to take the research further; funding support is required for the adoption on the SPE and final optimization using PStouch mobile device software. This research looked primarily at *P. falciparum*, and can be adapted to investigate *P. vivax* malaria, which has been counted among the neglected tropical diseases (NTDs).

Further collaboration with malaria researchers to obtain biomarker samples in culture medium supernatant for the assay will help reduce the overall cost of the research. There is the benefit from malaria eradication to look forward to. In addition, microscopic examination may be less used as the parasites attains eradication status and sub-microscopic, quantitative detection will support efforts to sustain re-introduction, re-surgence and re-infection of malaria in a low cost, easy to use, accurate immunosensor.

## **6.5 FUTURE WORK**

The results achieved in this research include the development of two novel malaria immunosensors for the detection of malaria infection in field conditions. Additionally, the immunosensor was tested against current commercially available immunochromatographic tests to ascertain the quantitative detection in relation to qualitative detection of malaria. However, there are several suggestions for further development to adopt the immunoassay for use on intuitive software in a hand-held device.

Future work development includes:

### **a) *Further optimization of the sensor***

Further research will be conducted to test whole blood samples using a different batch of sensors. Optimization will include:

- Sample preparation (stored samples and fresh samples)
- Other sample assay (saliva and urine for non-invasive testing for the soluble biomarkers).

### **b) *Conduction of assay using PStouch software on mobile device***

- The developed assay may be adopted for the detection of other infectious diseases like Schistosomiasis and Onchocerciasis.
- Further optimization will be conducted to determine optimum storage conditions over a period of six months.

### **c) *Design and construction of innovative platform for the immunosensor***

The idea is nascent but shows potential.

d) ***Funding for further research***

*Funding will be sought for the progress of the work (supported application to various funding bodies).*

## **6.6 FINAL CONCLUSIONS**

Malaria and other infectious diseases of global importance caused by mosquitoes result in morbidity, reduced productivity and mortality. Although elimination of malaria is in focus in some countries, many countries are yet to achieve this status. Understanding the socio-cultural influence on malaria transmission is crucial for future disease control. Therefore, a multi-prong approach is needed, combining basic research and various disease control measures, such as impact assessment and monitoring and evaluation in relation to use of intervention, perception, reaction and decision-making by the individual in an endemic area. Nevertheless, the diagnostic approach presented in this study can be easily integrated with the existing malaria intervention programmes, to contribute to provision of data, currently insufficient in sub-Saharan Africa for the projection of trends in malaria disease incidence.

The high sensitivity compared with immunochromatographic tests, combined with the portable and low cost of the developed immunosensor makes this approach highly suitable for the specific detection of past and active malaria infection, producing a powerful tool for malaria screening. With blood levels of LDH ( $\sim 5 \text{ ng mL}^{-1}$ ) and PfHRP 2 ( $\sim 10 \text{ ng mL}^{-1}$ ) the developed immunosensors can be taken forward for point of care device development.

Because malaria elimination globally is in focus, the need remains for even more sensitive tests such as biosensing field applicable tests that will support the eventual reduced skill in malaria detection as the disease continues to be eliminated.

## REFERENCES

- Abba, K., Kirkham, A. J., Olliaro, P. L., Deeks, J. J., Donegan, S., Garner, P. and Takwoingi, Y. (2014) "Rapid diagnostic tests for diagnosing uncomplicated non-falciparum or *Plasmodium vivax* malaria in endemic countries". The Cochrane Library 1-198.
- Abdallah, J. F., Okoth, S. A., Fontecha, G. A., Torres, R. E., Banegas, E. I., Matute, M. L., Bucheli, S. T., Goldman, I. F., de Oliveira, A. M. and Barnwell, J. W. (2015). "Prevalence of *PfHRP2* and *PfHRP3* gene deletions in Puerto Lempira, Honduras". *Malaria journal* 14: 19.
- Abdin, M., Israr, M., Rehman, R. and Jain, S. (2003). "Artemisinin, a novel antimalarial drug: biochemical and molecular approaches for enhanced production". *Planta Medica* 69: 289-299.
- Abdul-Ghani, R., Farag, H.F., Allam, A.F. and Azazy, A. A. (2014). "Measuring resistant-genotype transmission of malaria parasites: Challenges and prospects". *Parasitology research* 113: 1481-1487.
- Abdulkadir, M.K. and Tohill, I.E. (2010). "Development of an electrochemical immunosensor for fumonisins detection in foods" *Toxins* 2: 382-398.
- Accardo, A., Laurent, S.A., Mazarguil, H., Meyer, M., Robert, A. and Meunier, B. (2007). "Interaction of iron (II) – heme and artemisinin with a peptide mimic of *Plasmodium falciparum* HRP – II". *Journal of inorganic biochemistry* 101: 1739-1747.
- Adeoye, G. and Nga, I. (2007). "Comparison of Quantitative Buffy Coat technique (QBC) with Giemsa-stained Thick Film (GTF) for diagnosis of malaria". *Parasitology International* 56: 308-312.
- Aizawa, M., Morioka, A., Matsuoka, H., Suzuki, S., Nagumura, Y., Shinohara, R. and Ishiguro, I. (1976) An enzyme immunosensor for IgG, *Solid Phase Biochem.* 1: 319-328.
- Ajumobi, O., Sabitu, K., Nguku, P., Kwaga, J., Ntadom, G., Gitta, S., Elizeus, R., Oyibo, W., Nsubuga, P., Maire, M. and Poggensee, G. (2015). "Performance of and HRP-2 Rapid Diagnostic Test in Nigerian Children Less Than 5 Years of Age". *The American Journal of Tropical Medicine and Hygiene* 92: 828- 833.
- Akhouayri, I.G., Habtewold, T. and Christophides, G.K. (2013) "Melanotic Pathology and Vertical Transmission of the Gut Commensal *Elizabethkingia meningoseptica* in the Major Malaria Vector *Anopheles gambiae*". *PLoS ONE* 8: 10.

- Akinyi, O. S., Abdallah, J.F., Ceron, N., Adhin, M.R., Chandrabose, J., Krishnalall K. (2015). Variation in *Plasmodium falciparum* Histidine –Rich Protein 2 (*Pfhrp2*) and *Plasmodium falciparum* Histidine-Rich Protein 3 (*Pfhrp3*) Gene Deletions in Guyana and Suriname PLoS ONE 10: 5.
- Alii, J.A., Okonko, I.O., Abraham, O.A., Kolade, A.F., Ogunjobi, P.N., Solako, A. O., Ojezele, M.O. and Nwanze, J.C. (2010). “A serosurvey of blood parasites (*Plasmodium*, *microfilaria*, HIV, HBsAG, HCV antibodies) in prospective Nigerian blood donors”. *Research Journal of Medical Sciences*. 4: 255-275.
- American Mosquito Control Association (2014). <http://www.mosquito.org>
- Amodu, O.K., Adeyemo, A.A., Olumese, P.E., Gbadegesin, R.A. (1998). Intraleukocytic malaria pigment and clinical severity of malaria in children *Trans R Soc Trop Med Hyg*. 92: 54–56.
- Araya, G.D., Reda, H.L. and Tesema, A.G. (2015). “Utilization of Long Lasting Insecticidal Nets Among Households in Malarious Areas of Raya Alamata District, Tigray, Ethiopia”. *Science* 3: 216-221.
- Arya, S. K., Singh, P. S. and Malhotra, B. D. (2007). "Electrochemical Techniques in Biosensors" in Marks, R. S., Cullen, D. C., Karube, I., Lowe, C. R. and Weetall, H. H. (editors) *Handbook of biosensors and biochips*, John Wiley, Chichester: 342-377.
- Ariey, F., Witkowski, B., Amaratunga, C., Beghain, J., Langlois, A., Khim, N., Kim, S., Duru, V., Bouchier, C., Ma, L., Lim, P., Leang, R., Duong, S., Sreng, S., Suon, S., Chuor, C., Bout, D., Menard, S., Rogers, W., Genton. B., Fandeur, T., Miotto, O., Ringwald, P., Le Bras, J. and Berry A. (2013). A molecular marker of artemisinin-resistant *Plasmodium falciparum* malaria, *Nature* 505: 50-55.
- Arevalo-Herrera, M., Quinones, M. L., Guerra, C., Cespedes, N., Giron, S., Ahumada, M., Pineros, J.G., Padilla, N., Terrientes, Z., Rosas, A., Padilla, J.C., Escalante, A.A., Beier, J.C. and Herrera, S. (2012). “Malaria in selected non-Amazonian countries of Latin America”. *Acta Tropica* 121: 303-314.
- Atkinson, C.T. (2008). Avian malaria- *Parasitic diseases of wild birds* 1: 35-53.
- Atoba, T. and Adeyinka, D.A. (2013). “Morbidity pattern among the disabled in Ibadoan, Nigeria: A retrospective analysis”. *International Journal on Disability and Human Development* 12: 369-372.



- Aubailly, L Drucbert, A.S., Danzé, P.M and Forzy, G. (2011). Comparison of surface plasmon resonance transferrin quantification with a common immunoturbidimetric method. *Clin. Biochem* 44: 731–735.
- Avila, P.E., Kirchgatter, K., Brunialti, K.C.S., Oliveira, A.M., Siciliano, R.F. and Di Santi, S.M., (2002). Evaluation of a rapid dipstick test, Malar-Check™, for the diagnosis of *Plasmodium falciparum* malaria in Brazil. *Revista do Instituto de Medicina Tropical de Sao Paulo* 44: 293-296.
- Azikiwe, C.C. A., Ifezulike, C.C., Siminialayi, I. M., Amazu, L.U., Enye, J.C. and Nwakwunita, O.E. (2012). “A comparative laboratory diagnosis of malaria: Microscopy versus rapid diagnostic test kits”. *Asian Pacific Journal of Tropical Biomedicine* 2: 307-310.
- Baer, K., Klotz, C., Kappe, S.H., Schnieder, T., Frevert, U. (2007). Release of hepatic *Plasmodium yoelii* merozoites into the pulmonary microvasculature. *PLoS Pathog.* 3: 171.
- Bailey, J.W., Williams, J., Bain, B.J., Parker- Williams, J. and Chiodini, P.L. (2013). “Guideline: The Laboratory diagnosis of malaria”. *British journal of haematology* 163: 573-580.
- Bain, C.D., Troughton, E.B., Tao, Y.T., Evall, J., Whitesides, G.M., Nuzzo, R.G., (1989). Formation of monolayer films by the spontaneous assembly of organic thiols from solution onto gold. *J. Am. Chem. Soc.* 111: 321–335.
- Baker, D.A., Nolan, T., Fischer, B., Pinder, A., Crisanti, A. and Russell, S. (2011). “A comprehensive gene expression atlas of sex- and tissue-specificity in the malaria vector, *Anopheles gambiae*”, *BMC Genomics*, 12, 296.
- Baker, J., McCarthy, J. Gatton, M., Kyle, D. E., Belizario, V., Luchavez, J. Bell, D. and Cheng Q. (2005). Genetic Diversity of *Plasmodium falciparum* Histidine-Rich Protein 2 (*PfHRP2*) and Its Effect on the Performance of *PfHRP2*-Based Rapid Diagnostic Tests. *The Journal of Infectious Diseases* 192: 870-877.
- Baltzell, K.A., Shakely, D., Hsiang, M., Kemere, J., Ali, A.S., Bjorkman, A., Martensson, A., Omar, R., Elfving, K., Msellem, M., Aydin-Schmidt, B., Rosenthal, P.J. and Greenhouse, B. (2013). “Prevalence of PCR detectable malaria infection among febrile patients with a negative *Plasmodium falciparum* specific rapid diagnostic test in Zanzibar”. *American Journal of Tropical Medicine and Hygiene.* 88: 289-291.
- Baptista, F.G., Pamplona, A., Pena, A.C., Mota M.M., Pied, S., Vigario, A. M. (2010). Accumulation of *Plasmodium berghei*-infected red blood cells

- in the brain is crucial for the development of cerebral malaria in mice. *Infect Immun.* 78: 4033-9.
- Bard, J.F., Faulkner, L. R. (2001). *Electrochemical Methods: Fundamentals and Applications*. John Wiley and Sons, Inc.
- Baron, J.M., Higgins, J. M. and Dzik, W. H. (2011). "A revised timeline for the origin of *Plasmodium falciparum* as a human pathogen". *Journal of Molecular Evolution*, 73: 297-304.
- Basilico, N., Spaccapelo, R. and D'Alessandro, S. (2015). *Malaria Diagnosis, Therapy, Vaccines, and Vector Control in Human and Mosquito Lysozymes*, Springer: 19-43.
- Beare, N.A.V., Taylor, T., Harding, S.P., Lerallen, S. and Molyneux, M. E. (2006). Malarial retinopathy: A newly established diagnostic sign in severe malaria. *American Journal of Tropical Medicine and Hygiene* 75: 790–797.
- Bell, D., Wongsrichanalai, C., Barnell, J. W. (2006). Ensuring quality and access for malaria diagnosis: how can it be achieved? *Nat. Rev. Microbiol.*, 4: 7-20.
- Berg, P., Naebauer, A. & Ruge, I. (1989). An ion sensitive field effect transistor for biosensor applications. In: *Biosensors: Applications in medicine, environmental protection, and process control*, Schmid, R.R.D. & Scheller, F. (eds.), VCH Publishers, New York: 158-168.
- Bharaathi, S. and Nogami, M. (2001). "A glucose biosensor based on electrodeposited biocomposites of gold nanoparticles and glucose oxidase enzyme". *Analyst*, 126: 1919-1922.
- Bharathi, S., Nogami, M. and Ikeda, S. (2001). Novel electrochemical interfaces with a tunable kinetic barrier by self-assembling organically modified silica gel and gold nanoparticles. *Langmuir* 17: 1-4.
- Bio-rad-antibodies-<https://www.bio-rad-antibodies.com/hucal-monoclonals> (accessed, 2016).
- Binder M. (2014). Development of a *Botrytis*- specific immunosensor towards using pcr species identification PhD Thesis Cranfield University, 99-145.
- Brince, K.P., Kumar, S., Tripathy, S., Vanjari, S.R.K., Singh, V. and Singh, S.G. (2016). A highly sensitive self assembled monolayer modified copper doped zinc oxide nanofiber interface for detection of *Plasmodium falciparum* histidine-rich protein-2: Targeted towards rapid, early diagnosis of malaria. *Biosensors and Bioelectronics* 80: 39-46.

- Borgmann, S., Schulte, A., Nergebauer, S. and Schuhmann, W. (2011). Goelectrochemistry: fundamentals, applications and recent developments, *Advances in Electrochemical Science and Engineering*, 13 Wiley-VHC, Germany: 48-52.
- Borman, S. (2002). "Proteomics: Taking over where genomics leaves off". *Chem Eng News* 78: 31-37.
- Bosch, J., Paige, M.H., Vaidya, A.B., Bergman, L.W. and Hol, W.G.J. (2012). "Crystal structure of GAP 50 the anchor of the invasion machinery in the inner membrane complex of *Plasmodium falciparum*". *Journal of structural biology*. 178: 61-73.
- Bowers, K. M., Bell, D., Chiodini, P.L., Barnwell, J., Incardona, S., Yen, S., Luchavez, J. and Watt, H. (2009). Inter- rate reliability of malaria parasite counts and comparison of methods. *Malaria Journal*: 8, 267.
- Breslauer, D.N., Maamari, R.N., Switz, N.A., Lam, W.A. and Fletcher, D.A. (2009). Mobile phone based clinical microscopy for global health applications. *PloS one*, 47: 6320.
- Brown, L. (1993). The New shorter Oxford English dictionary on historical principles, Oxford [Eng.]: Clarendon.
- Bruce, D., Harvey, D., Hamerton, A.E. and Bruce, L. (1913). *Plasmodium cephalophi Proceedings of the Royal Society of London. Series B, Containing Papers of a Biological Character* 87: 45-47.
- Burrows, J.N., Leroy, D., Lotharius, J., Waterson, D. (2011). Challenges in antimalarial drug discovery. *Future Med.Chem* 3: 1401-1412.
- Cabrales, P., Zanini, G.M., Meays, D., Frangos J.A., Carvalho L.J. (2010). Murine cerebral malaria is associated with a vasospasm-like microcirculatory dysfunction, and survival upon rescue treatment is markedly increased by nimodipine. *Am J Pathol*. 176: 1306-15.
- Caminade, C., Kovats, S., Rocklov, J., Tompkins, A.M., Morse, A.P., Colon-Gonzalez, F.J., Stenlund, H., Martens, P. and Lloyd, S.J. (2014). "Impact of climate change on global malaria distribution". *Proceedings of the National Academy of Sciences of the United States of America* 111: 3286-3291.
- Canh, T. M. (1993). Biosensors. Chapman and Hall 10-11, 20 – 22.
- Cardoso, A.R., Cabral-Miranda, G., Reyes-Sandoval, A., Bachmann, M.F. and Sales, M.G.F. (2017). Detecting circulating antibodies by controlled surface modification with specific target proteins: Application to malaria. *Biosensors and Bioelectronics* 91:833-841.

- Cass, A. E., Davis, G., Francis, G. D., Hill, H. A. O., Aston, W. J., Higgins, I. J., Plotkin, E. V., Scott, L. D. and Turner, A. P. (1984). "Ferrocene-mediated enzyme electrode for amperometric determination of glucose". *Analytical Chemistry*. 56: 667-671.
- Casals-Pascual, C., Idro, R., Gicheru, N., Gwer, S., Kitsao, B., Gitau, E., Mwakesi, R., Roberts, D. J. and Newton, C.R. (2008). "High levels of erythropoietin are associated with protection against neurological sequelae in African children with cerebral malaria". *Proceedings of the National Academy of Sciences of the United States of America*. 105: 2634-2639.
- Castellanos, M.E., Diaz, S., Parsons, E., Peruski, L.F., Enriquez, F., Ramirez, J.L. and Padilla, N. (2015). "First imported *Plasmodium ovale* malaria in Central America: case report of a Guatemalan soldier and a call to improve its accurate diagnosis". *Military Medical Research* 2: 1, 3.
- Centres for Disease Control and Prevention (1994). *A. gambiae* mosquito photo. Credit James Gethany: CDC.
- Centres for Disease Control and Prevention (2012). Malaria Surveillance-United States.
- Centres for Disease Control and Prevention (2014). Malaria insecticide treated bed nets Photo credit: Maggie Hallahan.
- Charles, M., Coughlin, R. W., Paruchuri, E.K., Allen, B.R. & Hasselberger, F.X. (1975). Enzymes immobilized on alumina and stainless steel supports. *Biotech. and Bioeng.* 17: 203-210.
- Chomean, S., Potipitak, T., Promptmas, C. and Ittarat, W. (2010). Quartz crystal microbalance-based biosensor for the detection of  $\alpha$ -thalassemia 1 (SEA deletion). *Clinical Chemistry and Laboratory Medicine*, 48: 1247-1254.
- Coatney, G.R., Collins, W.E., Warren, M. and Contacos, P.G. (1971). *The Primate Malarias*. U.S. Department of Health, Education and Welfare, Bethesda, 366.
- Coleman, R.E., Maneechai, N., Rachapaew, N., Kumpitak, C., Soyseng, V., Miller, R.S., Thimasarn, K. and Sattabongkot, J. (2002). Field evaluation of the ICT Malaria Pf/Pv immunochromatographic test for the detection of asymptomatic malaria in a Plasmodium falciparum/vivax endemic area in Thailand. *The American journal of tropical medicine and hygiene* 66: 379-383.

- Collins, T.J. (2007). "Image for microscopy". *BioTechniques*, 43: 25-30.
- Cook, J., Reid, H., Iavro, J., Kuwahata, M., Taleo, G., Clements, A., McCarthy, J., Vallely, A. and Drakeley, C. (2010). "Research using serological measures to monitor changes in malaria transmission in Vanuatu". *Malaria Journal* 9: 169.
- Corran, P., Coleman, P., Riley, E. and Drakeley, C. (2007). "Serology: a robust indicator of malaria transmission intensity?". *Trends in parasitology* 23: 575-582.
- Cotter, C., Sturrock, H.J.W., Hsiang, M.S., Liu J., Phillips, A.A., Hwang, J., Gueye, C.S., Fullman, N., Goslin, R.D. and Feachem, R.G.A. (2013). "The changing epidemiology of malaria elimination: new strategies for new challenges". *Lancet* 382: 900-911.
- Cox, F. (2010). "History of the discovery of the malaria parasites and their vectors". *Parasit. Vectors* 3: 1- 5.
- Craig, M.H., Bredenkamp, B.L., Williams, C.V., Rossouw, E.J., Kelly, V.J., Kleinschmidt, I., Martineau, A. and Henry, G.F.J. (2002). Field and laboratory comparative evaluation of ten rapid malaria diagnostic tests. *Transactions of the royal society of tropical medicine and hygiene* 96: 258-265.
- Daghestani, H.N. and Day, B.W., (2010). Theory and applications of surface plasmon resonance, resonant mirror, resonant waveguide grating, and dual polarization interferometry biosensors. *Sensors* 10: 9630-9646.
- Darain, F., Park, S. U. & Shim, Y. B. (2003). Disposable amperometric immunosensorsystem for rabbit IgG using a conducting polymer modified screen-printedelectrode, *Biosens. Bioelectron* 18: 773 -780.
- Davies, M. J., Woolf, N., Rowles, P.M. and Pepper, J. (1988). Morphology of the endothelium over atherosclerotic plaques in human coronary arteries. *British heart journal* 60: 459 – 464.
- Davies, F., Collyer, S. D. and Higson, S. P. J. (2007). "Overview of Modern Analytical Needs", in Marks, R. S., Cullen, D. C., Karube, I., Lowe, C. R. and Weetall, H. H. (editors) *Handbook of biosensors and biochips*. John Wiley, Chichester: 23-39.
- Davies, F. and Higson, S.P.J. (2013). *Electrochemical Biosensors: Impedance Immunosensors*. Taylor and Francis group, 289-304.

- Delahunt, C., Horning, M.P., Wilson, B.K., Proctor, J.L. and Hegg, M.C., (2014). Limitations of haemozoin-based diagnosis of *Plasmodium falciparum* using dark-field microscopy. *Malaria Journal* 13:147.
- Demirev, P., Feldman, A., Kongkasuriyachai, D., Scholl, P., Sullivan, D. and Kumar, N. (2002). "Detection of malaria parasites in blood by laser desorption mass spectrometry". *Analytical Chemistry* 74: 3262-3266.
- Desai, S. (2013). Insights gained from *P. falciparum* cultivation in modified media. *The Scientific World Journal*.
- Desakorn, V., Dondorp, A. M., Silamut, K., Pongtavornpinyo, W., Sahassananda, D., Chotivanich, K., Pitisuttithum, P., Smithyman, A., Day, N.P. and White, N.J. (2005). "Stage-dependent production and release of histidine-rich protein 2 by *Plasmodium falciparum*", *Transactions of the Royal Society of Tropical Medicine and Hygiene*, 99: 517-524.
- de Oliveira, A.M., Skarbinski, J., Ouma, P.O., Kariuki, S., Barnwell, J.W., Otieno, K., Onyona, P., Causer, L.M., Laserson, K.F., Akhwale, W.S. and Slutsker, L. (2009). Performance of malaria rapid diagnostic tests as part of routine malaria case management in Kenya. *The American journal of tropical medicine and hygiene* 80: 470-474.
- de Souza Castilho, M., Laube, T., Yamanaka, H., Alegret, S. and Pividori, M. (2011). "Magneto immunoassays for *Plasmodium falciparum* histidine-rich protein 2 related to malaria based on magnetic nanoparticles". *Analytical Chemistry* 83: 5570-5577.
- Dirkzwager, R.M., Kinghorn, A.B., Richards, J.S., (2015). APTEC: aptamer-tethered enzyme capture as a novel rapid diagnostic test for malaria. *Chemical Communications* 51: 4697-4700.
- DiMaio, M.A., Pereira, I.T., George, T.I. and Banaei, N. (2012). Performance of BinaxNOW for diagnosis of malaria in a US hospital. *Journal of clinical microbiology* 50: 2877-2880.
- Dondorp, A.M., Desakorn, V., Pongtavornpinyo, W., Sahassananda, D., Silamut, K. (2005). Estimation of the total parasite biomass in acute falciparum malaria from plasma PfHRP2. *PLoS Med* 2: 788–797.
- Dondorp, A.M., Nosten, F., Yi, P., Das, D., Phyto, A.P., Tarning, J., Lwin, K.M., Ariey, F., Hanpithakpong, W. and Lee, S.J. (2009). "Artemisinin resistance in *Plasmodium falciparum* malaria". *New England Journal of Medicine* 361: 455-467.
- Druilhe, P., Moreno, L., Blanc C., Basseur, P.H., Jacquier, P. (2001). A calorimetric *in vitro* drug sensitivity assay for *Plasmodium falciparum*

- based on a highly sensitive double-site lactate dehydrogenase antigen-capture enzyme-linked immunosorbent assay. *Am J Trop Med Hyg* 64: 233–241.
- Duffy, P. and Fried, M. (2005). Malaria: New Diagnostics for an Old Problem *Am J Trop Med Hyg* 73: 482-483.
- Dutta, G., Nagarajan, S., Lapidus, L.J. and Lillehoj, P.B. (2017). Enzyme-free electrochemical immunosensor based on methylene blue and the electro-oxidation of hydrazine on Pt nanoparticles. *Biosensors and Bioelectronics*, 92: 372-377.
- Dzakah, E.E., Kang, K., Ni, C., Tang, S., Wang, J. and Wang, J. (2014). "Comparative performance of aldolase and lactate dehydrogenase rapid diagnostic tests in *Plasmodium vivax* detection". *Malaria journal* 13, 272.
- Dzurinko VL, Gurwood AS, Price JR. (2004). Intravenous and indocyanine green angiography. *Optometry* 75: 743-55.
- Eggins, B. (1996). *Biosensors: An introduction*. Wiley Teubner UK, Germany 69-73.
- Emery, A.N., Hough, J.S., Novais, J.M. & Lyons, T.P. (1972). Some applications of solid-phase enzymes in biological engineering. *The Chemical Engineer*. 71-76.
- Evans, J.A., Adusei, A., Timmann, C., May, J., Mack, D., Agbenyega, T., Horstmann, R.D. and Frimpong, E. (2004). High mortality of infant bacteraemia clinically indistinguishable from severe malaria. *Qjm* 97: 591-597.
- Fanjul-Bolado, P., González-García, M. B. and Costa-García, A. (2005). "Amperometric detection in TMB/HRP-based assays". *Analytical and Bioanalytical chemistry* 382: 297-302.
- Figueiredo S., K.C., Salim, V.M.M. and Borges, C.P., (2008). Synthesis and characterization of a catalytic membrane for pervaporation-assisted esterification reactors. *Catalysis Today*, 133, .809-814.
- Fisher, A. C. (1996). *Electrode Dynamics-Oxford Chemistry Primers*, Oxford Scientific publications 13: 45.
- Fitch, C. D., Cai, G., Chen, Y. and Shoemaker, J. D. (1999). "Involvement of lipids in ferriprotoporphyrin IX polymerization in malaria", *Biochimica et Biophysica Acta (BBA)-Molecular Basis of Disease*, 1454: 31-37.

- Fleischer, B. (2004). "Editorial: 100 years ago: Giemsa's solution for staining of plasmodia", *Tropical Medicine & International Health* 9: 755-756.
- Fogg, C., Twesigye, R., Batwala, V., Piola, P., Nabasumba, C., Kiguli, J., Mutebi, F., Hook, C., Guillerm, M., Moody, A. and Guthmann, J.P., (2008). Assessment of three new parasite lactate dehydrogenase (pan-pLDH) tests for diagnosis of uncomplicated malaria. *Transactions of the Royal Society of Tropical Medicine and Hygiene* 102: 25-31.
- Forney, J.R., Magill, A.J., Wongsrichanalai, C., Sirichaisinthop, J., Bautista, C.T., Heppner, D.G., Miller, R.S., Ockenhouse, C.F., Gubanov, A., Shafer, R. and DeWitt, C.C., (2001). Malaria rapid diagnostic devices: performance characteristics of the ParaSight F device determined in a multisite field study. *Journal of clinical microbiology* 39: 2884-2890.
- Forney, J.R., Wongsrichanalai, C., Magill, A.J., Craig, L.G., Sirichaisinthop, J., Bautista, C.T., Miller, R. S., Ockenhouse, C.F., Kester, K.E., Aronson, N. E., Andrsen, E.M., Quino-Ascurra, H.A., Vidal, C., Moran, K.A., Murray, C.K., DeWitt, C.C., Heppner, D.G., Kain, K.C., Ballou, W.R. and Gasser, R. A., Jr (2003). "Devices for rapid diagnosis of Malaria: evaluation of prototype assays that detect *Plasmodium falciparum* histidine-rich protein 2 and a *Plasmodium vivax*-specific antigen". *Journal, of clinical microbiology* 41:6 2358-2366.
- Foster, D., Cox-Singh, J., Mohamad, D.S., Krishna, S., Chin, P.P. and Singh, B., (2014). Evaluation of three rapid diagnostic tests for the detection of human infections with *Plasmodium knowlesi*. *Malaria journal* 131: 60.
- Frank, R. and Hargreaves, R. (2003). "Clinical biomarkers in drug discovery and development". *Nature Reviews Drug Discovery* 2: 566-580.
- Franke-Favard B., Janse, C.J., Cunha-Rodrigues, M., Ramesar, J., Buscher, P., Que, I. (2005) Murine malaria parasite sequestration: CD36 is the major receptor, but cerebral pathology is unlinked to sequestration. *Proc Natl Acad Sci U.S.A.* 102: 11468-73.
- Frasch, S. C., Henson, P. M., Nagaosa, K., Fessler, M. B., Borregaard, N. and Bratton, D. L. (2004). "Phospholipid flip-flop and phospholipid scramblase 1 (PLSCR1) co-localize to uropod rafts in formylated Met-Leu-Phe-stimulated neutrophils". *The Journal of biological chemistry* 279: 17625-17633.
- Freyssinet, J. (2003). "Cellular microparticles: what are they bad or good for? *Journal of Thrombosis and Haemostasis* 1:1655-1662.



- Frevert, U., Engelmann, S., Zougbede, S., Stange, J., Ng, B., Matuschewski, K. (2005). Intravital observation of *Plasmodium berghei* sporozoite infection of the liver. *PLoS Biol.* 3:192.
- Frosch, T., Koncarevic, S., Zedler, L., Schmitt, M., Schenzel, K., Becker, K. and Popp, J. (2007). In situ localization and structural analysis of the malaria pigment hemozoin. *The Journal of Physical Chemistry B* 111: 11047-11056.
- Gatton, M.L., Rees-Channer, R.R., Glenn, J., Barnwell, J.W., Cheng, Q., Chiodini, P.L., Incardona, S., Gonzalez, I.J. and Cunningham, J. (2015). "Pan-Plasmodium band sensitivity for *Plasmodium falciparum* detection in combination malaria rapid diagnostic tests and implications for clinical management". *Malaria journal* 14: 115.
- Gardiner, D.J. (1989). Practical Raman spectroscopy. Springer-Verlag. ISBN 978-0-387-50254-0.
- Garrett, N.L. Sekine, R., Dixon, W.A M. Tilley, Leann K. Bambery, R., Bayden. R Wood (2015). Bio-sensing with butterfly wings: Naturally occurring nano-structures for SERS-based malaria parasite detection *Phys Chem Chem Phys* <http://dx.doi.org/10.1039/C4CP04930F>.
- Gaye, O., Diouf, M., Dansokho, E.F., McLaughlin, G. and Diallo, S., (1998). Diagnosis of *Plasmodium falciparum* malaria using ParaSight F®, ICT malaria PF® and Malaria IgG CELISA® assays. *Parasite* 5: 189-192.
- Ge, R., Watt, R., Sun, X., Tanner, J., He, Q., Huang, J. and Sun, H. (2006). "Expression and characterization of a histidine-rich protein, Hpn: potential for Ni<sup>2</sup> storage in *Helicobacter pylori*", *Biochem.J*, 393: 285-293.
- Gething P.W., Smith, D. L., Patil, A.P., Tatem, A. J., Snow, R.W., and Hay, S. I. (2010) Climate change and the global malaria recession. *Nature* 465: 342–345.
- Gikunoo, E., Abera, A. and Woldesenbet, E. (2014). A novel carbon nanofibers grown on glass microballoons immunosensor: a tool for early diagnosis of malaria. *Sensors*, 14 8, 14686-14699.
- Gilad, J. (2008). October Evaluation of a Malaria Antigen Rapid Diagnostic Test (RDT) in a Non-Endemic Setting. In *46th Annual Meeting*. Ilsa.
- Gosser, D.K.J., (1993). Cyclic Voltammetry: Simulation and Analysis of Reaction Mechanisms; Wiley-VCH: Berlin, Germany 27-30.
- Grabias, B., Zheng, H., Mlambo, G., Tripathi, A. K. and Kumar, S. (2014). "A sensitive enhanced chemiluminescent-ELISA for the detection of< i>

- Plasmodium falciparum* circumsporozoite antigen in midguts of *Anopheles stephensi* mosquitoes". *Journal of microbiological methods* 108: 19-24.
- Grigg, M. J., William, T., Barber, B. E., Parameswaran, U., Bird, E., Piera, K., Aziz, A., Dhanaraj, P., Yeo, T. W. and Anstey, N. M. (2014). "Combining parasite lactate dehydrogenase-based and histidine-rich protein 2-based rapid tests to improve specificity for diagnosis of malaria Due to *Plasmodium knowlesi* and other Plasmodium species in Sabah, Malaysia", *Journal of clinical microbiology* 52: 2053-2060.
- Grobusch, M.P., Hänscheid, T., Krämer, B., Neukammer, J., May, J., Seybold, J., Kun, J.F., Suttorp, N. (2003). Sensitivity of hemozoin detection by automated flow cytometry in non- and semi-immune malaria patients. *Cytometry B. Clin. Cytom.* 55:46–51.
- Grubaugh, N. D., Petz, L. N., Melanson, V. R., McMenamy, S. S., Turell, M. J., Long, L. S., Pisarcik, S. E., Kengluacha, A., Jaichapor, B., O'Guinn, M. L. and Lee, J. S. (2013). "Evaluation of a field-portable DNA microarray platform and nucleic acid amplification strategies for the detection of arboviruses, arthropods, and bloodmeals". *The American Journal of Tropical Medicine and Hygiene*,. 88:245-253.
- Gulka, C. P.; Swartz, J. D.; Trantum, J. R.; Davies, K. M.; Peak, C. M.; Denton, A. J.; Haselton, F. R.; Wright, D. W. (2015). Coffee rings as low-resource diagnostics: detection of the malaria biomarker *Plasmodium falciparum* histidine-rich protein-II using a surface-coupled ring of Ni(II)NTA gold-plated polystyrene particles *ACS Appl. Mater. Interfaces*6: 6257–6263.
- Gupta, R. and Chaudhury, N.K. (2007). Entrapment of biomolecules in sol-gel matrix for applications in biosensors: Problems and future prospects. *Biosensors and Bioelectronics*, 22: 2387-2399.
- Guthmann, J.P., Ruiz, A., Priotto, G., Kiguli, J., Bonte, L. and Legros, D., (2002). Validity, reliability and ease of use in the field of five rapid tests for the diagnosis of *Plasmodium falciparum* malaria in Uganda. *Transactions of the Royal Society of Tropical Medicine and Hygiene* 96: 254-257.
- Hailu, T. and Kebede, T. (2014). "Assessing the performance of CareStart Malaria Pf/Pv Combo Test against thick blood film in the diagnosis of malaria in northwest Ethiopia". *The American Journal of Tropical Medicine and Hygiene* 90: 1109-1112.
- Haldar, K. and Mohandas, N. (2009). "Malaria, erythrocytic infection, and anemia", *Hematology / the Education Program of the American Society of Hematology*. American Society of Hematology. Education Program 87-93.

- Hasenkamp, S., Wong, E.H. and Horrocks, P. (2011). An improved single-step lysis protocol to measure luciferase bioluminescence in *Plasmodium falciparum*. *Malaria journal*. 11:1 42.
- Hasselberger, F.X., Allen, B., Paruchuri, E.K., Charles, M. & Coughlin, R.W. (1974). Immobilized enzymes: lactase bound to stainless steel and other dense carriers for use in fluidized bed reactors. *Biochemical and Biophysical Research Communications*. 57: 1054-1062.
- Hawkes, M., Conroy, A. L., Opoka, R. O., Namasopo, S., Liles, W. C., John, C. C. and Kain, K. C. (2014). "Use of a three-band HRP2/pLDH combination rapid diagnostic test increases diagnostic specificity for falciparum malaria in Ugandan children", *Malaria journal* 13: 43.
- Hayashi, T., N. Makiuchi, and M. Hara. (2009). Self-Assembled Monolayers with Chemical Gradients: Fabrication and Protein Adsorption Experiments, *Japanese Journal of Applied Physics* 48: 95503-95505.
- Helg, A., Mueller, M.S., Joss, A., Pörtl-Frank, F., Stuart, F., Robinson, J.A. and Pluschke, G., (2003). Comparison of analytical methods for the evaluation of antibody responses against epitopes of polymorphic protein antigens. *Journal of immunological methods* 276: 19-31.
- Henze, K., Morrison, H. G., Sogin, M. L. and Müller, M. (1998). "Sequence and phylogenetic position of a class II aldolase gene in the amitochondriate protist *Giardia lamblia*". *Gene* 222: 163-168.
- Herrera, S., Vallejo, A. F., Quintero, J.P., Arévalo-Herrera, M., Cancino, M. and Ferro, S. (2014). *Malaria Journal* 13:87.
- Higson, S. P. J. (2003). *Analytical Chemistry* Oxford University Press 268-271
- Ho, M. F., Baker, J., Lee, N., Luchavez, J., Arie, F., Nhem, S., & McCarthy, J. S. (2014). Circulating antibodies against *Plasmodium falciparum* histidine-rich proteins 2 interfere with antigen detection by rapid diagnostic tests. *Malaria journal*, 13: 480.
- Hobro, A.J., Konishi, A., Coban, C. Smith, N.I. (2013). Raman spectroscopic analysis of malaria disease progression via blood and plasma samples *Analyst* 138: 3927–3933.
- <http://www.sierrasensors.com> (2014).
- <http://www.abcam.com.jp/kits/elisa-kits> Abcam (2016) ELISA format.

- [http://phil.cdc.gov/phil/details\\_linked](http://phil.cdc.gov/phil/details_linked) Centres for Disease Control and Prevention (1994). Anopheles Mosquito: credit James D. Gathany.
- <https://www.innovabiosciences.com/b2b/lateral-flow-assay-development-service> (accessed 2017).
- Humphreys, M. (2001). *Malaria: Poverty, Race, and Public Health in the United States*. Johns Hopkins University Press 256:5.
- Hurdoyal, R., Achilonu, I., Choveaux, D., Coetzer, T.H. and Goldring, J.D., (2010). Anti-peptide antibodies differentiate between plasmodial lactate dehydrogenases. *Peptides* 31: 525-532.
- Hutter, E. and Maysinger, D. (2013). Gold-nanoparticle-based biosensors for detection of enzyme activity. *Trends in pharmacological sciences* 34: 497-507.
- Ittarat, W., Chomean, S., Sanchomphu, C., Wangmaung, N., Promptmas, C. and Ngrenngarmkert, W. (2013). "Biosensor as a molecular malaria differential diagnosis", *Clinica Chimica Acta*, 419, 47-51.
- Iglesias, N., Subirats, M., Trevisi, P., Ramírez-Olivencia, G., Castán, P., Puente, S. and Toro, C., (2014). Performance of a new gelled nested PCR test for the diagnosis of imported malaria: comparison with microscopy, rapid diagnostic test, and real-time PCR. *Parasitol Res.* 113, 2587–2591.
- Iqbal, J., Hira, P. R., Sher, A. and Al-Enezi, A.A. (2001). Diagnosis of imported malaria by Parasite lactate dehydrogenase and histidine-rich protein 2 (PfHRP-2)-based immunocapture assays. *Am J Trop Med Hyg.* 64: 20–23
- Iqbal, J., N. Khalid, P. and P. Hira. R. (2002). Comparison of two commercial assays with expert microscopy for confirmation of symptomatically diagnosed malaria. *J. Clin. Microbiol.* 40:4675-4678.
- Iqbal, J., Siddique, A., Jameel, M. and Hira, P. R. (2004). "Persistent histidine-rich protein 2, parasite lactate dehydrogenase, and panmalarial antigen reactivity after clearance of *Plasmodium falciparum* mono-infection". *Journal of clinical microbiology* 42: 4237-4241.
- Jacobsen, W., Bayer Aktiengesellschaft, (1994). *Spectroscopically correlated light scanning microscopy*. U.S. Patent 5,329,352.

- Jain, K.K., (2003). Nanodiagnosics: application of nanotechnology in molecular diagnostics. *Expert Review of Molecular Diagnostics*. 3:153-161.
- Jain, P., Chakma, B., Patra, S. and Goswami, P. (2014). "Potential Biomarkers and Their Applications for Rapid and Reliable Detection of Malaria", *BioMed research international*, Article ID 852645, 20 pages.
- James M.L., Gambhir S.S. (2012). A molecular imaging primer: modalities, imaging agents, and applications. *Physiol Rev*. 92: 897-965.
- Janse, C.J. and Van Vianen, P.H. (1994). Flow cytometry in malaria detection. *Methods in cell biology* 42: 295-318.
- Joshi, G., Chaudhary, N., Labana, Y. and Tailor, V. (2014). "Correlation of thrombocytopenia in urban children with malaria" *International Journal of Medical Science and Public Health*, 3, 4.
- Joshi V., Agurto C., Barriga, S. Nemeth, S., Soliz, P., MacCormick, I., Taylor, T., Lewallen, S. and Harding, S. (2016). Automated detection of retinal whitening in malarial retinopathy. *Proc. SPIE 9785, Medical Imaging: Computer-Aided Diagnosis 97852G* doi:10.1117/12.2217188.
- Kadara, O. R., Jenkinson, N. and Banks, C.E. (2009). *Sens. Actuators* 138: 556.
- Kakkilaya, B. S. (2011). <http://www.malariasite.com> (accessed 2014).
- Kang, Y., Shim, M., Kim, J., Ji, S., Lee, W. and Yang, J. (2015). "A Case of *Plasmodium malariae* Infection Imported from Guinea". *Laboratory Medicine Online*, 5: 33-37.
- Karas, M. and Bahr, U. (1986). Laser desorption mass spectrometry. *TrAC Trends in Analytical Chemistry* 5: 90-93.
- Karpen, M. E., De Haseth, P. L. and Neet, K. E. (1992). "Differences in the amino acid distributions of 310-helices and  $\alpha$ -helices". *Protein Science*, 1: 1333-1342.
- Karunamoorthi, K., Mulelam, A. and Wassie, F., (2009). Assessment of knowledge and usage custom of traditional insect/mosquito repellent plants in Addis Zemen Town, South Gonder, North Western Ethiopia. *Journal of ethnopharmacology* 121: 49-53.
- Kassa, F. A., Shio, M. T., Bellemare, M., Faye, B., Ndao, M. and Olivier, M. (2011). "New inflammation-related biomarkers during malaria infection", *PloS one*, 6, 10, e26495.

- Kifude, C.M., Rajasekariah, H.G., Sullivan, D.J., Stewart, V.A., Angov, E., Martin, S.K., Diggs, C.L. and Waitumbi, J.N. (2008). Enzyme-linked immunosorbent assay for detection of *Plasmodium falciparum* histidine-rich protein 2 in blood, plasma, and serum. *Clinical and vaccine immunology* 15: 1012-1018.
- Kim, T., Kim, H., Lee, S., Na, B., Lin, K., Cho, S., Kang, Y., Kim, D., Sohn, Y. and Kim, H. (2010). "Prevalence of *Plasmodium vivax* VK210 and VK247 subtype in Myanmar". *Malar J.* 9:195.
- Kim, J. Y., Kim, H. H., Shin, H., Sohn, Y., Kim, H., Lee, W. and Lee, H. (2012). Genetic variation of aldolase from Korean isolates of *Plasmodium vivax* and its usefulness in serodiagnosis Malaria Journal 11: 159.
- Kissinger, P.T. and Heineman, W.R. (1983). Cyclic voltammetry. *J. Chem. Educ.* 60: 702.
- Knapp, B., Hundt, E., Küpper, H.A. (1990). "*Plasmodium falciparum* aldolase: gene structure and localization". *Mol Biochem Parasitol.* 40 : 1–12.
- Krief, S., Escalante, A. A., Pacheco, M. A., Mugisha, L., André, C., Halbwx, M., Fischer, A., Krief, J., Kasenene, J. M., Crandfield, M., Cornejo, O. E., Chavatte, J., Lin, C., Letourneur, F., Grüner, A. C., McCutchan, T. F., Rénia, L. and Snounou, G. (2010). "On the diversity of malaria parasites in African apes and the origin of *Plasmodium falciparum* from Bonobos". *PLoS Pathogens* 6: 2.
- Laloo, D.G., Shingadia, D., Pasvol, G., Chiodini, P.L., Whitty, C.J., Beeching, N.J., Hill, D.R., Warrell, D.A. and Bannister, B.A. (2007). "UK malaria treatment guidelines". *Journal of infection* 54: 111-121.
- Landau, I. and Chabaud, A.G., (1978). Description of *P. cyclopsi* sp. - a parasite of the microchiropteran bat *Hipposideros cyclops* in Gabon (author's transl). *Annales de parasitologie humaine et comparée* 53: 247.
- Layek, R.K., Datta, A. and Dougherty, E.R. (2011). From biological pathways to regulatory networks. *Molecular BioSystems*, 7: 843-851.
- Layek, K., Kantam, M.L., Shirai, M., Nishio-Hamane, D., Sasaki, T. and Maheswaran, H. (2012). Gold nanoparticles stabilized on nanocrystalline magnesium oxide as an active catalyst for reduction of nitroarenes in aqueous medium at room temperature. *Green chemistry*, 14: 3164-3174.
- Layek, R.K. and Nandi, A.K., (2013). A review on synthesis and properties of polymer functionalized graphene. *Polymer*, 54: 5087-5103.

- Lee, N., Baker, J., Andrews, K. T., Gatton, M. L., Bell, D., Cheng, Q. and McCarthy, J. (2006). "Effect of sequence variation in *Plasmodium falciparum* histidine-rich protein 2 on binding of specific monoclonal antibodies: Implications for rapid diagnostic tests for malaria". *Journal of clinical microbiology* 44: 2773-2778.
- Lee, S., Song, K., Jeon, W., Jo, H., Shim, Y. and Ban, C. (2012). "A highly sensitive aptasensor towards *Plasmodium* lactate dehydrogenase for the diagnosis of malaria". *Biosensors and Bioelectronics* 35: 291-296.
- Leke, R. F., R. R. Djokam, R. Mbu, R. J. Leke, J. Fogako, R. Megnekou, S. Metenou, G. Sama, Y. Zhou, T. Cadigan, M. Parra, and D. W. Taylor. (1999). Detection of the *Plasmodium falciparum* antigen histidine-rich protein 2 in blood of pregnant women: implications for diagnosing placental malaria. *J. Clin. Microbiol.* 37:2992-2996.
- Lillehoj, P.B., Huang, M.C., Truong, N. and Ho, C.M., (2013). Rapid electrochemical detection on a mobile phone. *Lab on a Chip* 13: 2950-2955.
- Liu, W., Li, Y., Learn, G. H., Rudicell, R. S., Robertson, J. D., Keele, B. F., Ndjango, J. N., Sanz, C. M., Morgan, D. B. and Locatelli, S. (2010). "Origin of the human malaria parasite *Plasmodium falciparum* in gorillas". *Nature* 467: 420-425.
- Looareesuwan, S., Laothamatas, J., Brown, T.R., Brittenham, G.M. (2009). Cerebral malaria: a new way forward with magnetic resonance imaging (MRI). *Am J Trop Med Hyg.* 81: 545-547.
- Love, J.C., Estroff, L.A., Kriebel, J.K., Nuzzo, R.G. and Whitesides, G.M. (2005). Self-assembled monolayers of thiolates on metals as a form of nanotechnology. *Chemical reviews* 105: 1103-1170.
- Luo, S., Zhang, E., Su, Y., Cheng, T., Shi, C. (2011). A review of NIR dyes in cancer targeting and imaging. *Biomaterials* 32: 7127-7138.
- Luxton, R.W. and Kiely, J., (2009). Spot test: new technologies bring point-of-care testing into the 21st century. *European Biopharmaceutical Review* 64-70.
- Lynn, A., Chandra, S., Malhotra, P. and Chauhan, V. S. (1999). "Heme binding and polymerization by *Plasmodium falciparum* histidine rich protein II: influence of pH on activity and conformation", *FEBS letters.* 459: 267-271.
- Mahajan, R. and Gupta, P. (2010). "Proteomics: Taking over where Genomics Leaves off". *Czech J. Genet. Plant Breed.* 46: 47-53.

- Maiera Consultative Group on Diagnoses and Diagnostics (2011). A Research Agenda for Malaria Eradication: Diagnoses and Diagnostics. *PLoS Med* 8: e1000396.
- Mainini, V., Bovo, G., Chinello, C., Gianazza, E., Grasso, M., Cattoretti, G. and Magni, F. (2013). Detection of high molecular weight proteins by MALDI imaging mass spectrometry. *Molecular BioSystems* 9: 1101-1107.
- Maltha, J., Gillet, P., Bottieau, E., Cnops, L., van Esbroeck, M. and Jacobs, J. (2010). "Research Evaluation of a rapid diagnostic test, CareStart™ Malaria HRP-2/Pfhdh (Pd/pan) Combo Test for the diagnosis of malaria in a reference setting". *Malar J.* 9: 171.
- Maltha, J. and Jacobs, J. (2011). Clinical practice: the diagnosis of imported malaria in children *Eur J Pediatr.* 170: 821-829.
- Mann, A., Semenenko, I., Meir, M. and Eyal, S. (2015). Molecular imaging of membrane transporters' activity in cancer: a picture is worth a thousand tubes. *The AAPS journal* 17: 788-801.
- Marsh, K., Snow, R.W. (1999). Malaria transmission and morbidity. *Parassitologia* 41: 241-246.
- Martinez, A.W., Phillips, S.T., Carrilho, E., Thomas III, S.W., Sindi, H. and Whitesides, G.M. (2008). Simple telemedicine for developing regions: camera phones and paper-based microfluidic devices for real-time, off-site diagnosis. *Analytical chemistry* 80: 3699-3707.
- Mason, D.P., Kawamoto, F., Lin, K., Laoboonthai, A. and Wongsrichanalai, C. (2002). A comparison of two rapid field immunochromatographic tests to expert microscopy in the diagnosis of malaria. *Acta tropica* 82: 51-59.
- Mauritz, J.M., Tiffert, T., Seear, R., LautenschlÄger, F., Esposito, A., Lew, V.L., Guck, J. and Kaminski, C.F. (2010). Detection of *Plasmodium falciparum*-infected red blood cells by optical stretching. *Journal of biomedical optics* 15: 030517.
- Mawili-Mboumba, D.P., Akotet, M.K.B., Ngoungou, E.B. and Kombila, M., (2010). Evaluation of rapid diagnostic tests for malaria case management in Gabon. *Diagnostic microbiology and infectious disease* 66:162-168.
- McKeague M. and DeRosa, M. C. (2012). "Challenges and opportunities for small molecule aptamer development". *Journal of nucleic acids* 2012: 748913.
- Merwyn, S., Gopalan, N., Singh, A.K., Rai, G.P., Agarwal, G.S. (2011). Monoclonal antibodies against recombinant histidine-rich protein 2 of



- Plasmodium falciparum* and their use in malaria diagnosis Hybridoma, 30: 519–524.
- Metters, J. P., Tan, F., Kadara, R. O. and Banks, C. E. (2011). "New directions in screen printed electroanalytical sensors: an overview of recent developments". *Analyst* 136:1067-1076.
- Metzger, W.G., Mordmüller, B.G., Kremsner, P.G. (1995). Malaria pigment in leukocytes Trans R Soc Trop Med Hyg. 89: 637–638.
- Mfonkeu, J. B. P., Gouado, I., Kuate, H. F., Zambou, O., Zollo, P. H. A., Grau, G. E. R. and Combes, V. (2010). "Elevated cell-specific microparticles are a biological marker for cerebral dysfunctions in human severe malaria". *PLoS One*, 5: 10.
- Mistry, K. K., Layek, K., Mahapatra, A., RoyChaudhuri, C. and Saha, H. (2014). "A review on amperometric-type immunosensors based on screen-printed electrodes", *Analyst*, 139, 10, 2289-2311.
- Monošík, R., Stred'anský, M. and Šturdík, E. (2012). "Biosensors-classification, characterization and new trends". *Acta chimica slovacica* 5:109-120.
- Moody, A. (2002). "Rapid diagnostic tests for malaria parasites". *Clinical microbiology reviews* 15: 66-78.
- Morrin, A., Killard, A. J. and Smyth, R. M. (2007). "Electrochemical Characterization of Commercial and Home-Made Screen-Printed Carbon Electrodes", *Analytical Letters*, 36: 2021-2039.
- Morrissey, B.W. & Han, C.C. (1978). The conformation of gamma globulin adsorbed on polystyrene lattices determined by quasiaelectric light scattering *J. Colloid and Interface Sci.* 65: 423-431.
- Mubi, M., Janson, A., Warsame, M., Martensson, A., Kallander, K., Petzold, M. G., Ngasala, B., Maganga, G., Gustafsson, L.L. and Massele, A. (2011). "Malaria rapid testing by community health workers is effective and safe for targeting malaria treatment: randomised cross- over trial in Tanzania "PloS one, 6: 7.
- Mueller, T. R. and Adams, R. N. (1961). "Voltammetry at inert electrodes: II. Correlation of experimental results with theory for voltage and controlled potential scanning, controlled potential electrolysis, and chronopotentiometric techniques. *Analytica Chimica Acta* 25: 482-497.
- Munge, B. S., Fisher, J., Millord, L. N., Krause, C. E., Dowd, R. S. and Rusling, J. F. (2010). "Sensitive electrochemical immunosensor for

- matrix metalloproteinase-3 based on single-wall carbon nanotubes". *Analyst* 135:1345-1350.
- Murhandarwati, E. E., Wang, L., de Silva, H. D., Ma, C., Plebanski, M., Black, C. G. and Coppel, R. L. (2010). "Growth-inhibitory antibodies are not necessary for protective immunity to malaria infection". *Infection and immunity*, 78: 680-687.
- Murray CJ, Rosenfeld LC, Lim SS, Andrews KG, Foreman KJ, Haring D, Fullman N, Naghavi M, Lozano R, Lopez AD (2012). "Global malaria mortality between 1980 and 2010: A systematic analysis". *Lancet* 379: 413–31.
- Mwangi, T. W., Mohammed, M., Dayo, H., Snow, R. W. and Marsh, K. (2005). "Clinical algorithms for malaria diagnosis lack utility among people of different age groups". *Tropical Medicine & International Health* 10: 530-536.
- Mya, M., Saxena, R., Roy, A. and Roy, K. (2003). "Design and development of and immunosensor for the detection of malaria in field conditions". *Parasitology research* 89: 371-374.
- Myszka, D.G., (1999). Survey of the 1998 optical biosensor literature. *Journal of Molecular Recognition*, 12: 390-408.
- Nacer, A., Movila, A., Sohet, F., Girgis, N.M., Gundra, U.M., Loke, P. (2014). Experimental cerebral malaria pathogenesis--hemodynamics at the blood brain barrier. *PLoS Pathog.* 10:10.
- Nakabayashi, I., Tomida, T. & Kawashiro, K. (1985). Modification of titanium electrodes for detection of biological substances. *J. Electrochem. Soc.* 132: 2611-2613.
- Nanduri, V., Sorokulova, I. B., Samoylov, A. M., Simonian, A.L. Petrenko, V.A., Vadyanoy, B. (2007). Phage as a molecular recognition element in biosensors immobilized by physical adsorption, *Biosens. Bioelectron.* 22: 986-992.
- Nelson D.L. and Cox, M.M. (2005). *Principles of Biochemistry* 4th Ed. Lehninger, Freeman, New York 166.
- Nemiroski, A., Christodouleas, D.C., Hennek, J.W., Kumar, A.A., Maxwell, E.J., Fernández-Abedul, M.T. and Whitesides, G.M., (2014). Universal mobile electrochemical detector designed for use in resource-limited applications. *Proceedings of the National Academy of Sciences*, 11: 11984-11989.

- Nenkova, R., Ivanova, D., Vladimirova, J. and Godjevargova, T. (2010). New amperometric glucose biosensor based on cross-linking of glucose oxidase on silica gel/multiwalled carbon nanotubes/polyacrylonitrile nanocomposite film. *Sensors and Actuators B: Chemical* 148: 59-65.
- Nguyen, Q.T., Tsien, R.Y. (2013). Fluorescence-guided surgery with live molecular navigation-a new cutting edge. *Nat Rev Cancer* 13: 653-62.
- Newman, J. D. and Setford, S.J. (2006). Enzymatic biosensors. *Molecular Biotechnology* 32: 249-268.
- Newman, J. D. and Turner, A. P. F. (2007). "Historical Perspective of Biosensors and Biochip Development", in Marks, R. S., Cullen, D. C., Karube, I., Lowe, C. R. and Weetall, H. H. (editors) *Handbook of biosensors and biochips*. John Wiley, Chichester: 41-56.
- NEQAS UK For Microbiology (2013). <http://www.ukneqasmicro.org.uk/parasitology/index.php/blood-parasitology>
- Noland, G.S., Briones, N., Sullivan Jr. D. J. (2003). The shape and size of hemozoin crystals distinguishes diverse Plasmodium species, *Molecular and Biochemical Parasitology*, 130: 91-99.
- Nomura, T., Carlton, J. M., Baird, J. K., del Portillo, H. A., Fryauff, D. J., Rathore, D., Fidock, D. A., Su, X., Collins, W. E., McCutchan, T. F., Wootton, J. C. and Wellems, T. E. (2001) "Evidence for different mechanisms of chloroquine resistance in 2 Plasmodium species that cause human malaria", *The Journal of infectious diseases*, 183, 11, 1653-1661.
- Noh, M.F.M and Tothill, I.E., (2011). Determination of Lead (II) and Copper (II) in waste-water and soil extracts on mercury film screen-printed carbon electrodes sensor. *Sains Malaysiana* 40: 1153-1163.
- Noppadon T., Chatnapa D., Polrat W., Srivicha K., (2009). *Korean Journal of Parasitology*, Malaria diagnosis: A brief review 47: 93–102.
- Notomi, T., Okayama, H., Masubuchi, H., Yonekawa, T., Watanabe, K., Amino, N. and Hase, T. (2000). "Loop-mediated isothermal amplification of DNA". *Nucleic acids research* 28: 12.
- Odolini, S., Parola, P., Gkrania-Klotsas, E., Caumes, E., Schlagenhauf, P., López-Vélez, R., Burchard, G., Santos-O'Connor, F., Weld, L. and von Sonnenburg, F. (2012). "Travel-related imported infections in Europe, EuroTravNet 2009". *Clinical Microbiology and Infection*, 18: 468-474.

- Otto, A. (1968). Excitation of nonradiative surface plasma waves in silver by the method of frustrated total reflection. *Zeitschrift für Physik* 216: 398-410.
- Pagola, S. Stephens, P.W., Bohie, D.S., Kosar, A.D. and Madsen, S.K. (2000). The structure of malaria pigment  $\beta$ -haematin. *Nature* 404: 307-310.
- Patankar, T.F., Karnad, D.R., Shetty, P.G., Desai, A.P. and Prasad, S.R., (2002). Adult cerebral malaria: prognostic importance of imaging findings and correlation with postmortem findings. *Radiology*, 224 3, .811-816.
- Padial, M.M., Subirats, M., Puente, S., Lago, M., Crespo, S., Palacios, G., Baquero, M. (2005). Sensitivity of laser light depolarization analysis for detection of malaria in blood samples. *J Med Microbiol* 54:449–452.
- Pai, S., Qin, J., Cavanagh, L., Mitchell, A., El-Assaad, F., Jain R. (2014). Real-time imaging reveals the dynamics of leukocyte behaviour during experimental cerebral malaria pathogenesis. *PLoS Pathog.* 10: e1004236.
- Pancrazio, J.J., Whelan, J.P., Borkholder, D.A., Ma, W. and Stenger, D.A. (1999). Development and application of cell-based biosensors. *Annals of biomedical engineering*, 27: 697-711.
- Pandey, A., Bisht, H., Babbarwal, V., Srivastava, J., Pandey, K. and Chauhan, V. (2001). "Mechanism of malarial haem detoxification inhibition by chloroquine". *Biochem.J.* 355: 333-338.
- Park, Y., Diez-Silva, M., Fu, D., Popescu, G., Choi, W., Barman, I., Suresh, S. and Feld, M.S. (2010). Static and dynamic light scattering of healthy and malaria-parasite invaded red blood cells. *Journal of biomedical optics* 15: 020506.
- Parker, C. O. and Tothill, I. E. (2009). "Development of an electrochemical immunosensor for aflatoxin M1 in milk with focus on matrix interference" *Biosensors and Bioelectronics* 24: 2452-2457.
- Pattnaik, P. (2005). Surface plasmon resonance: applications in understanding receptor–ligand interaction *Appl. Biochem. Biotechnol.* 126: 79–92.
- Pang, L., Li, J., Jiang, J., Shen, G. and Yu, R. (2006). DNA point mutation detection based on DNA ligase reaction and nano-Au amplification: a piezoelectric approach. *Analytical biochemistry* 358 99-103.

- Pemberton, R.M., Cox, T., Tuffin, R., Drago, G.A., Griffiths, J., Pittson, R., Johnson, G., Xu, J., Sage, I.C., Davies, R. and Jackson, S.K., (2014). Fabrication and evaluation of a micro (bio) sensor array chip for multiple parallel measurements of important cell biomarkers. *Sensors* 14: 20519-20532.
- Perraut, R., Richard, V., Varela, M., Trape, J., Guillotte, M., Tall, A., Toure, A., Sokhna, C., Vigan-Womas, I. and Mercereau-Puijalon, O. (2014). "Comparative analysis of IgG responses to *Plasmodium falciparum* MSP1p19 and PF13-DBL1 $\alpha$ 1 using ELISA and a magnetic bead-based duplex assay (MAGPIX®-Luminex) in a Senegalese meso-endemic community", *Malaria journal*, 13: 410.
- Perkel, J. (2012). Structure of an antibody (<http://www.doublexscience.org/an-antibody-therapy-for-hemophilia-a/>).
- Pernia, A. M., Prieto, M.J., Orille, I.C., Martin-Ramos, J.A. and Costa-Garcia, A. (2009). "Development of optimized screen-printed immunosensors", *Instrumentation and Measurement, IEEE Transactions*, 58: 2181-2188.
- Phu, N.H., Day, N., Diep, P.T., Ferguson, D.J.P., White, N.J. (1995). Intraleukocytic malaria pigment and prognosis in severe malaria. *Trans R Soc Trop Med Hyg* 89: 200–204.
- Phyo, A. P., Nkhoma, S., Stepniewska, K., Ashley, E. A., Nair, S., McGready, R., Al-Saai, S., Dondorp, A. M., Lwin, K. M. and Singhasivanon, P. (2012). "Emergence of artemisinin-resistant malaria on the western border of Thailand: a longitudinal study", *The Lancet* 379:1960-1966.
- Pingarrón, J.M., Yáñez-Sedeño, P. and González-Cortés, A., (2008). Gold nanoparticle-based electrochemical biosensors. *Electrochimica Acta*, 53: 5848-5866.
- Piper, R., Lebras, J., Wentworth, L., Hunt-Cooke, A., Houze, S., Chiodini, P. and Makler, M. (1999). "Immunocapture diagnostic assays for malaria using *Plasmodium lactate dehydrogenase* (pLDH)". *The American Journal of Tropical Medicine and Hygiene*, 60: 109-118.
- Pisciota J. M. and Sullivan, D. (2007). Hemozoin: oil versus water *Parasitology International*, 7: 89-96.
- Ploemen, I.H, Prudencio, M., Douradinha, B.G., Ramesar, J., Fonager, J., van Gemert, G.J. (2009). Visualization and quantitative analysis of the rodent malaria liver stage by real time imaging. *PLoS One*. 4: e7881.

- Portnoy E., Vakruk<sup>1</sup>, N. Bishara, A., Shmuel. M., Magdassi, S. Golenser, J. and Eyal, S. (2016). Indocyanine Green Liposomes for Diagnosis and Therapeutic Monitoring of Cerebral Malaria. *Theranostics* 6: 167-176.
- Potchen, M.J., Kampondeni, S.D., Seydel, K.B., Birbeck, G.L., Hammond, C.A., Bradley, W.G. (2012). Acute brain MRI findings in 120 Malawian children with cerebral malaria: new insights into an ancient disease. *AJNR Am J Neuroradiol.* 33: 1740-6.
- Rakotonirina, H., Barnadas, C., Raherijafy, R., Andrianantenaina, H., Ratsimbaoa, A., Randrianasolo, L., Jahevitra, M., Andriantsoanirina, V. and Ménard, D., (2008). Accuracy and reliability of malaria diagnostic techniques for guiding febrile outpatient treatment in malaria-endemic countries. *The American journal of tropical medicine and hygiene.* 78: 217-221.
- Rathod, P. K., Ganesan, K., Hayward, R. E., Bozdech, Z. and DeRisi, J. L. (2002). "DNA microarrays for malaria". *Trends in parasitology* 18: 39-45.
- Read, J. A., Wilkonson, K. W., Trantes, B., Sessions, R. B., Brady, R. L. (1999). Chloroquine binds in the co factor binding site of *Plasmodium falciparum* lactate dehydrogenase. *J. Biol. Chem.* 274:10213-10218.
- Rechnitz, G.A. (1986). The development of biocatalytic membrane electrodes. *Anal. Chim. Acta* 180: 281-287.
- Redd, S., Kazembe, P., Luby, S., Nwanyanwu, O., Hightower, A., Ziba, C., Wirima, J., Chitsulo, L., Franco, C., Olivar, M., (2006). "Clinical algorithm for treatment of *Plasmodium falciparum* malaria in children *Lancet* 347: 223–227.
- Rénia L, Wu Howland S, Claser C, Charlotte Gruner A, Suwanarusk R, Hui Teo T, Russell B, Ng LF (2012). "Cerebral malaria: mysteries at the blood-brain barrier" *Virulence* 3: 193–201.
- Ricci, L., Viani, I., Piccolo, G., Fabio, A., Calderaro, A., Galati, L., Perandin, F., Vecchia, L., Manca, N., Dettori, G. and Turano, A. (2000). Evaluation of OptiMAL Assay test to detect imported malaria in Italy. *The new microbiologica* 23: 391-398.
- Rich, S.M., Leendertz, F.H., Xu, G., LeBreton, M., Djoko, C.F., Aminake, M.N., Takang, E.E., Dikko, J.L., Pike, B.L., Rosenthal, B.M. and Formenty, P., (2009). The origin of malignant malaria. *Proceedings of the National Academy of Sciences*, 106 35 .14902-14907.
- Richards, J. S., Arumugam, T. U., Reiling, L., Healer, J., Hodder, A. N., Fowkes, F. J., Cross, N., Langer, C., Takeo, S., Uboldi, A. D.,

- Thompson, J. K., Gilson, P. R., Coppel, R. L., Siba, P. M., King, C. L., Torii, M., Chitnis, C. E., Narum, D. L., Mueller, I., Crabb, B. S., Cowman, A. F., Tsuboi, T. and Beeson, J. G. (2013). "Identification and prioritization of merozoite antigens as targets of protective human immunity to *Plasmodium falciparum* malaria for vaccine and biomarker development", *Journal of immunology* (Baltimore, Md.: 1950). 191: 795-809.
- Richardson, D.C., Ciach, M., Zhong, K.J., Crandall, I. and Kain, K.C., (2002). Evaluation of the Makromed dipstick assay versus PCR for diagnosis of *Plasmodium falciparum* malaria in returned travelers. *Journal of clinical microbiology* 40: 4528-4530.
- Robertson, T. (2015). "Cold War landscapes: towards an environmental history of US development programmes in the 1950s and 1960s". *Cold War History*, ahead of print 1-25.
- Rogers D.J., and Randolph S.E. (2000). The global spread of malaria in a future, warmer world. *Science* 2 289:1763–1766.
- Ronkainen, N.J., Halsall, H.B. and Heineman, W.R. (2010). "Electrochemical biosensors". *Chemical Society Reviews* 39:1747-1763.
- Sainz-Elipe, S., Latorre, J. M., Escosa, R., Masià, M., Fuentes, M. V., Mas-Coma, S. and Bargues, M. D. (2010). "Malaria resurgence risk in southern Europe: Climate assessment in a historically endemic area of rice fields at the Mediterranean shore of Spain". *Malaria Journal* 9:221.
- Salam F. and Tothill I. E. (2009). Detection of *Salmonella typhimurium* using an electrochemical immunosensor *Biosensors and Bioelectronics* 24: 82630–2636.
- Sauerbrey, G. (1959). Use of a quartz vibrator for weighing thin layers on a microbalance. *Z. Phys.*, 155: 206-222.
- Schall, J.J. and Staats, C.M. (1997). Parasites and the evolution of extravagant male characters: *Anolis* lizards on Caribbean islands as a test of the Hamilton-Zuk hypothesis. *Oecologia*, 111: 543-548.
- Scholl, P. F., Kongkasuriyachai, D., Demirev, P. A., Feldman, A. B., Lin, J. S., Sullivan, D. J., Jr and Kumar, N. (2004). "Rapid detection of malaria infection in vivo by laser desorption mass spectrometry". *The American Journal of Tropical Medicine and Hygiene* 71: 546-551.
- Schuhmann, W., Lammert, R., Hämmerle, M. and Schmidt, H.L. (1991). Electrocatalytic properties of polypyrrole in amperometric electrodes. *Biosensors and Bioelectronics* 6: 689-697.

- Scouten, W.H., Luong, J.H. and Brown, R.S. (1995). Enzyme or protein immobilization techniques for applications in biosensor design. *Trends in biotechnology*, 13: 178-185.
- Scienceaid.co.uk, Laser desorption mass spectrometry (accessed 2015).
- Sharma, S.K., Sehgal, N. and Kumar, A. (2003). Biomolecules for development of biosensors and their applications. *Current Applied Physics* 3: 307-316.
- Sharma, M. K., Rao, V. K., Agarwal, G. S., Rai, G. P., Gopalan, N., Prakash, S., Sharma, S. K. and Vijayaraghavan, R. (2008). "Highly sensitive amperometric immunosensor for detection of *Plasmodium falciparum* histidine-rich protein 2 in serum of humans with malaria: comparison with a commercial kit". *Journal of clinical microbiology* 46: 3759-3765.
- Sharma, M. K., Agarwal, G.S., Rao, V.K., Upadhyay, S., Merwyn, S., Gopalan, N., Rai, G.P., Vijayaraghavan, R. and Prakash, S. (2010). "Amperometric immunosensor based on gold nanoparticles/alumina sol-gel modified screen- printed electrodes for antibodies to *Plasmodium falciparum* histidine rich protein-2". *Analyst* 135: 608-614.
- Sharma, M.K., Agarwal, G.S., Rao, V.K., Upadhyay, S., Rai, G.P. and Vijayaraghavan, R., (2011). Amperometric Biosensor for the Sensitive Detection of *Plasmodium falciparum* Histidine Rich Protein-2 Antigen. *Sensor Letters*, 9: 1363-1369.
- Sherman, I. W. (1979). Biochemistry of Plasmodium malarial parasites *Microbiological Reviews*, 43: 453–495.
- Shiff, C.J., Premji, Z. and Minjas, J.N., (1993). The rapid manual ParaSight®-F test. A new diagnostic tool for *Plasmodium falciparum* infection. *Transactions of the Royal Society of Tropical Medicine and Hygiene* 87: 646-648.
- Shrivastava, K. S., Gupta, R.K., Mahanta, J. and Lal Dubey M. (2014). Correlation of Molecular Markers of *Pfmdr1* – N 86Y and *Pfcrt* – K 76T, with In Vitro Chloroquine Resistant *Plasmodium falciparum* isolated in the malaria endemic states of Assam and Arunachal Pradesh, Northwest India. *PLoS One* 9:8.
- Sierra Sensors (2014) <http://www.sierrasensors.com>.
- Sikawar, B. Sharma, P., Srivastava, A., Agarwal, G S., Boopathi, M., Singh, B. and Jaiswa, Y. K. (2014). Surface plasmon resonance characterization of monoclonal and polyclonal antibodies of malaria for biosensor applications. *Biosensors and Bioelectronics* 60: 201-209.



- Silamut, K. (2000). *Plasmodium falciparum* staging in *in vitro* culture. Mahidol Oxford Research Unit Bangkok: 5.
- Singh, N., Mishra, A.K., Shukla, M.M., Chand, S.K. and Bharti, P.K., (2005). Diagnostic and prognostic utility of an inexpensive rapid on site malaria diagnostic test (ParaHIT f) among ethnic tribal population in areas of high, low and no transmission in central India. *BMC infectious diseases*, 5: 50.
- Singh, B. and Daneshvar, C. (2013). Human infections and detection of *Plasmodium knowlesi*. *Clinical microbiology reviews* 26: 165-184.
- Singhi, S., Chaudhary, D., Varghese, G. M., Bhalla, A., Karthi, N., Kalantri, S., Peter, J., Mishra, R., Bhagchandani, R. and Munjal, M. (2014). "Tropical fevers: Management guidelines", *Indian journal of critical care medicine: peer-reviewed, official publication of Indian Society of Critical Care Medicine*, 18: 62.
- Singer, L.M., Newman, R.D., Diarra, A., Moran, A.C., Huber, C.S., Stennies, G., Sirima, S.B., Konate, A., Yameogo, M., Sawadogo, R. and Barnwell, J.W., (2004). Evaluation of a malaria rapid diagnostic test for assessing the burden of malaria during pregnancy. *The American journal of tropical medicine and hygiene* 70: 481-485.
- Sinka, M. E., Bangs, M. J., Manguin, S., Rubio-Palis, Y., Chareonviriyaphap, T., Coetzee, M., Mbogo, C. M., Hemingway, J., Patil, A. P. and Temperley, W. H. (2012). "A global map of dominant malaria vectors". *Parasit Vectors* 5: 69.
- Situ, C. Mooney, M.H., Elliott, C.T Buijs J. (2010). Advances in surface plasmon resonance biosensor technology towards high-throughput, food-safety analysis *Trends Analyt. Chem.*, 29: 1305–1315.
- Slapeta, J. and Morin-Adeline, V. (2011). Tree of life web project (<http://tolweb.org/apicomplexa>) accessed 2014.
- Slomianny, C. (1990). Three-dimensional reconstruction of the feeding process of the malaria parasite. *Blood Cells* 16: 369–378.
- Solon, O. (2014). Perform blood tests with your smartphone screen. <http://www.wired.co.uk/news/archive/2014-03/17/smartphone-blood-test>.
- Song, W., Okamura, M., Kondo, T. and Uosaki, K. (2003). Electron and ion transport through multilayers of Au nanoclusters covered by self-assembled monolayers. *Journal of Electroanalytical Chemistry* 554: 385-393.

- Sousa, L. P., Mariuba, L. A., Holanda, R. J., Pimentel, J. P., Almeida, M. E., Chaves, Y. O., Borges, D., Lima, E., Crainey, J. L. and Orlandi, P. P. (2014). "A novel polyclonal antibody-based sandwich ELISA for detection of *Plasmodium vivax* developed from two lactate dehydrogenase protein segments", *BMC infectious diseases*, 14: 49.
- Staalsoe, T., Giha, H.A., Dodoo, D., Theander, T.G. and Hviid, L. (1999). Detection of antibodies to variant antigens on *Plasmodium falciparum*-infected erythrocytes by flow cytometry. *Cytometry Part A*, 35: 329-336.
- Stadtherr, K., Wolf, H. and Lindner, P. (2005). "An aptamer-based protein biochip". *Analytical Chemistry* 77: 3437-3443.
- Stoeva, S.I., Lee, J.S., Smith, J.E., Rosen, S.T. and Mirkin, C.A. (2006). Multiplexed detection of protein cancer markers with biobarcoded nanoparticle probes. *Journal of the American Chemical Society* 128: 8378-8379.
- Suenaga, E Mizuno, H. Penmetcha K.K.R (2012). Monitoring influenza hemagglutinin and glycan interactions using surface plasmon resonance Biosens. *Bioelectron* 32:195–201.
- Sugiyama M, Ikeda E, Kawai S, Higuchi T, Zhang H, Khan N, (2001). Cerebral metabolic reduction in severe malaria: fluorodeoxyglucose-positron emission tomography imaging in a primate model of severe human malaria with cerebral involvement. *Am J Trop Med Hyg.* 71: 542-5.
- Sullivan Jr, D. J., Ayala, Y. M. and Goldberg, D. E. (1996). "An unexpected 5' untranslated intron in the *P. falciparum* genes for histidine-rich proteins II and III", *Molecular and biochemical parasitology.* 83: 247-251.
- Sullivan D.J. (2002). Theories on malarial pigment formation and quinoline action. *Int J Parasitol* 32: 1645–1653.
- Sutherland, C.J., Tanomsing, N., Nolder, D., Oguike, M., Jennison, C., Pukrittayakamee, S., Dolecek, C., Hien, T.T., do Rosario, V.E., Arez, A. P., Pinto, J., Michon, P., Escalante, A. A., Nosten, F., Burke, M., Lee, R., Blaze, M., Otto, T.D. Barnwell, J.W., Pain, A., Williams, J., White, N.J., Day, N. P., Snounou, G., Lockhart, P.J., Chiodini, P.L., Imwong, M. and Polley, S.D. (2010). "Two non-recombining sympatric forms of the human malaria parasite *Plasmodium ovale* occur globally". *The Journal of infectious diseases* 201: 1544-1550.
- Takala – Harrison, S., Clark, T.G., Jacob, C.G., Cummings, M. P., Miotto, O., Dondorp, A.M., and Plowe, C.V. (2013). Genetic loci associated with delayed clearance of *Plasmodium falciparum* following artemisinin treatment in Southeast Asia. *Proceedings of the National Academy of Sciences* 110: 240-245.

- Tatem A.J, Guerra, C.A., Kabaria, C.W., Noor A.M., Hay S. I. (2008). Human population, urban settlement patterns and their impact on *Plasmodium falciparum* malaria endemicity. *Malar Journal* 7:218.
- Taylor, D.W. and Voller, A. (1993). The development and validation of a simple antigen detection ELISA for *Plasmodium falciparum* malaria. *Transactions of the Royal Society of Tropical Medicine and Hygiene* 87: 29-31.
- Ter Kuile, F.O., Parise, M. E., Verhoeff, F. H., Udhayakumar, V., Newman, R.D., van Eijk, A.M., Rogerson, S.J., Steketee, R.W. (2004). The burden of co-infection with human immunodeficiency virus type 1 and malaria in pregnant women in sub-saharan Africa. *Am J Trop Med Hyg* 71: 41– 54.
- Thongdee, P., Chaijaroenkul, W., Kuesap, J. and Na-Bangchang, K. (2014). "Nested-PCR and a New ELISA-Based NovaLisa Test Kit for Malaria Diagnosis in an Endemic Area of Thailand". *The Korean journal of parasitology*, 52: 377-381.
- Thrift, R.N., Forte, M. T., Cahoon, B. E., and Shore V. G. (1986). Characterization of lipoproteins produced by the human liver cell line, Hep G2, under defined conditions<sup>1</sup> *Journal of Lipid Research* 27: 236-250.
- Thompson, M., Dorn, W.H., Jrull, U.J., Tauskela, J.S., Vandenberg, E.T. and Wong, H.E. (1986). Biosensors based on plant and animal tissue. *Biosensors: Fundamentals and applications* (ed. A.P.F. Turner, I. Karube and G.S. Wilson), Oxford Univ. Press 30-59.
- Tjitra, E., Suprianto, S., McBroom, J., Currie, B.J. and Anstey, N.M. (2001). Persistent ICT malaria P.f/P.v Panmalarial and HRP2 antigen reactivity after treatment of *Plasmodium falciparum* malaria is associated with gametocytemia and results in false positive diagnoses of *Plasmodium vivax* in convalescence, *Journal of Clinical Microbiology*, 39: 1025-1031.
- Todokoro, H. and Ezumi, M. (1999). Scanning electron microscope US Patent 5: 358.
- Tombelli, S. (2012). Piezoelectric biosensors for medical applications. *Biosensors for Medical Applications* 41.
- Tothill, I.E., (2001). Biosensors developments and potential applications in the agricultural diagnosis sector. *Computers and Electronics in Agriculture*, 30: 205-218.

- Tothill, I.E., Turner, A.P.F. (2003). Biosensors. In: Caballero B, Trugo L, Finglas P, editors. Encyclopaedia of food sciences and nutrition. 2nd ed. Academic Press; ISBN: 0-12-227055-X
- Tothill, I. E. (2003). *Rapid and on-line Instrumentation for Food Quality Assurance*. Woodhead Publishing Limited, Cambridge.
- Tothill, I. E. (2009). "Biosensors for cancer markers diagnosis". *Seminars in cell & developmental biology*, Elsevier, 20 1: 55-62.
- Tothill, I.E. (2011). Emerging bio-sensing methods for mycotoxins analysis. *Prof. Dr. De Saeger S, editor. Determining mycotoxins and mycotoxigenic fungi in food and feed. Cambridge: Woodhead 359-84.*
- Tseng, D., Mudanyali, O., Oztoprak, C., Isikman, S.O., Sencan, I., Yaglidere, O. and Ozcan, A. (2010). Lensfree microscopy on a cellphone. *Lab on a Chip*, 10 14,1787-1792.
- Ulbrich, R., Golbik, R. & Schellenberger, A. (1991). Protein adsorption and leakage in carrier-enzyme systems. *Biotech and Bioeng*, 37, 28 & 287..
- Uludag, Y. (2011). Schematic of a biosensor (<https://yildizuludag.wordpress.com>) -accessed 2015.
- University of California - Los Angeles (2010). "How world's smallest 'coffee ring' may help biosensors detect disease." *Science Daily*, <[www.sciencedaily.com/releases/2010/05/100505143128.htm](http://www.sciencedaily.com/releases/2010/05/100505143128.htm)>.
- University of California (2013). Human parasite life cycle final, Scientists discover chemical modification in human malaria parasite DNA, Image credit: Le Roch Lab, UC, Riverside (<http://ucrtoday:ucr.edu>).
- Vander Jagt, D. L., Hunsaker, L. A. and Heidrich, J. E. (1981). "Partial purification and characterization of lactate dehydrogenase from *Plasmodium falciparum*". *Molecular and biochemical parasitology* 4: 255-264.
- Van Oss, C.J. & Singer, J.M. (1966). The binding of immunoglobulins and other proteins by polystyrene latex particles. *J. Reticuloendothelial Sot.* 3: 29-40.
- Verma, P., Biswas, S., Mohan, T., Ali, S. and Rao, D. N. (2013). "Detection of histidine rich protein and lactate dehydrogenase of *Plasmodium falciparum* in malaria patients by sandwich ELISA using in-house reagents". *The Indian journal of medical research* 138: 977-987.
- Vo-Dinh, T. and Cullum, B. (2000). "Biosensors and biochips: advances in biological and medical diagnostics". *Fresenius' journal of analytical chemistry*. 366: 540-551.

- Wan, Y., Lin, Z., Zhang, D., Wang, Y. and Hou, B. (2011). Impedimetric immunosensor doped with reduced graphene sheets fabricated by controllable electrodeposition for the non-labelled detection of bacteria. *Biosensors and Bioelectronics*, 26: 1959-1964.
- Wang, W., Liu, L., Song, S., Tang, L., Kuang, H. and Xu, C. (2015). "A Highly Sensitive ELISA and Immunochromatographic Strip for the Detection of *Salmonella typhimurium* in Milk Samples" *Sensors* 15: 5281-5292.
- Wanidworanun, C., Nagel, R.L., Shear, H. L. (1999). Antisense oligonucleotides targeting malarial aldolase inhibit the asexual erythrocytic stages of *Plasmodium falciparum*. *Molecular and Biochemical Parasitology* 102: 91-101.
- Wallach, M., Frölich, S. and Entzeroth, R. (2012). "Comparison of protective immune responses to apicomplexan parasites" *Journal of Parasitology Research* (<http://dx.doi.org/10.1155/2012/852591>).
- Webster, G.T., Tilley, L., Deed, S., McNaughton, D. and Wood, B.R. (2008). Resonance Raman spectroscopy can detect structural changes in haemozoin (malaria pigment) following incubation with chloroquine in infected erythrocytes. *FEBS letters*. 582:1087-1092.
- Wenisch, C., Spitzauer, S., Florris-Linau, K., Rumpold, H., Vannaphan, S., Parschalk, B., Graninger, W. and Looareesuwan, S. (1997). "Complement Activation in Severe *Plasmodium falciparum* Malaria", *Clinical immunology and immunopathology*, 85: 166-171.
- Werner, C., Stubbs, M. T., Krauth-Siegel, R. L. and Klebe, G. (2005). "The Crystal Structure of *Plasmodium falciparum* Glutamate Dehydrogenase, a Putative Target for Novel Antimalarial Drugs". *Journal of Molecular Biology*. 349: 597-607.
- White, N. J. (1997). "Assessment of the pharmacodynamic properties of antimalarial drugs *in vivo*". *Antimicrobial Agents and Chemotherapy*, 41: 1413-1422.
- Wilcox, B. A., Ellis, B. (2006). "Forests and emerging infectious diseases of humans". *Unasylva* 57. ISSN 0041-6436.
- Wilson, B. K., Behrend, M.R., Horning, M.P. and Hegg, M.C. (2011). Detection of malarial by-product hemozoin utilizing its unique scattering properties, *International Online Journal of Optics*, 19: 12190-12196.

- Wingard, L.B. Jr. (1987). Possibilities for biosensors based on neuro receptors, in Biosensors international workshop. (ed. R.D.Schmid) GBF Monographs, 10:133-137.
- Wollenberger, U., Spricigo, R., Leimkuhler, S. and Schroder, K. (2008). "Protein electrodes with direct electrochemical communication" in Biosensing for the 21<sup>st</sup> Century. Springer 19-64.
- Wong, E.H., Hasenkamp, S., Horrocks, P. (2011). Analysis of the molecular mechanisms governing the stag-specific expression a prototypical housekeeping gene during intrerythrocytic development of *P. falciparum*. *J Mol Biol.* 408:205-221.
- Worrall, E., Basu, S., Hanson, K. (2005). "Is malaria a disease of poverty? A review of the literature". *Tropical Health and Medicine* 10: 1047–59.
- Wood, B.R., Hermelink, A., Lasch, P., Bamberg, K.R., Webster, G.T., Khiavi, M.A., Cooke, B.M., Deed, S., Naumann, D. and McNaughton, D. (2009). Resonance Raman microscopy in combination with partial dark-field microscopy lights up a new path in malaria diagnostics. *Analyst* 134: 1119-1125.
- Wood, B.R., Bailo, E., Khiavi, M. A., Tilley, L. Deed, S., Deckert-Gaudig, T. (2011). Tip-enhanced Raman scattering (TERS) from hemozoin crystals within a sectioned erythrocyte *Nano Letter.* 11: 1868–1873.
- World Health Organization (2003). *Malaria rapid diagnosis: making it work.* Geneva, World Health Organization, (document RS/2003/GE/05(PHL)).
- World Health Organization (2004). *The use of rapid diagnostic tests.* Geneva, Roll Back Malaria, WHO Regional Office for the Western Pacific and UNDP/World Bank/WHO/UNICEF Special Programme for Research and Training in Tropical Diseases.
- World Health Organization (2006). Guidelines for the treatment of malaria. (<http://www.who.int>).
- World Health Organization (2011). World Malaria Report 1–248.
- World Health Organization (2014). Malaria fact sheet on malaria reduction (<http://www.who.int/>).
- World Health Organization (2014). Malaria map of incidence by countries. [http://gamapserver.who.int/mapLibrary/Files/Maps/Global\\_Malaria\\_EndemicCountries\\_2013](http://gamapserver.who.int/mapLibrary/Files/Maps/Global_Malaria_EndemicCountries_2013).

- World Health Organization (2015). Projected changes in malaria incidence rates from 2000 to 2015 / Malaria world map, taken from the World Health Organisation website <http://www.who.int/gho/malaria/en/> .
- World Health Organization Malaria fact sheet (2016). <http://www.who.int/malaria/news/2016/missinggenerdtperformance/en/>.
- Yakob, L., Lloyd, A.L., Kao, R.R., Ferguson, H.M., Brock, P.M., Drakeley, C. and Bonsall, M.B. (2017). *Plasmodium knowlesi* invasion following spread by infected mosquitoes, macaques and humans. *Parasitology* 1-10.
- Yamamoto, N., Nagasawa, Y., Sawai, M., Sudo, T., and Tsubomura, H. (1978) Potentiometric investigations of antigen–antibody and enzyme–enzyme inhibitor reactions using chemically modified metal electrodes. *J. Immunol. Methods*, 22: 309-317.
- Yap, A., Azevedo, M. F., Gilson, P. R., Weiss, G. E., O'Neill, M. T., Wilson, D. W., Crabb, B. S. and Cowman, A. F. (2014). "Conditional expression of apical membrane antigen 1 in *Plasmodium falciparum* shows it is required for erythrocyte invasion by merozoites", *Cellular microbiology*, 16, 5, 642-656.
- Yu, W., Mengersen, K., Dale, P., Ye, X., Guo, Y., Turner, L., Wang, X., Bi, Y., McBride, W. J. and Mackenzie, J. S. (2015). "Projecting future transmission of malaria under climate change scenarios: Challenges and research needs", *Critical Reviews in Environmental Science and Technology*, 45, 7, 777-811.
- Yuen, C. and Liu Q. (2012). Magnetic field enriched surface enhanced resonance Raman spectroscopy for early malaria diagnosis *J Biomed Opt*, 17. 017005.
- Zeitlin, L., Cone, R.A. and Whaley, K. J. (1999). "Using monoclonal antibodies to prevent mucosal transmission of epidemic infectious diseases", *Emerging infectious diseases* 5: 54-64.
- Zhao, H. and Waite, J. H. (2006). "Proteins in load-bearing junctions: the histidine-rich metal-binding protein of mussel byssus", *Biochemistry* 45: 14223-14231.
- Zhao Y, MacCormick, I. J, Parry, D.G. Beare, N.A., Harding, S.P., Zheng, Y. (2015). Automated Detection of Vessel Abnormalities on Fluorescein Angiogram in Malarial Retinopathy. *Sci Rep*. 5: 11154.
- Ziegler, J., Chang, R. T. and Wright, D. W. (1999). "Multiple-Antigenic Peptides of Histidine-Rich Protein II of *Plasmodium falciparum*:

Dendrimeric Biomineralization Templates", *Journal of the American Chemical Society* 121: 2395-2400.

Zhou, W., Huang, P.J., Ding, J., (2014). Aptamer-based biosensors for biomedical diagnostics *Analyst* 139: 2627.



## **APPENDICES**




# APPENDICES

## Appendix A Conference posters

Research updates were made during poster presentations

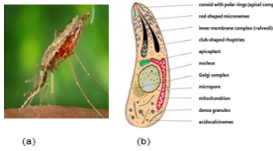
### Development of an Immunosensor for the Detection of Malaria

Aver Hemben and Ibtisam E. Tothill\*



---

Introduction



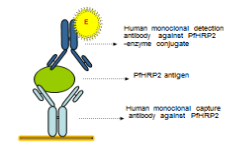
**Figure 1:** (a) Anopheles mosquito; (b) Apicomplexan

Malaria is a disease transmitted by the adult female Anopheles mosquito and caused by the Apicomplexan Plasmodium parasite. Four species of Plasmodium are responsible for human malaria: *Plasmodium malanae*, *Plasmodium ovale*, *Plasmodium vivax* and *Plasmodium falciparum*. *Plasmodium knowlesi*, the simian species typically affecting macaque monkeys is also known to affect humans. The symptoms are known to be similar in *P. falciparum* and *P. knowlesi* malaria and include headache, elevated body temperature, nausea, dizziness, loss of appetite and fatigue. Of all the forms of malaria, *P. falciparum* malaria is said to be the most lethal. Malaria even though preventable and curable, is transmitted easily and claims the lives of some of its victims, expectant mothers and children under the age of five being the most vulnerable.

Early detection is beneficial in reducing mortality rate and increasing productivity. To this end, a range of diagnostic methods have been developed to detect the disease including microscopy which has the advantage of enumerating parasites while other point of care devices rely on detecting specific biomarkers. Malaria biomarkers include aldolase, hemozoin, parasite glutamate dehydrogenase, parasite lactate dehydrogenase (pLDH) and *Plasmodium falciparum* histidine rich protein 2 (PfHRP2). To date different tests have been developed for the detection of these biomarkers, but all have limitations in being costly or lacking in sensitivity and specificity or being time consuming. Hence, the development of biosensors for malaria detection may overcome some of the limitations known in malaria diagnosis.

---

Principle and methodology


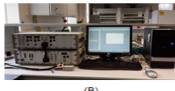


**Figure 2:** Schematic diagram of sandwich assay

*Plasmodium falciparum* histidine rich protein 2 (PfHRP2) as the biomarker was obtained along with the paired capture and detection (horse radish peroxidase-conjugate) antibodies. A sandwich ELISA format was then constructed in a microliter plate for the detection of the biomarker in order to screen and confirm the antibody affinity for PfHRP2 antigen prior to applying the assay to the electrochemical immunosensor. Screen-printed gold electrodes (SPGE) consisting of gold working electrode, carbon counter electrode and silver-silver chloride pseudo-reference electrode were fabricated using the facilities at DuPont Microcircuit Materials (Bristol, UK). Two types of gold working electrodes (JD 1 and JD 2) containing two different ink combinations were first characterised and compared using potassium ferricyanide (0.1, 0.5 and 1.0 mM). The optimum potential for the assay was then confirmed using the TMB - H<sub>2</sub>O<sub>2</sub> substrate system. The sandwich ELISA for the detection of *Plasmodium falciparum* histidine rich protein 2 was then applied onto the surface of the electrodes and the immunoreagents optimised for optimal immunosensor performance.

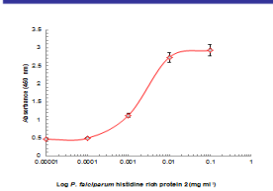
Batch no.	Carbon material
JD 1	BQ 221
JD 2	BQ 226

**Figure 3:** (A) the screen-printed electrode used, (B) Autolab potentiostat analyser attached to external terminal, USB and display unit.

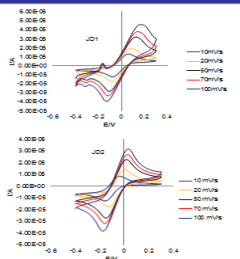
---

Results

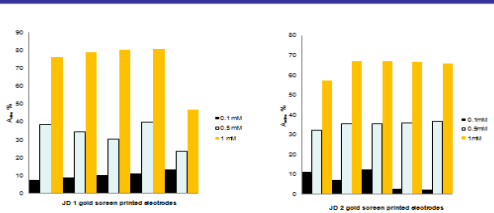


**Figure 4:** ELISA calibration plots for PfHRP2 antigen

Optimisation experiments were conducted for the ELISA assay before a calibration plot was conducted for the sandwich assay using PfHRP2 concentration range of 0.001 - 0.1 mg ml<sup>-1</sup>. The calibration plot is shown above.



**Figure 5:** JD 1 and JD 2 Cyclic voltammogram using Potassium ferricyanide [1.0 mM]



**Figure 6:** JD 1 and JD 2 active surface area

The electrochemical screen-printed gold electrodes were tested for their performance and the best electrode type selected for the development of the immunosensor. Optimization experiments are now being conducted for the PfHRP2 detection.

---

Conclusions

It can be seen from the results that the calibration plot for *Plasmodium falciparum* histidine rich protein 2 reached saturation after 0.01 mg ml<sup>-1</sup> analyte concentration. These results imply that good detection limit has been reached and confirms the affinity of the antibodies used for PfHRP2. The optimum potential applied to the electrochemical assay is found at -0.2 mVs<sup>-1</sup> confirming the results of earlier tests with the least potential for a reversible reaction at the highest current of 1.5 µA. The voltammograms show a variation in the current implying that the performance of the two batches is not equal. Further analysis reveals the higher A<sub>ox</sub>[%] of the JD 1 batch, but JD 2 gives a more reproducible CV signal.

[www.cranfield.ac.uk](http://www.cranfield.ac.uk)

Cranfield University, Cranfield, Bedfordshire, MK43 0AL, England, United Kingdom

Corresponding author: [i.tothill@cranfield.ac.uk](mailto:i.tothill@cranfield.ac.uk)

**Figure A-1:** British Society for Parasitology (BSP) Autumn Symposium held at Royal Veterinary College, Camden, London, UK (14<sup>th</sup> -15<sup>th</sup> September, 2015).

# Malaria Detection using an Electrochemical Biosensor

Aver Hemben and Ibtisam E. Tothill\*

Cranfield University, Cranfield, Bedfordshire MK43 0AL, England, UK.



## Introduction

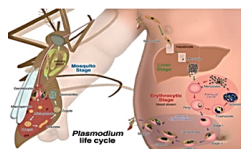


Figure 1: Plasmodium life cycle (UCR, 2013).

Malaria is a disease transmitted by the adult female Anopheles mosquito and caused by four species of Plasmodium parasite: *Plasmodium malariae*, *Plasmodium ovale*, *Plasmodium vivax* and *Plasmodium falciparum*. *Plasmodium knowlesi*, the simian species typically affecting Macaque monkeys is also known to affect humans. The symptoms are known to be similar in falciparum and knowlesi malaria and include headache, elevated body temperature, nausea, dizziness, loss of appetite and fatigue. Of all the forms of malaria, falciparum malaria is known to be the most lethal. Early detection of malaria is beneficial in reducing the mortality rate and increasing productivity. The malaria biomarkers include aldolase, hemozoin, parasite glutamate dehydrogenase, parasite lactate dehydrogenase (pLDH) and *Plasmodium falciparum* histidine rich protein 2 (PfHRP 2). pLDH and PfHRP 2 are commonly used in immuno-chromatographic tests to detect the former which is a pan-malaria glycolytic enzyme and the latter which is typically expressed on the surface of infected erythrocytes. PfHRP 2 is also known to persist after parasite clearance and can lead to false positives. The immunosensor provides quantifiable detection of the biomarker.

## Methodology

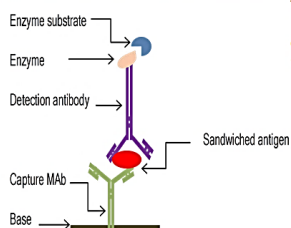


Figure 2: Sandwich assay format.

The sandwich assay was conducted in an ELISA and then applied to the gold screen-printed electrodes (DuPont Microcircuit Materials, Bristol, UK), following characterization by cyclic voltammetry, SEM and AFM scanning. The optimum potential for the assay was confirmed by amperometry using the TMB - H<sub>2</sub>O<sub>2</sub> system with HRP injection at -0.2 V s<sup>-1</sup>.



Figure 3: Gold screen-printed electrode.

Table 1: Electrode materials.

Batch no.	Carbon material
JD 1	BQ 221
JD 2	BQ 226



Figure 4: Autolab potentiostat analyser.

## Results

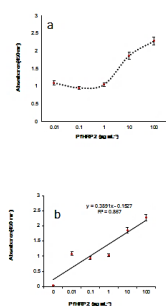


Figure 5: ELISA LOD was found to be 1.45 µg mL<sup>-1</sup>.

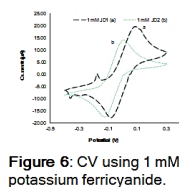


Figure 6: CV using 1 mM potassium ferricyanide.

Table 2: Active surface area

	JD 1		JD 2	
	Average	SD	Average	SD
<i>i</i> <sub>pa</sub> (µA)	19.88	±0.18	14.41	±0.32
<i>i</i> <sub>pc</sub> (µA)	0.09	±0.01	0.004	±0.001
<i>i</i> <sub>pc</sub> (µA)	0.02	±0.001	-17.43	±0.01
<i>i</i> <sub>pa</sub> (µA)	-0.079	±0.11	-0.13	±0.01
<i>i</i> <sub>pa</sub> / <i>i</i> <sub>pc</sub>	0.17	-	-0.83	-
<i>i</i> <sub>pc</sub> / <i>i</i> <sub>pa</sub>	-1.14	-	-0.83	-
<i>A</i> <sub>elec</sub>	0.18	-	0.15	-
<i>A</i> <sub>elec</sub> (%)	78.9	-	66.8	-

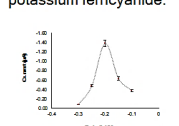


Figure 7: Optimum potential selection.

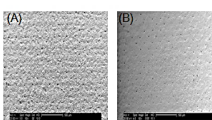


Figure 8: SEM of bare (A) and assayed (B) SPGE at 50 x magnification

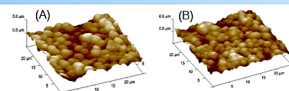


Figure 9: AFM of bare (A) and CM-Dextran coated (B) SPGE at 25 µm.

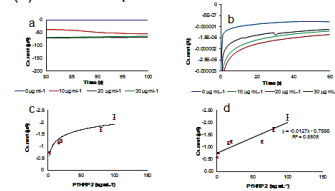


Figure 10: Optimization for sandwich assay (a,b) and standard curve (c) with linear regression (d) of P/HRP 2 immunosensor (LOD = 0.9 ng mL<sup>-1</sup>)

## Conclusions

The paired antibodies are suitable for the development of an immunoassay using JD2 electrodes for more stable results at the optimum potential confirmed from previous studies. It was also found that application of a polymer to the sensor surface inhibits the electron transfer by blocking the working electrode surface. The electrochemical measurements produced a 0.9 ng mL<sup>-1</sup> detection limit which is better than the ELISA assay. Further investigation will focused on amplifying the signal using colloidal gold.

[www.cranfield.ac.uk](http://www.cranfield.ac.uk)

Cranfield University, Cranfield, Bedfordshire MK43 0AL, England, UK.  
Corresponding author: [i.tothill@cranfield.ac.uk](mailto:i.tothill@cranfield.ac.uk).

The authors would like to express their thanks for the support of BSP in attending this Conference.

Figure A-2: BSP Spring Conference held at Imperial College, London, UK (April 11-13, 2016).

# Development of an Immunosensor for the Detection of Malaria

Aver Hemben, Jon Ashley and Ibtisam E. Tothill\*

Cranfield University, Cranfield, Bedfordshire MK43 0AL, England, UK.

Cranfield UNIVERSITY

## Introduction

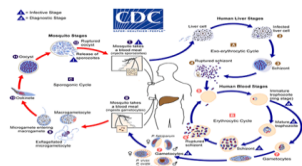


Figure 1: Plasmodium life cycle.

Malaria is a disease transmitted by the adult female Anopheles mosquito and caused by four species of Plasmodium parasite: *Plasmodium malariae*, *Plasmodium ovale*, *Plasmodium vivax* and *Plasmodium falciparum*. *Plasmodium knowlesi*, the simian species typically affecting Macaque monkeys is also known to affect humans. The symptoms are known to be similar in falciparum and knowlesi malaria and include headache, elevated body temperature, nausea, dizziness, loss of appetite and fatigue. Of all the forms of malaria, falciparum malaria is known to be the most lethal. Early detection of malaria is beneficial in reducing the mortality rate and increasing productivity. The malaria biomarkers include aldolase, hemozoin, parasite glutamate dehydrogenase, parasite lactate dehydrogenase (pLDH) and *Plasmodium falciparum* histidine rich protein 2 (PfHRP 2). pLDH and PfHRP 2 are commonly used in immuno-chromatographic tests to detect the former which is a pan-malaria glycolytic enzyme and the latter which is typically expressed on the surface of infected erythrocytes. PfHRP 2 is also known to persist after parasite clearance and can lead to false positives. The immunosensor provides quantifiable detection of the biomarker.

## Methodology

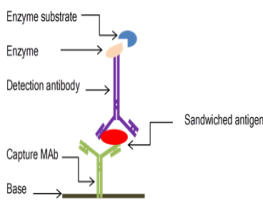


Figure 2: Sandwich assay format.

The sandwich assay was first conducted in an ELISA plate and then applied to the gold sensor chip based on screen-printing (DuPont Microcircuit Materials, Bristol, UK). Different electrode materials were used in different sensors (Table 1), which were characterised for optimal electrochemical performance. The sensor surface was also examined using SEM and AFM scanning. The optimum potential for the assay was confirmed by amperometry using the TMB - H<sub>2</sub>O<sub>2</sub> system with HRP injection at -0.2 V s<sup>-1</sup>. The immunosensor was then developed and optimized for PfHRP 2 detection.

Table 1: Electrode materials.

Batch no.	Carbon material
JD 1	BQ 221
JD 2	BQ 226

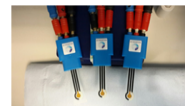


Figure 3: Sensors used.



Figure 4: Electrochemical analyser.

## Results

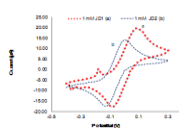


Figure 5: CV using 1 mM potassium ferricyanide.

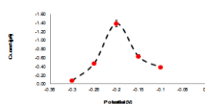


Figure 6: Optimum potential selection.

Table 2: Active surface area

T / mM	JD 1	JD 2		
I <sub>pa</sub> (μA)	19.88	0.18	14.41	±0.32
E <sub>pa</sub> (V)	0.09	0.01	0.004	±0.00
I <sub>pc</sub> (μA)	0.02	24.99	-17.43	±0.01
E <sub>pc</sub> (V)	-0.079	0.11	-0.13	±0.01
ΔE (V)	0.17	-	0.13	-
I <sub>pa</sub> / I <sub>pc</sub>	-1.14	-	-0.83	-
A <sub>active</sub>	0.18	-	0.15	-
A <sub>active</sub> (%)	78.9	-	66.8	-

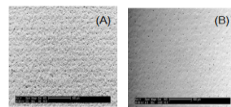


Figure 7: SEM of bare (A) and assayed (B) SPGE at 50 x magnification.

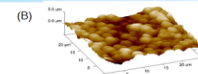


Figure 8: Electron Emission Spectrum of bare SPGE (A), topography in 3D of 25 μm by AFM.

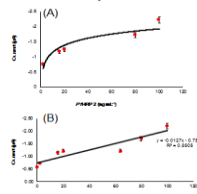


Figure 9: Sandwich assay standard curve (A) with linear regression (B) (LOD = 0.9 ng mL<sup>-1</sup>).

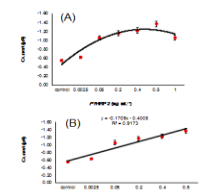


Figure 10: AuNP signal amplification (a) Linear regression (b) (LOD = 0.03 ng mL<sup>-1</sup>).

## Conclusions

The paired antibodies are suitable for the development of an immunoassay using JD2 electrodes for more stable results at the optimum potential confirmed from previous studies. It was also found that application of a polymer to the sensor surface inhibits the electron transfer by blocking the working electrode surface. The electrochemical measurements produced a 0.9 ng mL<sup>-1</sup> detection limit which is better than the ELISA assay developed in this work. Signal amplification using gold nanoparticles gave an LOD of 0.03 ng mL<sup>-1</sup>.

[www.cranfield.ac.uk](http://www.cranfield.ac.uk)

Acknowledgements: The authors would like to express their thanks to DuPont Microcircuit Materials, UK, for the screen-printed electrodes.

Corresponding author: [i.tothill@cranfield.ac.uk](mailto:i.tothill@cranfield.ac.uk)

DU PONT

Figure A-3: Biosensors Conference held at Swedish Conference and Exhibition Center, Gothenburg, Sweden (May 24<sup>th</sup> – 28<sup>th</sup>, 2016).



# Sensitive Amperometric Immunosensor for Malaria Detection

*Aver Hemben, Jon Ashley and Ibtisam E. Tothill\**

## Introduction



Figure 1: The *A. gambiae* mosquito

Malaria is a disease that is transmitted when an adult female *Anopheles* mosquito pierces the skin of a person injecting saliva containing one or more of the five *Plasmodium* parasites that infect humans. Red blood cells infected by *P. falciparum* express histidine rich protein 2 on the surface enabling sub microscopic detection of the biomarker in serum samples. Immunochromatographic and microscopic techniques have limited sensitivity leading to misdiagnosis.

Sensitive electrochemical biosensors such as screen-printed electrodes are among the earliest bio sensing instruments, signalling amperometric response of interacting bio molecules following oxidation of the enzyme substrate. Accuracy, portability and disposability make screen-printed electrodes suitable for early detection of malaria.

## Methodology

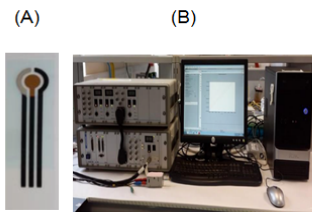


Figure 2: Dupont SPGE (A) and an electrochemical analyser (B).

Screen-printed gold electrodes (SPGEs) consisting of gold working electrode, carbon counter electrode (BQ 226) and silver-silver chloride pseudo-reference electrode were fabricated using the facilities at DuPont Microcircuit Materials (Bristol, UK). *PfHRP 2* was applied to the working electrode in a sandwich ELISA format using horse radish peroxidase conjugated detection antibody. AuNP obtained from BBI solutions (Cardiff, UK) were conjugated to the detection antibody to enhance the signal.

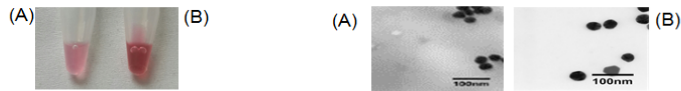


Figure 3: Working dilution of AuNP - Ab conjugate (A) stock solution (B).

Figure 4: TEM AuNP before (A) and after (B) antibody conjugation.

## Results

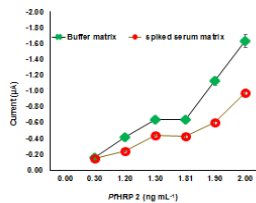


Figure 5: *PfHRP 2* standard curve binding assay in buffer and 100% serum matrices.

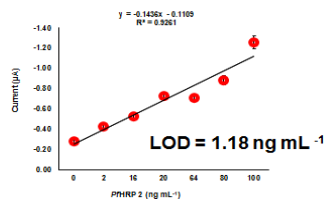


Figure 6: Serum Assay.

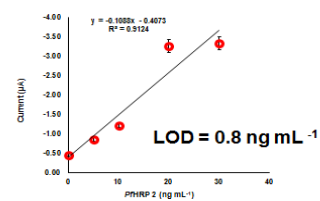


Figure 7: AuNP amplified serum assay.

## Conclusions

Amperometric detection of malaria using SPGE shows an enhanced signal with AuNP and is suitable for use in biomarker quantitation. Further studies will be conducted to compare sensitivity with immunochromatographic test.

Cranfield University, Cranfield, Bedfordshire, MK43 0AL, UK.

Contact e-mail: [i.tothill@cranfield.ac.uk](mailto:i.tothill@cranfield.ac.uk)

[www.cranfield.ac.uk](http://www.cranfield.ac.uk)



Acknowledgement:

Thanks to BSP for support to attend this event

Figure A-4: BSP Autumn symposium held at Durham University, Durham, UK, (14<sup>th</sup> - 16<sup>th</sup> September, 2016).



# Rapid and Sensitive Immunosensors for Malaria Detection

Aver Hemben, Jon Ashley, and Ibtisam E. Tothill\*

Cranfield University, Cranfield, Bedfordshire MK43 0AL, England, UK.

## Introduction

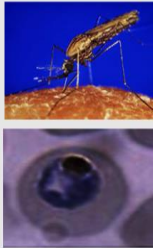


Figure 1: *Plasmodium falciparum* trophozoite.

Malaria is a disease transmitted by the adult female Anopheles mosquito and caused by: *Plasmodium malariae*, *Plasmodium ovale*, *Plasmodium vivax* and *Plasmodium falciparum*. *Plasmodium knowlesi*, the simian species typically affecting Macaque monkeys may also affect humans. Early detection of malaria is beneficial in reducing mortality rate and increasing productivity. The malaria biomarkers investigated in this work are parasite lactate dehydrogenase (pLDH) and *Plasmodium falciparum* histidine rich protein 2 (PfHRP 2). pLDH and PfHRP 2 are commonly tested using immuno-chromatographic tests (ICTs). However, a more rapid and sensitive test is required to detect the disease. A gold based working electrode was used to develop a rapid sensor for malaria detection using pLDH and PfHRP 2 as the biomarkers. The sensors signal was also enhanced using gold. The sensors were then tested with culture medium supernatant from Dd2<sup>Luc</sup> culture (6%) and compared against ICT sensitivity.

In a separate test, malaria sample (6% culture medium supernatant) was serially diluted and then analysed using the developed sensor and compared with optiMAL-IT kit.



Figure 5: Average amperometric signal of the culture medium supernatant (6% parasitaemia) in 3-fold serial dilution (A). Comparison with Immunochromatographic detection of LDH in serial dilution of culture medium supernatant using optiMAL-IT kit (B).

## Methodology



Figure 2: Autolab potentiostat analyser.

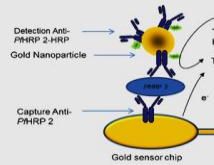


Figure 3: Gold nanoparticles amplified sandwich assay for the detection of malaria biomarkers on the sensor chip.

Enhanced sandwich assay for the detection of LDH was conducted with concentrations ranging from 0.001 ng mL<sup>-1</sup> to 10 ng mL<sup>-1</sup>. The analyte was diluted in buffer and 100% spiked serum and ELISA format applied to the gold screen-printed electrodes (DuPont Microcircuit Materials (Bristol, UK). The assay was conducted at optimum potential (-0.2 V) using the TMB-H<sub>2</sub>O<sub>2</sub> (mediator-substrate) system.

## Results

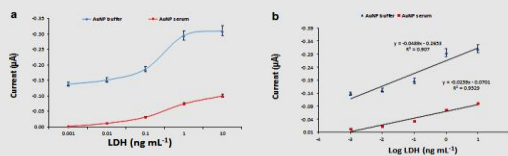


Figure 4: LDH AuNP enhanced assay standard curves (a) and linear regression (b) in buffer and 100% serum matrix.

The serum matrix affects electron transport. The signal is therefore lower in serum assay than in buffer assay. Limit of detection calculated by 3xSD of the blank + blank reading showed 14 pg mL<sup>-1</sup> 23 pg mL<sup>-1</sup> in buffer and serum assays respectively.

Faint bands are barely visible with 2% parasitaemia on optiMAL-IT. No bands seen at 0.007% parasitaemia. While the sensor showed a response even at 0.002% sample concentration.

The second ICT combo test for PfHRP 2 and pLDH in synchronous samples (4% and 0.5% parasitaemia) showed faint bands in the former and a strong band in latter for both biomarkers.

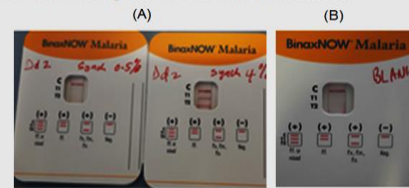


Figure 6: Immunochromatographic detection of PfHRP 2 and pLDH dissolved in synchronous samples 0.5% and 4% parasitaemia culture medium supernatant on BinaxNOW Malaria kit (A). Culture medium only (B).

Positive detection of PfHRP 2 and pLDH in synchronous samples (0.5% and 4% parasitaemia). Blank medium shows valid test negative internal control only.

## Conclusions

The paired antibodies used for the development of the immunosensor using the gold electrode produced a higher sensitivity than the ICTs. This was confirmed, since a signal was achieved with 0.002% sample concentration using the immunosensor when compared to the ICTs. The quantity in picogram mL<sup>-1</sup> of biomarker in culture medium supernatant was not determined.

These results predict a higher sensitivity with AuNP enhanced immunosensor. The developed immunosensor has potential as a point-of-care diagnostic assay alongside ICTs in malaria detection.

Corresponding author: Professor Ibtisam E. Tothill  
i.tothill@cranfield.ac.uk

## Acknowledgements:

The authors thank DuPont (Bristol, UK) for SPGEs and Professor P. Horrocks and team (Keele University, UK) for culture medium supernatant containing biomarkers.

www.cranfield.ac.uk



Figure A-5: Biosensors Conference on Lake Garda. Italy (7<sup>th</sup> -10<sup>th</sup> May, 2017).

Over the three-year period, updates of the research have been presented at conferences and symposia within and outside the UK, to gain exposure and improve presentation skills.

**Table A-1:** Presentation of the research.

S/no.	Venue		Year
1	BSP (Royal Vet. College, UK)	-	2015
2	BSP (Imperial College, UK)	-	2016
3	Biosensors (Gothenburg, Sweden)	-	2016
5	RME (Amsterdam, Netherlands)	-	2016
6	BSP (Durham University, UK)	-	2016
7	Cranfield University, UK	(RSB prize best student poster)	2017
8	<b>Oral presentation</b> , (Dundee, UK)		2017
9	Biosensors (Lake Giards, Italy)		2017



Article

## Development of an Immunosensor for *Pf*HRP 2 as a Biomarker for Malaria Detection

Aver Hemben <sup>1</sup>, Jon Ashley <sup>1,2</sup>  and Ibtisam E. Tothill <sup>1,\*</sup> 

<sup>1</sup> Surface Engineering and Nanotechnology Institute, Cranfield University, Cranfield, Bedfordshire MK43 0AL, UK; a.hemben@cranfield.ac.uk

<sup>2</sup> Department of Micro- and Nanotechnology, Technical University of Denmark, Produktionstorvet, 2800 Kgs. Lyngby, Denmark; jash@nanotech.dtu.dk

\* Correspondence: i.tothill@cranfield.ac.uk; Tel.: +44-0-750-076-6487

Received: 13 June 2017; Accepted: 12 July 2017; Published: 18 July 2017

**Abstract:** *Plasmodium falciparum* histidine-rich protein 2 (*Pf*HRP 2) was selected in this work as the biomarker for the detection and diagnosis of malaria. An enzyme-linked immunosorbent assay (ELISA) was first developed to evaluate the immunoreagent's suitability for the sensor's development. A gold-based sensor with an integrated counter and an Ag/AgCl reference electrode was first selected and characterised and then used to develop the immunosensor for *Pf*HRP 2, which enables a low cost, easy to use, and sensitive biosensor for malaria diagnosis. The sensor was applied to immobilise the anti-*Pf*HRP 2 monoclonal antibody as the capture receptor. A sandwich ELISA assay format was constructed using horseradish peroxidase (HRP) as the enzyme label, and the electrochemical signal was generated using a 3, 3', 5, 5' tetramethyl-benzidine dihydrochloride (TMB)/H<sub>2</sub>O<sub>2</sub> system. The performance of the assay and the sensor were optimised and characterised, achieving a *Pf*HRP 2 limit of detection (LOD) of 2.14 ng·mL<sup>-1</sup> in buffer samples and 2.95 ng·mL<sup>-1</sup> in 100% spiked serum samples. The assay signal was then amplified using gold nanoparticles conjugated detection antibody-enzyme and a detection limit of 36 pg·mL<sup>-1</sup> was achieved in buffer samples and 40 pg·mL<sup>-1</sup> in serum samples. This sensor format is ideal for malaria detection and on-site analysis as a point-of-care device (POC) in resource-limited settings where the implementation of malaria diagnostics is essential in control and elimination efforts.

**Keywords:** Malaria; *Pf*HRP 2; parasites; immunosensor; biosensor; nanoparticles

### 1. Introduction

Malaria is a serious disease that is caused by an Apicomplexan *Plasmodium* parasite that is transmitted by adult female *Anopheles* mosquitoes, which thrive in tropical and subtropical weather [1]. Malaria affects approximately 50% of the world's population, and causes millions of deaths [2]. According to the latest World Health Organisation (WHO), estimates, released in December 2016, there were 212 million cases of malaria in 2015, and 429,000 deaths [2]. From this, the African region accounted for the most global cases of malaria (88%), followed by the South-East Asia Region (10%) and the Eastern Mediterranean Region (2%). Despite control efforts, the disease continues to affect productivity, and therefore an effective diagnosis is required for the successful treatment and reduction of both complications and mortality [2].

The methods available for the detection of malaria include blood film microscopy, immunochromatographic tests, and serological tests. Blood film microscopy shows the highest specificity, as it depends on the detection of *Plasmodium* parasites in blood circulation, and in some cases is essential for epidemiological purposes [3]. This assay is known as the gold standard method for malaria diagnosis despite problems with its field accuracy, unacceptably high false-positive rates, errors in species identification, and its operator-dependence [4,5]. Alternative methods, such as laser desorption mass